Problems related to the estimation of rock and fluid properties from 3D and 4D seismic data

Hardianshah Bin Saleh

Submitted in accordance with the requirements for the degree of Doctor of Philosophy

The University of Leeds

School of Earth and Environment

February 2021

“Knowledge is that which benefits,

Not that which is memorized.”

-Imam As Syafie-

Declaration

The candidate confirms that the work submitted is his own and that appropriate credit has been given where reference has been made to the work of others.

Acknowledgments

This PhD research is the manifestation of collaboration of many colleagues at Leeds University. The contribution and support from them have keep my PhD journey progressing and become more meaningful.

First of all, I must express my great gratitude to my dedicated supervisor Prof. Quentin Fisher for his tremendous passion in guiding and helping me through the most critical and crucial moments during my PhD journey. I gained a lot from his knowledge and experience specially for my academic life. Also I am very grateful to my co-supervisors Associate Prof. Dr. Adam Booth for his supervision throughout this PhD project. His unique constructive critics, invaluable discussions and continual guidance have inspired me a lot. I also want to thank to Dr. Doug Angus to initiate and introduce the research project during my first year of PhD.

I would like to give my biggest thanks to my late father (1956-2017) for encouragement and motivation at beginning of my study. Also to the queens of my heart, my mum (Norwana) and my wife (Nora Norshafira) for emotional support and constant encouragement for the whole time while I was abroad. And not to forget to my beloved new born baby (Rayyan Harris) and all my family members for always being my strongest support and motivation.

I would like to thank the Institute of Applied Geophysics and people in room 8.12 of School of Earth and Environment for the help they have given me. I am very grateful for the enjoyable life in The University of Leeds with my office mates, friends and the Malaysian big family in Leeds. Thank you, David Price, Alif Aifaa Mohd Jelani, Peidhong Shi, Lin Shen, Pawan & Andy Cooke for be my friend and helper during my time in University life. Also to John Martin and Carlos Grattoni for their help and advice for the laboratory works.

I would also like to acknowledge The Government of Malaysia (Minister of Higher Education) Scholarship and Universiti Malaysia Sabah for their financial support of my PhD study. Her Royal Highness Raja Zarith Sofia for Zarith Sofiah's Initiative For Education Finance Assistance (ZSIEFA) during my critical time at the end of my study journey.

Abstract

For almost 100 years, seismic analysis has been used by the petroleum industry to map the subsurface to identify exploration targets and characterize discoveries. More recently seismic has also been used to extract additional information such as the changes in fluid saturation and rock properties. Interpretation of seismic data in terms of rock and fluid properties is difficult because it is intrinsically a non-unique problem. For example, changes in seismic velocity could be caused by variations in fluid saturation, stress or rock deformation amongst other variables.

Forward modelling of seismic properties is a potentially valuable way to increase certainty regarding the interpretations but relies on accurate rock physics models. The models used to assess rock properties of sandstones, based on correlations with properties such as porosity and clay content, are very imprecise. Many of the most commonly used rock physics models were tested against laboratory measurements of ultrasonic velocity and acoustic impedance. The simple Raymen-Hunt- Garnet (RHG) model appears to provide a far better fit to data than the rock physics models that take into account mineralogy. Overall, it appears that an accuracy of around 5% absolute porosity can be obtained from seismic velocity measurements of tight gas sandstones and the correlation with permeability is very poor. In other words, seismic velocities are not a good tool for identifying sweat spots in tight gas sandstone (TGS) reservoirs.

The most commonly used models for the stress-dependence of seismic properties are based on the assumption of the presence of penny-shaped cracks whose density and aspect ratio vary as a function of effective stress. These values are often calibrated based on ultrasonic velocity measurements made a the sample is loaded in a triaxial cell. New measurements show that much of the stress sensitivity is caused by damage and is probably not representative of subsurface conditions. The microfractures

present are far more complicated than the assumed penny-shaped cracks. There is also a large difference in values when measured during loading compared to unloading. Overall, the results indicate that seismic inversions based in current microstructural models should be treated with caution.

The effect of stress path change was simulated on field size scale based on properties and geometry of the Snøhvit field, Barent Sea, Norway. The ATRAK raytracing software was used to simulate seismic response as a result of changes in stress and fluid content that would be expected to occur due to reservoir depletion followed by water flooding. Output from ATRAK provide amplitude versus offset that allowed detailed seismic response for every stress and fluid change for each of the model layers. The predicted amplitude vs. offset (AVO) changes predicted by ATRAK suggest that both stress changes and fluid substitution has influence towards seismic response. The results also vary significantly if the microstructural model used to predict stress dependent velocities is based on laboratory measurements collected during primary loading or unloading; thus could lead to misinterpretation of seismic response.

Lists of Publications

Parts of the work in this thesis have been presented and published at international conferences.

Publication (Extended Abstract):

Saleh, H., Fisher, Q., Price, D. & Angus, D. 2017. Trends in Micro-Crack Properties of Sedimentary Rocks in Loading and Unloading Mechanism. 4th EAGE workshop on Rock Physics.

Saleh, H., Fisher, Q. & Martin. J. 2018. Geomechanics Stress Path Changes Induced Seismic Anisotropy: Misfit In Time-Lapse 4D Seismic Measurements. PETEX 2018.

Table of Contents

LIST OF FIGURES

LIST OF TABLES

LIST OF EQUATIONS

1 INTRODUCTION

1.1 Background and motivation

Petroleum (oil and gas) remains the most widely used energy resource. The exploration, appraisal and development of petroleum reservoirs can be both physically and economically risky partly due to the difficulty in characterizing the subsurface. Petroleum exploration runs the risks of having well blowouts due to encountering unexpectedly high subsurface pressures and most exploration wells are unsuccessful because they either fail to encounter petroleum or the reservoir quality is too poor to allow economic rates of production. In appraisal, collection of insufficient data can lead to very expensive mistakes particularly in the offshore environment. For example, petroleum extraction-induced compaction and sea floor subsidence have been reported in many reservoirs around the world (e.g., van Ditzhuijzen *et al.,* 1984; Nagel, 2001; Rickett *et al.*, 2006; Ruiz *et al.,* 2020). The Ekofisk reservoir in the Norwegian North Sea is a particularly well known example (Agarwal *et al.*, 2020). Petroleum production from Ekofisk between 1971 to 1985 as well as 10 years of water flooding (Hermansen *et al.,* 2000) caused the platform to sink around 2.5 meters deeper in the water as a result of the seafloor subsiding at up to 50 cm per year (Kvendseth, 1988). Jacking up the platform so that production could continue cost around $600 million. Once a field is under development there is often the need to drill infill wells to extract petroleum that is not being drained from existing wells. Often these infill wells can be incorrectly drilled into parts of the reservoir that have already been drained of petroleum; this again reduces the economic viability of projects.

For nearly 100 years, seismic measurements have been conducted to characterise the structure of the subsurface to improve the identification of structures that may contain petroleum as well as to assess optimal positions to drill production wells if exploration is successful. Over the past decades, analysis of seismic data has evolved to a stage where it is now used in an attempt to map static reservoir properties (e.g. porosity) and to monitor dynamic changes in the subsurface properties such as stress and fluid distribution resulting from petroleum extraction (Angus *et al.,* 2013). A particularly important method that is widely used in industry is time-lapse (4D) seismic. This technique involves conducting seismic surveys before and at different stages in the production history of a reservoir in an attempt to identify changes in the distribution of phases (i.e. gas, oil and brine).

A key issue with these advanced seismic methods is that the interpretation of the seismic data is often non-unique and always needs to be compared to a model to determine the property that is required. In the case of static seismic surveys rock physics models are required to relate the measured differences in seismic impedance with properties such as porosity. Interpretation of time-lapse seismic surveys is even more complicated because changes in seismic properties could have many causes including variations in the fluid phases present in the rock, changes in pore pressure and/or stress, as well as subsurface deformation. In reservoirs whose properties are particularly sensitive to changes in stress it is often necessary use geomechanical models to assess the likely causes of changes in seismic properties (i.e. changes in saturation vs changes in stress and/or deformation) identified from 4D seismic data (e.g., Minkoff *et al*., 2003; Angus *et al*., 2015).

Although advanced seismic methods are widely used in industry it is probably fair to argue that there remains a significant amount of uncertainty regarding the accuracy to which they can measure the properties for which the surveys have been conducted. The research conducted during this thesis aims to address some of this uncertainty. It specifically addresses the accuracy to which porosity can be determined from seismic data obtained from tight gas sandstone reservoir and the impact of that uncertainties in the input parameters of geomechanical models have on the interpretation of 4D seismic.

1.2 Reservoir monitoring

Monitoring stress and pressure changes within the subsurface is of considerable benefit to avert drilling or reservoir depletion related problems (Doornholf *et al.*, 2006; Herwanger & Koutsabeloulis, 2011; He *et al.*, 2015). Hence, significant approach have been made in monitoring and predicting changes in physical properties within the subsurface related to petroleum extraction (Angus *et al.*, 2015) and one of the key instruments for this is time-lapse or 4D seismic. This method has significantly improved since the 1990's and led to more quantitative approaches such that hydrocarbon migration, fluid saturation and pore pressure could be estimated from the seismic data (Angelov, 2009).

Clear changes in seismic attributes, such as amplitude and arrival times, have been observed above, within and below petroleum reservoirs (Hawkins, 2008) that are clearly caused by development activities. These changes are relatively small, but they tend to build up over large zones and are referred as geomechanical effects. To predict changes in the stress field and layer thickness, as well as the variations in the overburden and underburden, the use of geomechanical forward modelling is recommended (e.g., Hawkins, 2006; Angelov, 2009). The remainder of this introductory chapter will followed by an overview of the thesis aims, objectives and structure of this thesis.

1.3 Thesis overview

1.3.1 Aims and objectives

The overall aim of this research was to improve understanding of problems related to the estimation of rock and fluid properties from the interpretation of 3D and 4D seismic data. It has achieved this aim by addressing three objectives:

- Assessing the factors that control the ultrasonic velocity response of dry sandstone and the implications for the prediction of porosity.
- Measuring stress dependent ultrasonic velocities of sandstones and then assessing the causes of the stress dependency and the implications for the use of such measurements in interpreting 4D seismic.
- The latter objective is partially achieved by incorporating the output of a coupled fluid flow-geomechanical model into seismic modelling software (ATRAK) to assess how uncertainties in the input parameters for the geomechanical model impact interpretations of 4D seismic.

The workflow adopted in this research is shown in **Figure 1-1**.

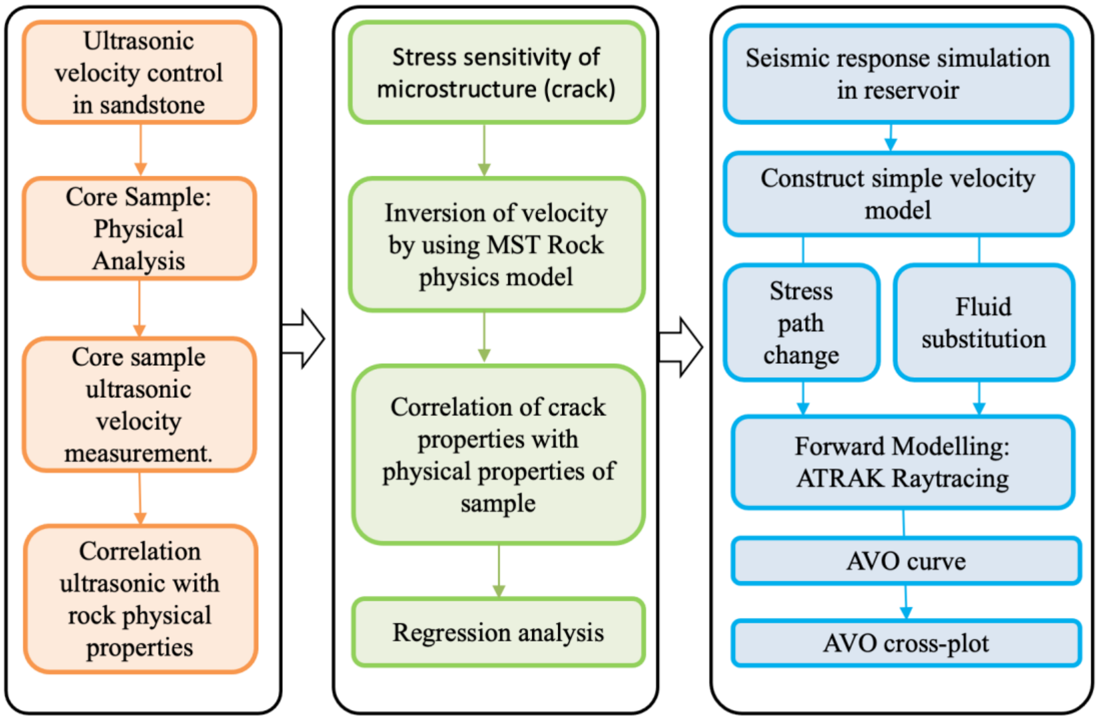

Figure 1-1 Research workflow.

1.3.2 Thesis outline

The structure of this thesis is summarized in **Table 1-1**. The following chapter (**Chapter 2**) provides a detailed review of key topics that are relevant to this research. There are three objectives this thesis are presented in the following three chapters. **Chapter 3** addresses the factors that control ultrasonic velocity response in sandstone. The analysis was carried out based on ultrasonic results from wide range of sandstone sample from various reservoir. To analyse the control factors, the ultrasonic results from the sample were correlated with various physical properties of the sample such as mineralogy, grain size, porosity and permeability. A detailed discussion for the results is also provided in this chapter.

Chapter 4 addresses the controls on stress dependent ultrasonic velocities such as variations in the microstructure such as crack density and aspect ratio during loading and unloading. The velocity from all the samples that were measured in the laboratory during loading and unloading cycles were inverted using a microstructural, MST, rock physics model to produce crack properties (aspect ratio and density) . Inverted crack properties then allow an analysis to be carried out as to how these related to changes in stress sensitivity. The output from analysis was then correlated with other rock properties (grain size, microstructural etc.) to investigate if any of these properties impacted influence towards crack development.

Chapter 5 addresses how uncertainties in the input parameters for geomechanical models, such as whether rock physics models were based on laboratory measurements collected during loading vs. unloading impact the interpretation of 4D seismic. The forwarded seismic response was modelled by incorporating the results of ultrasonic velocity measurements collected during loading and unloading into a coupled fluid flow-geomechanical model. This model is broadly based on the Snøhvit field reservoir in the Barent Sea, Norway. The ATRAK raytracing software was used to model the seismic response during the depletion and re-inflation of the reservoir. The characteristic of the seismic response was analysed using amplitude versus offset, AVO, cross-plots. Finally, **Chapter 6** presents conclusions and recommendations for further work.

Table 1-1 General thesis structure

CHAPTER	CONTENT
CHAPTER 1: INTRODUCTION	• Background and motivation • Aims and objective • Timetable and thesis structure
CHAPTER 2: QUANTITATIVE SEISMIC ANALYSIS: LABORATORY & FIELD MEASUREMENTS	• Ultrasonic measurement for porosity determination • Field 2D or 3D seismic measurement for porosity estimation • Seismic method for field monitoring

	• Rock physics • Stress dependant rock physics models • Stress path hysteresis: Loading vs unloading • Geomechanical properties change induced anisotropy • Fluid flow substitution • Seismic forward modelling
CHAPTER 3: CONTROLS OF ULTRASONIC VELOCITY OF SANDSTONE: IMPLICATIONS FOR THE ESTIMATION OF RESERVOIR PROPERTIES FROM SEISMIC DATA	• Velocity-porosity relationships • Rock physics models for velocity-porosity relationships • Correlation of velocity with grain size • Correlation of wave velocity and mineralogy • Velocity impedance with porosity • Velocity impedance-porosity: Grain size, mineralogy and pore size. • Sensitivity and scatter trend of ultrasonic velocity in low porosity rock.
CHAPTER 4: ROCK PHYSICS INVERSION & CRACK CHARACTERISTIC	• Physical meaning of crack density and aspect ratio • Impact of quartz and clay content on crack properties • Loading versus unloading • Laboratory versus subsurface velocities • Comparison with Microcrack image • Implications of results
CHAPTER 5: SEISMIC SIMULATION DURING STRESS PATH CHANGE: CASE STUDY OF SNØHVIT FIELD	• Shifted synthetic and AVO response during loading and unloading. • AVO cross-plot for stress path change.

	• Impact of changes in fluid saturation & stress path on seismic attributes
CHAPTER 6: CONCLUSSION & SUGGESTION	• Conclusion • Suggestion for future work

2 QUANTITATIVE SEISMIC ANALYSIS: LABORATORY AND FIELD MEASUREMENT

2.1 INTRODUCTION

Seismic or wave velocity has been widely used to characterise rock properties. For example, the ultrasonic or high frequency wave propagation approach has been used in the laboratory to measure physical properties of rock sample (e.g., Kohout *et al.,* 2013). This ultrasonic velocity approach is one of the most important tools for reservoir evaluation specially to determine reservoir parameters such as porosity from wire line log data (Hosseini *et al.,* 2019). Correlations established from laboratory measurements of ultrasonic velocities and other petrophysical properties are then used to interpret wire-line log measurements of sonic slowness (e.g., Vilhelm *et al.,* 2016; Hosseini *et al.,* 2019). However, well data is only 1D in nature due to the large distance between the wells. Hence, the 2D or 3D seismic method is implemented to provide more detailed reservoir characterization and correlate information between wells (e.g. Soleimani *et al.,* 2020). Recently, it is a commonly used in petroleum exploration, where well data are carefully tied with 2D or 3D seismic data to evaluate subsurface (e.g., Dubey & Das, 2019).

2.1.1 Ultrasonic measurement for porosity determination

Porosity is one of the most important physical properties in the petroleum reservoir (e.g. Tiab & Donaldson, 2016). Technically, measuring porosity is important to identify reservoir potentials to store hydrocarbon and the properties also dictate the reservoir development and production plans. Measuring porosity is also important because it is strongly correlated with other important physical properties and much use is made of these correlations in reservoir characterization studies. For example, elastic constants and seismic attenuation depend almost linearly on porosity, density, electric resistivity, thermal conductivity and seismic velocities depend inversely on porosity whereas permeability has an exponential or pore-law relationship with porosity.

Porosity can be measured in several ways such as the gas pycnometry, Archimedes water immersion method, or X-ray micro-tomography (Rasilainen *et al.*, 1996, Schön, 2004). Most of these methods tend to contaminate the rock sample during measurement process, therefore, ultrasonic measurement methods were develop for rapid and non-destructive porosity measurements. Practically, ultrasonic method will be used if the porosity measurement is required over a huge area of a rock formation (Kohout *et al.,* 2008). The ultrasonic method has been widely used to determine porosity of solid samples, with a proper calibration from other materials or rocks of interest, this method consider as a reliable and proven method in porosity determinations (Kohout *et al.,* 2013; Saether *et al.,* 2016; Garia *et al.,* 2019).

Plots of physical properties vs. porosity (see Schön, 2004) reveal considerable scatter. This scatter may be caused by differences in grain size, packing density, structure of the minerals and their bonding, and lithological variation (Schön, 2004). This scatter also directly influences velocity-porosity relationships. It is currently unclear which rock properties control the scatter of velocity-porosity data.

2.2 Field 2D or 3D seismic measurement for porosity estimation

Cores or wire-line log data from reservoirs sample just a small proportion of the reservoir let along the subsurface in general (Mojeddifar *et al.,* 2015; Soleimani *et al.*, 2020). Considering the complexities of the geology, errors will occur if it assumed that such data fully represent the whole subsurface (Somasundaram *et al.,* 2017). Thus, seismic measurements are used to help characterize the subsurface not sampled by core or wire-line logs. The field seismic measurements such obtained using 2D/3D seismic reflection methods are often used to delineate, correlate and image the structure of subsurface (Mojeddifar *et al.,* 2015; Cox *et al.,* 2020). Technically, the 2D / 3D seismic reflection methods involve the generation of elastic waves that are transmitted into the subsurface. The waves are then refracted or reflected back to the surface when they encounter an interface that represents a contrast properties in elastic properties; the way in which they are reflected or refracted can be predicted using Snell's law (e.g. Nayfeh, 1995). The arrivals of the reflected or refracted waves are then recorded on the surface and processed to create an image of the subsurface (Cox *et al.,* 2020).

It is far more difficult to estimate the porosity directly from seismic data, than it is from ultrasonic measurements made on core samples (Baker *et al.,* 2015). Estimation of porosity using seismic data has been carried out by various researchers and in various forms in different field by using compressional wave (P-wave) data (e.g. Dufaut and Landrø, 2007; Dufaut *et al.* 2018; Holt Rune *et al.,* 2018; Landrø *et al.,* 2019; Soleimani *et al.,* 2020). Essentially, inversion methods are required to make porosity estimates from field seismic data. Past studies have shown that inversion of seismic data into acoustic impedance (AI) is widely used in hydrocarbon exploration to estimate petrophysical properties (Mojeddifar *et al.,* 2015). It is common that acoustic impedance is used to estimate porosity, based on an empirical relationships between acoustic impedance and porosity (Richardson & Briggs, 1993; Mojeddifar *et al.,* 2015). However, the acoustic impedance-porosity relationship differs from area to area because the microstructure and mineralogy of rocks vary laterally and vertically. Thus, in many cases, in a large area, porosity cannot be estimated directly from the acoustic impedance using a single transform function (Anderson 1996). All these predictions should become even more accurate as wells are added.

2.2.1 Seismic method for field monitoring

Besides being used as porosity estimation tools in the reservoir, seismic also widely used to monitor changes in fluid saturation in the subsurface. Production simulation modelling and monitoring using techniques such as time-lapse (4D) seismic are playing an ever-increasing role in helping industry to optimise reservoir management (Lumley, 2001; Mandal *et al.*, 2011). Predictive simulation models have traditionally been built based upon estimates of the porosity distribution in the subsurface, the flow properties of the reservoir (i.e., permeability, capillary pressure and relative permeability), the saturation of fluids present as well as their pressure-volume-temperature (PVT) behaviour (Aminzadeh & Dasgupta, 2013; Thai *et al.*, 2017). It is practically impossible to know all of these properties in detail, so flow models are generally calibrated, a process often referred to as history matching, based on measurements such as production rates and downhole pressure measurements (e.g., Dean & Chean, 2011, Zhang *et al.*, 2014). The large number of unknowns regarding the different controls on reservoir and fluid properties means that history matching always provides non-unique solutions (e.g., Tavassoli *et al.,* 2004; Rwechungura *et al.*, 2011). In other words, just because a simulation model can reproduce production rates and downhole fluid pressures doesn’t mean that it accurately represents the way in which fluids flow in the subsurface. To help provide better constrained simulation models it has now become common practise to attempt to image changes in fluid saturation in the subsurface by conducting and comparing repeat 3D seismic surveys; this is known as 4D seismic or time-lapse seismic (Lumley, 2001; Razaei *et al.,* 2020).

Time lapse (4D) seismic surveys are now used throughout industry in an attempt to monitor changes and deformation in the subsurface (**Figure 2-1**). Generally, the 4D seismic method can be categorised into two classes: reflection amplitude methods and travel-time methods. Travel-time shifts embody the path-averaged combined influence of velocity changes and strains. On the other hand, seismic reflection amplitude changes are sensitive to perturbations in localized properties, such as the change of density and velocity across a boundary. The reflectivity changes on the top and bottom of reservoir horizons are due to a combination effects of rock deformation, pore pressure and fluid saturation changes. For example, the time-lapse seismic reflection Amplitude Variation with Offset (AVO) approach were applied with various degrees of success to discriminate between changes in fluid saturation and pressure in reservoir (e.g., Landrø, 2001; Stovas & Landrø, 2005; Herwanger & Koutsabeloulis, 2011; He, 2015). In some cases, hydrocarbon extraction induced reservoir compaction can results seismic anisotropy and hence distort the AVO response for wide-azimuth and long-offset data (e.g., Herwanger & Horne, 2009). This is complicated by the fact that reservoir compaction also can result in stress arching, which, as explained in more detail later in this chapter. Generally, stress arching is the results of vertical stresses within the overburden being transferred to the side burden of the reservoir and potentially lead to shear stresses appeared in the overburden (e.g., Segall *et al.*, 1994; Setarri, 2002; Herwanger & Koutsabeloulis, 2011; Segura *et al.*, 2011; He, 2015).

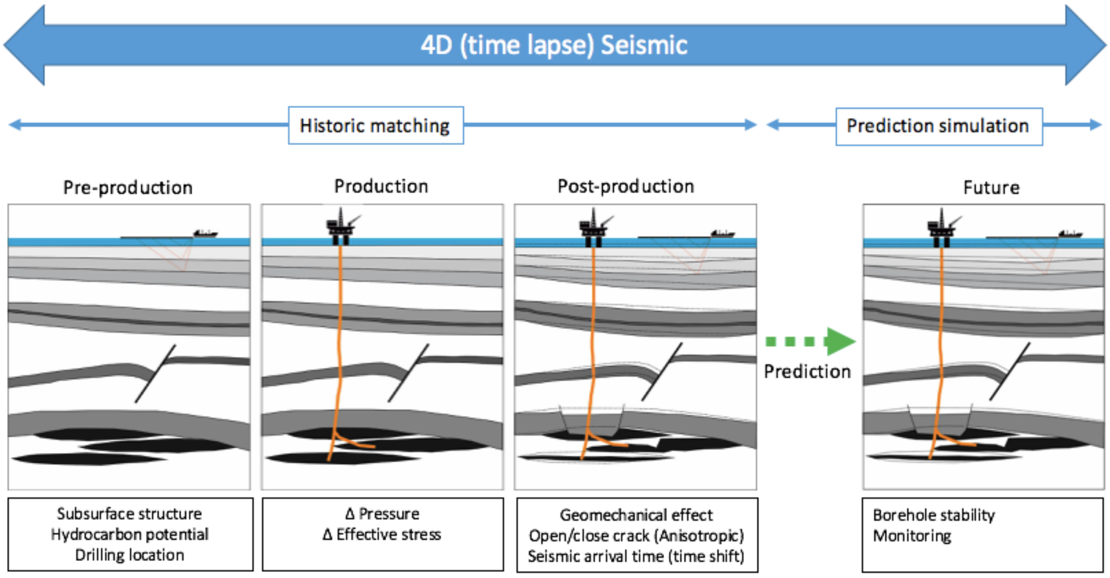

Figure 2-1 *4D seismic monitoring consist of pre-production, production and post production data which able to predict reservoir characteristic (simulation) (after Herwanger & Koutsabeloulis, 2011).*

An issue regarding the interpretation of 4D surveys and indeed conducting production simulation modelling is that the properties (e.g., porosity, density, permeability) of some reservoirs can be very sensitive to changes in stress. Stress sensitivity of reservoir properties both increases the complexity of modelling fluid flow and make it difficult to assess whether changes detected using 4D seismic are caused by changes in fluid saturation or reflect stress-related changes in the seismic properties of the reservoir. A subject that has emerged in recent years, which attempts to address these problems is seismic geomechanics. A central feature of seismic geomechanics is the use of results of coupled fluid flow - geomechanical models to improve interpretions of 4D seismic data b. In theory, this should allow 4D to be interpreted in terms of changes in both geomechanical and fluid substitution effects.

Seismic geomechanics is very much an emerging technology and some early results have identified a significant mismatch between predictions from coupled fluid flow – geomechanical models and 4D seismic data (DeGenaro *et al.*, 2008; Angus *et al.*, 2011). One possible explanation for these discrepancies is that many geomechanical models do not take into account the fact that many subsurface properties, including seismic velocities, are anisotropic.

2.2.2 Reservoir modelling: Geomechanical and fluid flow

Petroleum production induced pore-pressure and temperature changes, which results in changes in stress leading to deformation both in and around the reservoir. Compactional deformation within the reservoir may lead to reductions in both porosity and permeability, which may significantly impact fluid-flow in the reservoir (e.g., Heffer *et al.*, 1994; Fredrich *et al.*,1996, 1998; Longuemare *et al.*, 2002; Settari *et al.*, 2002; Angus *et al.*, 2011; Yang *et al.*, 2018;). In theory, it is possible to model changes in stress, rock properties and fluid saturation, which can be combined with 4D seismic data to both improve the interpretation of the 4D data and improve the reservoir model itse;f. This subsequent improved understanding of the subsurface can then be used to improve reservoir planning such as identifying the location of in-fill wells. For more than a decade, there have been many research has been carried on reservoir-geomechanical modelling and various coupling approach have been developed (e.g., Hatchell *et al.*, 2003; Barkved & Kristiansen, 2005; Staples *et al.*, 2007; Herwanger & Horne, 2009). These coupled simulation approach have been used to assess the relative importance of fluid saturation and stress changes due to production related geomechnaical effects such as compaction and subsidence (Molenaar *et al.*, 2004; He, 2015; Verdon *et al.*, 2008). Besides that, the same simulation approach also has been used to assess the sensitivity of seismic properties to variations in various rock and fluid properties. For example, many studies have been conducted to investigate how the properties of cracks/fractures, such as their crack aspect ratio and density, impact 4D seismic data (e.g., Hatchell *et al.*, 2003; Minkoff *et al*. 2003; Herwanger & Horne, 2009; Angus *et al*., 2011).

2.2.3 Misfit of predicted and measured seismic data

Ideally, the results of coupled flow - geomechanical models, which can be used to model stress and fluid saturation changes would be consistent with 4D seismic data. This is often not the case and the results of forward seismic modelling are sometimes inconsistent with 4D seismic data (e.g., Angus *et al.*, 2015; Souza *et al.,* 2018). The specific reasons for the mismatch between measured and predicted values is still poorly understood; a range of possibilities exist including: -

- Unclear rock physical properties that controlling factors on velocity response (Salah *et al.,* 2018) and the relationship of seismic response towards various type of rocks.
- Seismic anisotropy condition in the reservoir could affect the seismic response and characteristic (e.g., Bandyopadhyay, 2009).
- The capability of rock physics to model realistic physical properties such as crack properties.
- Failure to properly account for the stress dependency of subsurface velocities (e.g., Price *et al.,* 2017).
- The effects of stress path change (loading and unloading) towards seismic velocity response (Van Der Linden *et al.,* 2006).
- It is often assumed that the crack distribution is isotropic in the unstressed state (Brahmah & Sircar, 2014).

The seismic properties of rocks could be affected by a range of variables such as grain size, mineralogy, heterogeneity, fracture content and properties. It is known that porosity has a significant impact on ultrasonic velocities. However, velocity-porosity relationships have significant scatter, which is likely to be controlled by other rock properties, but the specific details of such controls are still poorly understood. Consequently, it is challenging to use seismic velocities to accurately predict porosity (Salah *et al.*, 2018).

Petroleum production can result in changes in stress as well as seismic velocity. Therefore it is important to account for how such stress changes impact seismic velocity in comparison to the changes that are caused by variations in fluid saturation. Previous researchers have shown that stress dependant wave velocity relationships are nonlinear (e.g. Holt *et al.,* 1997; Pervukhina, *et al.*, 2010). It is common practise to estimate the stress dependence of velocities by conducting ultrasonic velocity measurements on core samples from the subsurface. These measurements are made using a wavelength of 0.5 to 1 MHz, which is around four to five orders of magnitude higher than controlled source seismic (i.e. 10 to 80 Hz), on core plugs that are often not saturated with fluid and will have undoubtedly experienced a significant amount of damage during and following the core (e.g. Price *et al.,* 2017).

The seismic properties of rocks may also vary significantly depending upon the orientation at which the seismic waves propagate – this is referred to as seismic anisotropy. Seismic anisotropy can result from the preferential alignment of minerals, cracks and pores (e.g., Batzle *et al*., 2006). It can also develop if an isotropic material is placed under anisotropic stress conditions and therefore could be controlled by how the stresses within and around a reservoir evolve during production (e.g., Bandyopadhyay, 2009). Clearly, if subsurface rocks have an intrinsic seismic anisotropy or are prone to develop a seismic anisotropy due to the development of stress anisotropy then models used to help the interpretation of 4D seismic data need to take into account both intrinsic and extrinsic seismic anisotropy.

2.3 ROCK PHYSICS

Rock physics is a term used to describe the relationships between rock properties, such as porosity, lithology, and fluid saturation, and elastic properties, seismic velocity and seismic impedance (e.g., Hitlerman, 1970; Anderson *et al*., 1995; Anderson &

Cardimona, 2002; Mavko *et al*., 2009; Ahmadi *et al.*, 2013; Grana, 2014). Rock physics models also being used to predict how seismic properties respond to pressure and fluid saturation changes (e.g. Lang & Grana, 2019). A key aim of seismic geomechanics is to combine rock physics models with seismic attribute analysis (e.g., amplitude, velocity etc.) to provide insight into stress changes which could be useful for building and calibrating geomechanical model (e.g., Avseth, 2007, 2010). In theory, changes in pressure and fluid saturation in the reservoir can be estimated by using rock physics models as part of the process of inverting 4D seismic data.

2.3.1 Stress dependant rock physics models

Rock physics models have recently become increasingly important in the petroleum industry as a way to model the impact of production-related stress change on seismic velocities (e.g., Guilbot and Smith, 2002; Herwanger and Koutsabeloulis, 2011; Angus *et al.*, 2015). Laboratory studies show that the strains due to stress changes have a non-liner impact on the elastic properties of rocks (e.g., Nur and Simmons, 1969). Various models have been used to account for this nonlinearity (Verdon *et al.*, 2008) including empirically studies (e.g. Minkoff *et al*., 2004), Hertz-Mindlin contact forces (Makse *et al*., 1999), third-rank elasticity tensors (Prioul *et al*., 2004), and microstructural modelling (e.g., Zatsepin and Crampin, 1997; Shapiro and Kaselow, 2005; Sayers, 2002; Tod, 2002; Hall *et al.*, 2008).

The non–linear, stress-dependent, rock physics models have been applied to estimate the impact of reservoir production on seismic velocities (Angus *et al.*, 2012). Price *et al.*, (2017) compared of stress-dependent rock physics models with experimental data on the stress dependence of the velocity of core samples of sedimentary rocks and found that all models gave a relatively good fit to observed data on the stress dependence of both P- and S-wave data (**Figure 2-2**). Overall, the experimental results unequivocally show that stress has a major impact on seismic velocities but the fact that the models are consistent with the data does not necessarily prove that the models are correct. The stress dependence of seismic velocities is particularly significant during loading at low-confining stresses, but the stress dependence decreases as confining stresses increase and is less during experiments conducted during while stresses are gradually increased (primary loading) compared to those conducted in which the sample is confined at a pressure and then measurements conducted as the pressure is reduced – a stress path commonly referred to as unloading (Asef & Najibi, 2013). Such behaviour is often explained by the gradual closure of cracks or discontinuities as confining pressure is increased (Verdon *et al*., 2008).

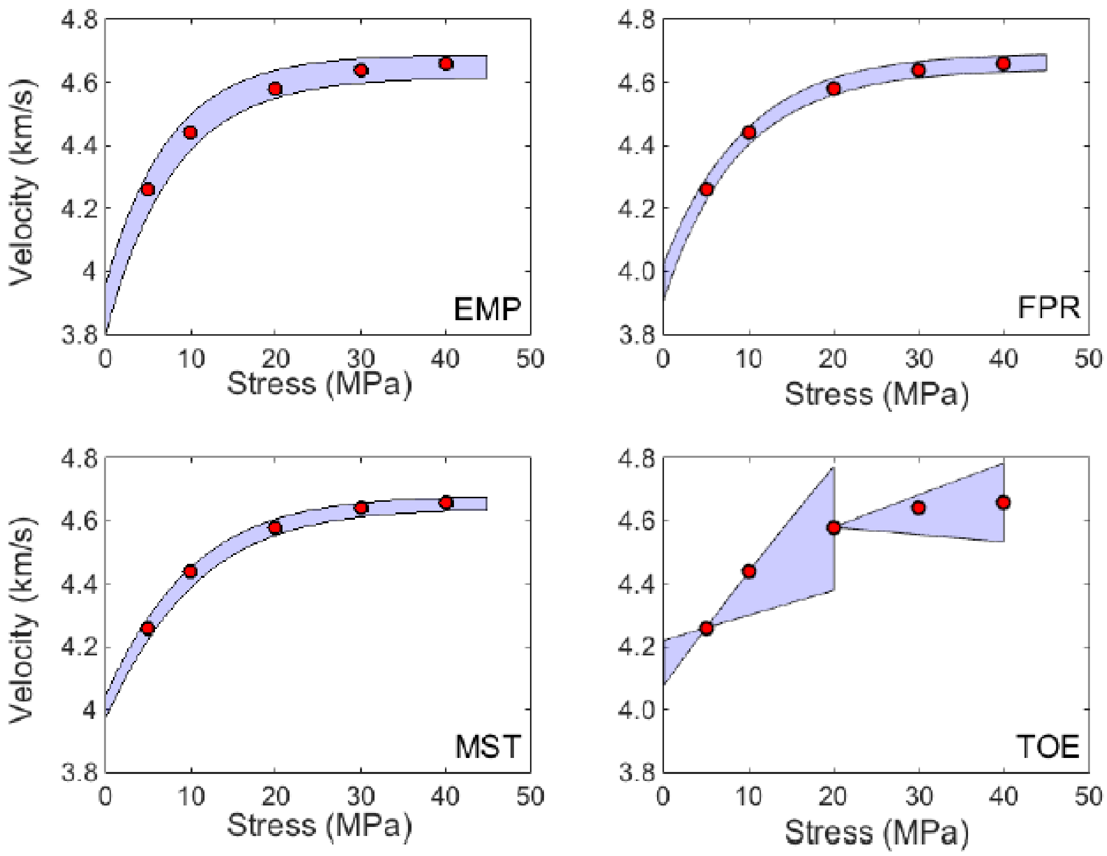

Figure 2-2 *Four non-linear rock physics models: an empirical (EMP) model, a first principle (FPR) model, a micro-structural (MST) model and a third-order elasticity (TOE) (Price et al., 2017).*

2.3.2 Stress path hysteresis: Loading vs. unloading

Total stress and pore pressure acting on a rock have a significant impact on the opening of closing of micro-cracks (Zhu & Shao, 2017) and hence seismic properties. Many previous studies have assumed that stress changes on ultrasonic properties were controlled by changes in crack properties and have been based on experiments conducted during primary loading rather than during unloading or loading that has followed several cycles of loading and unloading (e.g., Angus *et al.*, 2009; Angus *et al.*, 2012). Concentrating on changes in velocity during primary loading has two key problems. First, loading may simply be reversing damage that occurred during coring or sample preparation. Secondly, this stress path is perfectly reasonable in reservoirs undergoing pressure depletion as this increases stress, but petroleum production can also result in a reduction in stress (e.g. unloading) within the reservoir close to injectors or above compacting reservoirs (Holt *et al.*, 2016). The latter is important because there is significant evidence from laboratory experiments that seismic velocities at a given effective stress may be different during loading and unloading (e.g. Bhuiyan *et al.*, 2013).

2.3.3 Intrinsic controls on ultrasonic velocity

Experiments show that the relationship between ultrasonic velocities (both P and S wave) and stress is non-linear at low confining pressures (i.e <2000 psi) as a consequence of the 'extrinsic' effects such as stress change. At the higher confining pressures, which are in the range of those likely to be encountered in and around petroleum reservoirs, the relationship becomes approximately linear due to the 'intrinsic' effects (**Figure 2-3**). The transition from non-linear to linear velocity change is largely sample dependent (Ullemeyer et al, 2011). The variation of stress dependency of velocity between samples has several known causes including differences intrinsic factors (i.e. porosity, mineralogy, grain alignment, fracture content etc.) as well as how the properties of the sample have been affected by processes that have occurred during and following cutting, extracting and processing core taken from the subsurface (e.g., Siegesmund 1996).

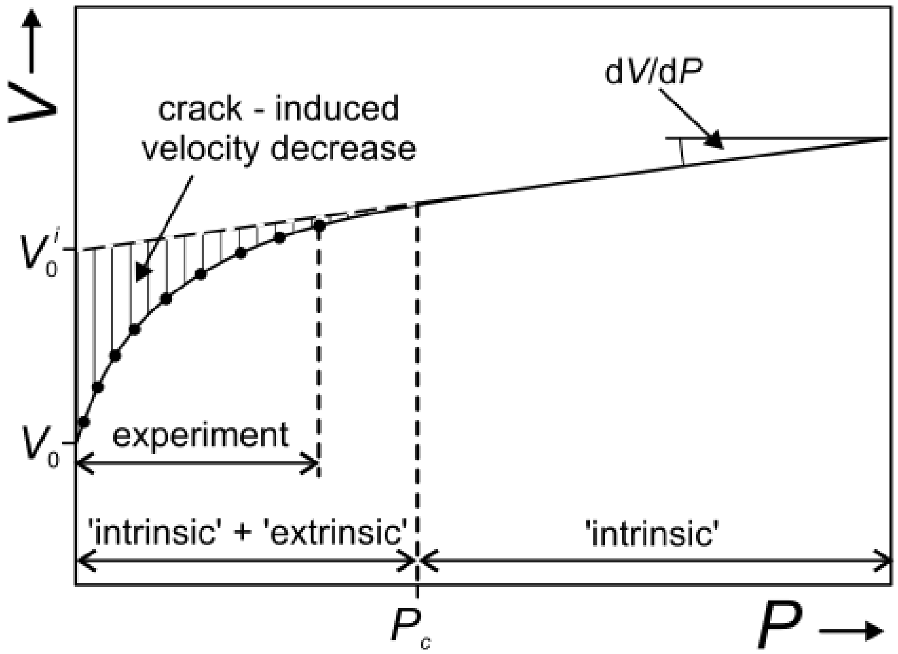

Figure 2-3 *Relationship between velocity and confining pressure (Ullemeyer et al., 2011).*

2.3.4 Oversimplification of rock physics models

Rock physics models are generally based on simplified representations of rocks. For example, microstructural models (MST), such as used by Hall *et al.* (2008), assume the stress dependence of velocities is controlled the deformation of penny-shaped cracks. Such a simplified model fails to account for the stress path dependence of ultrasonic velocities (e.g. **Figure 2-4**). It is also not clear why a rock physics model based on the presence of penny-shaped cracks is being used to interpret the results from experiments conducted on samples with such complex microstructures (**Figure 2-5**). Oversimplifying this microstructure by representing it as a series of penny-shaped cracks could lead to errors if these models are used to interpret changes in subsurface velocity because they do not represent the total characteristic of reservoir (Wang, 2001). A further problem related to the use of rock physics models based on laboratory data is the on which velocity measurements are made will be damaged and this could be the main cause for the stress-dependency of ultrasonic velocity measurements. Clearly, industry relies on core analysis studies to improve reservoir evaluation (e.g., Al-Saddique *et al.*, 2000). However, it is unclear how properties measured in the laboratory relate to how the same rocks would respond in the subsurface. It is also worth remaining fully aware that laboratory measurements are conducted on core samples taken from depths of 1 to 7 km to the surface within a few hours and then transported to a core analysis facility before core plugs are taken, cleaned and dried. Difficulties also exist regarding how to upscale the results to take into account the impact of heterogeneity.

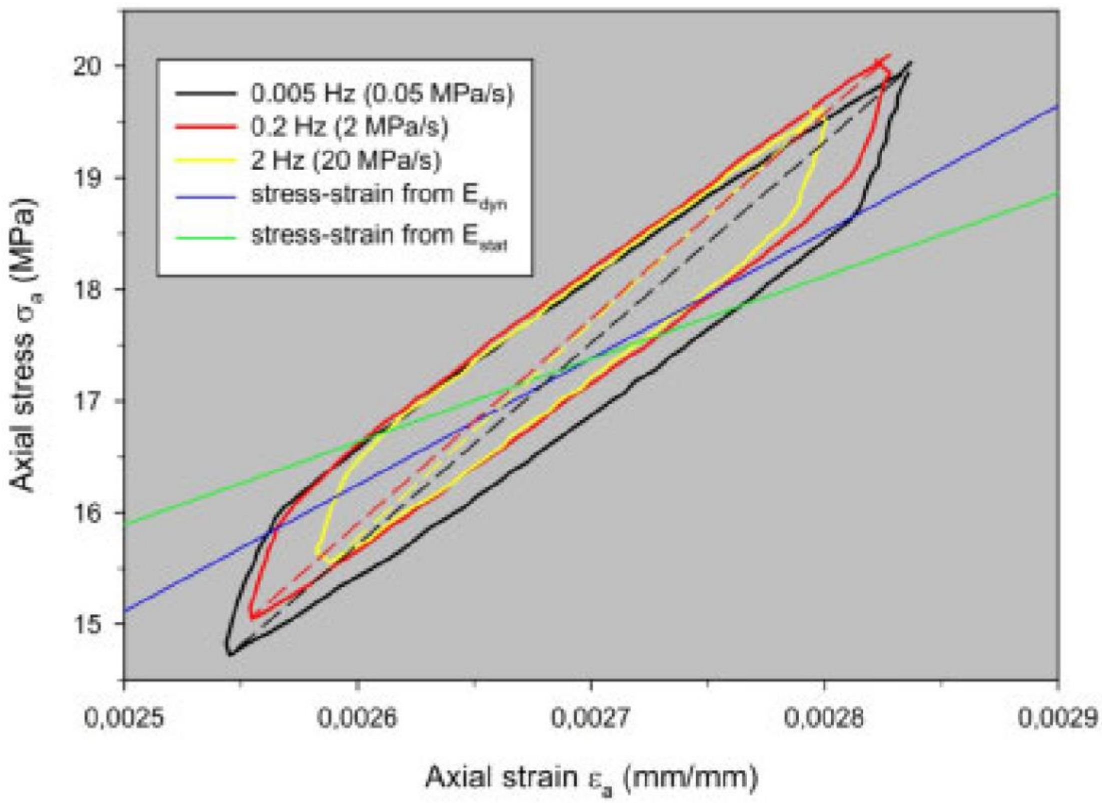

Figure 2-4 *Hysteresis in velocities hysteresis loops of a weak (left) and a strong (right) sandstone at different frequencies (Alber, 2006).*

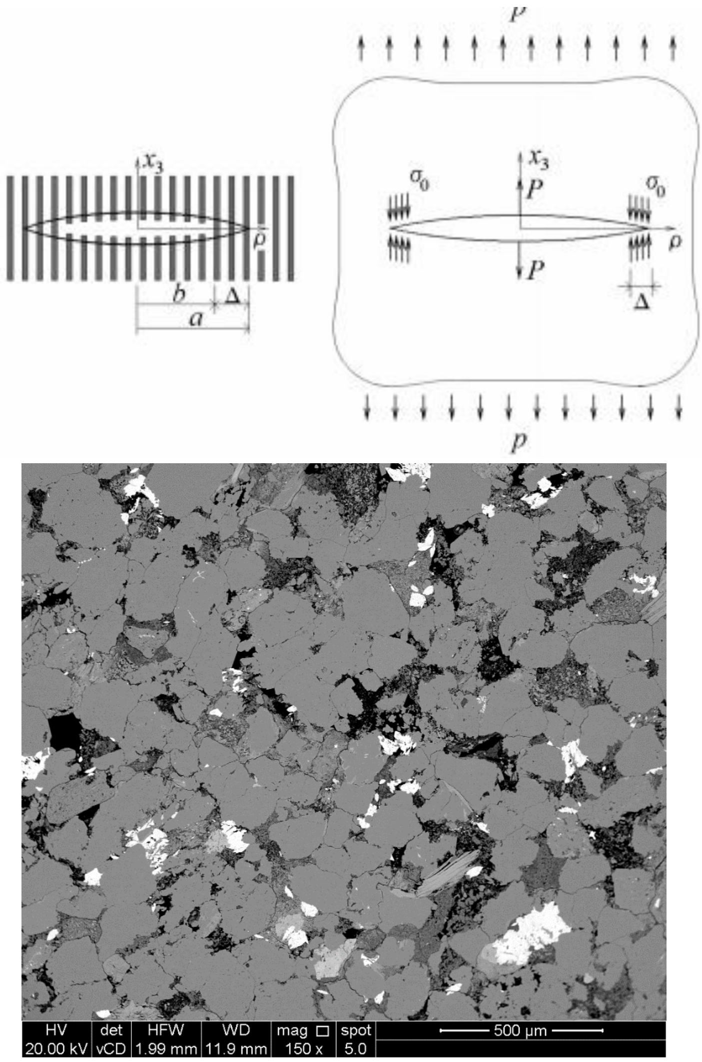

Figure 2-5 *Compares (top) the geometry of a penny-shaped crack that are assumed to control the elastic properties of rocks (from Grekov, 2009), to, (bottom) a back-scattered electron micrograph of a sandstone.*

2.4 GEOMECHANICAL PROPERTIES CHANGE INDUCED ANISOTROPY

Many core analysis measurements on which rock physics models are based are conducted under hydrostatic conditions. However, subsurface stresses vary in different directions (i.e. the stress is isotropic). It is possible that applying an anisotropic stress to a rock can result in seismic anisotropy. In particular, laboratory test on rock samples clearly proved and demonstrate that the velocity of wave propagation is dependent on the net confining pressure (e.g. King, 1966). An increment in compressive stress will typically lead to an increase in P and S wave velocity. It may therefore be assumed that velocity changes will be anisotropic when the change in stress state is non-hydrostatic. Indeed one advantage of the MST models is that they take allow the calculation of both the stress and directional dependence of ultrasonic properties. This is achieved by calculating the size and shape of penny-shaped cracks as a function of the applied stresses (i.e. cracks close when orientated perpendicular to the maximum compressive - Nur & Simmons, 1969). The large scale such in reservoir which technically, detectable amounts of seismic anisotropy can be produced by stress changes in and around (over- and side-burden) a producing reservoir (e.g. Angus *et al.*, 2016).

2.4.1 Reservoir stress path

Production from hydrocarbon reservoirs causes decline in the pore fluid pressure and increases the effective stress acting on the rock. Over time and depending upon the rock strength, this increase in stress can introduce compaction (e.g., Sayers, 2010; Segura *et al.*, 2011). The amount of compaction is partially controlled by the relative changes in effective horizontal and vertical stresses. The ratio of effective horizontal stress to effective vertical stress is known as the reservoir stress path, K, i.e.:

$$\boldsymbol{K} = \frac{\Delta\boldsymbol{\sigma'}_{\boldsymbol{h}}}{\Delta\boldsymbol{\sigma'}_{\boldsymbol{v}}}$$

Equation 2-1

where $\Delta\sigma'_h$ represent the minimum change in effective horizontal stress and $\Delta\sigma'_v$ represents the vertical effective stress at the pre-production state. Analysis of stress path, K in reservoir able to investigate the variations of the stress anisotropy and also reservoirs deformation. For example, activity during petroleum extraction can induce changes in the vertical effective stress that as well as horizontal effective stress due to compaction or depletion. For certain extend, stress anisotropy may develop as a result in changes in effective stress, could cause significant elastic anisotropic in seismic velocity (e.g., Sayers, 2010).

Understanding how reservoir stress path changes during production is important for predicting reservoir compaction, fault reactivation well bore stability etc (Hettema *et al.*, 2000; Holt, 2016). It is often assumed that it is easy to calculate how changes in pore pressure, Pp, impact effective stresses, σ', using Terzaghi's (Terzaghi, 1943) effective stress principal (**Equation** 2-2) or the Biot-Willis (Biot & Willis, 1957) effective stress law (**Equation** 2-3), which takes into account poroelastic effects:-

$$\Delta\sigma' = \Delta\sigma - \Delta P_p$$

Equation 2-2

where σ is the total stress.

$$\Delta\sigma' = \Delta\sigma - \alpha\Delta P_p$$

Equation 2-3

where α is the effective stress coefficient for volume change often referred to as Biot's parameter (Biot & Willis 1957). Usually, α is assumed to be equal to 1. In real reservoir condition, it may vary between 0 and 1 with typical values being between 0.3 and 1 (e.g., Fatt, 1959; Franquet & Abass, 1999; Segura *et al.*, 2011).

It is, however, now well known that changes in pore pressure may change horizontal stress, a processes known as horizontal stress-pore pressure coupling (Hillis, 2001). Also, it is usually assumed that the total vertical stress will stay constant during depletion because it is controlled by the weight of the overburden, which does not change. However, the depletion of a very compliant reservoir that is overlain by stiffer material can result in the overburden being partially supported by parts of the reservoir that have not undergone depletion/compaction - a process known as stress arching (Segura *et al.*, 2011). Reduction in vertical effective stress in the overburden results reservoir compaction and usually accompanied by stretching effects to the overburden. In the field, reservoirs usually do not fully undergo uniaxial deformation and heterogeneity of subsurface leads to stress arching as well as strong shear stresses in the overburden (e.g., Segall *et al*., 1994; Setarri, 2002; Herwanger & Koutsabeloulis, 2011; Segura *et al*., 2011). It is not possible to model stress arching in a predictive manner using conventional production simulation models and this is one of the key reasons that industry uses coupled fluid flow- geomechanical models (e.g., Osorio *et al.*, 1998; Angus *et al.*, 2011)

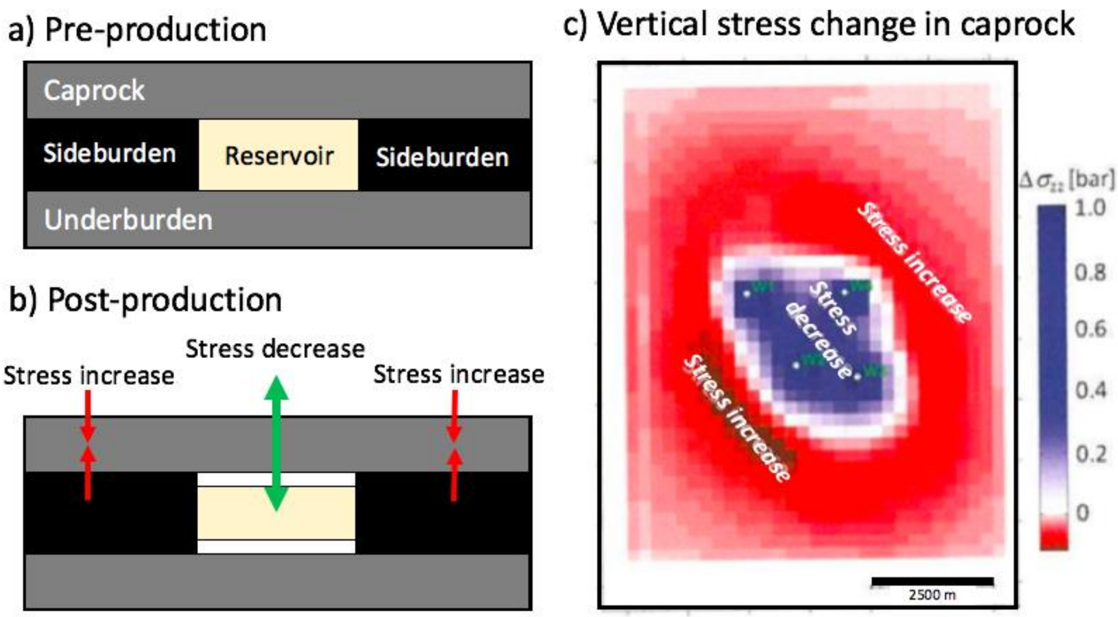

Figure 2-6 *Stress arching in the overburden. (a) and (b) show schematically the expected behaviour of vertical stress change in caprock. (c) Plan view of modelling results (Herwanger & Koutsabeloulis, 2011).*

These two processes of stress arching and horizontal stress pore pressure coupling mean that in many circumstances it is not possible to calculate changes in effective stress using these simple formulae and instead more complex geomechanical modelling is required (e.g. Segura et al., 2011). Reservoir stress path coefficients are often used to describe the change in the total stress $\Delta\sigma$ as a function of the change in pore pressure ΔP_p (subscripts "v" and "h" denote vertical and horizontal directions) γ_v

and γ_h are also called "arching coefficient" and "depletion coefficient" respectively and can describe as below:

$$\gamma_v = \frac{\Delta\sigma_v}{\Delta P_p}\ ;\ \ \gamma_h = \frac{\Delta\sigma_h}{\Delta P_p}$$

Equation 2-4

Stress path coefficients can be determined by repeated leak-off tests conducted at different stages of depletion or re-inflation. Alternatively, they could be estimated from coupled flow – geomechanical models. The way in which pore pressure changes impact stress effective stress can be represented on a Mohr circle diagram (**Figure 2-7** It is often assumed that changes in pore pressure result in the movement of the Mohr circle but do not change its size (**Figure 2-7a**). However, this is often not the case because changes in pore pressure cause changes in the total horizontal stress but not changes in the total vertical stress as generally this is fixed by the weight of the overburden. A reduction in pore pressure, which often occurs as a result of petroleum production, reduces the total horizontal stress (Hillis, 2001) resulting in an expansion of the Mohr circle (**Figure 2-7b)**, which contributes to an increase in deviatoric stress. Injection of pore fluids can have the opposite effect (**Figure 2-7c**). It is important to note that increasing and decreasing pore pressure can lead to stress path hysteresis (Santarelli *et al.*, 2008; 2013) increasing the risk of shear failure (**Figure 2-7d**).

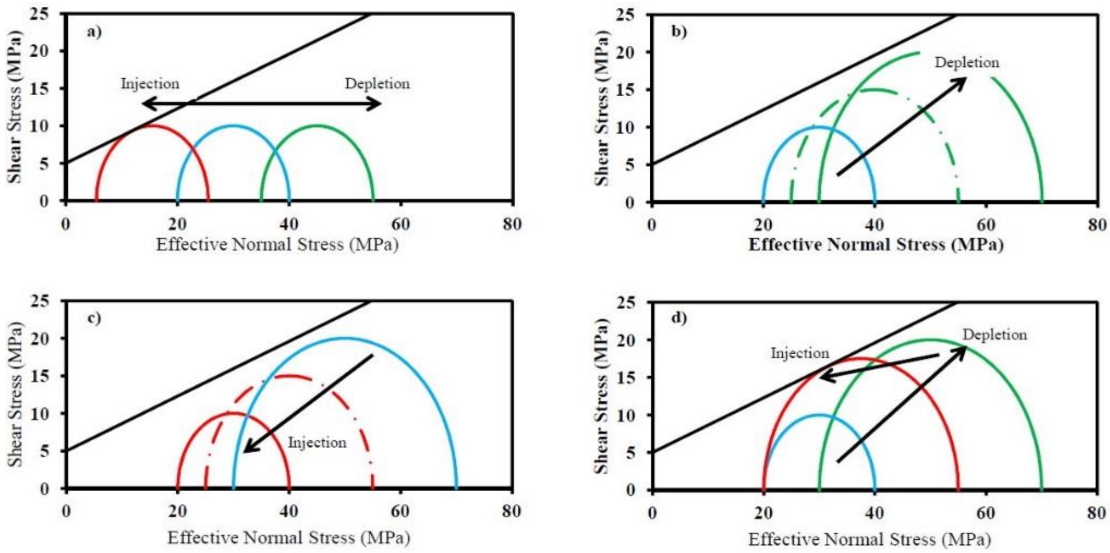

Figure 2-7 *Mohr circle evolution with pore pressure change during injection and depletion (Lynch et al., 2013); a) represents the case where changes in pore pressure do not change total horizontal stress; b) represents the case where a reduction in pore pressure decreases totally horizontal stress; c) represents the case where the changes in pore pressure effect the horizontal stress to the same extent during reinjection as they did during depletions; d) represents a case where depletion of pore pressure decreased the horizontal stress significantly but reinjection did not impact total horizontal stress to the same extent as occurred during depletion.*

2.4.2 Loading and unloading

Variation of P-wave velocity during uniaxial loading can be linked to micromechanical properties such as the presence of cracks, which may close or form as a result of stress changes (e.g., Ding & Bong, 2016Mavko *et al*., 1995; Sayers & Kachanov, 1995; Tod, 2002). It is possible that cracks behave in a different manner during loading and unloading, which will result in hysteresis in velocity-stress relationships. Indeed, 4D seismic data from petroleum reservoirs indicates that the sensitivity of wave velocity is higher during unloading than during loading (e.g., Herwanger & Koutsabeloulis, 2011) where overburden most likely experience unloading during loading or depletion of the reservoir. Based on this observation, the crack behaviour during loading is slightly different during unloading which led to give different velocity response during stress path.

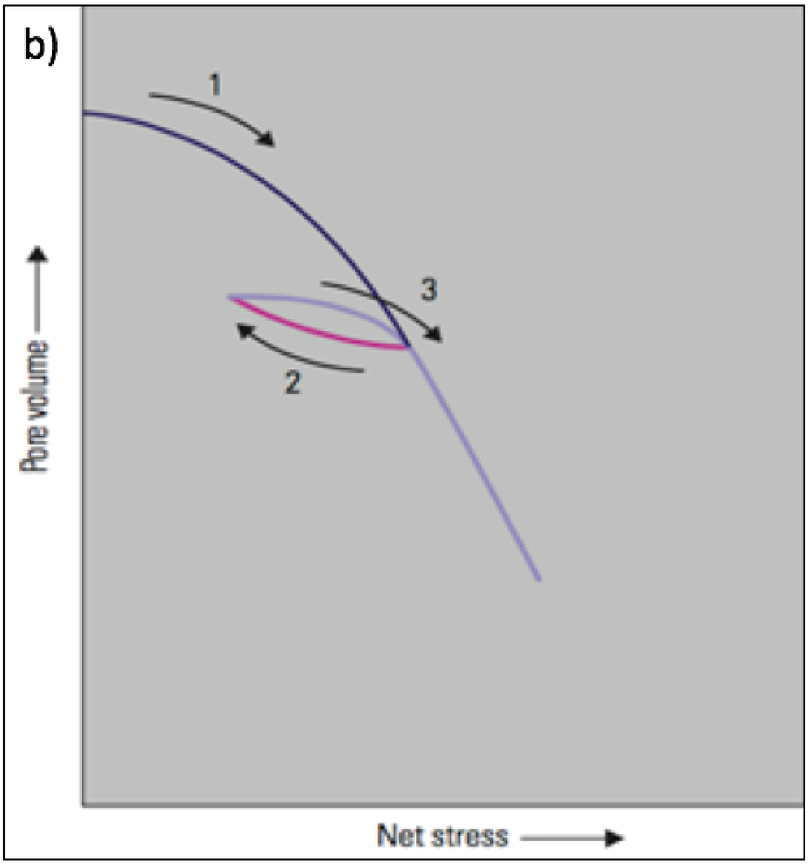

Figure 2-8 *Compaction hysteresis shows the Influence of stress towards pore volume (Doornholf, 2006; Herwanger & Koutsabeloulis, 2011).*

It is also important to remember that deformation is often inelastic. Increasing the net stress on material that is in a plastic state causes a reduction in volume (Phase 1 in **Figure 2-8b**). If the material is unloading, the volume rebound is not as large during loading, and it is often close to the elastic response (Phase 2 in **Figure 2-8b)**. Reloading the material initially causes a quasi-elastic response, until the previous high net-stress state is reached (Phase 3 in **Figure 2-8b**). At that point, the material again follows the plastic yield line (Doornholf, 2006). The wave velocity's change during these two phases (loading & unloading), as shown in **Figure 2-9,** has quantified using a metric known as the R-factor (Hatchell & Bourne, 2005). R-factor links fractional change of P-wave velocity ($\nabla V_{PO}/V_{PO}$) to the vertical change (ε_{zz}) as shown in **Figure 2-9**. It allows the use of a single parameter model to investigate time-lapse time-shift caused by (vertical) velocity change and vertical strain (Herwenger & Koutsabeloulis, 2011).

R-factors vary with the physical condition of rock such as strain, stress and also influence by type of rocks (e.g., Hatchell & Bourne, 2005; Jansen *et al*., 2006; Staples *et al*., 2007).

$$\frac{\nabla V_{PO}}{V_{PO}} = -R\varepsilon_{zz}$$

Equation 2-5

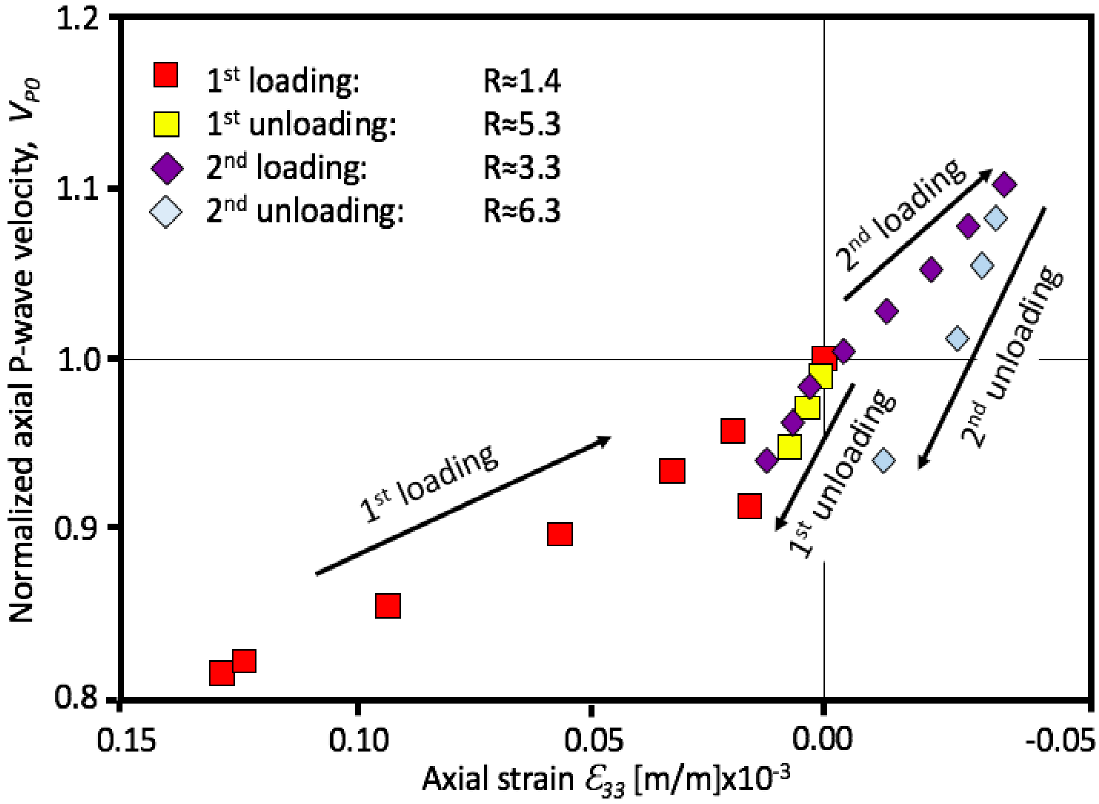

Figure 2-9 *Vertical velocity as function of vertical strain experiment during loading and unloading of an artificial claystone sample (Holt et al., 2008 in Herwenger & Koutsabeloulis, 2011).*

The R-factor approach attempts to fit the observed nonlinear stress-velocity response with a linear model, which is like other typical rock physics models. This also means that, the R-factor approached also has limited in its applicability as in rock physics model (e.g. Verdon, 2012). Furthermore, the model only taken account the response of vertical P-wave towards vertical strain (Verdon, 2012). Based on more details observations, the horizontal deformation also influence the vertical P-wave velocity, although this effects is considered as a second order effect (Verdon, 2012). Essentially, the seismic waves do not only travel vertically, but also shows a range of inclinations about the subvertical during seismic reflection acquisition. Therefore, the R-factor approach could be less efficient when involving wider offset-arrivals distance (e.g. Herwanger, 2007; Verdon, 2012).

2.5 FLUID FLOW AND SUBSTITUTION

The previous section has described the impact of stress changes on seismic properties. However, the key reason why industry conducts time-lapse seismic is to understand fluid flow in the subsurface and identify upswept hydrocarbons. The most commonly used method to estimate the impact of changes in phase saturation on seismic properties is by using a method called fluid substitution first developed by Gassmann (1951).

The Gassmann's model is widely used in petroleum rock physics and usually being used to simulate fluid substitution within rocks with spherical and interconnected pores at low frequencies (Misaghi *et al.*, 2010). Gassmann's formulation is straightforward and require simple input parameters (e.g. bulk modulus) which usually can be directly measured (in the lab) or assumed. This is among the main reasons that makes its widely applied in reservoir simulation exercises (Han & Batzle, 2004; Abe *et al.,* 2018) .

Gassmann's theory successfully assess the effects of fluid substitution towards seismic velocities for both isotropic and anisotropic media (Brown & Korringa, 1975) at lower than 1000Hz frequencies of seismic data. The pore pressure response during seismic wave passes through a rock can equilibrate in which case the following formula from Gassmann and also can be used to calculate the bulk modulus of the rock:

$$K_{SAT} = K_{DRY} + \frac{\left(1 - \frac{K_{DRY}}{K_M}\right)2}{\frac{\emptyset}{K_{FL}} + \frac{1 - \emptyset}{K_M} - \frac{K_{DRY}}{K_M^2}}$$

Equation 2-6

where K_{SAT} is bulk modulus for saturated rock and K_{DRY} is bulk modulus for dry rocks, K_{FL} is fluid bulk modulus, K_M represent mineral modulus, and φ is porosity. Compressional of P-wave velocity (V_P,) for saturated rock is influenced by changes in three properties bulk modulus ($K = K_{SAT}$), shear modulus, μ, and bulk density, ρ. In particular, this relationship could be describe as follow:

$$V_P = \sqrt{\frac{K + \frac{4}{3}\mu}{\rho}}$$

Equation 2-7

Appearance of fluid did not give any significant effect on the shear wave velocity or S-wave (V_S) as a results that fluids cannot sustain shear. S-wave velocity (Vs) can be expressed as follow:

$$V_S = \sqrt{\frac{\mu}{\rho}}$$

Equation 2-8

where μ is equivalent to μ_{DRY} which is shear modulus for dry rock. Shear and bulk moduli at of the rock at initial condition can be calculated by using data that acquired from well log (He, 2016). But care needs to be taken because the measurements are taken at different frequencies and the well log data will need to be upscaled so that it is representative of what will be sampled by seismic waves.

Another widely used fluid substitution model is a model developed by Brown and Korringa (1975), which basically an extended formulation of the Gassmann's equation (Wollner & Mavco, 2017). Unlike Gassmann equation, Brown and Korringa equations allow for randomly mixed mineralogy with interconnected pores (Mavko & Mukerji, 2013; Saxena *et al.,* 2015). Brown and Korringa equations require to replace the mineral bulk modulus with two less intuitive constants, which usually are unknown. Even though virtually all rocks are considered as heterogenous and more closely represented by Brown and Korringa's equation, it is difficult to determine constant that require by this equation. As a results, this practical difficulties makes this equation seldom used in many simulation approach (Mavko & Mukerji, 2013; Saxena *et al.,* 2015).

2.6 SEISMIC FORWARD MODELING

Seismic forward modelling by using ray-based approaches simply can be defined as a seismic forward realization of a given geological model, which describes the forward process of propagating waves from sources to scatters down in the subsurface and back to the receivers. Forward modelling is a useful prediction of the real behaviour of the subsurface even though it typically simplifies the structure and dynamic behaviour of the real subsurface (e.g. Kerebes, 2004; Mondal *et al.,* 2020). The output from forward modelling such as synthetic seismograms gives an opportunity to assess the robustness of the seismic response under controlled conditions. Moreover, this also allow more control on linking specific properties such as the change of velocity/reflectivity towards subsurface conditions (He, 2016).

Seismic forward modelling is also considered a good method to produces seismic realizations of a given geological model (Carcione *et al.,* 2002; Fagin, 1991; Krebes, 2004; Sayers & Chopra, 2009; He, 2015), and is useful for understanding complex imaging problems, for processing and algorithm testing, therefore important role to solve forward and inverse problems (Sayers, 2009). The output from the modelling can be used to validate the geological model by comparing the synthetic data with the field data (Anderson & Cardimona, 2002; Sayers & Chopra, 2009; Alaei, 2012; Phadke & Ramanjulu, 2012). Moreover, the modelling could aid understanding the link between geomechanical process and seismic observation that involving stress-induced seismic attributes (Herwanger & Koutsabeloulis, 2011).

The ray tracing method was the earliest numerical approach to produce seismic synthetics. Nowadays, this approach still be the most common approach being used specially for seismic and algorithms studies (He, 2017). This ray-based methods tracking the ray paths that passes through an elastic model that is built up by smoothly varying velocities and horizons or reflecting interfaces. The ray theory in this approach is based on an asymptotic solution, which allow to models the ray paths of transported energy during transmission and reflection in elastic model. One of the advantage of using ray-based methods is, it allow a simple physical observation in the wave propagations since it modelled only the primary first arrivals (e.g., Cerveny & Hron, 1980) which is one of the advantages over full-waveform simulation. For the numerical solutions in the ray equation, there are two main approach can be considered. The first one is a finite-difference solution (e.g., Noble *et al.,* 2014) which capable to produce fast algorithm to produce travel-times. While the second one is using Hamiltonian method or also known as method of characteristic to solve the ray equation.

Ray-based methods are widely used in many seismic numerical modelling related studies. This method being used to help seismic interpretation and also to produce velocity model. As the complete wavefield such a full waveform seismic is not taken into account, the ray-based method indicates more simple and efficient approach compared to full waveform solutions, especially when dealing with massive and complex subsurface models. However, this technique also has its limitation and restriction when dealing sharp velocity variation. To perform this technique, it will require an additional smoothing procedure for the velocities and surfaces in the model (e.g., Carcione *et al*., 2002; He 2017) and for certain cases in real field, this smoothed structure did not appear.

2.6.1 Ray-based modelling of Amplitude Versus Offset (AVO)

The AVO (amplitude variation with offset) technique appraises variations in seismic reflection amplitude with changes in distance between shot points and receivers. AVO analysis give better evaluation of reservoir rock properties, including porosity, density, lithology and fluid content (Feng & Bancroft, 2006). AVO analysis allowed execution of seismic data to determine a rock's fluid content, porosity, density, seismic velocity or identify shear wave information as well as fluid indicators (hydrocarbon indications) (Hussein *et al.*, 2020). The analysis is based on the Zoeppritz equations, which is basically the relationship between the reflection coefficient and the angle of incidence (Fawwad *et al.*, 2020). There are numerous expressions for the linear approximation of Zoeppritz's equation, each with different emphasis. Bortfeld (1961) emphasized the fluid and rigidity terms which provided insight when interpreting fluid-substitution problems, Aki and Richard's equation emphasized the contribution of variations in the P- and S- wave velocities and density (Feng & Bancroft, 2006).

Computing an accurate offset-to-angle transform is crucial to predicting subsurface lithology and fluid properties from seismic data. Whereas a conventional normal move out, NMO-based transform is increasingly inaccurate with increasing angles, especially in the presence of anisotropy, a ray-based method allows accurate calculation of angle gathers. It also allows computation of converted wave angle gathers in P-wave times, thereby offering a convenient way to jointly analyse primary and mode-converted reflection responses in AVO=AVA applications. The ray-based approach will in principle places a stronger constraint on model estimation because it accurately models large-angle travel-time. Therefore, the ray-based approach potentially can be used to compute angle gathers effectively from observed seismic data and to match them iteratively with synthetic angle gathers in a multicomponent pre-stack waveform inversion scheme (Mukhopadhyay & Subhashis, 2011).

With the proliferation of professional talks and publications regarding AVO cross-plotting, the technique is widely accepted as an important facet in AVO analysis. AVO cross-plotting can be a diagnostic tool for classifying AVO responses (Foster *et al.*, 1993; Castagna and Swan, 1997; Castagna *et al.*, 1998), and for identifying hydrocarbon deposits when performed correctly (Ross, 1995; Verm and Hilterman, 1995). A priori information is crucial, since it serves as a benchmark between prospect and analogy. The need for seismic cross-plotting arises from the complexities of the subsurface, the non-uniqueness of elastic seismic responses, and the desire to display multiple attributes simultaneously. In general, the primary attributes extracted for AVO analysis are the intercept and the gradient, which are obtained from velocity corrected common depth point, CDP records (Ross, 2000).

2.6.2 Time lapse time shift.

The seismic velocity and thicknesses of formations may be changed as a result of stress and strain redistributed that is associated with petroleum production. These changes often manifest themselves as significant time differences on migrated 4D images (**Figure 2-10**). The results from some recent research provides encouragement that 4D time shifts can be converted to meaningful stress changes and used to constrain the reservoir and geomechanical models (e.g., Avseth *et al.*, 2013; Avseth *et al.*, 2016). Such information is useful in detecting the depleted parts of a reservoir and better anticipate wellbore stability problems or reservoir monitoring purposes (e.g., Staples *et al*., 2006; Hawkins, 2007).

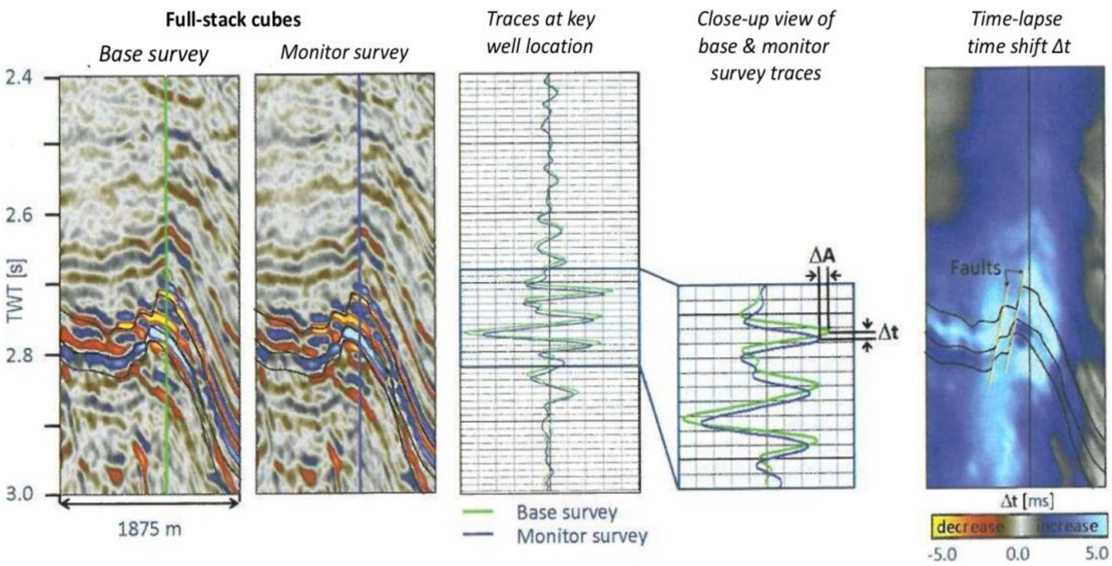

Figure 2-10 *Principles for time-lapse time-shift seismic monitoring (Herwanger & Koutsabeloulis, 2011).*

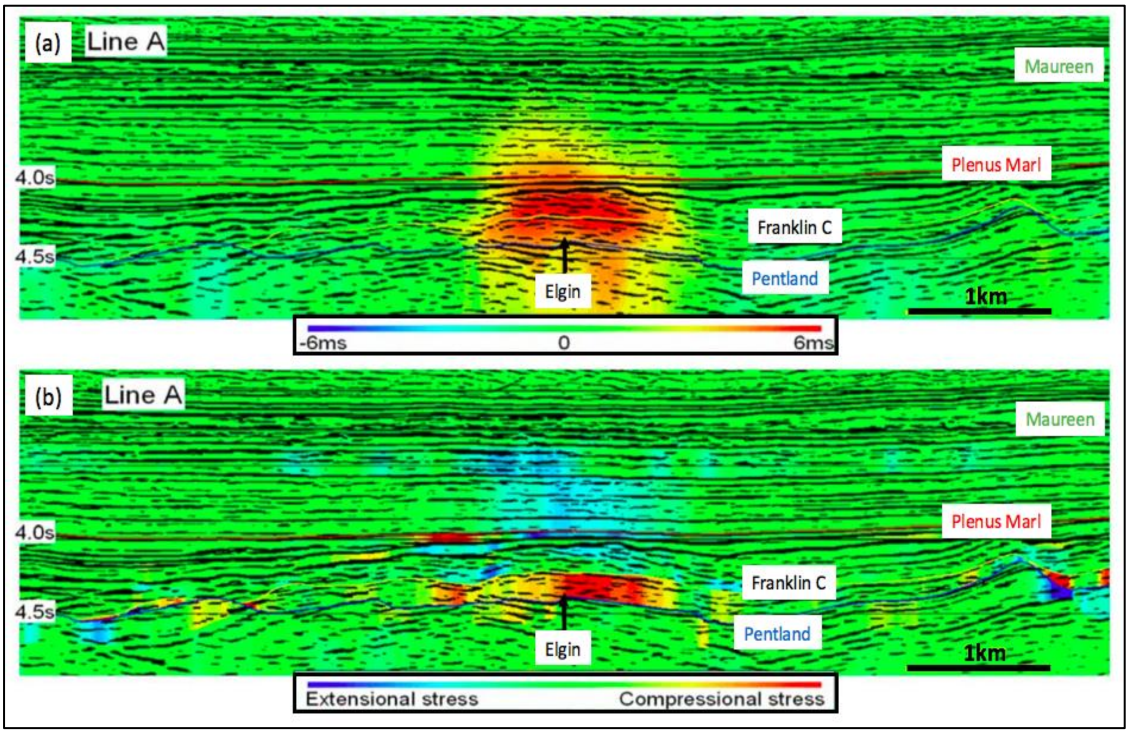

Figure 2-11 *a) 4D time shifts across Elgin. b) Estimated 4D stress across Elgin (Hawkins, 2008).*

The effects of geomechanics on 4D time-shifts have been observed in the Elgin and Franklin HPHT (**Figure 2-11**). Positive time-shifts accrue in the overburden are larger than the negative time-shifts that accrue inside the reservoir (Hatchell, 2006) and this indicates that the sensitivity of seismic waves is larger for rock expansion than for rock compaction. Measurement of overburden time-lapse time-shift can be compared with predicted time-shift from geomechanical model. Differences between observed and predicted data are then used to guide changes in the simulation model until agreement between observation and prediction is reached. Thus, the time-lapse seismic observation serves as an important calibration tool for the geomechanical model (Herwanger & Koutsabeloulis, 2011).

2.7 SUMMARY

Seismic method are widely used to estimate static rock properties and detect changes in fluid saturation during the production of oil and gas reservoirs. From the laboratory measurement until the field seismic survey, the seismic data are useful to predict rock characteristics with the helps from rock physics model. The rock physics model also being used to produce a dynamic reservoir simulator such as coupled fluid-geomechanical in order to mimic and simulate the real reservoir condition. But in certain case, there are misfit between measured and calculated data in the simulator which comes from various factors (discussed earlier in this chapter).

Rock physics model were built to link velocity wave with rock properties such as porosity. There are remain unclear about the major control on velocity-porosity relationship and what cause the scatter in most rock physics model. Intrinsic controls such as porosity, mineralogy, grain alignment, and crack properties may give significant influence towards relationship. Besides that, the other factor that could results scatter or misfit in the rock physics model is oversimplify of crack realization (penny-shaped cracks) in the model. The crack realization is important consideration since implementation of stress in the rock have a significant impact on the opening of closing of micro-cracks (e.g. Zhu & Shao, 2017) which also impacted the seismic properties.

Moreover, the evidence from laboratory experiments also indicates that seismic velocities response are different during loading and unloading at a given effective stress (e.g. Bhuiyan *et al.,* 2013).

Production from hydrocarbon reservoirs causes decline in the pore fluid pressure and increases the effective stress acting on the rock and may introduce compaction (loading). There are variation of wave velocity during loading which can be linked to micromechanical properties such as the presence of cracks, which may close or form a new crack as a result of stress changes (e.g., Ding & Bong, 2016; Mavko *et al*., 1995; Sayers & Kachanov, 1995; Tod, 2002). The stress arching effects in depleted reservoir suggest that the stress not evenly distributed among in the subsurfae, which may cause some of the subsurface such as over- and side-burden could experience unloading. It is possible that cracks behave in a different manner during loading and unloading, which will result in hysteresis in velocity-stress relationships. 4D seismic data from petroleum reservoirs indicates that the sensitivity of wave velocity is higher during unloading than during loading as well as during fluid substitution.

Seismic forward modelling considered a good method to produces seismic realizations and ray-based methods are widely used in many seismic numerical modelling related studies. This method being used to help seismic interpretation and also to produce velocity model. The implementation of time-lapse seismic method has been proven method to serves as an important calibration tool for the geomechanical model. This method also indicates a good potential and capability for investigate the impact of stress and fluid change towards seismic properties.

3 CONTROLS OF ULTRASONIC VELOCITY OF SANDSTONE: IMPLICATIONS FOR THE ESTIMATION OF RESERVOIR PROPERTIES FROM SEISMIC DATA.

Porosity is one of the most important rock properties because it allows the calculation of the volume of present within subsurface reservoirs. Porosity can be measured rapidly and accurately if core material is available. Unfortunately, core is expensive to obtain so it is only possible to obtain accurate porosity measurements from an extremely small proportion of subsurface reservoir which is being characterized. Wire-line logs provide data that allows porosity to be determined within sections of boreholes from which core has not been taken. The accuracy of such measurements depends on the extent that robust and well constrained relationships can be identified between the wire-line log data and accurate measures of porosity obtained from core. Even if wire-line log data provides an accurate measure of porosity it is still the case that boreholes only sample a small proportion of a reservoir. Indeed, drilling wells is extremely expensive and it would be far preferable to be able to estimate subsurface porosity without having to make such large investments as drilling wells, obtaining core and measuring core properties. Significant efforts have therefore been made at developing methods to estimate the porosity of subsurface reservoirs from seismic data. This has the advantage that data can be collected over a large area without the need to drilled expensive wells. An obvious disadvantage is that wave length of controlled source seismic data means that any estimates of porosity will have a low resolution (i.e. the seismic could sample 30 x 30x 30 m blocks).

A key reason for the interest in estimating porosity from seismic data is that laboratory studies (e.g., Wyllie *et al.*, 1958; Raymer *et al.,* 1980; Krief *et al.,* 1990; Rybach & Bunterbarth, 1982) have identified reasonable correlations between porosity and ultrasonic velocities (e.g., porosity with velocity). These empirical relationships are valid only to the particular dataset and may not be valid for other rock types (Garia *et al.,* 2019). The impact of variables such as the type and distribution of minerals, distribution of pores (size and orientation), frameworks grains (size, sorting and packing) and the cementing material on wave velocities is not known to a sufficient extent that wave velocities and their stress dependence can be estimated for the wide range of rock types present within the subsurface (Garia *et al.*, 2019).

Many studies have focused on estimating the porosity of conventional reservoirs from seismic data but have focused on characterizing porosity within unconventional reservoirs such as tight gas sandstones. This chapter attempts to fill this knowledge gap by investigating the possibility of estimating the porosity of tight gas sandstones from seismic data. It attempts to achieve this goal by determining the intrinsic controls on seismic velocity. In particular, it attempts to identify correlations between ultrasonic velocities measured from various rock types with a wide range of other physical properties analyses including microstructural data obtained using SEM and optical microscopy, quantitative mineralogy, porosity & permeability. Although many studies have examined velocity measurements in tight sandstones, little work has been done to the complex relationships between composition, grain arrangement, porosity and pore microstructure in these rocks (Smith *et al.*, 2009).

As well assessing the possibility of estimating porosity from seismic data, another key objective of the research reported in this chapter is to increase understanding of the fundamental controls on the P- and S-wave velocities of sandstones so as to improve the interpretation of stress-dependent velocity data reported in Chapter 4.

3.1 METHODS

3.1.1 Samples analysed

The ultrasonic velocities and petrophysical properties of around 375 sandstone reservoirs core plugs were measured in the laboratory **(Table** 3-1**)**. The sample were categorised based on the age of the sample, which range from Cambrian up to Triassic. Around 70% of the samples were from North Sea, UK, reservoirs with ages ranging from Carboniferous up to Middle Jurassic and maximum burial depths of 2500 to 5100 m. The remaining samples were collected from reservoirs in a range of countries including Australia, Germany, Oman, and Ukraine. Rock samples from Permian (Europe) group are the highest number of samples with 177 while only 3 samples were analysed from the Cretaceous (**Table** 3-1). Wider range of physical properties of the sandstone is beneficial in determining the major factors that control on stress dependence ultrasonic velocities behaviour.

Table 3-1 *Sample rock group details.*

Rock sample group	No. of sample	Depth (m)
Cambrian	58	4339 - 5294
Carboniferous	68	2808-5368
Cretaceous	3	3429-3448
Jurassic	20	3740-6199
Palaeocene	10	3536-3538
Permian (Australia)	15	3938-3963
Permian (Europe)	177	2438-4900
Triassic	15	2551-4324
Late Cambrian-early Ordovician	9	3798

3.1.2 Ultrasonic velocity measurements

Ultrasonic velocity measurements were carried out using the pulse transmission technique (Birch, 1960) with the apparatus shown in **Figure 3-1a**. In general, core plugs that were 1.5-inch diameter and 2-inch long were used for the measurements. These had been cleaned in a Soxhlet extractor using a 50:50 mixture methanol-toluene/dichloromethane and oven dried for at 60°C for 24 hours. The system has a compact design with an internally heated easy loading triaxial cell with acoustic transmission platens and data acquisition electronics. The acoustic system is made of 3 channels (P, S_1, S_2) piezo ceramic stacks integrally built into the axial platens, which can record one compressional (P) and two orthogonally polarized shear waves (S_1 and S_2). Transducers around 1 cm diameter were installed to record all the wave signal. The P-wave velocities are measured at 1 MHz frequency and the S-wave velocity at 0.6 MHz. Standard tests are performed at ambient temperature with an axial stress equal to the confining pressure to ensure good contact with acoustic transducers (incorporated in stainless steel loading platens). The ultrasonic velocity is calculated from the sample length and travel time measured by transducers located at both ends of the cored sample (e.g. Zhong *et al.*, 2014).

The *P*- and *S*-wave sonic transducers were contained within the ends of the platens that were used to apply the axial load to each rock specimen. The ends of each platen were fortified by a 10 mm thick titanium disc. The programmable (compression/tension) testing machine (**Figure 3-1b**) used to apply the axial load has a maximum capacity of 250 kN where in this experiment, the 0-50 kN load range was used. A triaxial cell, of the Hoek-type design (**Figure 3-1c),** was used to apply the confining pressure (maximum 5000 psi) to each plug and includes instrumentation to measure lateral strain. The core plugs were placed in an internal jacket to separate them from the silicon oil that was used as the confining fluid. The jacket is composed of thin Viton rubber, which enables it to conform completely to the plug's shape, even at low confining pressures. The transducers are energized by a bespoke transducer-pulsar unit and the receiver transducer signal is displayed and captured on a high-speed digital PC oscilloscope (**Figure 3-1d**), which allows the sonic signals to be analysed after a test is concluded. The transducers were calibrated using aluminium bars of different lengths before the experiment commenced.

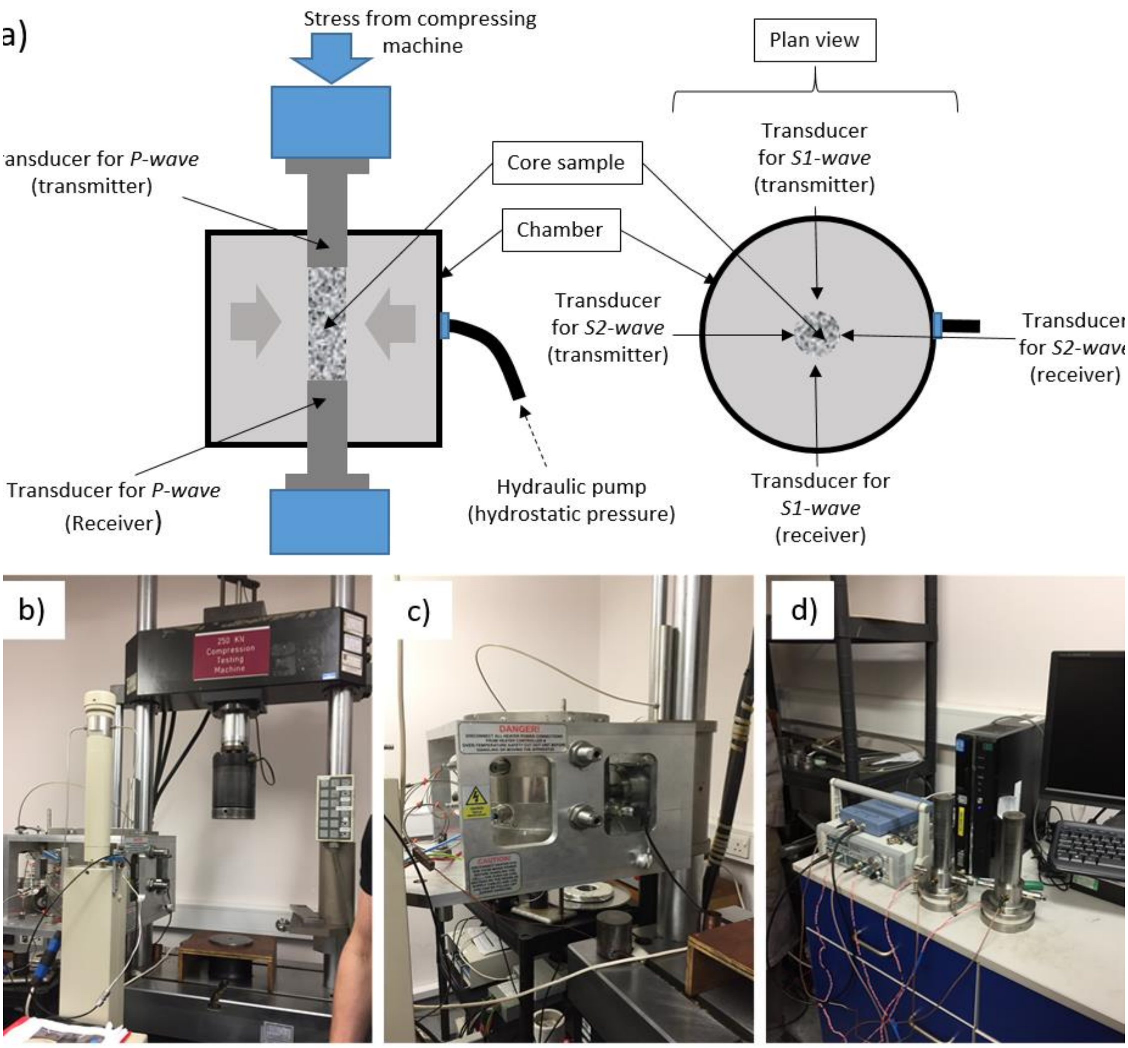

Figure 3-1 *a) Instrumentation arrangement, b) compression testing machine, (c) hydrostatic pressure chamber for tri-axial test, (d) transducer and transducer receiver with oscilloscope.*

Acoustic coupling between the end-platens and the porous rock plugs was facilitated by a thin layer of viscous honey smeared on the platen ends, which were then covered by a 0.1 mm thick disc of lead sheet to prevent contamination of the plug and to enhance the acoustic coupling. The loading frame used to apply the axial load is programmable. The instrument is calibrated annually to UKAS (United Kingdom Accreditation Service) standards. The double lip test sleeves have bonded inserts, at 90 degrees around the circumference, connected to cantilevers to measure radial deflection.

3.1.3 Porosity

A helium gas expansion porosimeter is used to determine the grain volume of the dry samples, which is then combined with the bulk volume to calculate porosity. The porosimeter is first calibrated to obtain the volumes of the reference and sample chambers. A core plug is then placed in the sample chamber and helium gas is allowed to expand into the reference chamber at a predetermined pressure, which is typically around 100 to 200 psig. About 30 seconds is allowed for pressure equilibrium and then the pressure indicated by the transducer digital readout is recorded as the starting pressure. The gas is then allowed to expand into the sample chamber and resulting lower pressure is recorded after the system has reached equilibrium. The grain volume, *GV*, of the sample is calculated using the ideal gas law equation whilst the bulk volume, *BV*, is determined by measuring the sample diameter and length with a calliper. Finally, the porosity, *ø*, is calculated by using equation as follow:

$$\emptyset = \frac{BV - GV}{BV}$$

Equation 3-1

3.1.4 Mineralogy: Quantitative X-Ray Diffraction (QXRD)

The intensity of an X-ray diffraction (XRD) pattern of a randomly orientated mineral is proportion to the amount present within a mixture (e.g., Hardy and Tucker, 1988). XRD has therefore frequently been used to quantify the proportions of minerals present within rocks. To make such analysis it is necessary to construct calibration curves based on the XRD analysis of mixtures containing different proportions of an internal standard such as corundum (Brindley, 1984). Sample preparation is difficult due to the requirement to produce a sample with a random orientation of minerals so previously, QXRD has been regarded as semi-quantitative (Hillier, 1999). A spray-dry technique is now commonly used hat appears to produce samples for XRD analysis without significant preferred orientation, even when they contain significant proportions of clay (Hillier, 1999; 2000). The development of this technique has simplified the sample preparation stage without sacrificing the quality of the analysis and allows truly quantitative analysis to be conducted.

XRD analysis was conducted on samples prepared using the spray dry technique using a Philips PW1050 Goniometer with a Philips PW1730 CuKα X-Ray tube (graphite monochromator). The data was analysed using Hiltonbrooks HBX data acquisition and Diffraction Technology's TRACE software which using the International Centre for Diffraction Data Powder Diffraction Files for the database of phase identification.

The spray dry sample preparation technique involves grinding the sample with a standard (20 wt. % corundum) and then spraying a slurry of the mixture through an air brush into a vertically orientated tube furnace to form ~30 μm wide spherical aggregates with random mineral orientation. The spheres are then top loaded into a specimen holder and then analysed using XRD. The diffraction results obtained are analysed by either reference intensity ratio (RIP) or a Rietvold method to produce mineralogical analyses that are accurate at the 95% confidence level to $\pm X^{0.35}$, where X is the concentration in wt. %. In all cases, the X-ray powder diffraction patterns were recorded from 2-75^{o} 2θ.

3.1.5 Linear and multiple regression analysis: PETMiner

Linear regression is a statistic analysis which is used to establish relationships between dependant and independent variables (e.g Abraham and Ledolter, 2006). A linear relationship is fitted to the data that has a slop and intercept that produce the closest match to the data. In this chapter, linear regression analysis was implemented to investigate the correlation between velocity-porosity relationship and other rock properties such as microstructural, mineralogy and grain size. Previous researchers have also used regression analysis to produce correlation on velocity, porosity and clay content (e.g. Shi & Yang, 2001). Simple linear regression is a function that allows predictions about one variable based on the information that is known about another variable. The independent variable is the parameter that is used to calculate the dependent variable or outcome which can be describe as follow equation:

$$y = \beta_0 + \beta_{1x} + \varepsilon$$

Equation 3-2

β_0 = y-intercept of the regression line
β_1 = the slope
ε = model error

PETMiner software being used to perform the regression analysis in this chapter and chapter 4. PETminer is a visual analysis tools that design for petrophysical properties analysis. Dealing with wide range or huge data analysis able to conducted smoothly as results of capabilities that provided by the software such as:

- PETMiner able to replaces points with images (e.g., Computerized tomography, CT scan or Scanning electron microscope, SEM images) with capability to run on both high-definition and ordinary displays. This makes dealing with huge data or comparative analysis could be carried out easily (Harrison *et al.*, 2017; Harrison *et al.*, 2018; Fisher, 2019).

- Ability to plot multidimensional data with X-Y-Z plots that also able to include another 4th and 5th parameter by varying size and colour of points. This complete visualization could be carried out in a single operation (Harrison *et al.*, 2018; Fisher, 2019).
- PETMiner saves projects it saves the definition of all plots in a visualization, which allows reports to be updated with new data easily. The software system also capable to split plots by attributes (partitioning) and makes any bulk operations on the plots could be proceed smoothly (Harrison *et al.*, 2018; Fisher, 2019).
- Range of fitting functions available which provide more flexible in understanding data correlation. Latest version of this software has data mining or machine learning compatibility and could run decision tree analysis, Neural networks, Naïve Bayes etc. (Fisher, 2019).

PETMiner also has limitation dealing with many data points that may cause clutter and occlusion of the data points (images) if carried out via small display. This could avoided by using bigger display, but it may require additional cost to have such display. However, in practice image data points were only used when plots were segmented by rock type or the source rock samples and this could minimize the potential of clutter problem. The images also could be rescaled interactively in order to get a better view of general images plotting pattern (Harrison *et al.*, 2018).

In the PETMiner software, used to analyse data in this project, the regression analysis allows the reasons for outliers to be determined (i.e. points can be replaced by

CT scans to assess whether fractures are the reason why a sample is an outlier), leading to improved regression equations and more accurate estimations of trends (Harrison *et al.,* 2016). Despite of this improvement, it is rare that a dependent variable is explained by only one variable. In this case, multiple linear regression (MLR) could be used. MLR analysis attempts to explain a dependent variable using more than one independent variable (e.g. Breiman and Friedman, 1997; Al-Mudhafar & Al-Isawi, 2015; Lorenzen, 2018). Multiple regressions are based on the assumption that there is a linear relationship between both the dependent and independent variables. It also assumes no major correlation between the independent variables. The population regression line for p explanatory variables x_1, x_2, ... , x_p is defined to be:

$$Y = \beta_o + \beta_1 xi_1 + \beta_2 xi_2 + \cdots + \beta_p xi_p + \varepsilon$$

Equation 3-3

Y = Dependent or predicted variable
x_i *= Independent variables*
β_o *= Y-intercept*
β_1 *= Regression coefficients*
β_p *= slope coefficient*
ε *=model random error (residual).*

3.2 RESULTS

3.2.1 Ultrasonic: P-wave and S-wave

A summary of *Vp* and *Vs* measured at 5000psi confining pressure for each of the stratigraphic rock types is presented in **Table 3-2.** P-wave velocities vary between 3110 to 5568 m/s with the highest P-wave velocity indicated by the rock sample from Carboniferous (5568 m/s) and the lowest is Permian (Europe) with 3119 m/s. While the porosity and permeability of the samples range from 0.006 to 0.241 and 0.0007 to 24.03mD respectively (**Table 3-3).** Based on routine core analysis (RCA), the Cretaceous have the highest porosity rock sample with average of 0.155 while Permian (Australia) rock samples have the lowest porosity with average of 0.027. In term of permeability, the Permian (Europe) samples have the highest permeability with average of 5.934 mD and the Jurassic samples have the lowest permeability with average of 0.003 mD.

Table 3-2 P- and S- wave velocity at pressure of 5000psi

Sample	P-wave, Vp (m/s) at 5000psi		S-wave, Vs (m/s) at 5000psi	
	Velocity range	Average	Velocity range	Average
Cambrian	4319 - 5236	4850	2687-3426	3096
Carboniferous	3805 - 5568	4621	2485 - 3429	2950
Cretaceous	3528 - 4003	3811	2223 -2531	2413
Jurassic	4089 - 5014	4404	2637 - 3345	2870
Palaeocene	3351 - 4978	3705	2223 - 3121	2405
Permian (Australia)	4554 - 5487	4901	2811 - 3451	3020
Permian (Europe)	3110 - 5286	4307	1987 - 3344	2810
Triassic	4250 - 5400	4803	2825 - 3165	3032
Default	4199 - 5252	4747	2963 - 3370	3151

Table 3-3 Porosity and permeability of rock sample (Routine core analysis)

Sample	Porosity (RCA)	Average	Permeability (RCA)	Average
Cambrian	0.018 – 0.148	0.074	0.011- 24.03	2.118
Carboniferous	0.027 – 0.136	0.066	0.017 - 15	0.964

Cretaceous	0.143 – 0.176	0.155	0.45 – 1.79	1.18
Jurassic	0.0187 – 0.115	0.074	0.001 – 0.006	0.003
Palaeocene	0.047-0.235	0.192	0.004-3.90	1.80
Permian (Australia)	0.006 – 0.071	0.027	0.0007 – 0.021	0.006
Permian (Europe)	0.015 - 0.241	0.1004	0.17 - 239	5.934
Triassic	0.0179 – 0.129	0.077	0.02 – 4.23	0.78
Default	0.016 – 0.091	0.058		

3.2.2 Mineralogy

The mineralogy of the samples is summarised in **Table *3-4*,** which indicates wide variation of mineral percentage among the rock sample. The results also show that quartz and clay (kaolin, illite and chlorite) are volumetrically the most important phases present. The Cambrian samples have the highest quartz content with ranging 76.6 to 94.0% among the sample in this group. The Carboniferous samples have the highest clay content with average of 21.3%. Other minerals present include albite, K-feldspar, calcite, dolomite, mica, illite-smectite, kaolinite, chlorite and clay; the volumes of these minerals present are highly variable. Palaeocene samples have a slightly higher albite content (10.65-26.51%) than the other samples.

Table 3-4 *Range of mineral percentage in 300 rock samples, value in the bracket indicate the average percentage of mineral in particular rock sample.*

Sample	Quartz	Albite	K-feldspar	Calcite	Dolomite	Mica	Illite-smectite	Kaolinite	Chlorite	Total clay
Cambrian	76.6 - 93.9	0 - 1.8	1.1 - 8.9	0	0	0 - 8.5	0 - 5.4	0 - 3	0 - 5.2	4.2 - 14.4
Carboniferous	39 - 90.1	0 - 17.9	0 - 9.1	0 - 23.2	0 - 19.7	0 - 24.7	0 - 21.1	0 - 17.1	0 - 10.1	5.8 - 50.2
Cretaceous	N/A	N/A	N/A	N/A	N/A	N/A	N/A	N/A	N/A	N/A
Jurassic	39.4 - 94.9	0 - 9.0	0 - 10.2	0 - 11.3	0 - 3	0 - 23.5	0 - 13.2	0 - 6.7	0 - 12.4	0 - 46.4
Palaeocene	21.7 - 51.0	10.6 - 26.5	2.8 - 5.9	0 - 0.5	7.6 - 53.2	3.1 - 4.9	2.4 - 12.5	0 - 1.4	0.91 - 3.9	10.9- 17.8
Permian (Australia)	20.2 - 51.8	12.7 - 32.9	0 - 4.6	0 - 22.2	0 - 1.1	2.4 - 9.3	3.8 - 13.8		9.1 - 29.7	19 - 46.2
Permian (Europe)	63.1- 88.6	0 - 9.4	0 - 7.5	0 - 3.6	0 - 21.2	0 - 16.8	0 - 17.5	0 - 13.1	0 - 8.0	1.8 - 27
Triassic	56.0 - 76.4	7.7 - 17.8	0 - 6.5	0 - 5.5	0 - 9.3	3.9- 14.9	0 - 7.6	0 - 1.5	0 - 2.6	9.4 - 15.6
Default	41.2 - 76.3	4.8 - 26.3	2.4 - 13.6		1.7 - 10.6	0 - 22.1	0 - 9.3	0 - 1.5	1.7 - 11.6	1.7 - 37.0

3.2.3 Grain size and microstructure

In addition, grain size of the samples varies from silts to medium grained sands (**Table *3-5***). Fine grained size sands are the most common BSEM images were analyzed to divide the samples into a series of microstructural rock types. Five rock types were identified:-

- **Low clay** – generally quartz cemented sandstone with low (<5%) concentrations of clay (**Figure 3-2**).
- **Pore filling** – contains clays that partially fill pores. Kaolin is one of the main pore filling clays (**Figure 3-3**)

- **Pore-lining clays** – here fine-grained clays coat grains and are particularly effective at blocking pore throats; illite is a particularly common grain-coating clay (**Figure 3-4**)
- **Cemented** – here the pore space between the framework grains has been largely filled by cements such carbonates or sulphates (**Figure 3-5**)
- **Glauconitic** – these sandstones have a large concentration of glauconite pellets (e.g **Figure 3-6**).

The grain-size and rock types of the samples analysed are provided in (**Table *3-5*).**

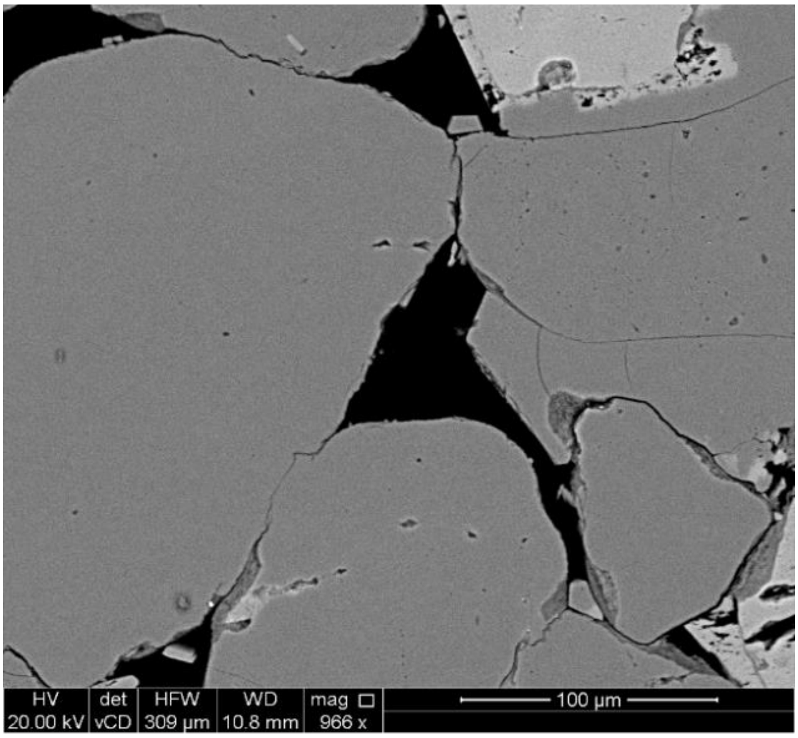

Figure 3-2 *BSEM image showing sample with a very low clay content.*

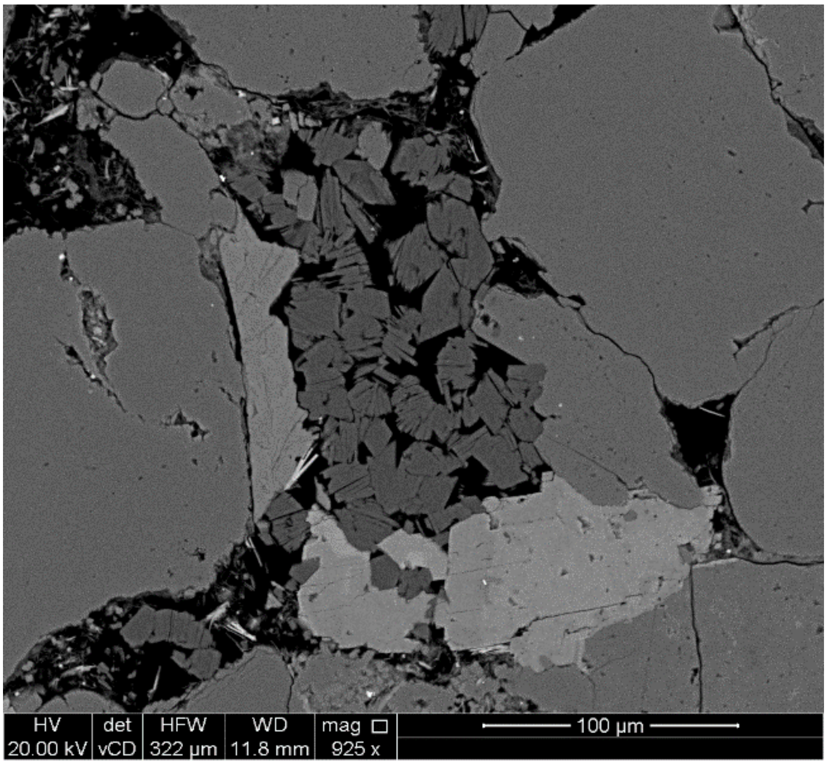

Figure 3-3 *BSEM image of sample with pore filling clays.*

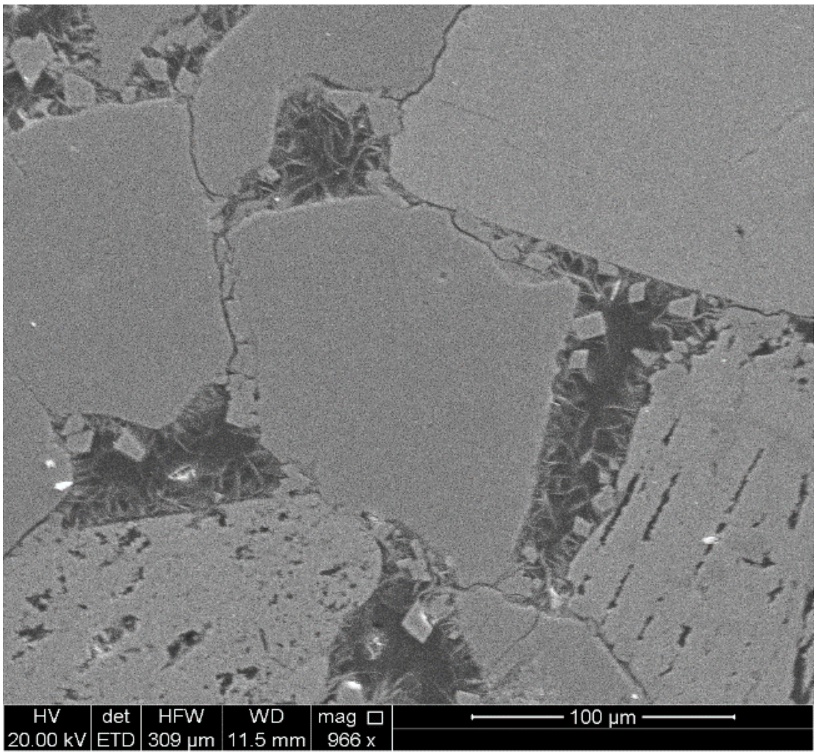

Figure 3-4 *SEM image of sample with pore lining clays.*

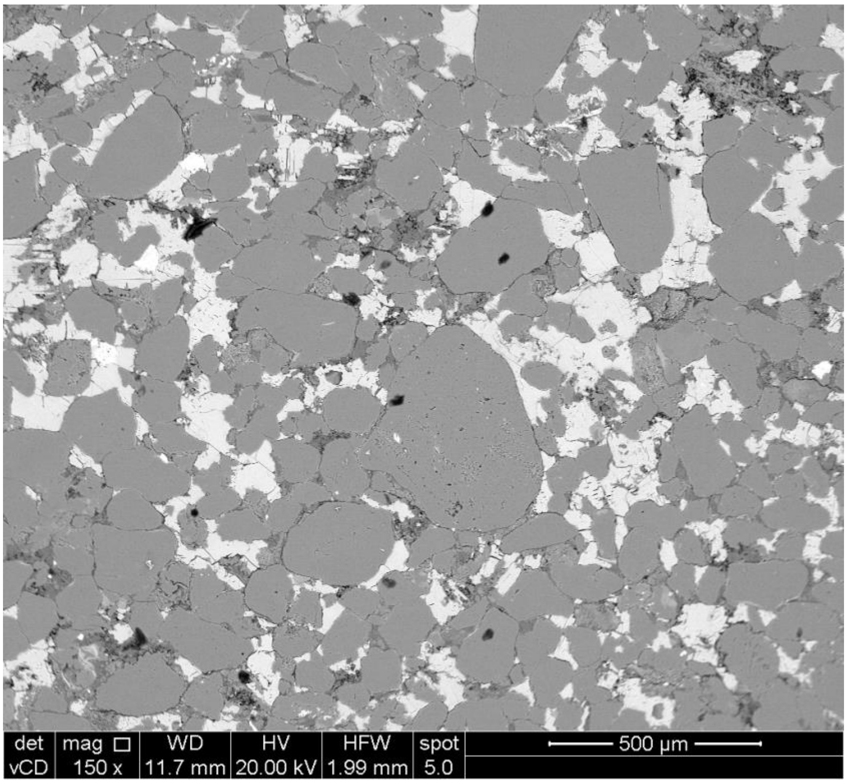

Figure 3-5 *BSEM image which is highly cemented*

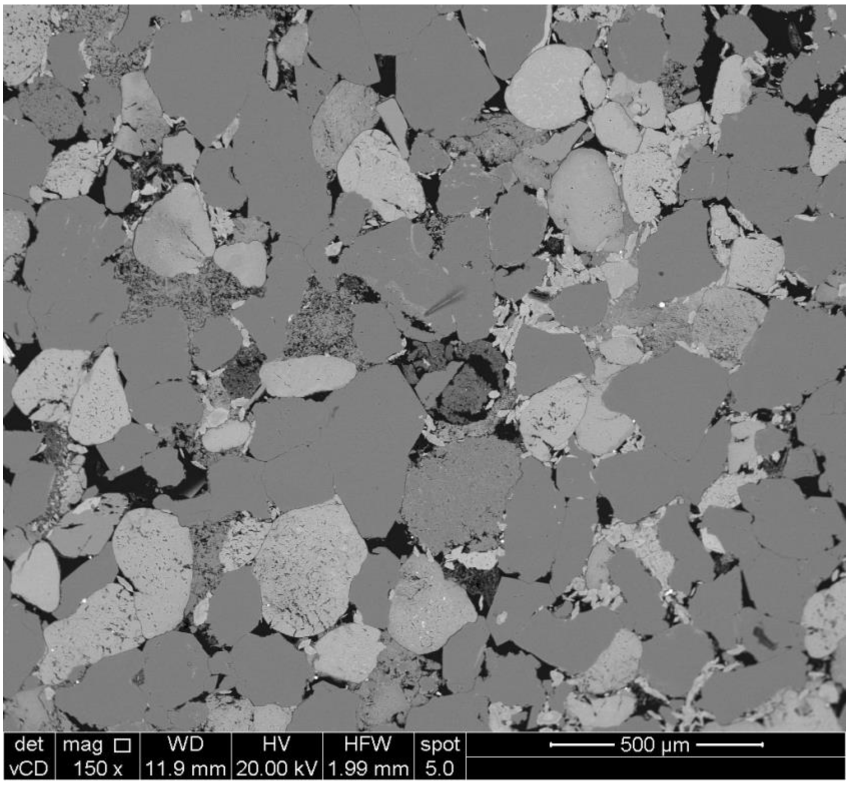

Figure 3-6 *BSEM image of s sample containing large amounts of glauconite.*

Table 3-5 *Grain size and microstructural type.*

Sample group	Grain size	Microstructural rock type
Cambrian	Very fine to medium	Low clay (dominant) and pore filling
Carboniferous	Clay to medium	Grain coating, low clay and pore filling
Cretaceous	Upper fine	Glauconitic
Jurassic	Silt to upper fine	Pore filling (dominant) and low clay
Palaeocene	Lower fine to upper fine	Pore filling (dominant) and cemented
Permian (Australia)	Upper fine to medium	Low clay
Permian (Europe)	Very fine to medium	Grain coating, pore filling, low clay and cemented
Triassic	Very fine to upper fine	Grain coating, pore filling and low clay
Default	Silt to upper fine	Low clay (dominant) and pore filling

3.3 DISCUSSION: CONTROLS ON ULTRASONIC VELOCITIES

Parameters such as density, rock type, shape and grain size, porosity, pore fluid, confining pressure, temperature, bedding planes and joint properties (filling materials, roughness, fluid content, orientation, etc.) has been suggested could influence the ultrasonic wave velocities (Fener, 2011; Chawre, 2018). However, it is unclear how those parameters give significant controls on wave velocity properties. Here, linear regression identifies relationships between ultrasonic velocities and porosity, grain size, mineralogy and microstructural rock type. This kind of analysis is based on the least square curve fitting method, which is also widely used as a statistical procedure for matching a straight line or curve to a set of measurements (e.g., Greenfield & Graham, 1996; Chatterjee & Mukhopadhyay, 2002; Jeng *et al.*, 2004; Yu *et al.*, 2016). The regression analysis also a good indicator of the mutual effects of the different measured parameters upon another (Abd El-Aal *et al.*, 2020), which help in reveal interdepended factor for velocity properties.

The data visualization and mining software PETMiner (Harrison *et al.*, 2018), was used to conduct the regression analyse and identify the key controls on the scatter of data on velocity-porosity plots. The software has an interactive visualization display for analysing the petrophysical properties of core samples, which also able to plot numerical (e.g., petrophysical properties, wave velocity) and image of the data (e.g., CT scans, micrographs, core sample image) simultaneously (Kaminskaite, 2019). For instance, the correlation of velocity and porosity with every single plot shows the CT scan results for each of the sample provides clear visualization to identify general trend on rock physical properties (**Figure 3-7**).

Examination of the CT, SEM images as well as the core plugs identified several samples that were fractured (**Figure 3-8**). It is known that fractures have a significant impact on velocities (Nur, 1971), so these samples were removed from the dataset prior to conducting the regression analysis. The outlier was remained in the plot in **Figure 3-7** to give general overview regarding of the scatter with the data set but did not give any influence towards regression output.

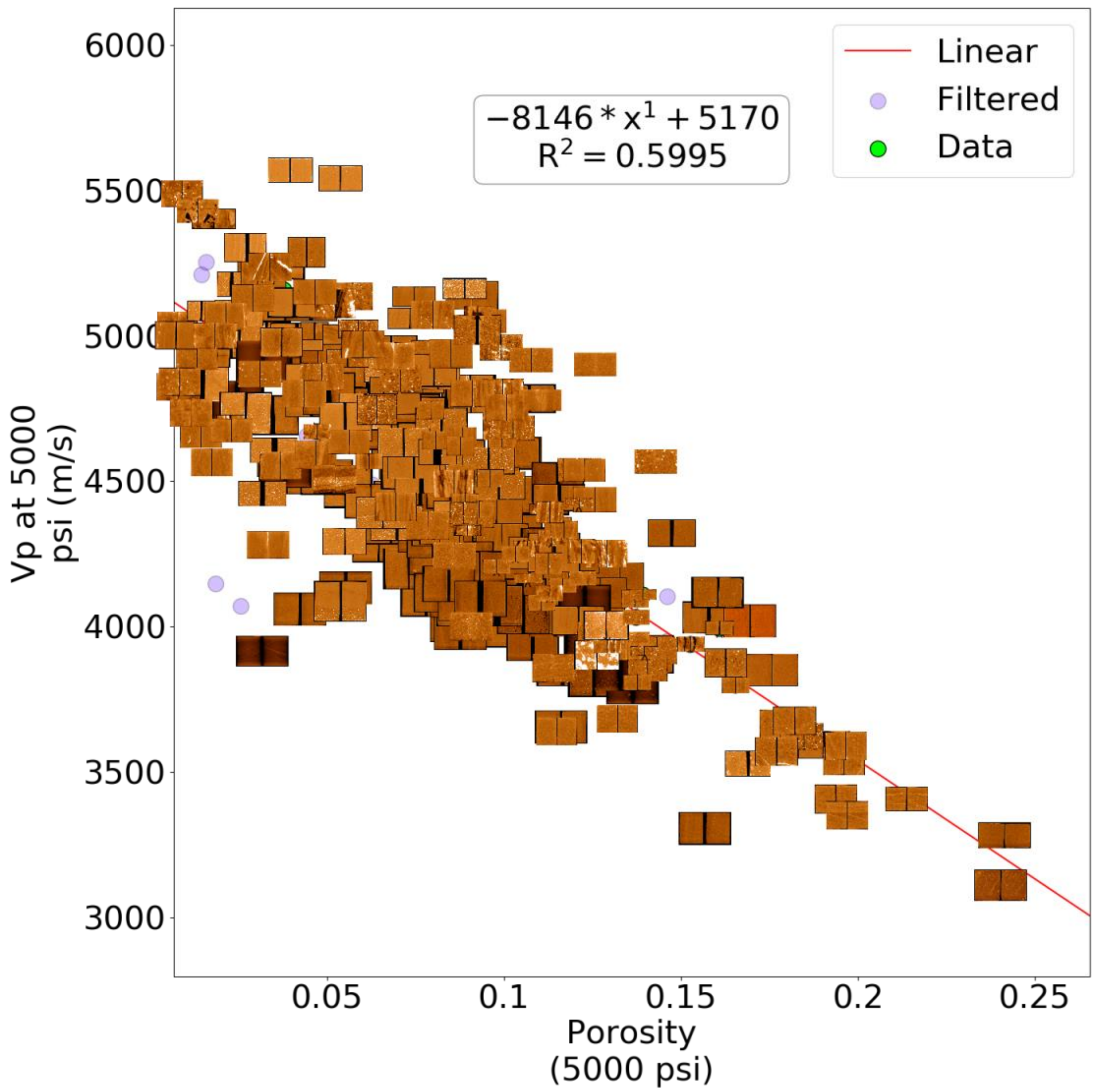

Figure 3-7 *Velocity-porosity relationship with CT scanned photo of general physical properties (crack, laminar or bedding) for each of the sample. There are 13 rock samples were taken out and considered as outlier (blue shade colour).*

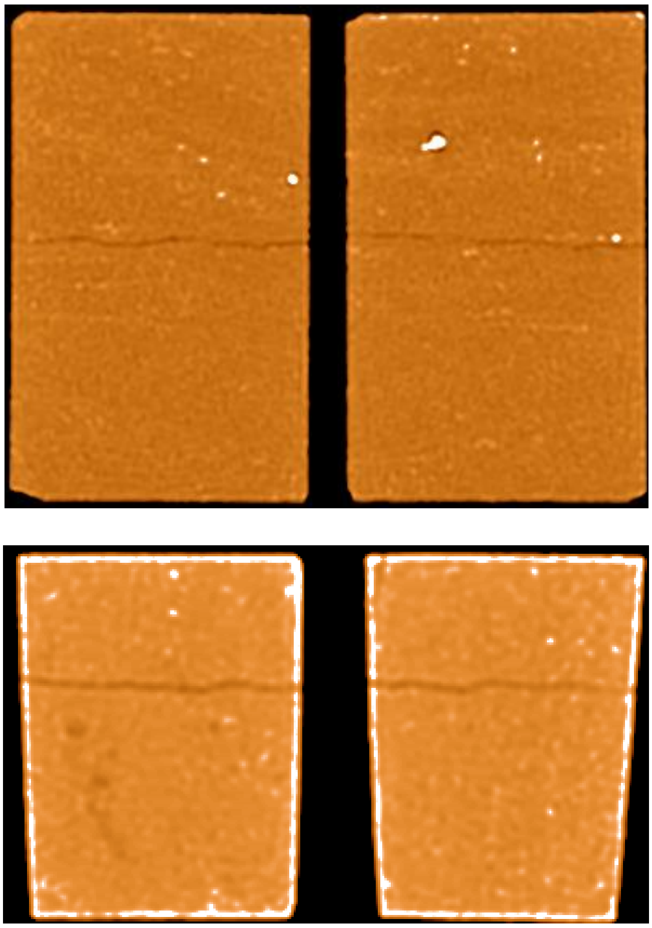

Figure 3-8 *CT scans showing the presence of fractures in a Carboniferous & Middle Jurassic samples.*

3.3.1 Velocity-porosity relationships

The results (**Figure 3-9** & **Figure 3-10**) indicate P and S wave velocity is inversely related to porosity for the wide range type of rock samples analysed (R^2 = 0.60). Such a strong relationship between velocity-porosity also shown previous studies (e.g. Abd El-Aal *et al.*, 2020).

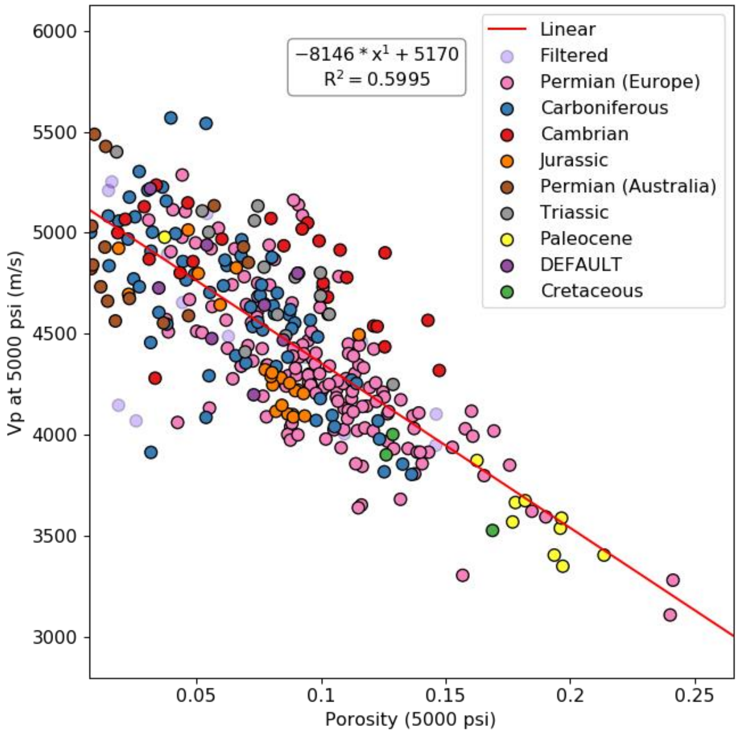

Figure 3-9 *Vp at 5000 psi plotted as a function of porosity with group colour coded. Samples containing fractures have been filtered out (blue) and are not included in the regression.*

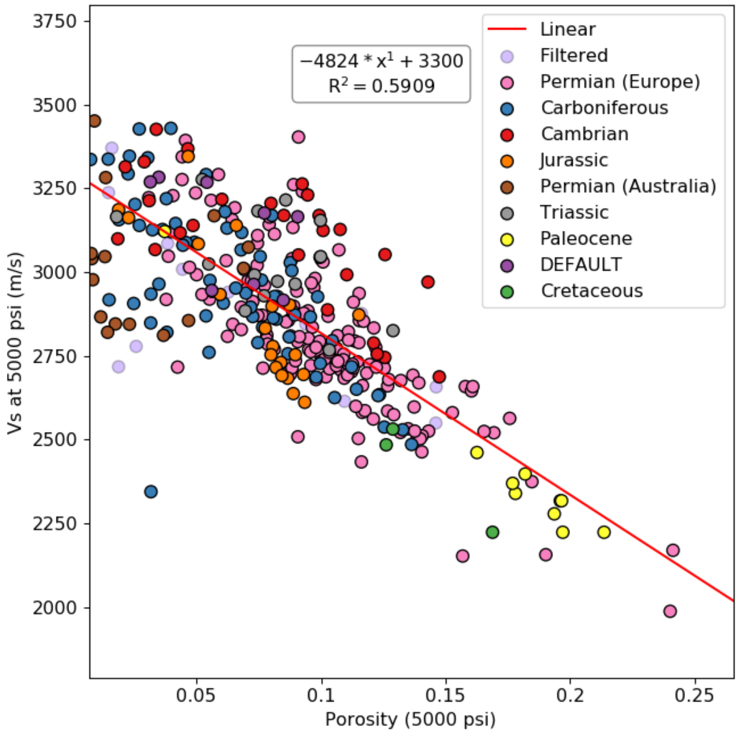

Figure 3-10 *Vs at 5000 psi plotted as a function of porosity with group colour coded. Samples containing fractures have been filtered out (blue) and are not included in the regression.*

3.3.2 Rock physics models for velocity-porosity relationships

A large number of empirical rock physics models have been developed to predict the ultrasonic and seismic velocities of rocks (e.g., Wyllie *et al.*, 1958; Kuster & Toksöz, 1974; O'Connell & Budiansky, 1974; Budiansky & O'Connell, 1976; Raymer *et al.*, 1980; Han, 1986; Krief *et al.*, 1990; Mavko *et al.*, 1998; Katahara, 1999). Each of these models define the rock properties (e.g., pores and matrix) differently and as a result it produces significantly different velocity-porosity relationship (Smith *et al.*, 2009). One of the earliest and most widely used models to describe the relationship between porosity and velocity is the Wyllie time-average equation (Wyllie *et al.*, 1958; & **Equation 3-4)**, which is an empirical relationship that lacks a theoretic foundation. The Wyllie time-average equation, which also most commonly used in wire-line log analysis to calculate porosity.

$$\frac{1}{V_p} = \frac{\emptyset}{V_{Pfl}} + \frac{1-\emptyset}{V_{P0}}$$

Equation 3-4

where V_P, $V_{P\text{-}0}$ and $V_{P\text{-}fl}$ are the P-wave velocities of the saturated rocks, of the minerals within the rock and the pore fluid respectively.

Another commonly used relationship is the Raymer-Hunt-Gardner (Equation **3-5**) relationship (Raymer *et al.*, 1980), which again is an empirical relationship lacking a theoretical foundation.

$$V_P = (1-\emptyset)^2 V_{P0} + \emptyset V_{Pfl}$$

Equation 3-5

Han (1986) developed a with slightly different approach and provided an empirical relationship between velocity, clay content, *C*, and porosity (**Equation 3-6**).

$$V_P = 5410 - 6350\emptyset - 2870C$$

Equation 3-6

According to Habib *et al.* (2016), Han's model does not take into account other fluids, such as oil and/or gas, which could exist in pores. Therefore, the model is unable to invert P-impedance data for rock and fluid properties. Krief *et al.* (1990) introduced a model to overcome this problem by assumingthat the fluid is compressible, with no viscosity, porosity is uniformly distributed and most of the input parameters are similar to the Gassmann/Biot equation (**Equation 3-11**) except there is no requirement to solve for K_{dry}. The relationship of P-wave and S-wave velocity with density and bulk modulus can be expressed in **Equation 3-7** and **Equation 3-10**. The bulk modulus, *K*, is used to calculate porosity (**Equation 3-8** and **Equation 3-11**). The Biot compressibility constant, β_B can be derived from **Equation 3-12**.

$$V_P^2 = \frac{K + \frac{4}{3}\mu}{\rho_b}$$

Equation 3-7

$$K = K_{ma} + (1 - \beta_B) + \beta_B^2 M_B$$

Equation 3-8

$$\mu = \mu_{ma} \times (1 - \beta_B)$$

Equation 3-9

$$K = \rho_B V_p^2 - \rho_B \frac{4}{3} V_s^2$$

Equation 3-10

$$1/_{M_B} = \frac{\beta_B - \emptyset}{K_{ma}} + \frac{\emptyset}{Kf}$$

Equation 3-11

$$1 - \beta_B = (1 - \emptyset)^{3/_{1-\emptyset}}$$

Equation 3-12

Where;

ρ_B = Bulk density

β_B = Biot compressibility constant

K_{ma} = Matrix bulk modulus

Kf = Bulk modulus for fluid

μ_{ma} = Matrix shear modulus

$\emptyset$ = Porosity

M_B = Rock and fluid biot coefficient

Other rock physics models use theoretical mixing laws and bounds to predict the elastic properties. For example, the Voight upper bound (*MV)*, and Reuss lower bound (*MR)* are commonly used to estimate velocities and elastic properties. The Voight-Reuss-Hill, VRH, method (**Equation 3-15)** is used to calculate the elastic modulus of an unsaturated rock (Rosid *et al.*, 2016).

$$M_V = \sum_{i-1}^{N} f_i M_i$$

Equation 3-13

$$\frac{1}{M_R} = \sum_{i-1}^{N} \frac{f_i}{M_i}$$

Equation 3-14

$$M_{VRH} = \frac{M_V + M_R}{2}$$

Equation 3-15

Where:

M_v = Voight elastic modulus
M_R = Reuss elastic modulus
f_i = i^{th} mineral fraction
M_i = i^{th} elastic modulus mineral
M_{VRH} = Voight-Reuss Hill elastic modulus

In the case of a rock, the mineral matrix components are similar enough that a simple Voigt-Reuss-Hill average is sufficiently accurate (Chung and Buessem, 2004). Pores, pore filling fluids, clays and cements must be considered separately as they can significantly change the effective moduli.

The different rock physics models discussed above are compared to the laboratory measurements in **Figure 3-11.** Overall, the RHG model provides a better fit to the data in comparison to the other models. Even though the model is simple and lacks a theoretical foundation it provides a good fit to the velocity-porosity data as indicated with model linear line (green) with the regression line (red) from all the sample.

The Krief and VRH rock physics models tend to slightly overestimate the velocity, but the fit is slightly improved for samples with a porosity >10%. The VRH may provide better approximation for both two-phase composites and polycrystals if the two Hashin-Shtrikman bounds are considered (Watt *et al.,* 1976). The Han equation gives a larger misfit as the porosity increases. Therefore, when used to estimate porosity, the RHG relationship provides are far more accurate prediction than the Wyllie relationship.

The Wyllie relationship severely underestimates the velocities and gives the worst prediction for velocity-porosity relationship compare to other rock physics model. The simple analytical expression in this model should be applied only to fully saturated rocks (Dvorkin & Nur, 1998; Dvorkin *et al.,* 200). Thus, simple approach taken by Wyllie's model is not suitable for a wide variation type of rocks.

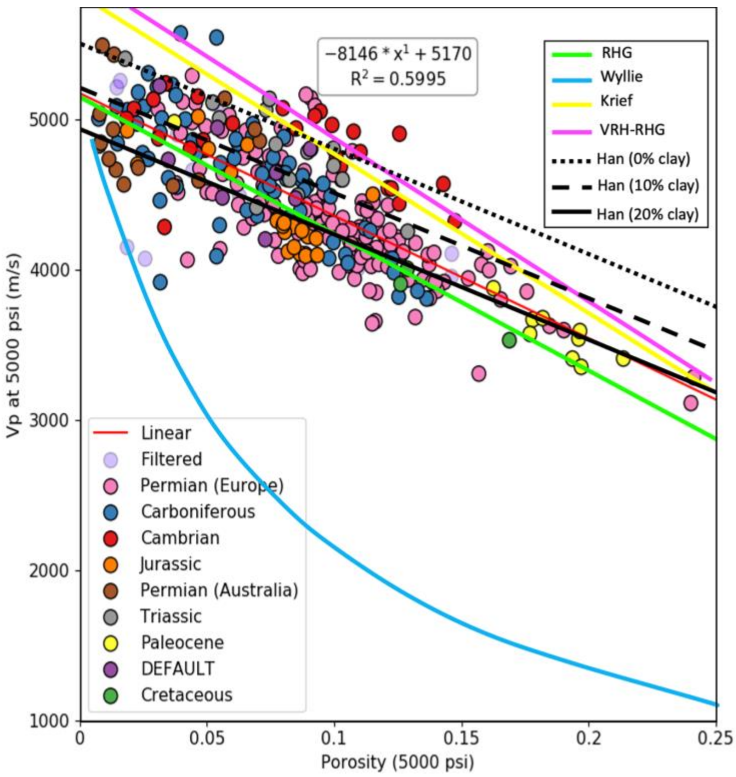

Figure 3-11 *Plot of porosity vs Vp measured at 5000 psi; samples containing fractures have been filtered out (blue) and are not included in the regression. Green line represents Raymer-Hunt-Gardner (RHG), blue line represents Wyllie, yellow line Krief, magenta line represents Voigt-Reus-Hill (VRH) and black line represent Han equation (with different percentage of clay content).*

3.3.3 Correlation of velocity with grain size

Establishment of porosity-velocity relationship could suggest that any parameters associated with porosity (size and shape) could influence velocity. Grain sorting and packing significantly impacts porosity, average number of contacts per grain and percentage of grains contacts (Gaither, 1953). The percentage of contact types is also a function of grain shape. Thus, grain size could be an interdependent factor that influences the velocity.

Grain-size does not appear to influence porosity-velocity relationships (**Figure 3-12** and **Figure 3-13).** Analysis of relationships for individual grain-sizes produces acceptable regression values. For instance, correlation of velocity-porosity among ultrafine sand dominated rock sample shows regression of 0.57 for V_p and 0.54 for V_s

(**Figure 3-14)**. Correlation of velocity and porosity with samples that are dominated by clay sized grains (0.98–3.9 μm) show better R^2 values 0.83 for V_p (0.83) and V_s (0.91) (**Figure 3-15**).

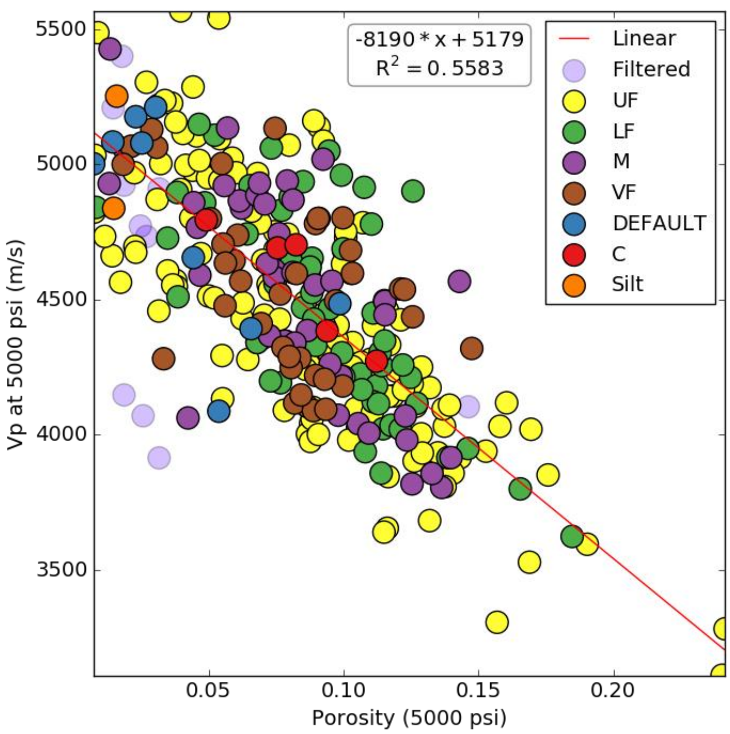

Figure 3-12 *Relationship of P-wave velocity - porosity with colour coded to grain size.*

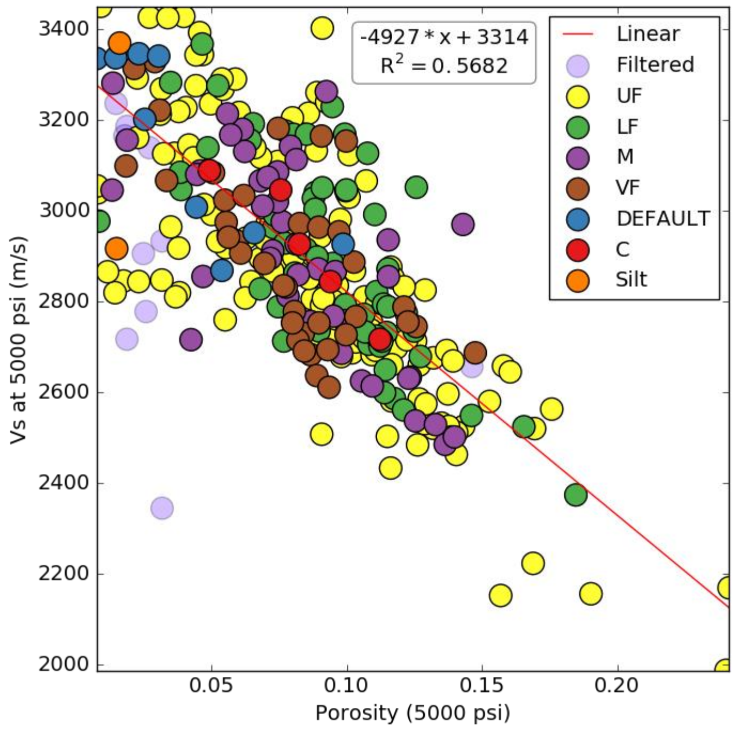

Figure 3-13 *Relationship of S-wave velocity - porosity with colour coded to grain size.*

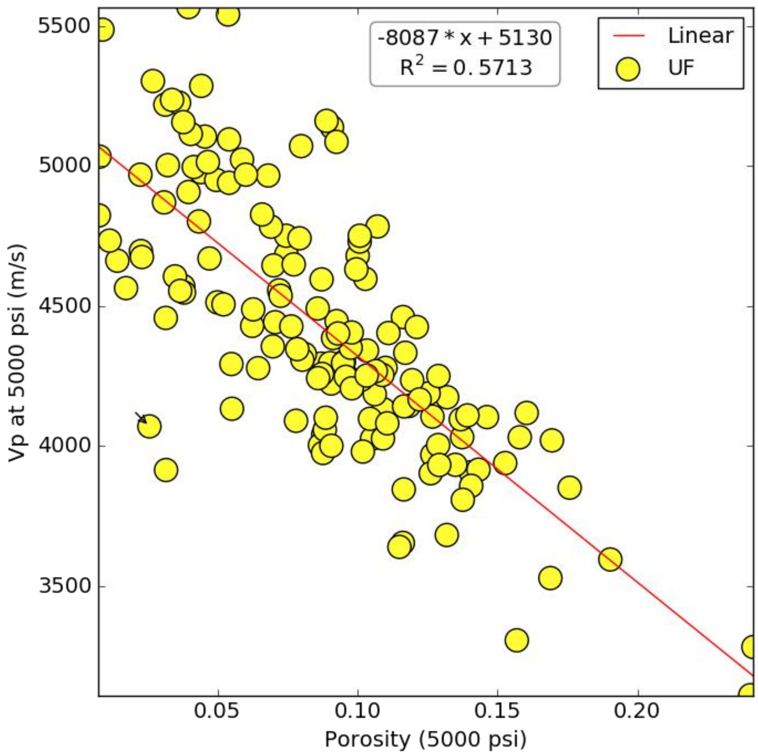

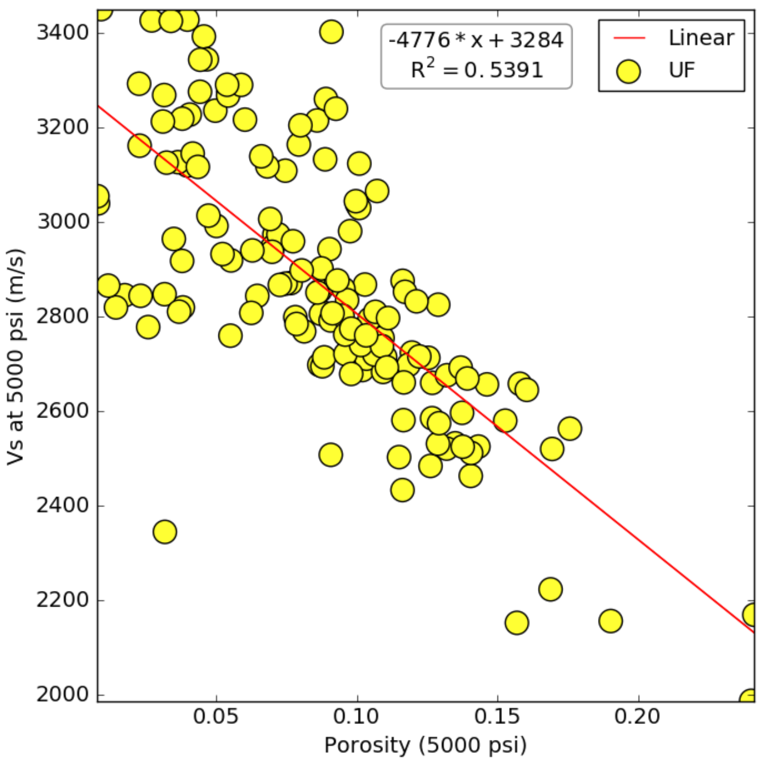

Figure 3-14 *Relationship of V_p and V_s towards porosity with ultrafine grain size dominate rock sample.*

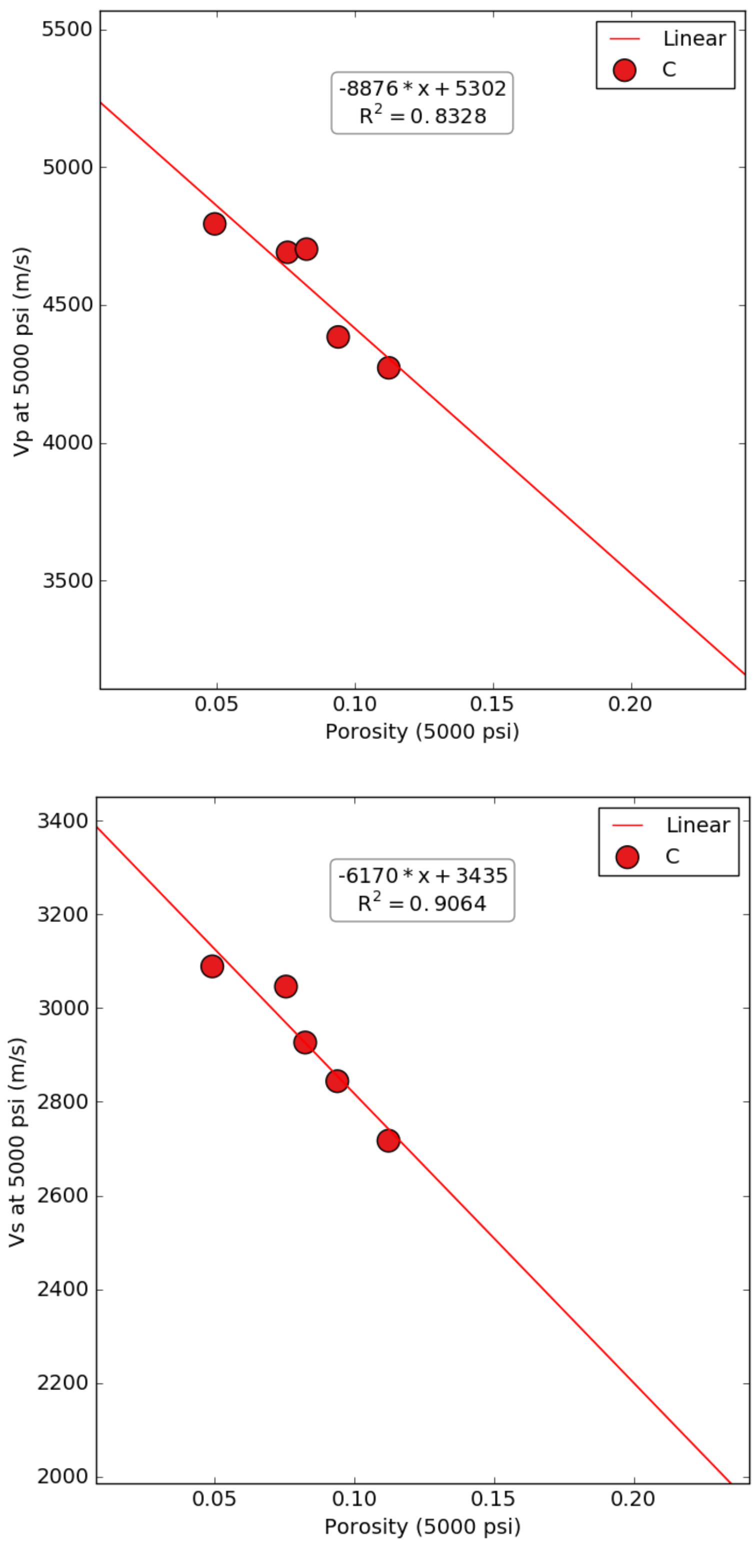

Figure 3-15 *Relationship of V_p and V_s towards porosity with clay grain size dominated rock sample.*

3.3.4 Correlation of wave velocity and mineralogy

There is no clear correlation between wave velocity with mineral abundance in the samples analysed. In particular, regression analysis of velocity versus porosity gave very low R^2 values ranging from 0.01 to 0.058 values (**Figure 3-16)**. The results also colour coded with types of mineral (e.g., quartz, clay, mica, carbonate and albite) and there is no clear indicator towards any of those mineral apearances have direct corelation with velocity-porosity relationship.

Even though the volume of mineral did not give direct correlation with the velocity, experiments conducted by Vernik & Nur (1992) indicate that small amounts of clays will substantially lower velocities. Han (1986) also included clay content in a model to refine the relationship between velocity and porosity (**Equation 3-6**), which could indicate that clay minerals might influence velocity-porosity relationships. **Figure 3-17** shows the plots of velocity against individual mineral volumes of quartz, clay, carbonate and albite; all have poor correlations. Samples with a higher volume of albite, clay and carbonate (**Figure 3-17a**, **Figure 3-17b** and **Figure 3-17d**) tend to have higher velocities. The velocity-porosity relationship shows more scatter in samples containing <10% of clay. This is consistent with increased scatter in the velocity-quartz relationship in samples with a high quartz content(**Figure 3-17**c).

The fact that most clays are not frame-supporting means that they do not play a major role in the transmission of elastic waves. Overall, it is clear that mineral volume are not strongly correlated with velocity even for abundant minerals such quartz and clay.

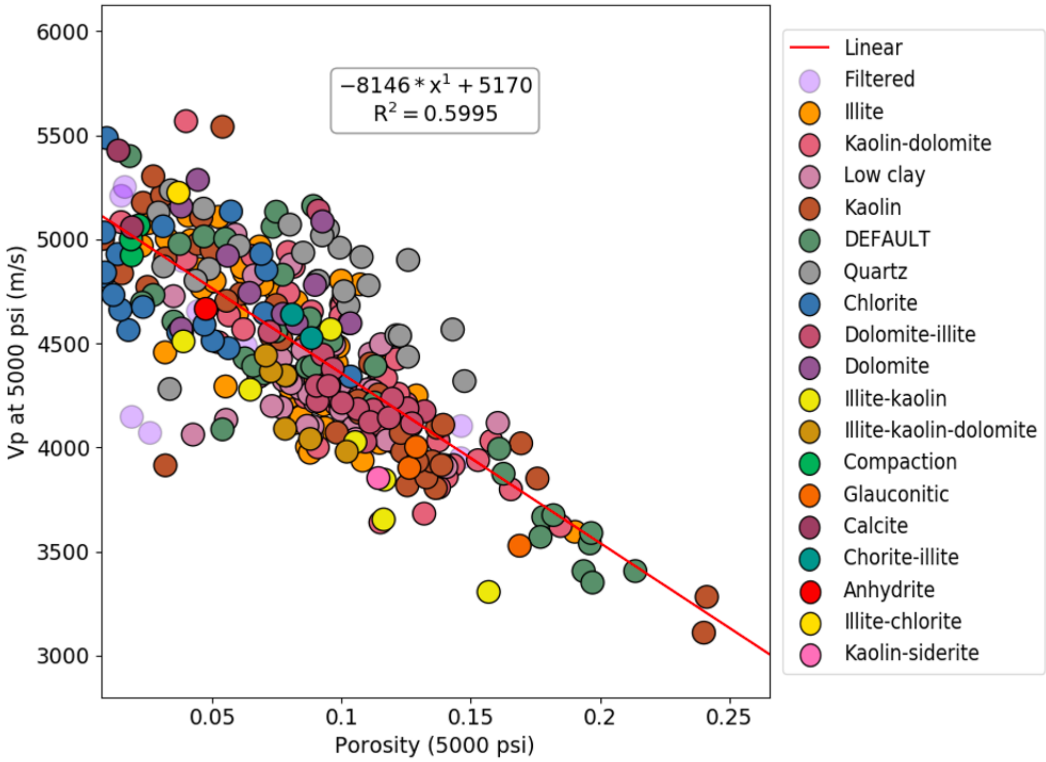

Figure 3-16 *Vp at 5000psi as function of porosity with colour coded of mineralogy.*

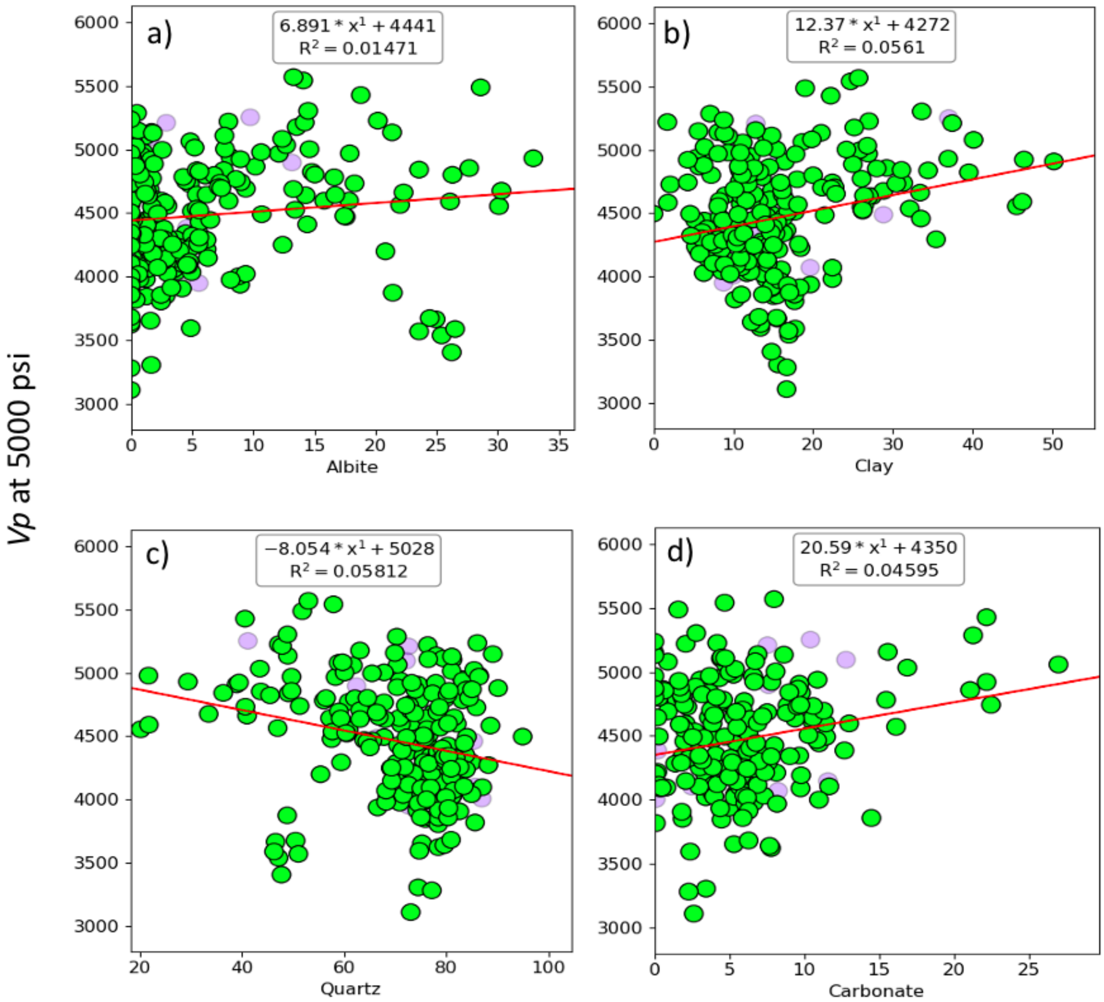

Figure 3-17 *P-wave Velocity as a function of mineral percentage; a) albite, b) clay, c) quartz & d) carbonate.*

3.3.5 Relationship between velocity impedance and porosity

Velocity impedance is the product of bulk density and velocity (Andreassen *et al.*, 2007). In well log data, P-wave impedance contains most of the porosity information (Harris *et al.*, 2009). Indeed, previous research also suggests that seismic impedance from seismic inversion data can be used to locate zones of low and high porosities in reservoirs (Cemen *et al.*, 2014).

Overall, the laboratory measurements show a better relationship between wave impedance and porosity than between velocity and porosity (**Figure 3-18** and **Figure 3-19**). Correlation between *Vp* impedance towards porosity shows R^2 of 0.80 (**Figure

3-18). The correlation of Vs impedance with porosity shows a R2 value of 0.81 (**Figure 3-19**). Vp and Vs impedance shows a reliable correlation with higher porosities whilst give more scatter for lower porosity samples. This also could suggest that seismic impedance might be useful for identifying areas with high porosity. Although, it should be noted that density is closely correlated with porosity, which in effect means that plots of velocity impedance vs. porosity are very similar to plotting the product of velocity and porosity against porosity; this will always provide a better correlation than simply plotting porosity against velocity.

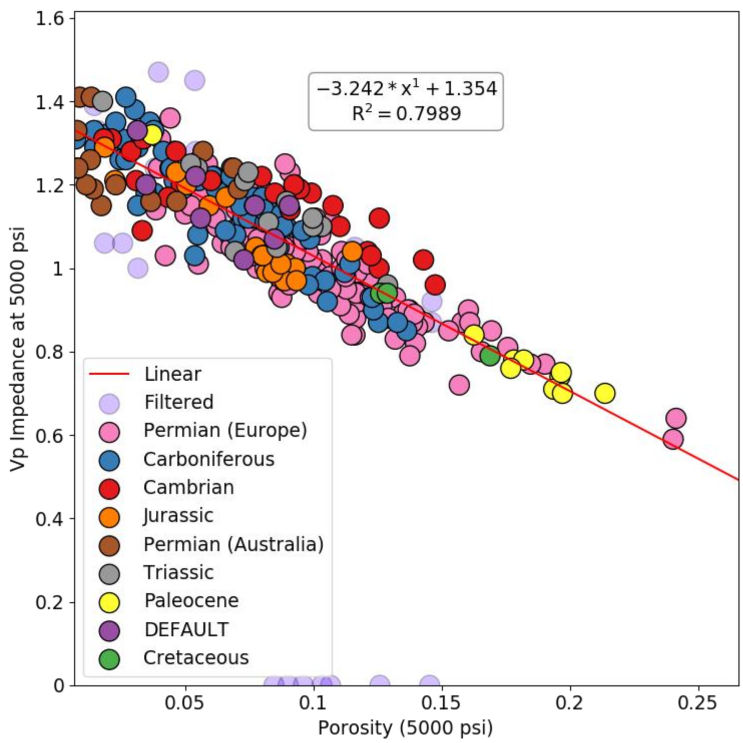

Figure 3-18 *Vp impedance measured at 5000 psi plotted as a function of porosity. Samples containing fractures have been filtered out (blue) and are not included in the regression.*

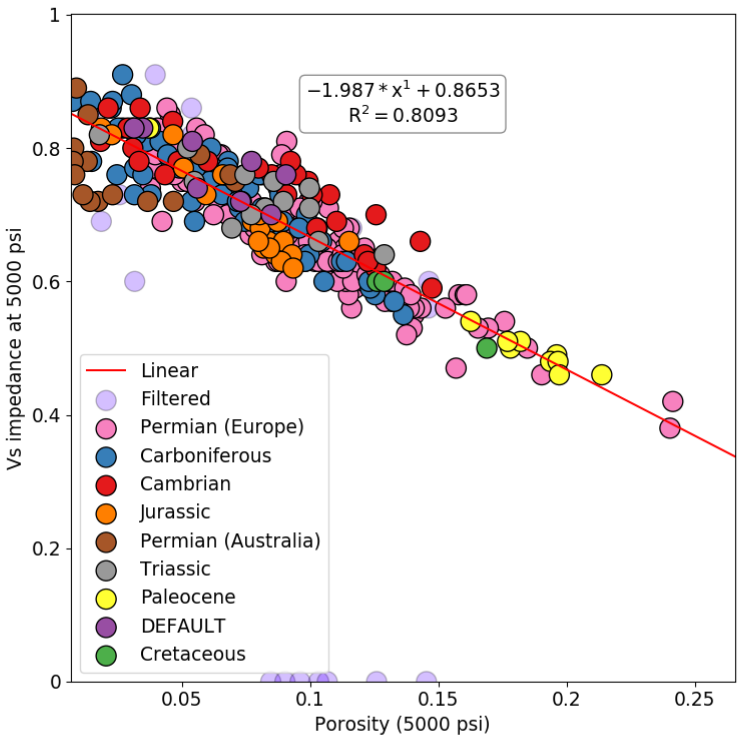

Figure 3-19 *Vs impedance measured at 5000 psi plotted as a function of porosity. Samples containing fractures have been filtered out (blue) and are not included in the regression.*

3.3.6 Velocity impedance-porosity: Grain size, mineralogy and pore size

The relationship between velocity impedance and porosity does not seem to be impacted by grain size. The plot of Vp impedance versus porosity with points coloured according to grain size (**Figure 3-20**) fails to reveal any significant underlying relationships. This is also the case when velocity impedance vs. porosity data are coloured according to their mineralogy. The plot of *Vp* impedance versus porosity with function of selected mineral content in the sample (**Figure 3-21)** shows **an** unclear pattern as a result of the type and volume of mineralogy did not give any significant impact towards the relationship of Vp impedance and porosity. Similarly, correlation with individual type of mineral (albite, clay, quartz & carbonate) (**Figure 3-22**) indicate poor correlation with R2 less than 0.1. While Cemen *et al.* (2014) suggest that the relationship of acoustic impedance-porosity should be used only for thick sandstone (reservoirs). This may conclude that, the usage of velocity impedance-porosity tend to be less efficient when involving clean sandstone or very high clay (shale) of reservoir.

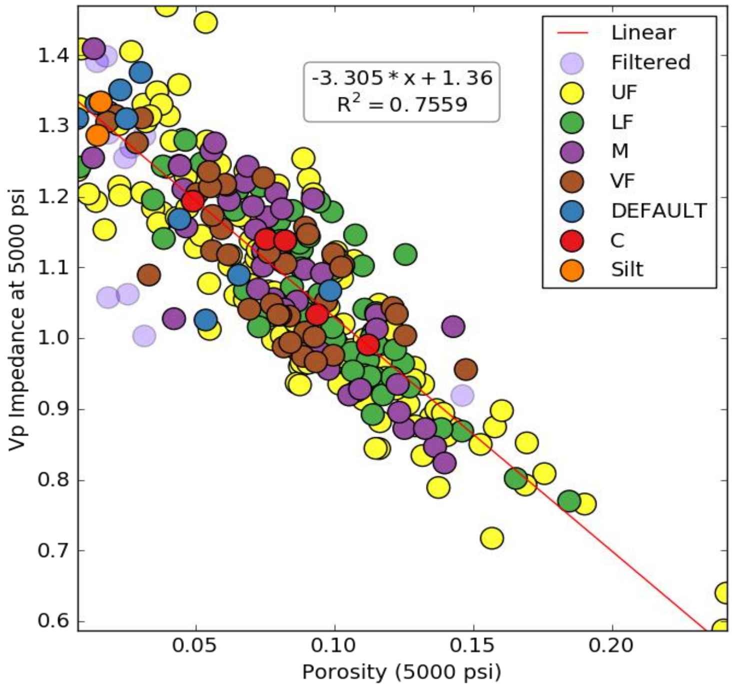

Figure 3-20 *Porosity as function of Vp impedance with the color coded to the grain size (UF: upper fine, LF: Lower fine, VF: very fine, F: Fine, M: medium, C: Clay & Silt)*

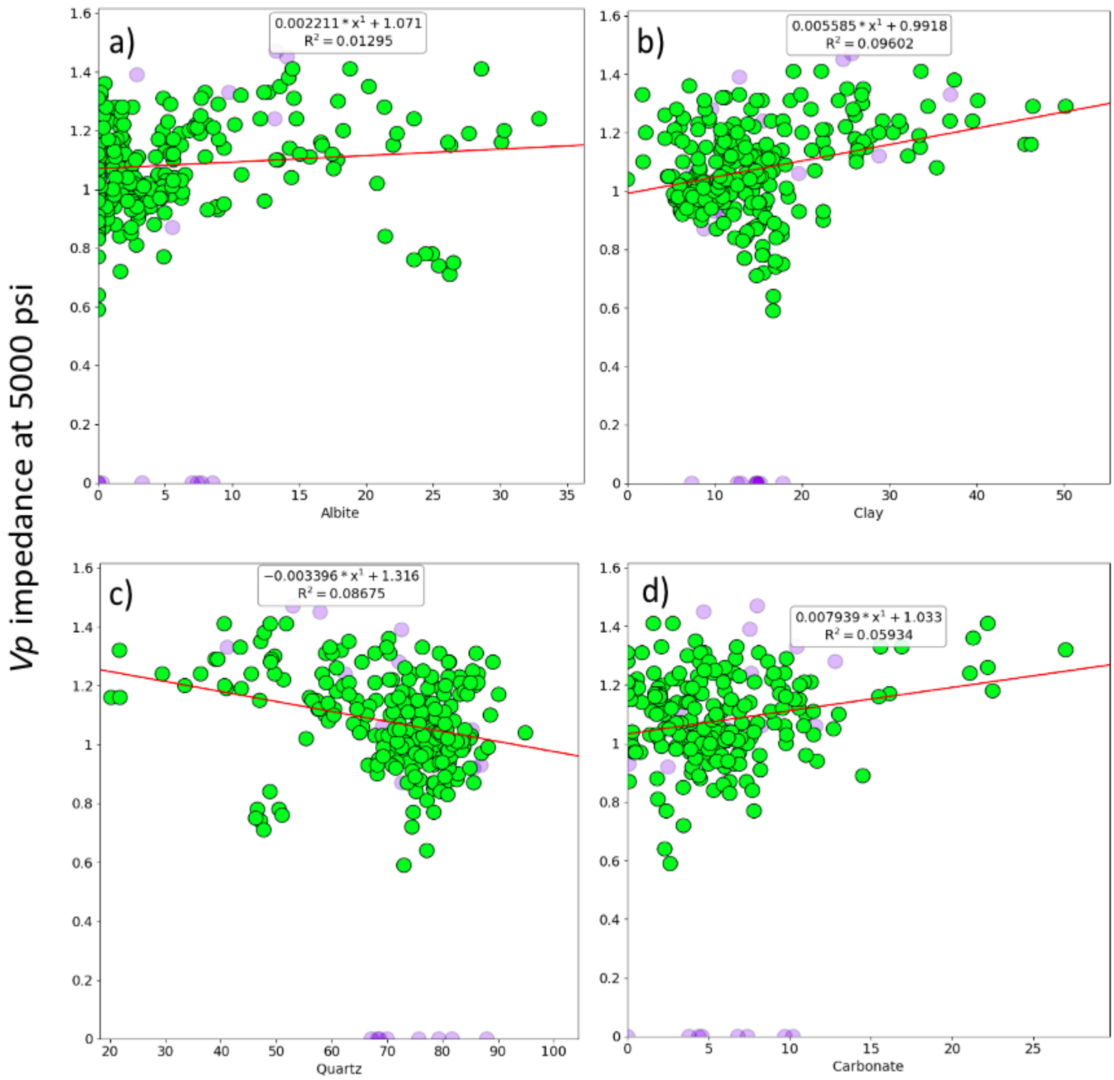

Figure 3-21 *P-wave Velocity as a function of mineral percentage; a) albite, b) clay, c) quartz & d) carbonate.*

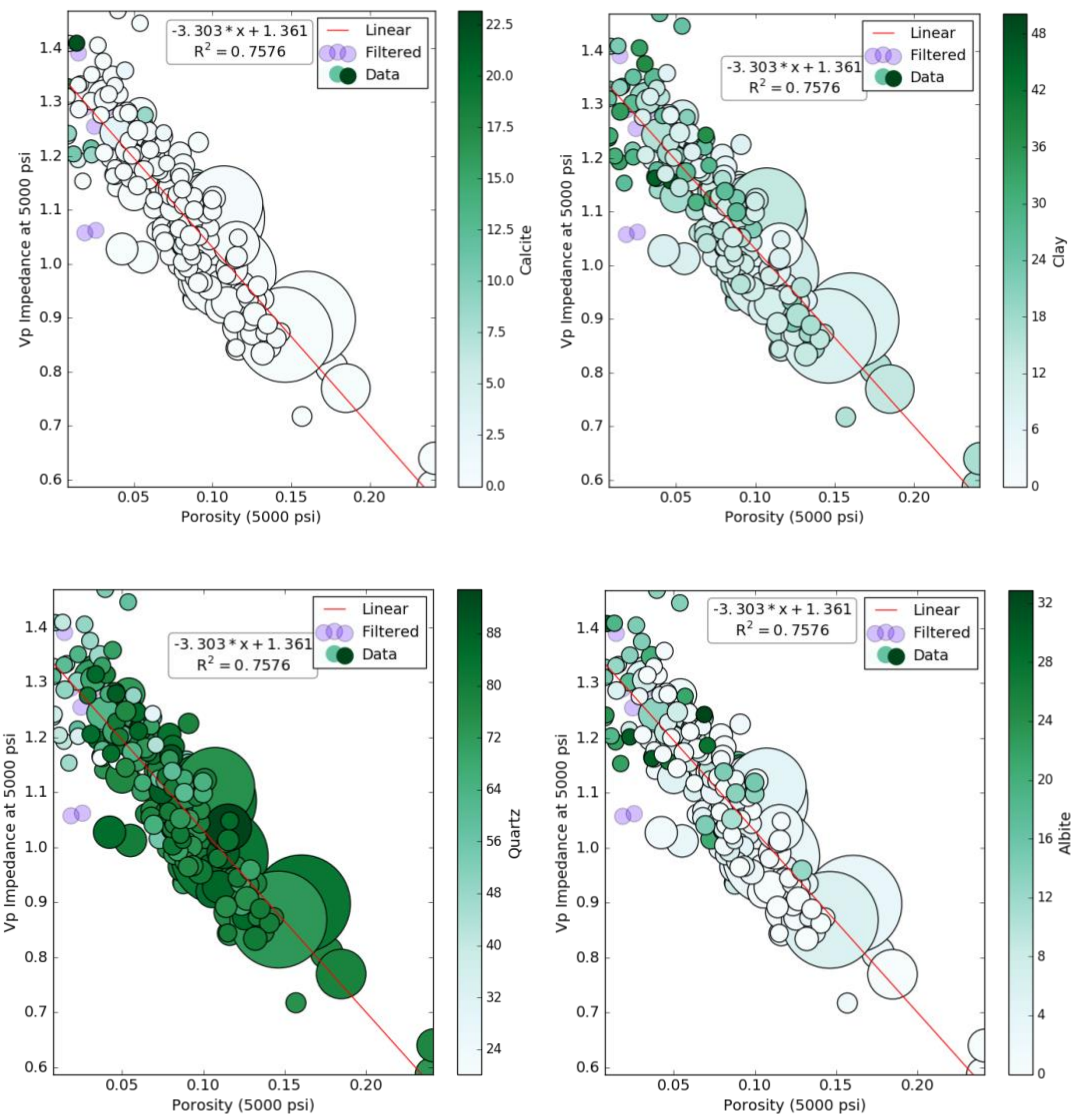

Figure 3-22 *Vp impedance vs porosity with circle size of the diagram represents the peak pore radius of a) calcite, b) clay c) quartz d) albite and the green colour intensity indicate the percentage of those mineral.*

Colouring points according to different properties does no easily explain the cause of scatter seen around the best-fit relationship to the porosity and ultrasonic velocity data obtained using linear regression analysis Multiple linear regression (MLR) analysis was carried out to allow more of a quantitative assessment of causes of scatter. This also allow any mineral among the rock sample were remove in order to improve the regression (predicted). Finally these two regression; measured and predicted were compared to shows the impact of appearances any of these mineral. Any significant improvement in the regression coefficient obtained using MLR analysis could indicate if the mineral could the influence velocity-porosity relationship or not.

The regression model of predicted vs. measured (**Figure 3-23**) shows a correlation coefficient of 0.671 for the entire dataset. Removing anhydrite, siderite, magnesite, barite, microcline and pyrite from the equation almost did not give any significant changes to the coefficient value. This due to the volume of those mineral within the rock sample considerably low. Correlation with all mineral but carbonate (**Figure 3-24**) slightly increased correlation coefficient from 0.671 to 0.676.

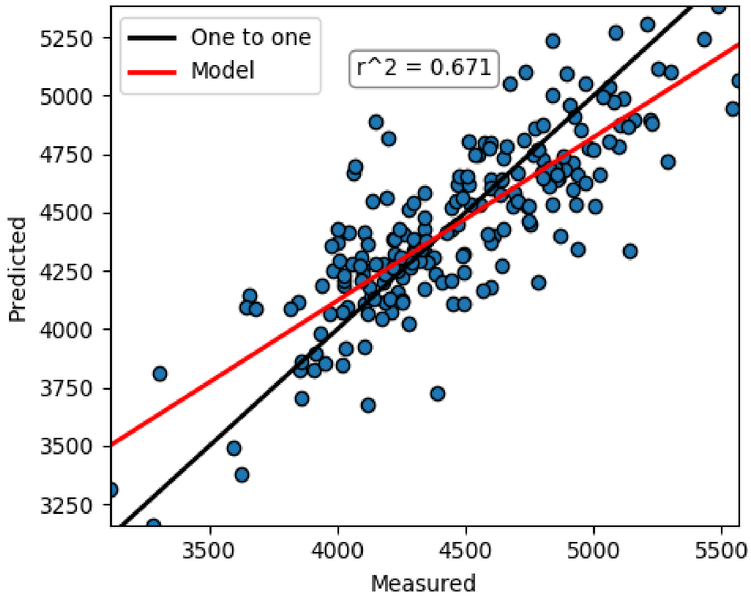

Figure 3-23 *Multiple regression model of predicted and measured relationship of velocity and porosity towards mineralogy.*

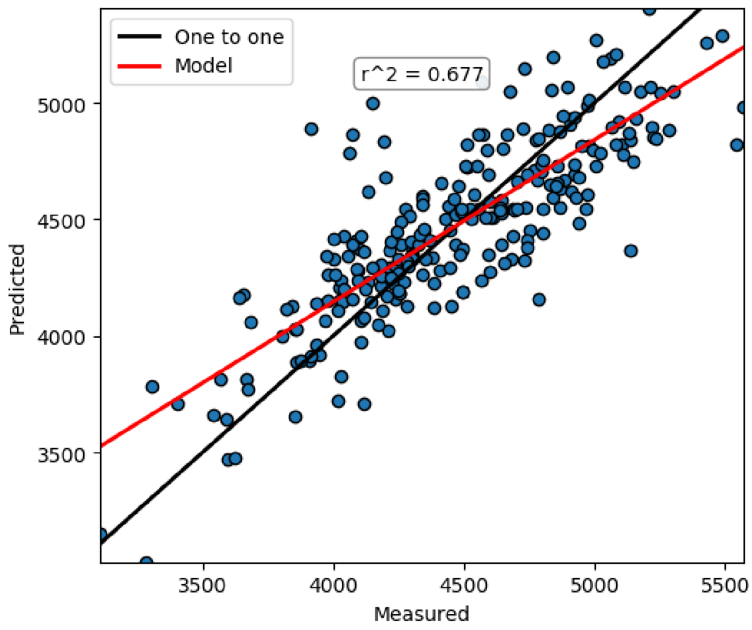

Figure 3-24 *Multiple regression model of predicted and measured relationship of velocity and porosity towards all mineralogy but carbonate.*

Both linear and multiple linear regression (MLR) analysis did not identify any significant improvement in the ability to estimate porosity from velocity by taking into account other minerals present. Improvement by removing carbonate show small improvement (0.006) in the regression analysis, while removing other minerals shows even smaller improvement.

3.3.7 Trend of ultrasonic velocity in low porosity rock

V_p and V_s impedance clearly show a strong negative correlation with porosity. However, this relationship is weaker at porosities below 10% (**Figure 3-25** and **Figure 3-26)**. This information indicates that velocity impedance should be used with great care for identifying sweet spots in low porosity sandstone reservoirs. This also could explain why low porosity reservoir such as tight gas sandstones reservoir (e.g., Swarbrick, 2012) give more challenge in order to predict the rock properties behaviour and indicate how crucial the calibration with local data should be done to get better inverted or predicted data.

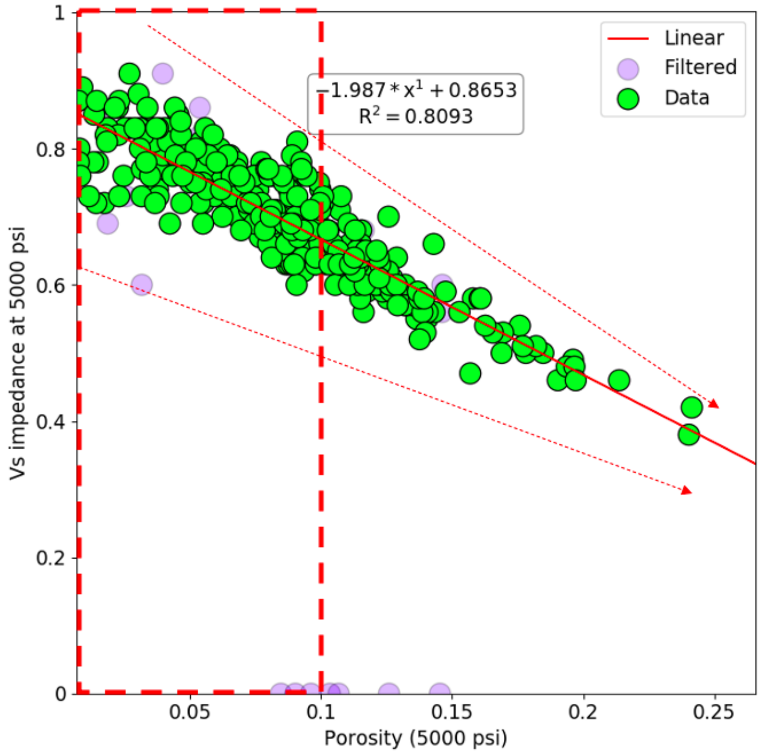

Figure 3-25 *Sensitivity of ultrasonic P-wave velocity impedance towards porosity.*

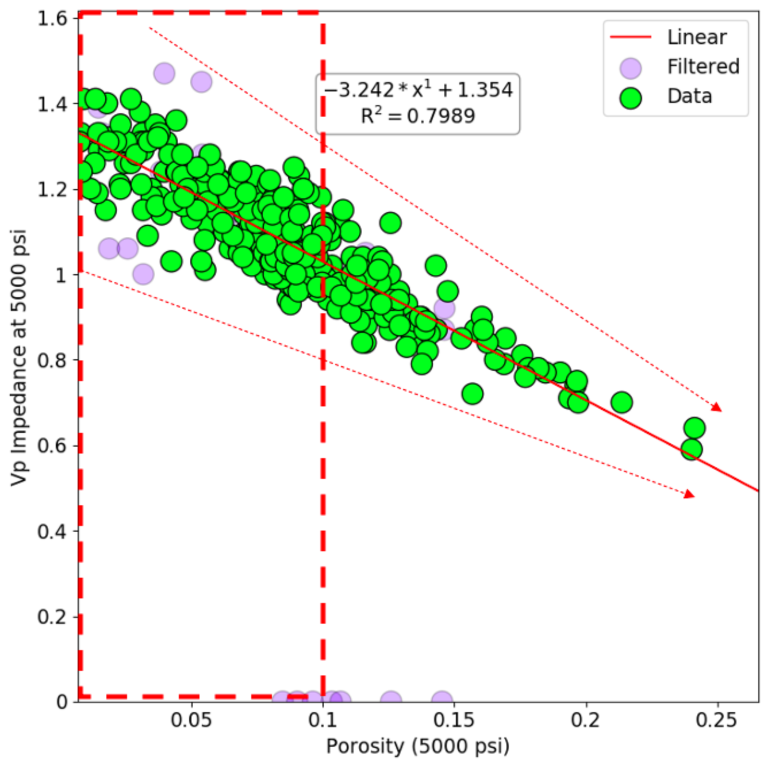

Figure 3-26 *Sensitivity of ultrasonic S-wave velocity impedance towards porosity.*

3.4 CONCLUSION

The ultrasonic velocities of a wide range of tight sandstones have been analysed and the results have been integrated with other properties such as porosity, grain-size and mineralogy. A wide range of standard rock physics models have been tested against the data. The Raymer-Hunt-Garner, RHG, equation produces the best fit to the velocity-porosity data. Other rock physics model (e.g Wyllie, Han, Krieff and VRH) tend to over or underestimate the porosity.

There are no significant improvements when velocity-porosity or velocity impedance-porosity relationship were correlated to mineralogy, grain size or pore radius. Ultrasonic velocities and impedance of sandstones are best correlated with porosity. However, at low porosities considerable errors can arise by estimating porosity from velocities. This also means that surface seismic methods that measure impedance or impedance contrast are a potentially useful tool for identifying porosity-related sweet spots reservoirs, but the data can be misleading indicator of porosity within low porosity (<10%) reservoirs.

4 ROCK PHYSICS INVERSION & CRACK CHARACTERISTIC

4.1 INTRODUCTION

Time lapse (4D) seismic surveys are now used throughout industry in an attempt to monitor fluid saturation changes in the subsurface (Herwenger *et al.,* 2016; Yang *et al.,* 2018; Asaka *et al.,* 2018). However, it is recognized that differences in time lapse surveys may not only be caused by changes in fluid saturation. The specific reasons for the mismatch between measured and predicted values is still poorly understood. Often, the results of forward seismic modelling show misfit when compared to measured seismic properties (e.g., Angus *et al.*, 2015; He *et al*., 2016). One potential reason is that the simulation models don't take into account stress changes.

The introduction of the coupled flow-geomechanical models is becoming an important method to take assess the impact of stress changes on 4D seismic. Coupled flow-geomechanical modelling has proven to produce better predictions of fluid flow and deformation in and around stress sensitive reservoirs (e.g., Heffer *et al.* 1994; Fredrich *et al.* 1996, 1998; Longuemare *et al.,* 2002; Settari *et al.,* 2002; Molenaar *et al*., 2004; Angus *et al*., 2010). The simulations usually rely on rock physics models to estimate the impact of stress on seismic velocity (e.g., Hitlerman, 1970; Anderson *et al*., 1995; Anderson & Cardimona, 2002; Ahmadi *et al*., 2013). Even though coupled flow-geomechanical provides better predictions, they still often do not match 4D seismic (measured and calculated) especially when involving rock in reservoirs that have experienced signficant pressure and stress changes (e.g., Hawkins *et al*., 2007; Herwenger & Koutsabeloulis, 2011).

This chapter attempts to assess whether the discrepancies between modelled and measured 4D seismic could be due to errors or inadequacies in the rock physics models from which the stress dependency of subsurface velocities are predicted. A series of laboratory experiments have been conducted to improve understanding of the stress dependence of seismic properties as well as their dependence on stress path (i.e., loading vs unloading). In addition to the velocity measurements, the microstructure of the samples was recorded using SEM and other basic properties of the samples were determined including mineralogy, porosity and permeability. The velocity-stress data from the laboratory measurements was then inverted by using a stress dependant rock physics models to predict crack properties (aspect ratio and crack density); in this case the microstructure (MST) rock physics model was used. An attempt to determine the controls on the crack properties was then made using data mining techniques (e.g., decision tree analysis). The results from these experiments are then discussed paying particularly emphasis on the differences of in-situ and predicted (model) crack properties.

The implications of the misfit (predicted and measured) and uncertainties from 4D seismic responses from coupled fluid flow-geomechanical models could potentially produce missed judge of the real field condition. This situation also could produce miss interpretation towards the changes and deformation that related to reservoir depletion such as surface subsidence and stress arching in the reservoir. Moreover, underestimate or overestimates the geomechanically related stress change could lead to missed calculated the production rates.

4.1.1 Stress dependant Rock physics model

Elastic wave velocities in sandstone are strongly related with stress under which the measurements are made due to the presence of stress sensitive discontinuities within the rock such as microcrack, fracture and grain boundaries (Sayers, 2010). This relationship indicates that the rocks have stress dependent wave velocities when their constitutive behaviour shows non-linear elasticity (Holt *et al.*, 1997). This also proven by laboratory measurements conducted under hydrostatic conditions, which show that velocities-stress relationships to be non-linear (e.g., Nur and Simmons, 1969; Prioul, 2004; Prioul *et al.*, 2004). The rock physics models have been developed in order to relate changes in effective stress, fluid saturation and pore pressure with seismic attributes (Angus *et al.*, 2007; Verdon *et al.*, 2008; Angus *et al.*, 2015). These rock physics models have now become an increasingly integral part of quantitative seismic interpretation (e.g., Todd, 2002; Avseth, 2010). Moreover, it has become a key technology to solve problem that related in petroleum geophysics such as predicting rock behaviour and reservoir characterization (e.g., Rob & Mike, 2014; Abe *et al.*, 2018).

The stress dependence of ultrasonic velocities is also particularly significant in during the loading phase of laboratory experiments conducted at low confining pressures (e.g., Gurevich, 2004). The stress dependence of ultrasonic velocities is also often less during unloading than loading (Gardner *et al.*, 1965). The most common explanation for these observations is that seismic velocities are impacted by the presence of small cracks or discontinuities between grain boundaries at low pressures. These cracks close when the samples are placed under higher confining pressures (Verdon *et al.*, 2008).

Laboratory measurements indicate that there are two major controls on the velocity-pressure relationship; (i) the presence of microcracks, which close as confining pressure is increased, and, (ii) the crystal lattice of the rock constituents (e.g. Birch 1960: Ullemeyer *et al., 2011*). Laboratory measurements show that the velocity–confining pressure relationship is very non-linear at low pressures as a result of the 'extrinsic' effects such as crack closure due to stress increases. On the other hand, the velocity-pressure relationship tends to become more linear at higher confining pressures due to the 'intrinsic' effects such as the orientation of minerals within the rock having a more dominant impact (Birch, 1960; Ullemeyer *et al.*, 2011). The wave velocity at low confining pressures is dominated by the orientation distribution and aspect ratio of cracks (e.g., Crampin, 1984; Siegesmund *et al.,* 1993). There is still unclear the main controls on wave velocity change due to crack closure (Garia *et al.,* 2019). While, for high pressure (e.g., in the lower crust, upper and lower mantle), the wave velocity highly influences by mineral preferred orientation (e.g., Mainprice & Nicolas, 1989, Karato, 1998; Mainprice *et al.,* 2000) and elasticity of the rock constituents (e.g., Mainprice *et al.,* 2000; (Ullemeyer *et al.,* 2011). Thus, the transition from non-linear to linear velocity change (the 'crack closure pressure') is largely sample-dependent (Ullemeyer *et al.,* 2011).

Various models have been used to account for this nonlinearity (Verdon *et al.,* 2008) and explain how behaviour differs between different lithologies (Price, 2018). The models such as empirically determined relationships (Minkoff *et al.,* 2004) or those based on Hertz-Mindlin contact force mechanics (Makse *et al.,* 1999), third-rank elasticity tensors (Prioul *et al.,* 2004) and microstructural (MST) properties (Todd, 2002, Shapiro and Kaselow, 2005; Price *et al*., 2017) were established to define the non-linear relationship between velocity and stress. The MST model is a particularly popular rock physics model because it defined to be based on fundamental physical concepts and is relatively simple for the user to visualize and understand. The MST model assumes the rock contains penny shaped cracks, which open and close depending upon the stress conditions (Price, 2018). However, the assumption of penny shaped cracks in the rock physics model is likely over-simplification when compare to the in-situ crack characteristic during stress change.

In quantitative seismic interpretation (e.g., Avseth *et al*., 2005), rock physics models usually correlate the seismic attributes (e.g., amplitude) with reservoir physical properties (e.g., porosity, clay-content, grain sorting, cements type and microstructural). Porosity and permeability heterogeneity are often linked to the facies architecture inherited from the original depositional system as well as to subsequent rock diagenesis (Gutierrez *et al.,* 2002). There is still uncertainty in rock physics modelling thus, some researcher suggests to constrained input parameters (e.g., compositional maturity and textural maturity) as guided by sequence stratigraphic to reduce the uncertainty (Dutta *et al.,* 2006). In this experiment, the rock sample that measured in the laboratory were classed based on the stratigraphy as shown in **Table 4-1**.

Table 4-1 *Core sample classification.*

Age/stratigraphy	Number of samples	Depth (m)
Carboniferous	67	2808-5368
Jurassic	20	3740-6199
Rotliegend	133	2438-4900
Triassic	15	2551-4324

*Mid Jurassic included in Jurasic, Namurian & Westphalian in Carboniferous

4.2 METHODS

A series of laboratory measurements have been undertaken to improve understanding of the stress dependence of ultrasonic velocities. Around 280 core plugs of sandstone from gas reservoirs were provided by industry. Around 70% of these were from the UK and Dutch sectors of the North Sea region with ages range from Carboniferous to Upper Jurassic within depth of 2500-5100 m. The remaining samples were from a range of countries including Australia, Germany, Oman, and Ukraine.

4.2.1 Quantitative X-Ray Diffraction, QXRD

The mineralogy of the samples was measured by quantitative X-ray diffraction QXRD) using the method of Hillier (1999). The spray dried samples were analysed using a

Philips PW1050 Goniometer and Philips PW1730 CuKα X-Ray tube, which has a graphite monochromator. The data then were analysed using Hiltonbrooks HBX data acquisition and Diffraction Technology's TRACE software to provide a quantitative measure of the mineralogy.

4.2.2 Stress dependant ultrasonic measurement.

The instrumentation for measuring ultrasonic velocity in the rock sample was the same with the previous chapter (**3.2.2 Ultrasonic velocity measurement**). In the experiments reported in this chapter, ultrasonic velocities were measured during loading and unloading where the ultrasonic velocity reading was recorded for every 1000psi change or interval with range of pressure were applied between 0 to 5000psi. The ultrasonic signal then processed by using the Picoscope 6 software, where the P-, S1 and S2-wave velocity were determined by using first arrival picking and provide the stress dependant velocity curve.

4.3 MICROSTRUCTURAL, MST ROCK PHYSICS INVERSION.

The MST rocks physics model, based on Sayers and Kachanov (1995), was used to calculate the stress-dependent elasticity resulting from micro-crack deformation using the excess compliance approach. Although the non-linear microstructural rock-physics model is not a rigorous description of the true microstructure of the rock, it does provide an accurate means of predicting the averaging effects of the microstructure in relations to wave properties. Furthermore, this effective medium model is very attractive conceptually because it is formulated in terms of two initial parameters: effective initial crack density, e^o and effective initial aspect ratio, a^o, which can be linked to rock microstructure (Angus *et al.*, 2009).

In particular, the elastic compliance of a rock, S_{ijkl}, is the inverse of elasticity, C_{ijkl}. This elastic compliance also can be describe as the sum of the intrinsic compliance of the rock matrix in the absence of discontinuities, S^0_{ijkl}, plus with the additional extrinsic compliance ΔS_{ijkl} as a results of the appearance of grain contacts and cracks (**Equation 4-1**). The additional compliance due to cracks, can be expressed in terms of a second- and a fourth- rank crack density tensor α_{ij} and β_{ijkl} given in **Equation 4-2.**

$$S_{ijkl} = S^0_{ijkl} + \Delta S_{ijkl}$$

Equation 4-1

$$S_{ijkl} = \frac{1}{4}\left(\delta_{ik}\alpha_{jl} + \delta_{il}\alpha_{jk} + \delta_{jk}\alpha_{il} + \delta_{il}\alpha_{ik}\right) + \beta_{ijkl}$$

Equation 4-2

Where;

Second-rank crack density,

$$\alpha_{ij} = \sum_{m} B_T^m\, n_i^m\, n_j^m\, S^m$$

Fourth-rank crack density,

$$\beta_{ijkl} = \frac{1}{V}\sum\nolimits_{m}(B_N^m - B_T^m)n_i^m n_j^m n_k^m n_l^m S^m$$

δ_{ij} = Kronecker delta.
V = Volume
B_N^m = Normal crack compliance
B_T^m = Tangential crack compliance across the m^{-th}

The scalar crack assumption, $\beta_{ijkl} = 0$, applies when the value of B_N / B_T equals to 1 and any crack set can be described by the three orthogonal components of the second-rank crack tensor α_{ij} (Sayers & Kachanov, 1995). Although it has been shown that the scalar crack assumption is not universally valid for most real rocks (e.g., Angus *et al*., 2009; Angus *et al.*, 2012; Choi *et al*., 2014). Hall *et al*. (2008) and Verdon *et al*.

(2008) observe that the scalar crack assumption is still a valid approximation to predict the general characteristics of stress dependent velocity and anisotropy.

The MST formulation of Sayers (2002) and Hall *et al.* (2008) provides only a single second- and fourth-rank crack density value per stress measurement. A model for the density of cracks is developed, which depends on both the aspect ratio and orientation of the cracks and furthermore, depends on both the applied stress and fluid pressure (Tod, 2002). Tod (2002) introduces a second-rank crack density term, α_{ij}, which decreases exponentially with increasing effective crack normal stress $\sigma\ (n_i)$ and the analytical second-rank crack tensor defined in **Equation 4-3** & **Equation 4-4**. If the rock were assume is isotropic, the second-rank crack density tensor α_{ij} (**Equation 4-3**) and the normalization constant, h_i (**Equation 4-5**) can be expressed as in **Equation 4-6** (Price *at al.*, 2017).

$$\alpha_{ij} = \begin{cases} \dfrac{\epsilon_{i(\sigma(n_i))}}{h_i}, & if\ i = j \\ 0, & if\ i \neq j \end{cases}$$

Equation 4-3

Where;

$$e_{i(\sigma(n_i))} = e^0\ exp\left[-\frac{2(1-v_b)}{\pi\mu_b a^0}\ \sigma(n_i)\right]$$

Equation 4-4

a^0 = Initial aspect ratio

e^0 = Initial crack density at zero applied stress.

v_b = Poisson's ratio

μ_b =Shear modulus of the matrix assuming zero compliant porosity rock.

h_i = Normalisation term, defined by as;

$$h_i = \frac{3E_i(2 - v_i)}{32(1 - v_i^2)}$$

Equation 4-5

$$\alpha_{11} = \alpha_{22} = \alpha_{33}$$

$$h_1 = h_2 = h_3$$

Equation 4-6

The rock physics model was fitting with the velocity versus stress data that measured in the laboratory by using inversion scheme. In the inversion scheme, the parameter ranges are allowed to span large orders of magnitude and use the neighbourhood algorithm (NA) (e.g., Sambridge 1999). The objective function defined as the model misfit between either both the P- and S-wave velocity data or individually for each of the wave type. This algorithm was implements a Bayesian integration of NA ensemble and it also was developed as a compliment to the NA sample (Price *et al.,* 2017). It should be noted that a^0 obtained during the inversion is the length divided by the width of the cracks. This may lead to some confusion because as the value of a^0 increases the aspect ratio of the cracks decreases. To make the understanding become easier to read, a^0 were refer as the aspect ratio value, which is the inverse of aspect ratio.

4.4 MICROSTRUCTURAL: MICROCRACKS IMAGING

Carbon-coated polished thin sections of all samples were examined using SEM. A TESCAN VEGA3 SEM was used to obtain low magnification images that provide an excellent overview of the general microstructure of each sample, which allows regions of interest to be identified for high resolution analysis. A FEI Quanta 650, field emission environmental SEM, fitted with an Oxford Instruments INCA 350 EDX system/80mm X-Max SDD detector to help identify the minerals present was used to examine the samples under higher magnification. The mineralogy and diagenetic history of all samples was determined, and digital images were saved as 8-bit TIFF files for further analysis.

4.5 LARGE DATA ANALSIS: WEKA & PETMINER

The dataset collected during this study is quite large and difficult to interpret without specialized data visualization and data mining software. The results collected during the study were therefore loaded into the PETMiner data visualization and data mining software (Harrison *et al.,* 2019). The advantages and details about PETMiner Software has been discussed in previous chapter (3.1.5). The data output (e.g., crack properties data) also were analysed using the WEKA data-mining software (Holmes *et al.,* 1994; Hall *et al.,* 2009). The Waikato Environment for Knowledge Analysis (WEKA) came about through the perceived need for a unified workbench that would allow researchers easy access to state-of- the-art techniques in machine learning. Nowadays, WEKA is recognized as a landmark system in data mining and machine learning (Hall *et al.,* 2009). Weka programme which is a collection of machine learning algorithms for data mining tasks which contains tools for data pre-processing, classification, regression, clustering, association rules, and visualization.

Data classification

The main physical attributes in the analysis is the crack properties from the rock samples. Crack appearances has significant influence towards the seismic propagation and attributes (e.g. Pointer *et al.,* 2000; Shen *et al.,* 2020). Microstructural (MST) rock physics model were used to invert wave velocity to get the crack properties (crack density & aspect ratio). The purpose of this analysis is to identify whether the physical properties of cracks (crack density & aspect ratio) have a direct control towards seismic velocity. The crack properties then classified (binned) based on the four category.

The crack density and aspect ratio values were classified into 4 major class (bin) as follow; (i) all high (crack density & aspect ratio); (ii) high value of crack density with low value of aspect ratio; (iii) high value of aspect ratio with low value of crack density, and (iv) all low (crack density & aspect ratio). The WEKA software was then used to identify the controls on which class the samples belong and produce decision tree to classified the sample. During the classification analysis, classifier called J48 were used which is build-in within Weka program. This classifier is based on C4.5 algorithm (Quinlan, 1993) which allow number of parameters are learned directly from data through a process known as model training (Hall *et al.*, 2009; Sammut & Webb, 2011).

Generally, decision tree classifier provide clear, simple and easy to understand output that makes this classifier being used in many diverse area (Szczerbicki, 2001). C4.5 by Quinlan (1993) is among the most popular decision tree algorithm and attained the highest accuracy compare to other classification algorithms (e.g. Iterative DiChaudomiser 3, ID3; Classification and Regression Trees, CART; and C5.0) based on empirical results (Salzberg, 1994; Hssina *et al.*, 2014; Maaliw *et al.*, 2017; Darmawan, 2018).

Most of decision tree tend to be overfitting in order to correctly classifies every sample which finally produce inaccurate classification or wrong prediction (Salzberg, 1994). To handle such problem, C4.5's algorithms employ a pruning method known as single pass pruning process to reduce overfitting effects. In practice, this approach proven works quite well and better than pruning approach that implemented by other algorithm (Quinlan, 1993; Salzberg, 1994). C4.5 also implement "Information gain" approach to overcome overly sensitive in typical classifiers (e.g. ID3) when dealing with large numbers of data. This computation approach does not create anything new within the data but being used to measure a gain ratio which finally being used to evaluate the splitting attribute (Quinlan, 1993; Hssina *et al.*, 2014). The approach implemented in C4.5 makes this decision tree algorithm stands out compare to other decision tree algorithm (e.g. Hssina *et al.*, 2014).

4.6 RESULTS

4.6.1 Microstructural analysis

The sandstone samples range from very fine to medium grained and are moderately to very well-sorted. The samples have a very varied mineralogical composition and diagenetic history. The samples were classified into three basic rock types that have: (i) a low clay content; (ii) grain-coating clay, and (iii) pore-filling clay (**Table 4-2**). The samples with a low clay content tended to be composed of quartz, feldspar with authigenic quartz and dolomite/ferroan dolomite. Samples with the grain-coating rock type generally contain detrital quartz and feldspar together with authigenic grain-coating illite, carbonates, quartz and occasionally anhydrite. The authigenic quartz in these samples tends to occur as outgrowths instead of syntaxial overgrowths reflecting the inhibition of its growth on detrital quartz due to the presence of grain-coating clays. The samples with pore-filling clay tends to be composed of detrital quartz and feldspar and contains authigenic kaolin within the space between the detrital grains; variable amounts of carbonate cements are also present. In some cases, the kaolin and K-feldspar have dissolved resulting in the precipitation of illite. This illite seems to have replaced the kaolin and tends not to form grain coats. Authigenic quartz is common in sandstones with pore-filling clays but tends to occur as overgrowths on detrital quartz grains.

Table 4-2 *Basic rock type for all the core sample*

Age/stratigraphy	Basic rock type
Carboniferous	Pore filling (39), grain coating (25) and low clay (3)
Jurassic	Pore filling (18) and low clay (2)
Rotliegend	Pore filling (33), grain coating (84) and low clay (16)
Triassic	Pore filling (10) and low clay (5)

* Namurian & Westphalian were combined in Carboniferous

4.6.2 Mineralogy

The mineralogical composition of the samples shows a wide variation with quartz being by far the most common mineral present occupying an average of 72% of the grain volume **Table 4-3**). Other minerals present include variable amounts of feldspars (albite and K-feldspar), carbonates (dolomite and calcite), mica, and clay (kaolin, illite-smectite, and chlorite).

Table 4-3 *Mineralogy of the samples analysed*

Mineral	**Range (%)**	**Average (%)**
Quartz	20.2 – 90.1	72
Albite	0 – 32.9	5.3
Microcline	0 – 9.1	2.9
Calcite	0 – 23.2	0.6
Dolomite	0 - 21.2	3.6
Mica	0 - 24.7	4.8
Kaolin	0 – 15.7	2.7
Chlorite	0 - 29.7	2.4
Illite-smectite	0 - 17	4.6

4.6.3 Ultrasonic velocities during loading and unloading

In general, there are significant variation between velocity-pressure none-linear relationship during loading and unloading (e.g**., Figure 4-1**). P-wave and S-wave velocities vary between 2593 to 5348 m/s and 1379 to 4203 at 1000 m/s respectively when first loaded to 1000 psi confining pressure (**Table 4-4)**. Velocities increase to 3595 to 5568 m/s and 2156 to 4617 m/s respectively when loaded to 5000 psi confining pressure. Reduction of confining pressure back to 1000 psi results in P-wave and S-wave velocities that vary between 2832 to 5407 m/s and 1150 to 3426 m/s respectively. The loading and unloading behaviour of both P- and S-wave velocities is non-linear (**Figure 4-1**). The ratio of P-wave velocity measured at 5000 psi to that measured at 1000 psi is 1.03 to 1.49 during loading (**Figure 4-2**) and 1.00 to 1.36 during unloading. The ratio of S-wave measured at 5000 psi to that measured at 1000 psi was 1.06 to 1.47 during loading and 1.04 to 1.36 during unloading. In other words, both P- and S-wave velocities are slightly more stress dependent during loading than unloading.

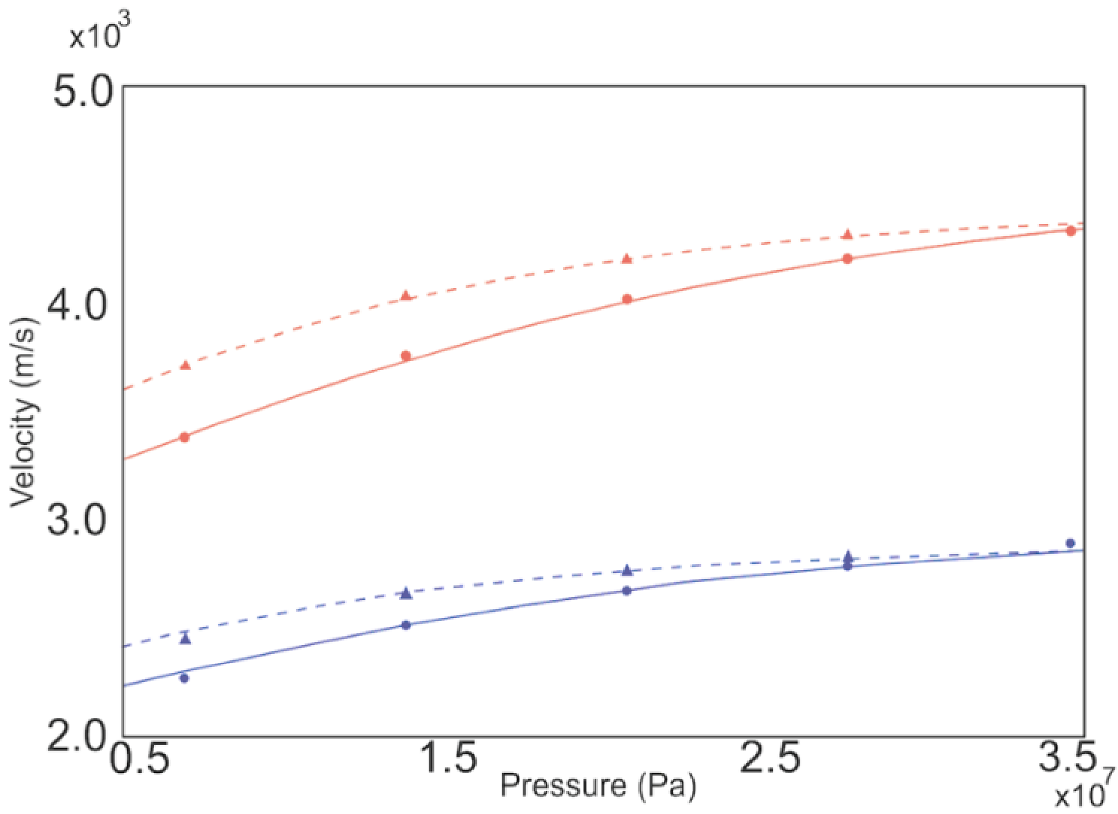

Figure 4-1 *Ultrasonic signal for P-wave (red) and S-wave (blue) during loading (solid line) and unloading (dashed line)*

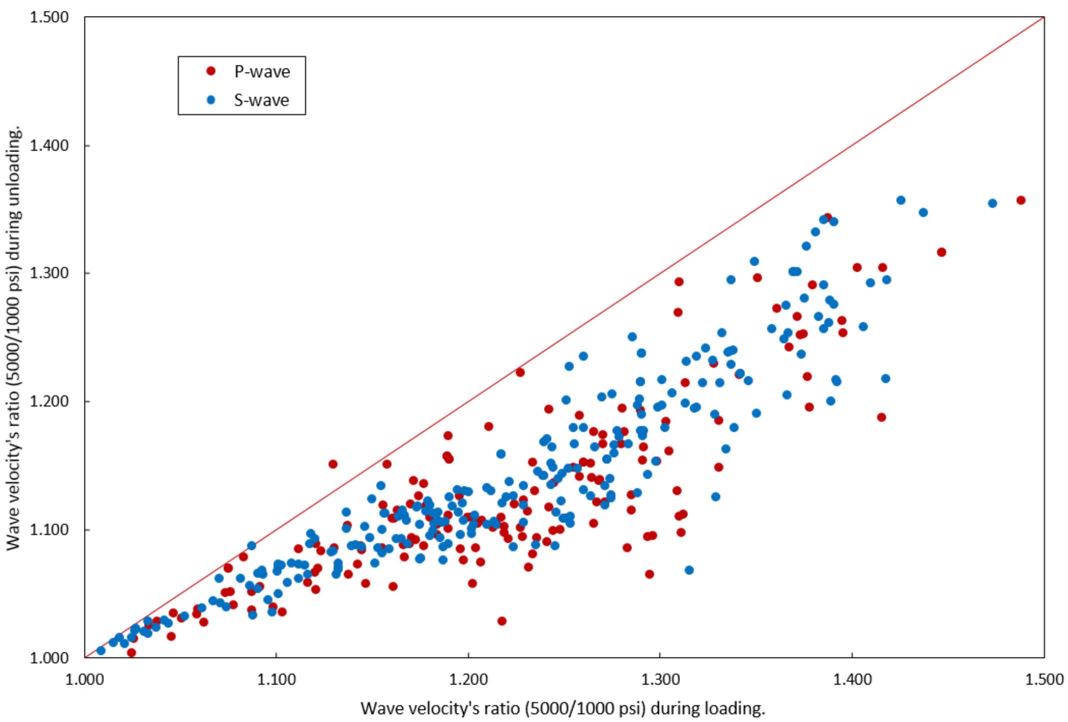

Figure 4-2 *Cross plot of wave velocity ratio at 5000:1000 psi for both loading and unloading.*

Table 4-4 *Velocity range for P and S-wave during load and unload with velocity ratio at 5000/1000 psi.*

Stress path	Wave type	Velocity range (m/s)	Range of velocity ratio (5000/1000 psi)
Loading	P-wave	2593 to 5348 at 1000 psi	1.03 to 1.49
		3595 to 5568 at 5000 psi	
	S-wave	1379 to 4203 at 1000 psi	1.01 to 1.56
		2156 to 4617 at 5000 psi	
Unloading	P-wave	2832 to 5407 at 1000 psi	1.00 to 1.36
	S-wave	1150 to 3426 at 1000 psi	1.01 to 1.39

4.6.4 Rock physics inversion: Crack density and aspect ratio

Inversion based on the MST rock physics model has used to estimate crack properties (aspect ratio& crack density) for all 79 rock samples in which velocities were measured during loading and unloading (**Table 4-5**). Generally, the result shows the crack properties have significant changes during loading and unloading which indicate the crack response differently during stress path change.

Table 4-5 *Crack properties during loading and unloading*

Crack properties	Loading			Unloading		
	Min	Max	Mean	Min	Max	Mean
Aspect ratio	0.00007	0.00085		0.00006	0.00095	
Crack density	0.01546	0.69719		0.00966	0.35397	
Vpgr	3186.48	6061.23		3660.51	7555.79	

Vsgr	1986.34	3810.74	2058.16	4278.59

Cross-plot between aspect ratio, a^o during loading and unloading (**Figure** 4-3**)** shows that the value dominated at lower part of 1:1 linear line, which indicates that a^o is higher during loading than unloading. The measured velocity data and that inverted using MST model shows a good fit for both loading and unloading (e.g., **Figure 4-1**). The aspect ratio value is higher during loading than unloading for 90% of the samples (**Figure** 4-3**a**). In other words, the inversion results indicate that the aspect ratio of cracks is higher during unloading than loading. The results can be divided into two groups according to how the aspect ratio of cracks differ during loading and unloading (**Figure** 4-3**a**). For 80% of the samples, the aspect ratio value during unloading is within 50% that measured during loading. However, for 20% of the difference between aspect ratio during loading and unloading is greater. The crack density is on average 60% higher during loading than unloading **(Figure** 4-3**b**). Less than 10% of samples have a crack density that is higher during loading than unloading.

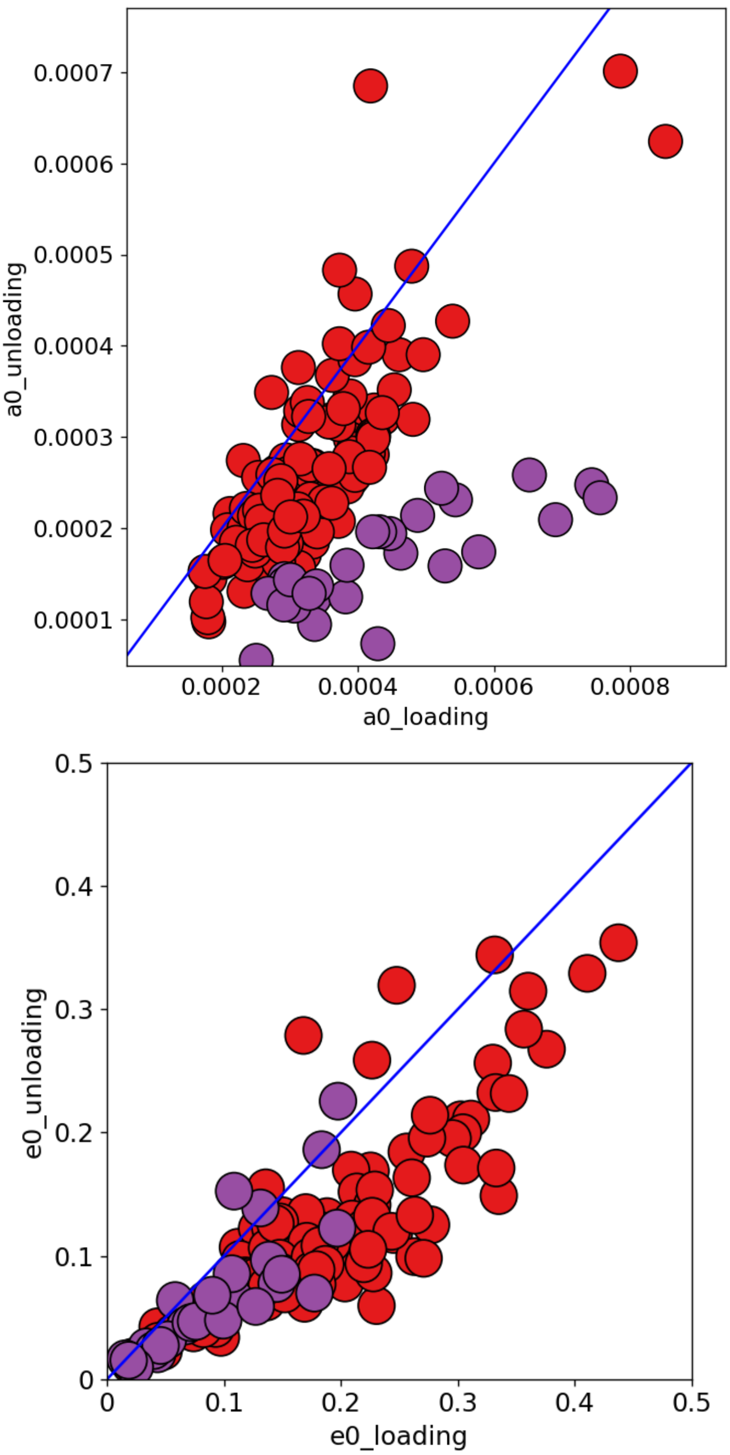

Figure 4-3 *Top) Cross-plot of aspect ratio vale, a^o, during loading and unloading, Bottom) cross-plot of crack density during loading and unloading. The samples are coloured purple if the aspect ratio value during loading is more than double that during unloading.*

Inverted a^o and e^o during loading and unloading are plotted against each other in **Figure 4-4** . Aspect ratio values during loading range from 6.7E-05 to 8.5E-04 (average = 3.5E-04) whereas crack density values during loading range from 0.015 to 0.70 (average = 0.2). The values tend to decrease significantly during unloading with a^o varying between 5.5E-05 to 9.5E-04 (average = 2.6E-04) and e^o varying between 0.01 to 0.35 (average = 0.11). The results also indicate that the range of a^o values during unloading is larger than during loading. The range of crack density values is similar during loading and unloading.

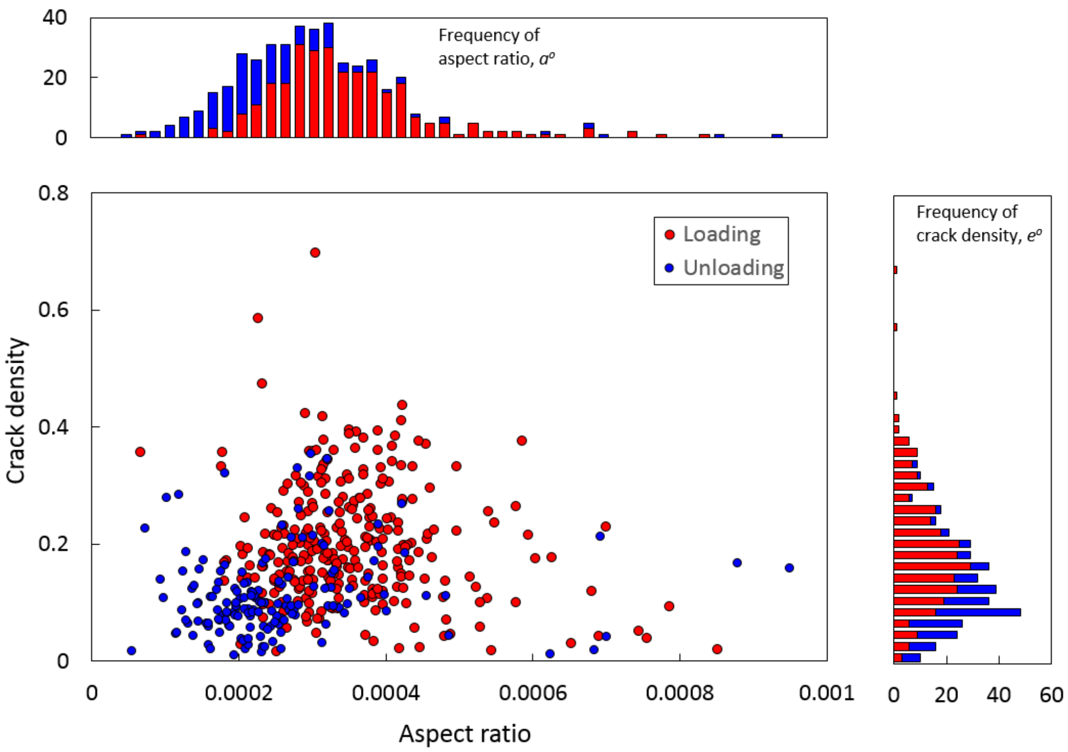

Figure 4-4 *Cross plot of inverted crack density, e^o versus aspect ratio, a^o for 289 sample of load (red) and 154 sample for unloading (blue circle) with the left part indicates the frequency of crack properties during load and unload.*

4.6.5 Crack density and aspect ratio: prediction and classification

Output from classification tree generated by Weka J48 method started with crack density value in unloading, which shows value more than 0.135 tend to create low value (small) for crack density and aspect ratio during loading. This indicate that, whenever crack size and density considerably small, the stress path changes (loading and unloading) has gave low influence in crack development and changes. But whenever the crack volume considerably high (more than 0.135), it shows there are variation of crack development when stress changes are implemented.

Samples with a crack density during unloading of more than 0.135 tended to produce more variation on aspect ratio (unload) where lower than 0.00016 tend to produce high value of crack density (load) and higher than 0.00016 tend to create lower crack density and aspect ratio during loading. Basically, with known value of crack density during unloading, it is possible to predict the behaviour of crack characteristic (aspect ratio and crack density) during unloading. Cross plot between classification with selected mineral are constructed as shown in **Figure 4-5** to assess if there any possibility of mineral type could influence crack characterization.

In general, there are relatively small and almost no significant relationship between the porosity of the samples and the crack properties (aspect ratio and density) during loading or unloading. But analysis with single mineral indicates for mineral some correlation for certain types of mineral. For instance, aspect ratio during loading and unloading for mineral quartz shows significant changes specifically with the sample with all low value of e_o & a_o *(All low values, AL for* e_o & a_o*) and* e_oH (High velue for e_o) decreasing significantly unloading compared to loading. But this situation is not really obvious in crack density for both different stress path changes. In conclusion, value of a_o and e_o has shown significant changes during stress path changes but relatively small changes that influence by the appearance of mineral which it's really hard to predict the crack characteristic with type of mineral that exist in the rock sample. This prediction problem also makes the classifier (machine learning) failed to predict clear attribute that could control velocity and crack properties. Thus, prediction based on percentage of mineral appearance in the rock sample still unable to predict real behaviour of crack in the rock sample. .

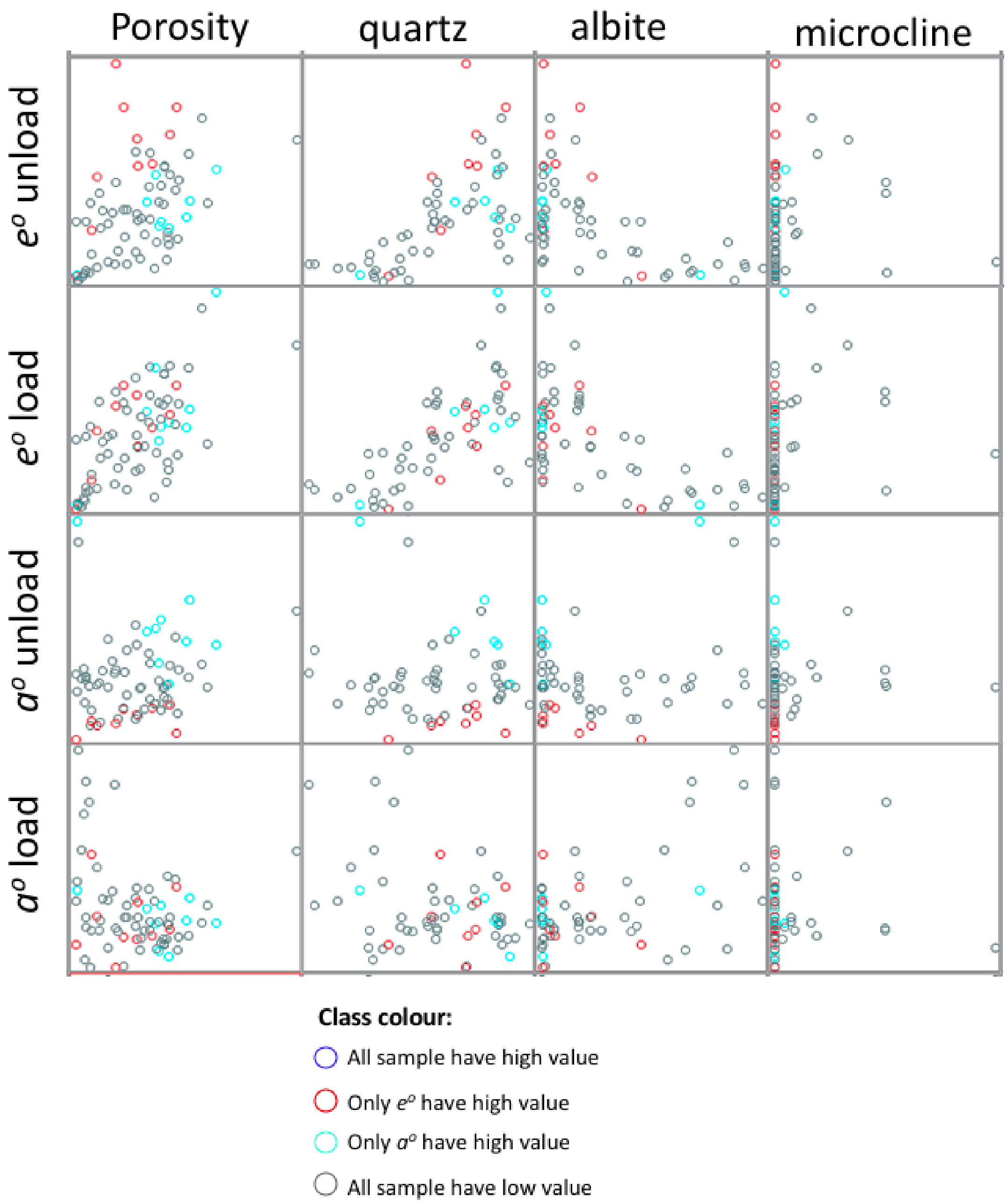

Figure 4-5 *Plot matrix of crack density and aspect ratio during loading and unloading with porosity, mineral quartz, albite and microcline.*

4.7 DISCUSSION

4.7.1 Physical meaning of crack density and aspect ratio.

The results indicate that there are significant differences in a^o and e^o during loading and unloading. The general reduction in e^o from loading to unloading is consistent with the opening and closing of cracks during loading and unloading rather than the formation of new cracks. A strong correlation exists between crack density and the ratio of maximum and minimum V_p within the pressure range of 1000 to 5000 psi (**Figure 4-6**). Data mining failed to identify similar relationships between aspect ratio values and ultrasonic velocities. A sensitivity study was therefore conducted by using the microstructural, MST model to assess the impact of a^o and e^o on velocity – stress relationships. **Figure 4-7** confirms that the stress dependence of the ultrasonic velocities increases as the crack density increases. The aspect ratio value appears to be related to the curvature of the velocity – stress data (**Figure 4-8)**. For example, the velocity of samples with a low aspect ratio values (i.e., long thin cracks) tends to increase rapidly as confining pressure is increased and then velocity tends to be less stress sensitive at higher confining pressures; this results in a distinct non-linearity to the stress vs. velocity relationship. On the other hand, the velocity of samples with high aspect ratio values (i.e., more sphere-like cracks) tends to have a more linear relationship with stress.

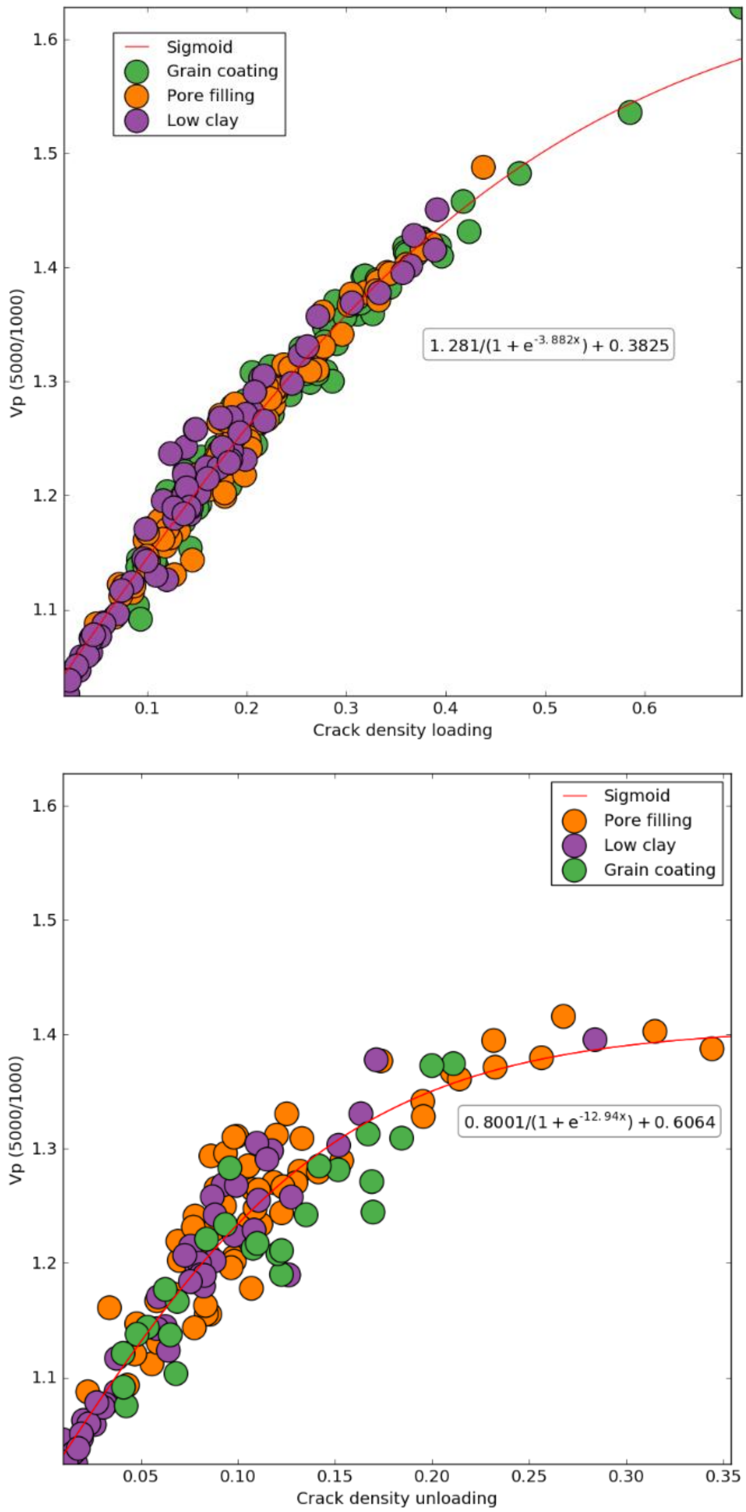

Figure 4-6 *Crack density versus Vp (5000/1000) measured during a) loading, and (b) unloading.*

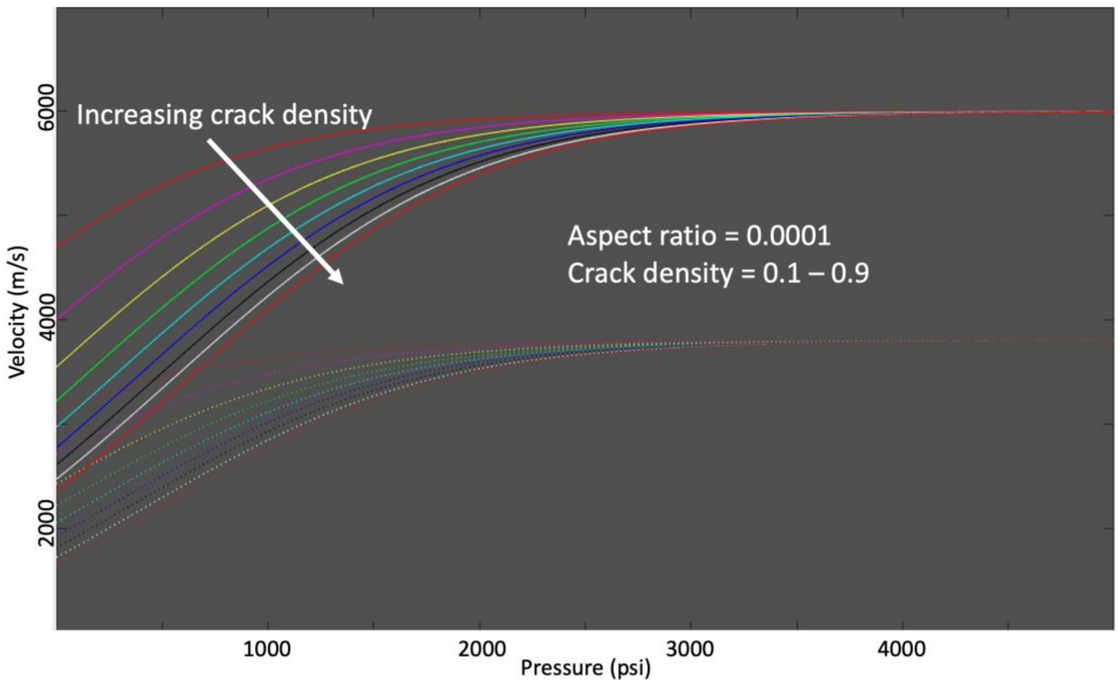

Figure 4-7 *The pressure versus wave velocity (P-wave indicate by solid line & S-wave indicate by dotted line) curve's changes with crack density value are increased from 0.1 to 0.9.*

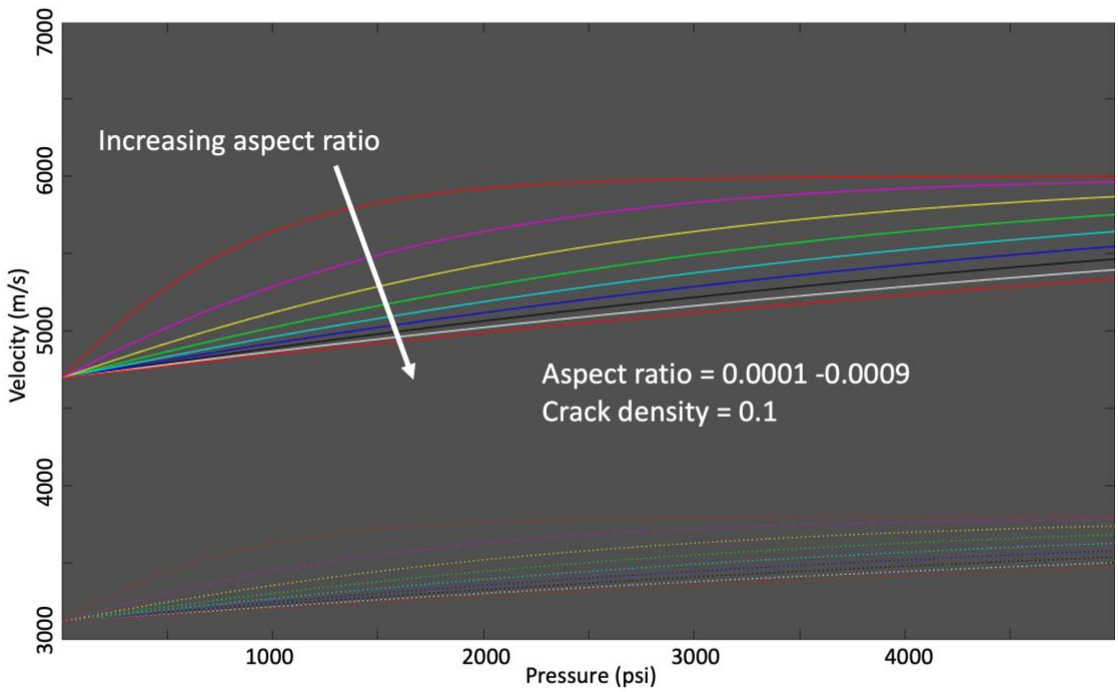

Figure 4-8 *The pressure versus wave velocity (P-wave indicate by solid line & S-wave indicate by dotted line) curve's changes with aspect ratio value are increased from 0.0001 to 0.0009.*

4.7.2 Impact of quartz and clay content on crack properties

It has been shown that crack density and aspect ratio values obtained from inverting ultrasonic velocity data based on the MST model may not be directly related to the density and shape of fractures within the samples. However, their impact on velocity is similar to what their names imply, and the terms are therefore useful for describing the manner in which the ultrasonic velocities vary as a function of stress. Data mining functionality in the PETMiner software was used to identify key relationships between crack density and aspect ratio with rock properties such as mineralogy, porosity, surface area, NMR T2 distributions, etc. but no strong controls were identified. Data analysis did identify some weaker controls on crack density and aspect ratio. For example, samples with a low quartz and high clay content appear to have lower crack densities (**Figure 4-9**)

To further controls on aspect ratio and crack density, the PETMiner software was used to replace individual points on cross plots with images such as SEM micrographs, as well as photographs and CT scans of the core plugs. This did not provide particularly useful information regarding controls on crack density. However, a plot of aspect ratio value against porosity with data points replaced by BSEM images proved more informative (**Figure 4-10**). In particular, the minimum aspect ratio value for a given porosity appears to increase with increasing porosity. The BSEM images indicate that grain contacts tend to become longer with decreasing porosity. This is consistent with low porosity rocks having long grain contacts due to cementation and grain contact quartz dissolution whereas the grain contacts of higher porosity samples could be controlled by the elastic deformation of the touching grains (i.e., they are Hertzian contacts). The aspect ratio value of the samples varies widely for a given porosity. Examination of the micrographs appears to suggest that samples with low porosities for a given aspect ratio value tend to contain more intragranular clays (**Figure 4-10**). Pore-filling and grain coating clays do not support the framework of the grains sandstones so effectively mean that samples with these rock-types have a higher effective porosity and hence shorter grain-contacts than if the porosity was filled with framework-supporting cements. The presence of clays at grain-contacts makes the samples more compliant at low stresses and therefore decreases their aspect ratio value.

Overall, data mining has failed to identify strong links between a^o and e^o and other key properties of the rocks. Potential microstructural controls on a^o and e^o have been identified but these are subtle. Quartz and clay have a better correlation with crack density during loading compared to the other minerals (**Figure 4-9**). However, the relationship is weaker for a^o and e^o measured during unloading. Two explanations as to why the controls on a^o and e^o are difficult to identify are that: (i) a^o and e^o are controlled by several rock properties and these vary from sample to sample, and (ii) a^o and e^o are controlled by damage to the rock during and following drilling and that such damage is dependent on external factors (e.g., trip speed, weight on bit etc.) that are not taken into account during the current analysis.

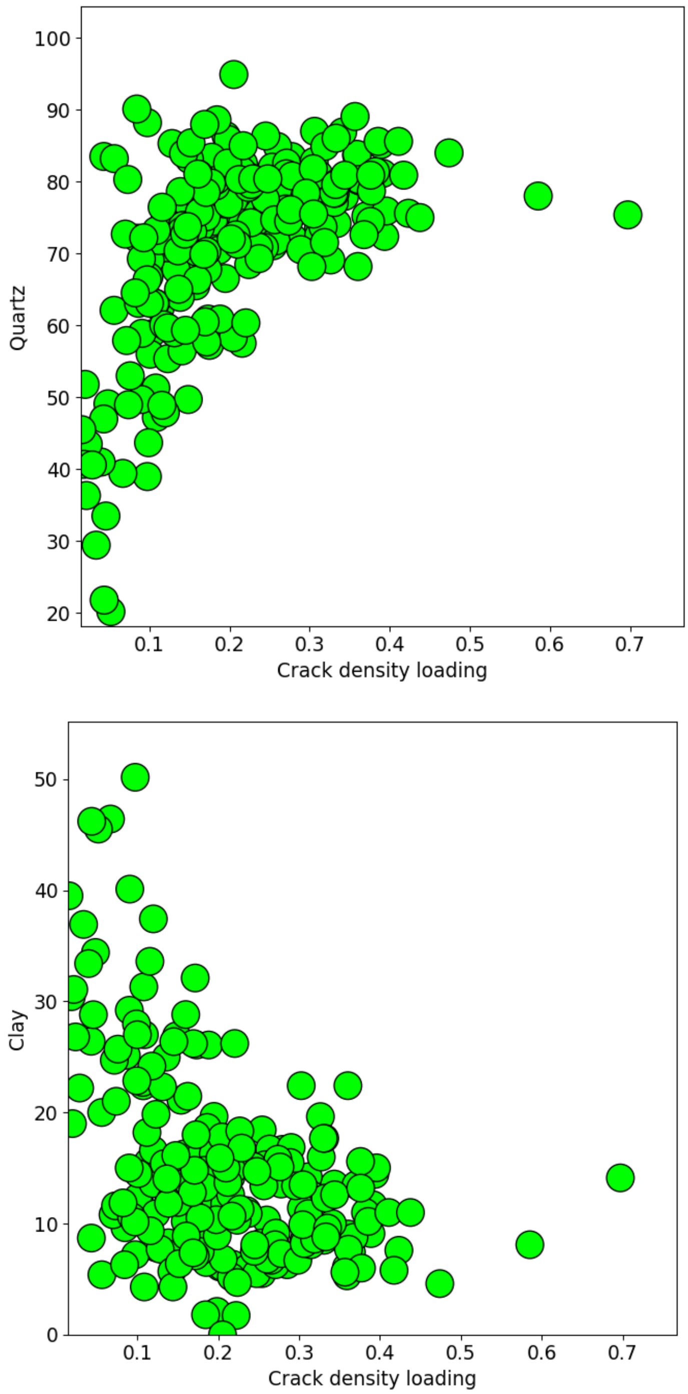

Figure 4-9 *Plot of crack density during loading against (top) quartz content and (bottom) clay content.*

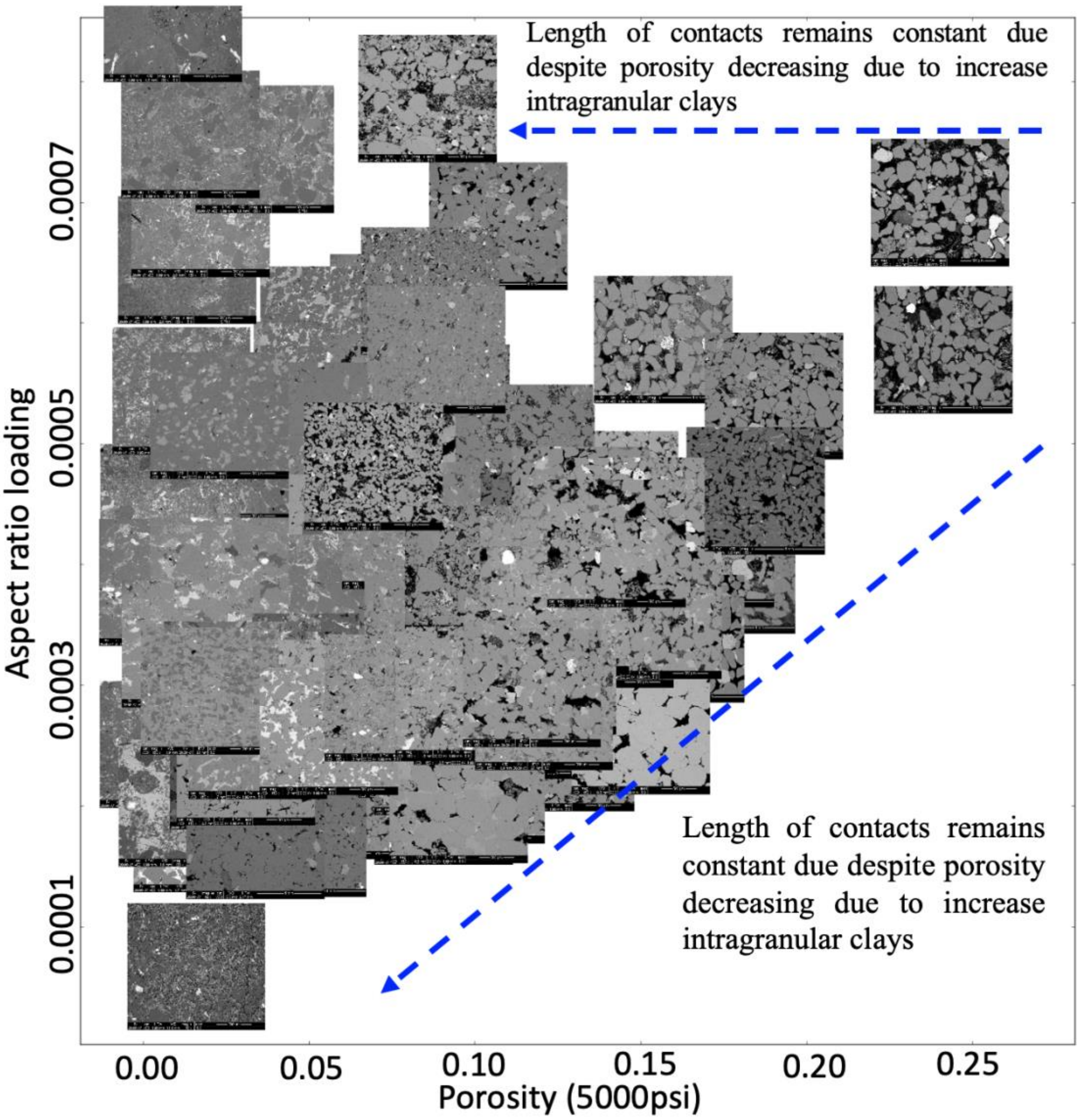

Figure 4-10 *Plot of porosity versus aspect ratio loading with data points replaced by BSEM images.*

4.7.3 Loading versus unloading

Several studies have previously noted that significant hysteresis of the elastic properties of porous rocks takes place during loading and unloading cycles (e.g., Plano and Cook, 1995; Tutuncu *et al*., 1998). Various mechanisms have been provided to explain this hysteresis including frictional sliding along grain contacts or cracks (e.g., Plano and Cook, 1995; Nihei *et al.,* 2000; David *et al.*, 2012) as well adhesion contact adhesion hysteresis (Sharma & Tutuncu, 1994).

The aspect ratio during loading divided by the aspect ratio during unloading seems to correlate with the aspect ratio during unloading (**Figure 4-11**). This is consistent with aspect ratios being partially controlled by the length of grain contacts. **Figure 4-12** plots aspect ratio during loading divided by that measured during unloading ($a^o{}_L/a^o{}_{UL}$) against porosity with data points being replaced by BSEM micrographs. In general, $a^o{}_L/a^o{}_{UL}$ tends to decrease with increasing porosity. The samples with low porosity show large differences in the $a^o{}_L/a^o{}_{UL}$ (i.e., 1 to 6). Examination of the micrographs indicates that the lower values tend to have clay between grain contacts whereas the higher values tend to have more quartz-quartz contacts. It is possible that the differences are controlled by grain adhesion. A higher clay content between the grain contacts makes them more compliant as the result of the low porosity value and high aspect ratio values. High aspect ratio value with high porosity caused by small Hertzian contact. In particular, the separation distance between two contacting grains will controlled by the surface forces between them and the external force applied (Sharma & Tutuncu, 1994). It is also showed that the surfaces do not follow the same path as they brought together and pulled apart, which may explain some of the differences in ultrasonic velocity during loading and unloading (Sharma & Tutuncu, 1994).

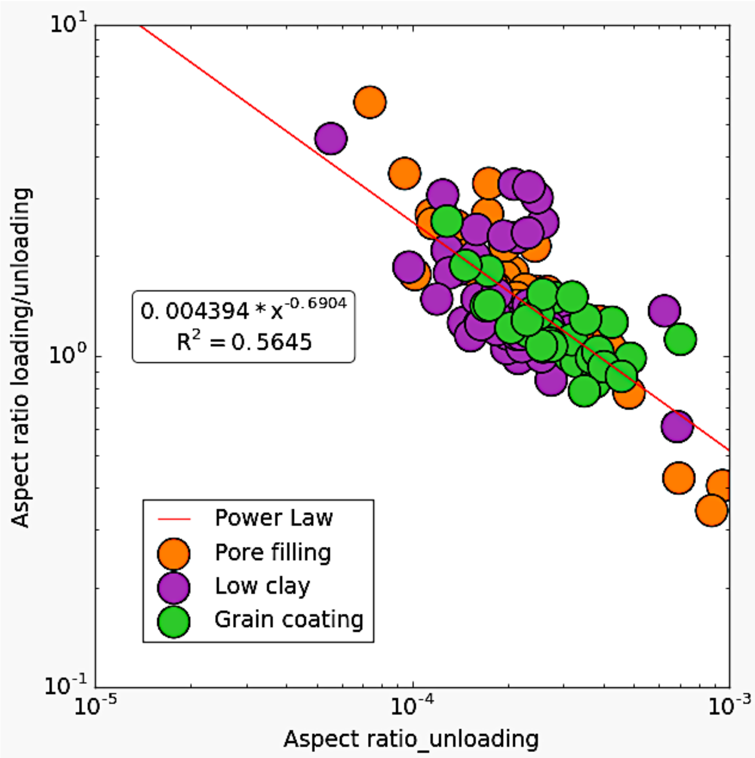

Figure 4-11 *Cross plot of aspect ratio (unloading) vs aspect ratio (loading/unloading).*

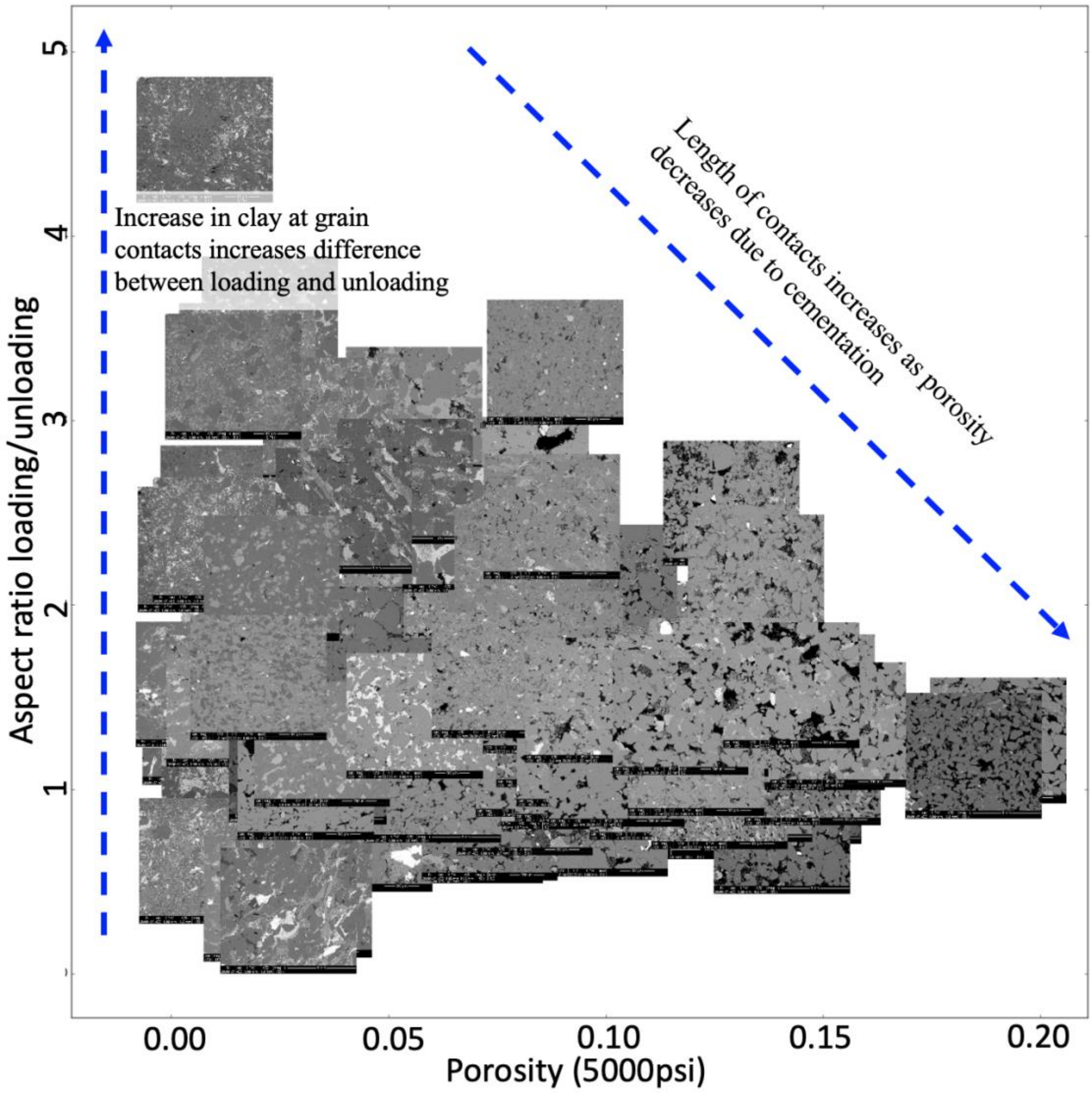

Figure 4-12 *Plot of porosity vs aspect ratio loading/unloading.*

4.8 Laboratory versus subsurface velocities

The rock physics models used to predict the stress sensitivity of seismic velocities are generally based on laboratory measurements of ultrasonic velocities. It is important to question whether these laboratory measurements are representative of the subsurface. The fracture networks that were observed after injecting Fields metal into the rock at low confining pressures rapidly closed as confining pressure was increased. It seems very unlikely that such fracture networks existed in the subsurface and were most likely formed as the samples were brought to the surface. If this is the case, the velocity measurements conducted at low stress are certainly not representative of subsurface values and there remain questions as to whether the high-pressure values are also representative of subsurface values.

4.8.1 Comparison with microcrack images

To improve our understanding on the shape and crack appearance, I tried to compare the crack model shape (penny shape) with the in-situ crack. Eardley (2017) has produced research work to visualize the in-situ cracks at different stresses by injecting molten Fields metal into the rock and then analysing the distribution of the solid metal after the sample had cooled. BSEM images from the research show that the distribution of Fields metal in the tight gas sandstone shows significant differences depending on the stress conditions. The Fields metal in the sample confined to 1500 psi appears to be concentrated along laterally continuous fracture that have formed between grain boundaries **(Figure 4-13**). Increasing confining pressure results in the closure of these laterally persistent fractures and the concentration of Fields metal in pores of the rock (**Figure 4-13**). In some cases, isolated pods of Fields metal remain at grain boundaries (**Figure 4-13**) but overall, most has been expelled into adjacent pore space or out of the sample completely.

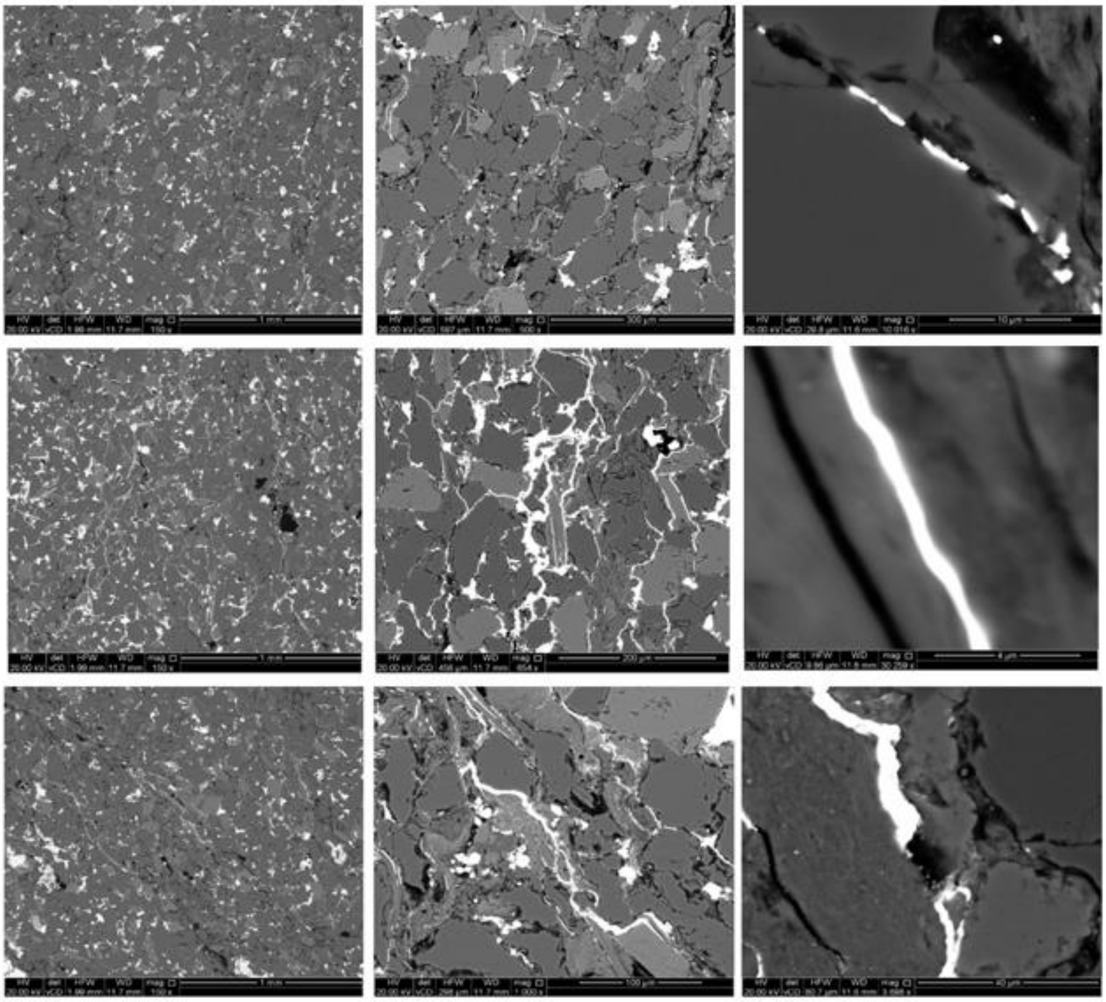

Figure 4-13 *Distribution of Fields metal (bright areas) at 1500psi, top, 2500 psi (middle) and to 5000 psi (bottom) confining pressures (Eardley, 2017).*

The influence of crack development or deformation should be taken account as well as fluid substitution in the reservoir because of geomechanical effect that occur in subsurface as discussed earlier. But normally the non-linear rock physics models assume that only elastic deformation occurs, thus the permanent deformation of pre-existing cracks and pores or any development of new cracks is ignored. Although the influence of plastic deformation can be modelled by using porosity-velocity relationships (e.g., Avseth *et al.*, 2010) these could ignored the important geomechanical effects, such as shear-band formation due to shear-enhanced compaction that could lead to induced seismic anisotropy (Price *et al.*, 2017).

The Fields metal experiments indicate that the sandstones contain a high density of anastomosing fracture arrays at low stresses formed by the coalescence of dilated grain-boundaries; these have a very different structure to the simple penny shaped cracks on with the MST model is based. It appears that a^o and e^o are essentially parameters that provide the best fit to velocity vs. confining pressure data and do not have the same physical significance as their names imply. Instead, crack density can be regarded as a parameter that provides an indicator of the absolute stress sensitivity of the rocks and aspect ratio provides a measure of the rate at which stress sensitivity changes as a function of confining pressure.

4.8.2 Implications of results

Overall, it appears that the crack density and aspect ratio terms are essentially parameters to fit measurements of ultrasonic velocity vs. confining pressure. It is also likely that the fracture networks that exist in the laboratory were probably not present in the subsurface. It seems incorrect to generate rock physics models based on these data and then attempt to extrapolate them to subsurface conditions. The impact of core damage is made worse by the fact that many rock physics models used to predict subsurface velocity changes are based on ultrasonic velocities measured in the first loading cycle rather than those measured during unloading or better still those collected after multiple loading and unloading cycles.

The results conducted during this study indicate that the MST model that is used in the interpretation of ultrasonic velocity data is far too simple compared to the complex fracture patterns that seem to be present at low confining pressures. However, although the assumption used in the MST model that fractures have a penny-shaped geometry is far from reality, it should be noted that the ultrasonic waveforms have dominant wavelengths much greater than the average diameter of the mineral grains

(Fine to medium sand with 0.0025-0.002mm) and their contacts. Even the model still provides a good fit to velocity versus stress data but the usage of this model to predict the impact of stress changes on seismic velocities in the subsurface should be taken more carefully. This is due to the physical assumptions behind these models are unrealistic and it still could be argued that it is better to simply use empirical relationships between stress and velocities (e.g., Price *et. al*., 2016).

The experimental results show that crack properties (a^o and e^o) have slightly different value in two different stress paths. On the other hand, it poses a doubt regarding the uncertainties of rock physics model to invert stress-velocity into crack properties for both of stress path condition, where the rock physics model constructed and considered only by velocity measurement during loading data. Note that, the reservoir could experience depletion or unloading during petroleum extraction. This stress path could be change into loading with implementation of water flooding. For most of the reservoir will experience loading at stress starting at 3000-5000psi. Ignoring the stress path change in the rock physics models may result is a poor correlation (scattered) in some of the crack properties analysis.

4.9 CONCLUSION.

The MST rock physics model has been used to invert the stress dependence of ultrasonic velocities into the crack properties, aspect ratio and crack density. These values are significantly different if measurements were made during loading or unloading. Strong correlations were not identified between either aspect ratio or crack density and either the composition of the sandstones, their basic petrophysical properties or their microstructure. These do not appear to be natural and instead formed as a result of damage during or following coring. These unnatural crack trend also did not show any clear trend by machine learning analysis either. The fractures containing the solidified

Field's (Eardley, 2017) metal also have a geometry that doesn't resemble the simplified penny shaped cracks assumed in the MST model. It is possible that the stress dependence of the properties of the samples is controlled by a range of extrinsic and intrinsic, which is why strong correlations are not identified between either aspect ratio or crack density and the microstructural, mineralogical or petrophysical properties of the samples.

Overall, the results indicate that great care should be taken when using the MST model used in the current study, or similar rock physics models, which have been calibrated with laboratory measurements of the stress dependence of ultrasonic velocities, to predict the stress dependence of seismic velocities in the subsurface. Most importantly it is quite likely that estimating stress sensitivity from laboratory tests overestimates how seismic velocities are likely to change as a result of stress changes resulting from petroleum extraction. This questions whether the rock physics models are useful in predicting changes in seismic velocity resulting from subsurface deformation. The results from this study would tend to suggest that simulations of seismic based on laboratory measurements of seismic velocities could overestimate the influence to roll that stress changes have on 4D seismic.

5 SEISMIC SIMULATION DURING STRESS PATH CHANGE

5.1 INTRODUCTION: SEISMIC SIMULATION

The previous chapter discussed the effect of stress path change (loading and unloading) on the relationship between porosity and velocity as well as the impact of crack properties on ultrasonic velocities. It appears that there is an unpredictable relationship of crack properties between loading and unloading cycles possibly due to sample damage (discussed in Chapter 4). This also could indicate that surface seismic survey may inherit the prediction error specially when involving time lapse seismic techniques that being used for monitor reservoir (e.g., Roste *et al.*, 2007) that experience stress path change. Although it is probably more likely that the damage occurred to the samples during or following coring.

In real world situation, reservoirs could experience stress path changes. For example, a depleted reservoir usually experiences loading as a result of primary or secondary production. As an oil field matures and production rates decline, water flooding or carbon dioxide injection is undertaken to increase oil recovery (Fink, 2015; Huang *et al.,* 2017), which would re-inflate (unload) the reservoir if the processes increase pressure. In this chapter, I build a simplified model of the Snøhvit Field within the package MpGeoflow. I then compare simulated seismic response when the model is populated with Vp & Vs values gathered during loading with those gathered during unloading. The seismic response comparison was produced with implementation of seismic time-lapse method, a well-known technique for estimating reservoir production-induced physical changes (Lumley, 2001; Nguyen *et al.*, 2015). Besides simulating the geomechanical impacts on seismic response during loading and unloading, the model also assessed how changes in fluid saturation would impact seismic. The Gassmann fluid substitution theory (Gassmann, 1951) was used to model the seismic response and velocity change as a result of variations in fluid saturation in the reservoir.

5.2 BUILDING THE GEOMECAHNICAL MODEL

Geomechanical models have many purposes in reservoir management such as predicting reservoir compaction and sea floor subsidence, predicting long-term well-bore integrity and optimization of drilling (Zoback, 2007; Vejbæk *et al.,* 2014). The basis for all geomechanical applications is an accurate knowledge of the subsurface stress state and the mechanical properties of rocks present; in combination these form a geomechanical (or mechanical earth) model. To increase trust in their predictions, these models need to be compared with field observations. For example, time shifts observed in the overburden, in time-lapse seismic data, are commonly ascribed to reservoir compaction and ensuing overburden elongation and associated velocity reductions (Hatchell and Bourne, 2005). The link between these time-shifts and the overburden elongation is now being used as a field-wide calibration tool for geomechanical models (Staples *et al.,* 2007; Herwanger and Koutsabeloulis, 2011; Herwanger *et al.,* 2013). To build a geomechanical model that creates simulated seismic response the workflow shown in **Figure 5-1** was followed; each of the steps are described below.

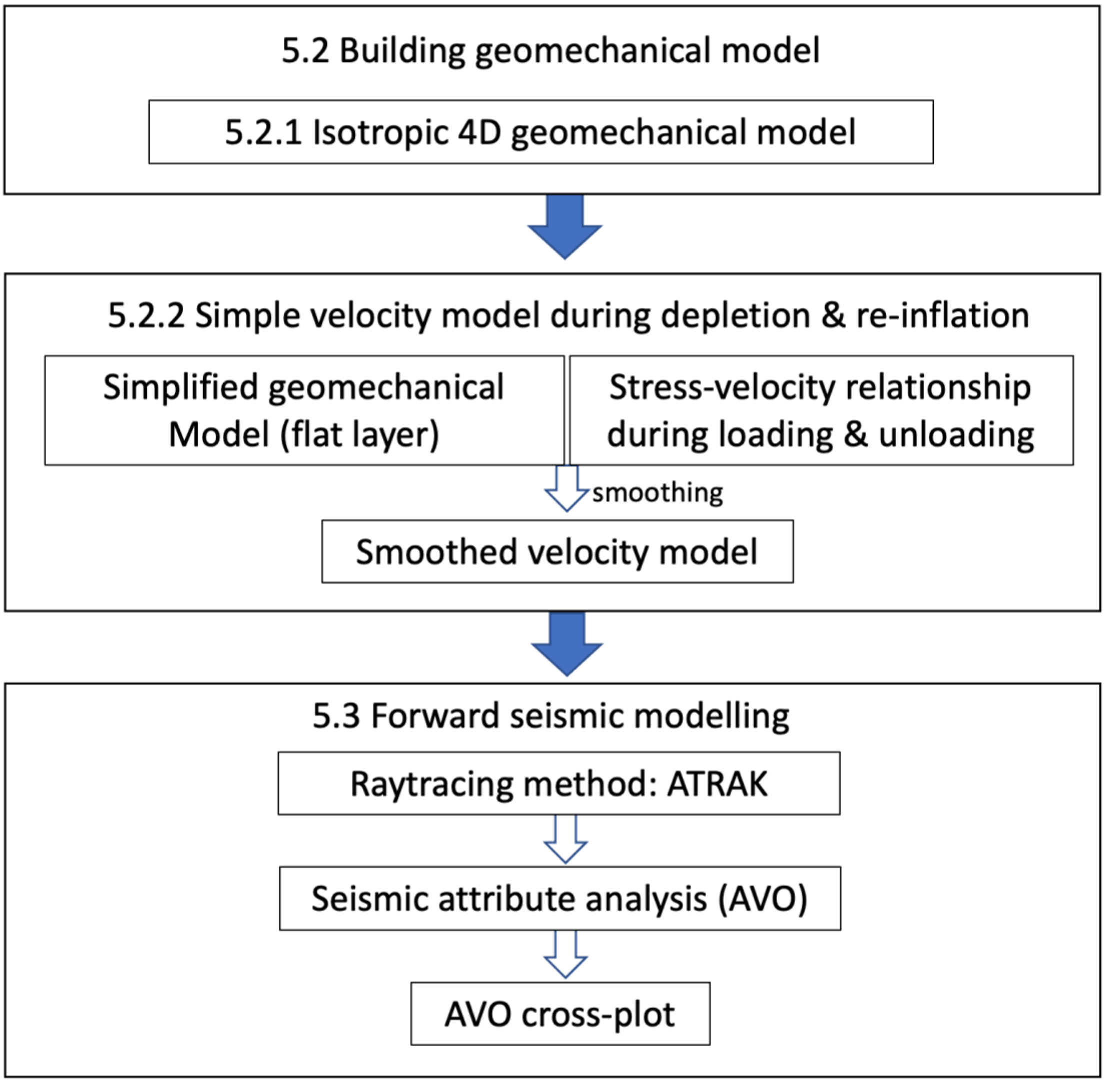

Figure 5-1 *Building model and seismic simulation flow chart.*

5.2.1 4D geomechanical model

The isotropic 4D coupled flow-geomechanical model was developed by MP Geomechanics Ltd., based on geological data from Snøhvit field in the Barent Sea (Botrill, 2016; Roach, 2017)The model consists total of 10 layers of surface and average velocity for each layer shown in (**Figure 5-2**). The inversion of Snøhvit geomechanical model (Roach, 2017) produces velocity models (*Vp* and *Vs*) within the Snøhvit field reservoir and includes three major faults as shown lower part of **Figure 5-2.** The model also simulated that the model uplifted approximately 22 cm at top reservoir after 10 years (2008-2018) of injection and around 10 cm of surface heave (**Figure** 5-3).

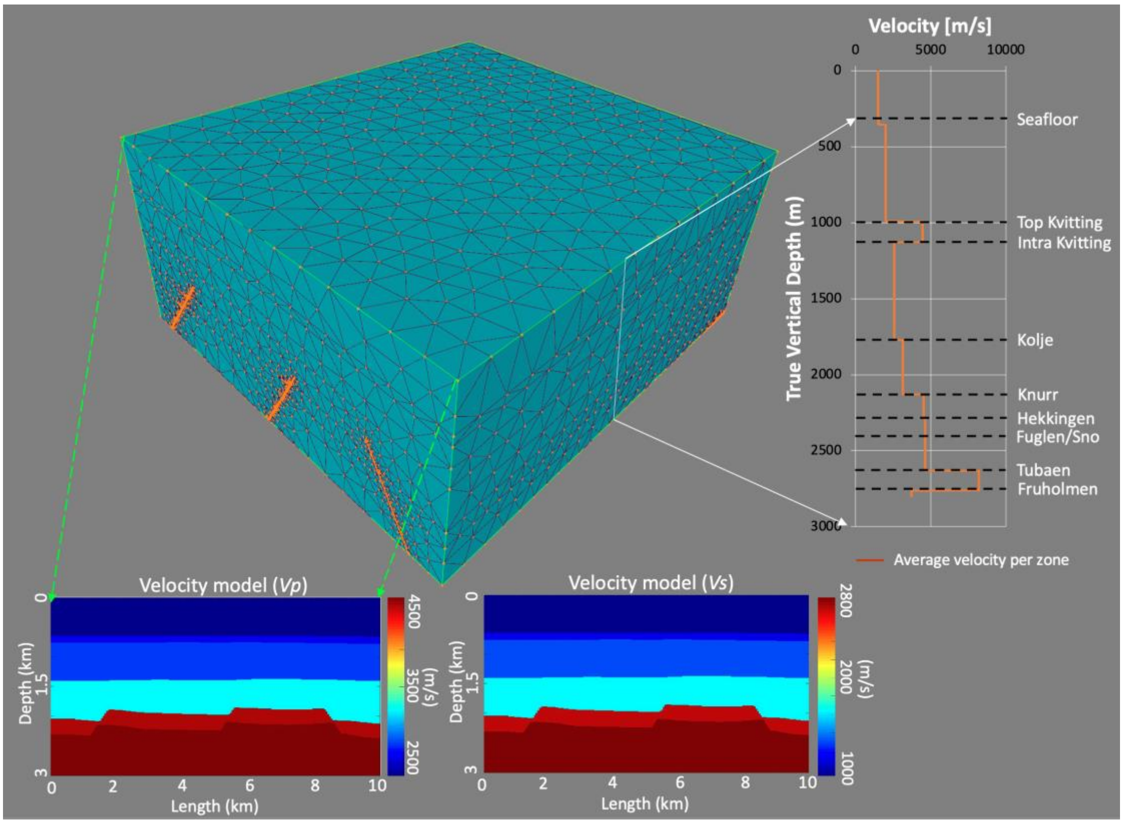

Figure 5-2 *Fully coupled hydro-geomechanical Snøhvit Field model. Extracted velocity model (Vp and Vs) from Snøhvit isotropic 4D geomechanical model.*

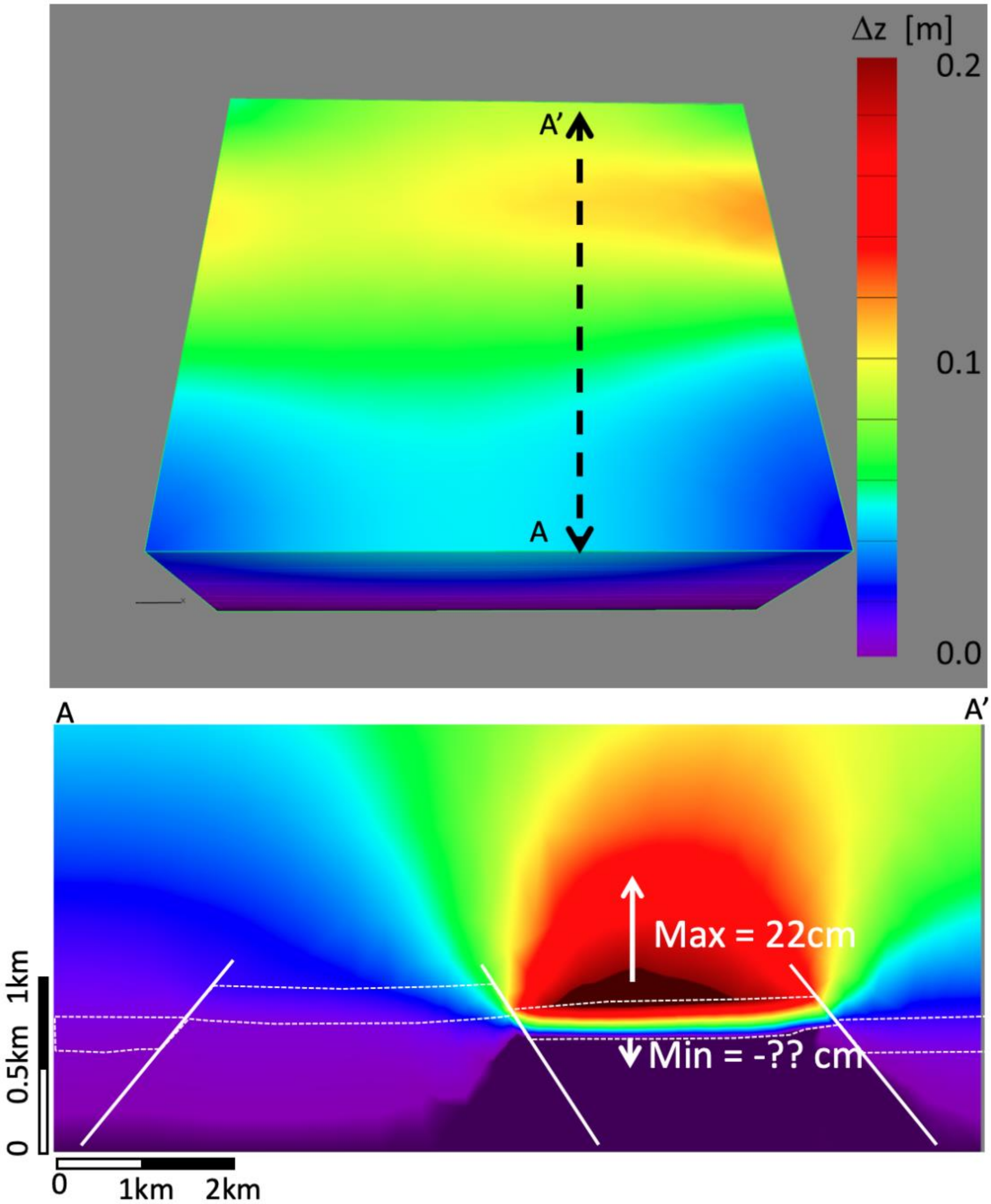

Figure 5-3 *Vertical displacement after 10 years (2008-2018) of injection and around 10 cm of surface heave and approx. 22 cm uplift at top reservoir.*

5.2.2 Simple velocity model during depletion and re-inflation.

As highlighted in **Figure 5-1**, the isotropic 4D Snøhvit geomechanical model in the Barent Sea is being used as basis to create a simple velocity model. This simple model consists of 6 layer, where the first layer is the water body and followed by 5 rock formation layers. The velocity (*Vp* & *Vs*) and density for the model for every layer shown in **Figure** 5-4**.** In this simulation, the influence of complex formation layering structure is neglected in order to focus on the impact of stress path change and fluid substitution induced perturbations on seismic properties. Thus, the flat layer velocity models (**Figure 5-5a**) were produced with fixed rock properties (e.g., *Vp, Vs* and density) followed by smoothing procedure with using high-frequency filter (**Figure 5-5b**). The main function of high-frequency filter is to remove any of the estimated travel-time shifts that are much smaller or larger than the specified values (e.g., Zacek, 2002; Selwood, 2010). This filtering approach may change slightly the velocity gradient within the horizon or layer to layer boundaries in the input model. The effects from smoothing procedure may alter the input model significantly (e.g. sharp structural edges), but the effect are considerably low when using simple (flat) structural input model as used in this analysis. The smoothed velocity procedure is compulsory (He, 2016) to allow seismic simulation (raytracing) were performed to analyse seismic response in the next stage..

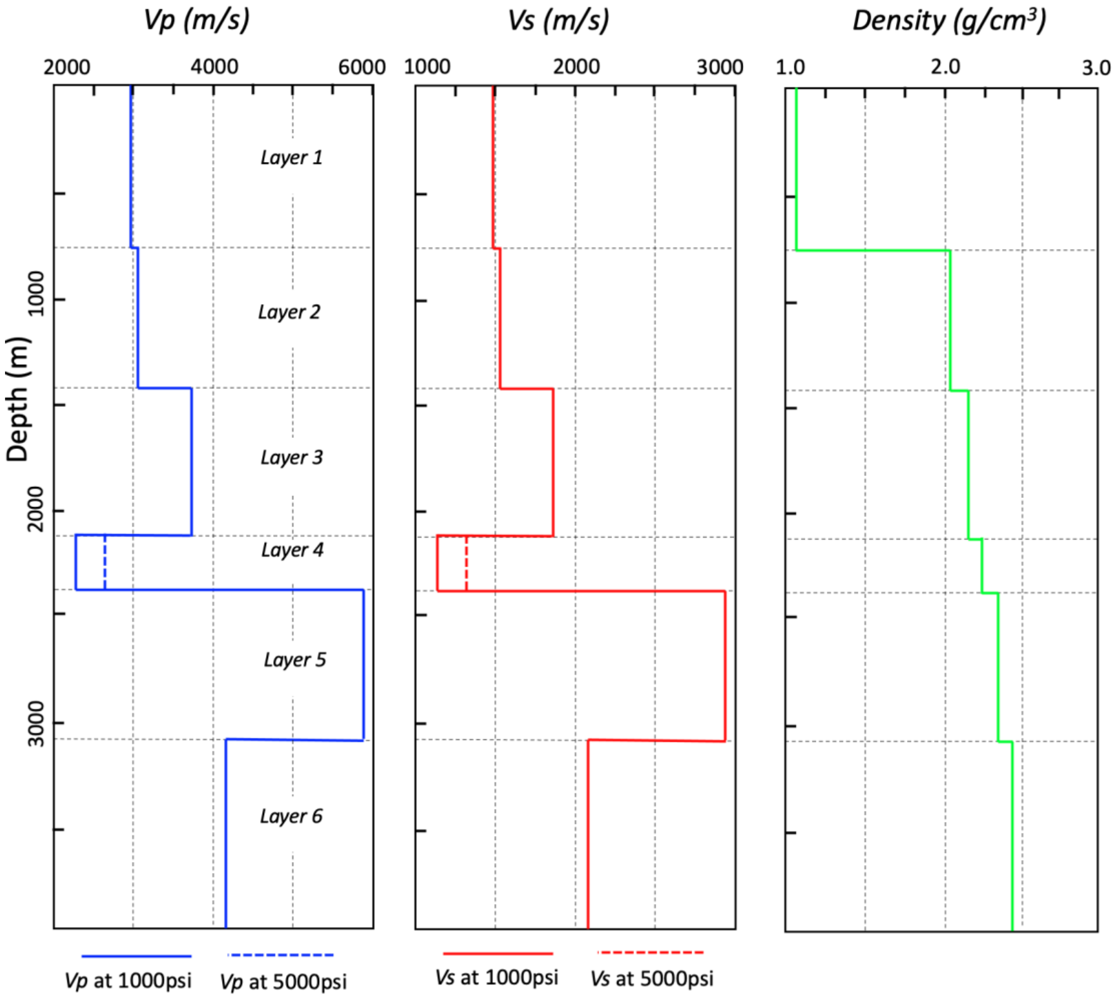

Figure 5-4 *Vp, Vs and density for every layer extracted from simplified geomechanical model.*

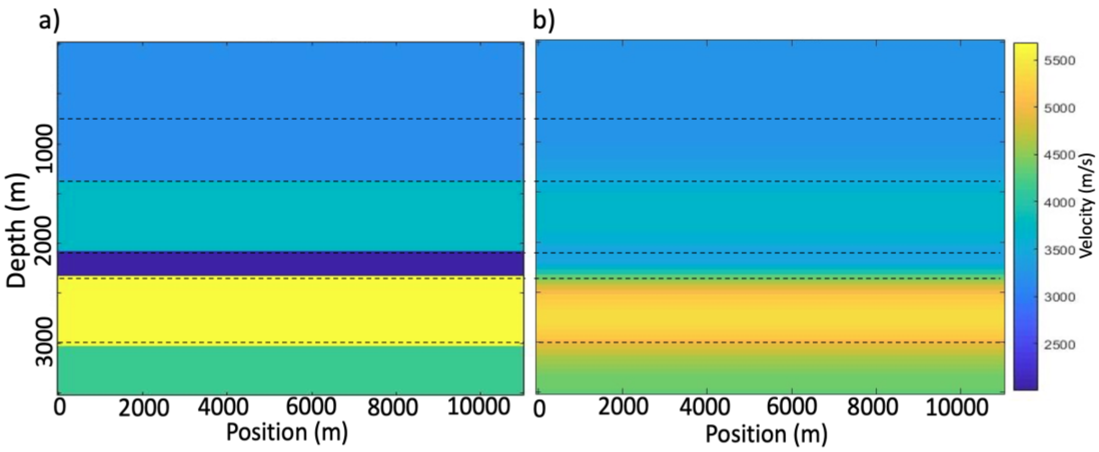

Figure 5-5 *a) Extracted and simplified Vp velocity model and b) smoothed Vp velocity model. The same smoothing procedure also applied for Vs velocity model.*

Velocity-stress relationships for the reservoir layer were measured in the laboratory to mimic stress changes during depletion and re-inflation experienced by the reservoir layer. This velocity-stress relationship (*Vp* and *Vs*) was measured using core samples of Upper Jurassic rock. The velocity measurement was also conducted by using the propagation of ultrasonic waves along rock cores under various confining pressures and later on added with fluid properties by using Gassmann theory that will discuss in section 5.3.2. This stress and fluid changes try to simulate stress changes in the reservoir in the field (e.g., Kern and Richter, 1981; Barruol and Kern, 1996; Burlini *et al*., 2005; Llana-Funez and Brown, 2012). The confining pressure were set to increase from 0 psi (0 MPa) up to 5000 psi (36 MPa) at a constant rate at 75 N/s and ultrasonic velocities (*P* & *S* wave) were measured at 1000, 2000, 3000, 4000 and 5000 psi. The confining pressure was then reduced with the same rate as during loading mechanism and ultrasonic velocities measured during unloading at 4000, 3000, 2000 and 1000 psi (**Figure 5-6*a***).

Finally, the simple velocity model with dimension of 11000 x 11000m and depth up to 3500 m were produced (**Figure 5-6*b***). The reservoir layer properties is based on the measurement in the laboratory, while velocity-pressure for overburden (3 layers) and under-burden (2 layers) remain constant and isotropic, as I assume these layers were sturdy and did not experience significant deformation as a consequence of production from followed by injection into the reservoir. This velocity model is then used in seismic forward modelling to simulate the seismic response.

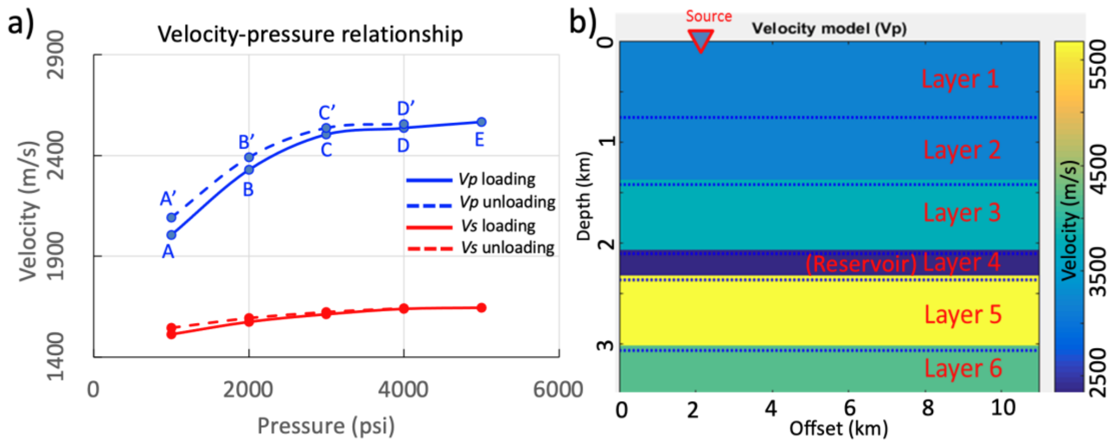

Figure 5-6 *a) Velocity-pressure relationship (Vp and Vs) of reservoir layer in layer 4 that acquire from core sample in the laboratory test. b) Simple velocity model with 6 horizons.*

5.3 FORWARD SEISMIC SIMULATION: RAYTRACING METHOD (ATRAK)

The raytracing method is used to model seismic propagation and can be adapted to simulate the seismic response of rock layers that are undergoing deformation as a result of pressure depletions. The ATRAK program (Guest & Kendall, 1993) is the raytracing software, which was used here to trace the propagation of seismic energy from various angles and monitor the seismic character under a range of stress paths. ATRAK program is constructed based on asymptotic ray theory and Hamiltonian solution. This approach allows travel-time effects to be studied in varying heterogeneous or anisotropic media and capable to analyse any distortion in amplitude or waveform (He *et al*., 2015).

5.3.1 AVO curve to AVO cross-plot: Gradient analysis.

ATRAK was used to calculate seismic response by using ray tracing approach (**Figure 5-7a**) and produce synthetic seismic gather as shown in **Figure 5-7b**. The gathers are conditioned so that they reference the same two-way time and the amplitude is extracted across a given time which also to represent the normal moveout, NMO procedure (**Figure 5-7c**).). In this analysis, the angle variations in amplitude for each reflecting interface in the AVO curve represent all the amplitude data as a single point on a cross-plot of intercept and gradient (**Figure 5-7d)**.

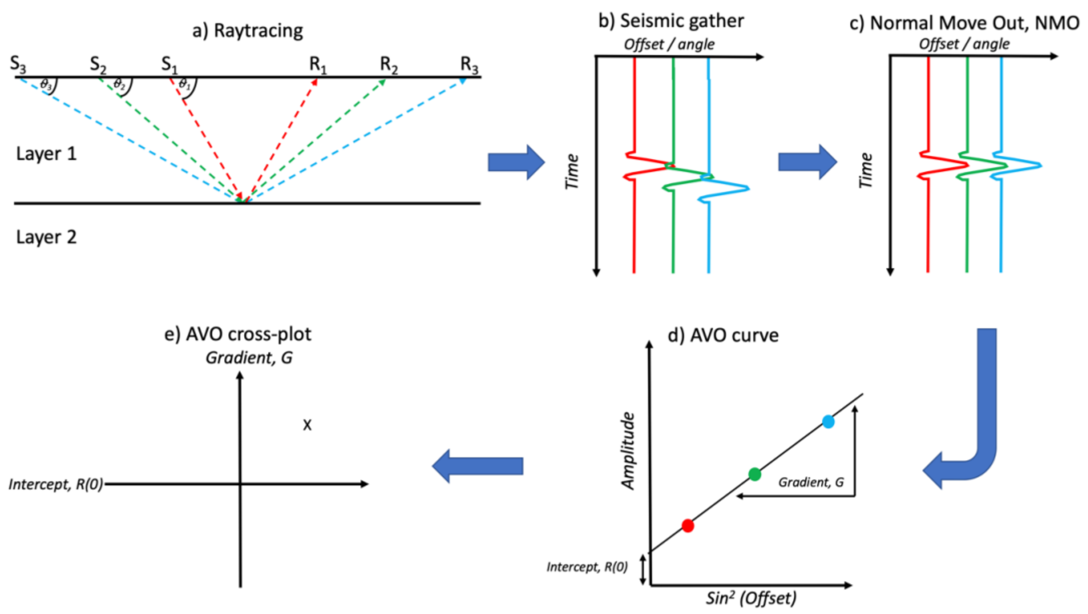

Figure 5-7 *Methodology for the construction of an AVO cross-plot from synthetic seismic and AVO curve.*

ATRAK programme by default calculate seismic as a function of offset instead of angle (degree). Thus, the offset need to convert into angle. Offset and angle are analogous but the relationship between the two is nonlinear relationship, that must first be taken into consideration in processing and analysis systems that normally require the angle to be used instead of offset (e.g., Russell, 2004). The incident angle is estimated from offset using as follow equation:

$$sin^2\theta = \frac{x^2 V_i^2}{V_r^2 (V_r^2 t_0^2 + x^2)}$$

Equation 5-1

Where;

x = Offset
V_i = Interval velocity
V_r = RMS velocity
t_0 = Zero offset two way time.

In this analysis, only angles of incidence less than 30° were considered since incident angle with more than 30° will require the third term in Shuey's approximation (involving S-wave) (Feng & Barncroft, 2006) and assumes small values for the angles normally observed in reflection seismology (Sheriff and Geldart, 1995). Each amplitude is then plotted against Sin^2 (offset) and a best-fit line is fitted using the 2-term Shuey Approximation (Shuey, 1985; Avseth *et al.*, 2005) which represents the how reflection amplitude varies as a function of offset into two components Intercept (*R*) and gradient (*G*) by using follow equations:

$$Intercept, R(\theta) \approx R(0) + G\, Sin^2\theta$$

Equation 5-2

Where;

$$R(0) = \frac{1}{2}\left(\frac{\Delta V_P}{V_P} + \frac{\Delta\rho}{\rho}\right)$$

$\Delta\rho = \rho_1 - \rho_2$
$\Delta V_P = V_{P1} - V_{P2}$

And

$$Gradient, G = \frac{1}{2}\frac{\Delta V_p}{V_p} - 2\frac{V_s^2}{V_P^2}\left(\frac{\Delta\rho}{\rho} + 2\frac{\Delta V_s}{V_s}\right)$$

Equation 5-3

In the formula above V_{P1} and V_{P2} are the P-wave velocities above and below given interface respectively. While ρ_1 and ρ_2 are densities above and below interface (Avseth *et al.*, 2005). The gradient (G) and intercept of this line are then plotted against each other (**Figure 5-7*e***) (e.g., Ross, 2010) and the process is repeated for all changes is pressure and stress path.

The advantage of the gradient vs. intercept plot is that a great deal of information can be presented and trends can be observed in the data that would be impossible to display on a standard offset (or angle) versus amplitude plot (e.g., Castagna *et al.*, 1998). The cross-plot is a useful way of examining differences in AVO responses that may be related to lithologic or fluid-type variations (Simm *et al.*, 2000).

5.3.2 Gassmann fluid substitution: hydrocarbon and water

The fluid type will affect the seismic response due to bulk moduli changes (Berryman, 2007). So, as well as taking into account the impact of geomechanical changes the analysis also considered the influence of changes in pressure and fluid saturation on seismic characteristics. Gassmann fluid substitution theory (Gassmann, 1951; Smith *et al.*, 2003) was used to calculate the impact of changes in fluid composition on seismic velocities.

Four stages of fluid properties were created to demonstrate the fluid substitution in the reservoir (**Table 5-1**). At the first stage, it was assumed that the reservoir was saturated with 80% hydrocarbons and 20% brine. For every stage, the ratio of hydrocarbon to water were changed as the secondary recovery procedure (i.e., water flooding) was conducted. This hydrocarbon to water ratio was continually changed until 100% water saturation was achieved during stage 4. During the fluid substitution procedure (from stage 1 until 4), *Vp* and *Vs* response were estimated by using Gassmann fluid substitution formula as shown in **Equation 5-4** until **Equation 5-9**. This *Vp* and *Vs* were then used to produce the new velocity model, which is then input into ATRAK for raytracing analysis. This step was repeated for every fluid substitution stage to produce synthetic seismic for every fluid ratio that exist in the pore space in the reservoir and the results were compare for seismic attributes analysis during fluid substitution.

Table 5-1 Fluid ratio in the reservoir during fluid substitution

Fluid substitution	Fluid properties (%)	
stages	Hydrocarbon	Water
1	80	20
2	50	50
3	20	80
4	0	100

The Gassmann theory most commonly used as theoretical approach for fluid substitutions. The equation relates the saturated bulk modulus of the rock (K_{sat}) to its porosity ($\emptyset$), the bulk modulus of the porous rock frame (K^*), the bulk modulus of the mineral matrix (K_0), and the bulk modulus of the pore-filling fluids (K_{fl}) as:

$$K_{sat} = K^* + \frac{(1 - \frac{K^*}{K_o})^2}{\frac{\emptyset}{K_{fl}} + \frac{(1 - \emptyset)}{K_o} - \frac{K^*}{K_o^2}}$$

Equation 5-4

Before using **Equation 5-4**, the properties of the rock need to be defined, including porosity, fluid properties (in every stages), matrix bulk modulus and the bulk modulus of the porous rock frame. All these properties could be defined and acquired through laboratory measurement. Whether from velocity measurements in the laboratory or from wireline log data, the saturated bulk modulus of a rock, K_{sat}, can be related to its compressional velocity (Vp), shear velocity (Vs), and bulk density (ρ_B) using the following relationship:

$$K_{sat} = \rho_B \left(V_p^2 - \frac{4}{3} V_s^2 \right)$$

Equation 5-5

The fluid and grain density also need to be known to perform fluid substitution. The relationship between the fluid density (ρ_{fl}), porosity (ϕ), grain density (ρ_g), and bulk density (ρ_B) can be simplified as follow:

$$\rho_B = \rho_g (1 - \emptyset) + \rho_{fl} \emptyset$$

Equation 5-6

The fluid substitution analysis involving substitution of two types of fluid, implying a two-component hydrocarbon-water system, can be represented as in as follow:

$$K_{fl} = \left[\frac{S_w}{K_w} + \frac{1 - S_w}{K_{hc}} \right]^{-1}$$

Equation 5-7

Where:

K_{fl} = the bulk modulus of fluid

K_w= the bulk modulus of the water

K_{hc}= the bulk modulus of the hydrocarbon

S_w= water saturation

Finally, the *Vp* and *Vs* could be determined by using **Equation 5-8** & **Equation 5-9** respectively.

$$V_p = \sqrt{\frac{K + \frac{4}{3}\mu}{\rho}}$$

Equation 5-8

Where K and μ are the bulk and shear moduli.

$$V_s = \sqrt{\frac{\mu}{\rho}}$$

Equation 5-9

5.4 RESULTS

A simple velocity model (**Figure 5-6*b***) was used as the input model for seismic simulation analysis by using ATRAK. The input model for ATRAK is considered as 2.5D, where there is variation in X and Z axis, and the Y-axis is assumed to be infinite. There is no variation in structure such as major fault or compartmentalization effects along the X direction due to smoothing procedure during building the velocity model. All the seismic response in the results in this section were trace by using ATRAK by using this smoothed velocity model.

5.4.1 Forwarded model: Synthetic seismic during loading and unloading.

The ATRAK program computes the transmission coefficient and reflection for each of the ray as a function of azimuth and offset, then generates synthetic seismograms. The output of the program consists of three components; a ray-traced model, synthetic seismic and amplitude versus offset (AVO). **Figure 5-8** show the traced seismic wave simulated via a convolutional step where an assumed source wavelet is convolved at the simulated travel times for each of the horizons. There are 5 horizons in the model since there are 6 rock layers. The ATRAK program managed to trace the seismic propagation for all the layers in the simple velocity model that was built earlier (Section 6.2). The seismic source is located at *X*=3500m and all the reflected waves are traced up to 4000m from the surface; receiver locations are fixed at the surface, spanning 0 to 11,000 mm.

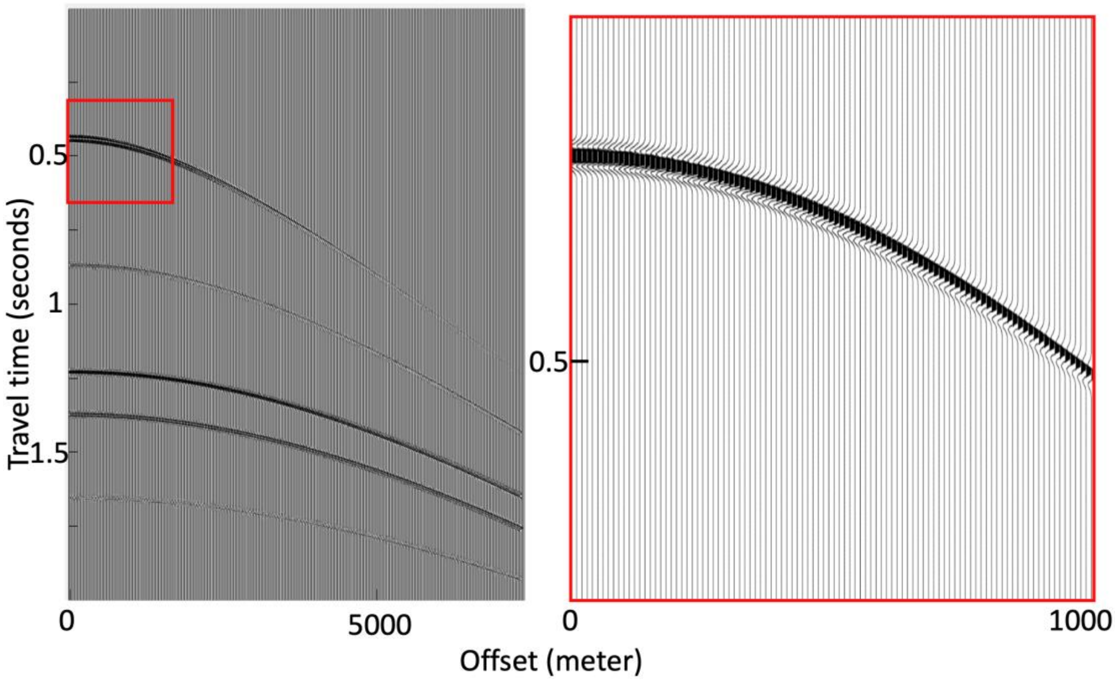

Figure 5-9 shows the results of the synthetic seismic response that was produced based on the traced seismic wave propagation in the model. This synthetic seismic generated by ATRAK are produced by interpolation of travel-time curves and convolution with a specified wavelet, and the results also show the amplitude change with offset. The seismic sources (located at 2500m) were simulated by using a zero-phase Ricker wavelet with temporal sample of 1ms and central frequency of 30Hz. The multiple source-receiver offsets are vary from to 7500 m. The receiver spacing are set 12.5 m in this simulation.

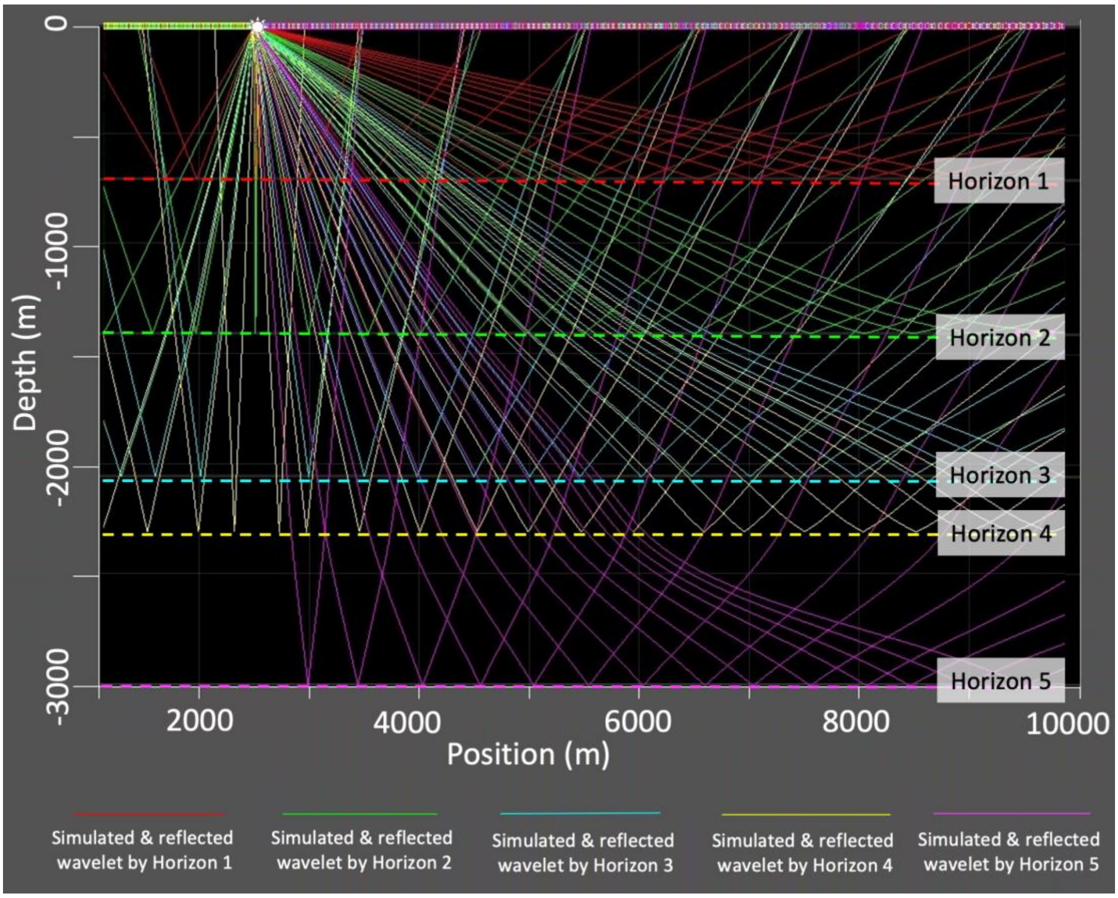

Figure 5-8 *Raytracing in ATRAK with the seismic wave is traced up through all the five horizons of velocity model with depth of 3000m and 10000m of length.*

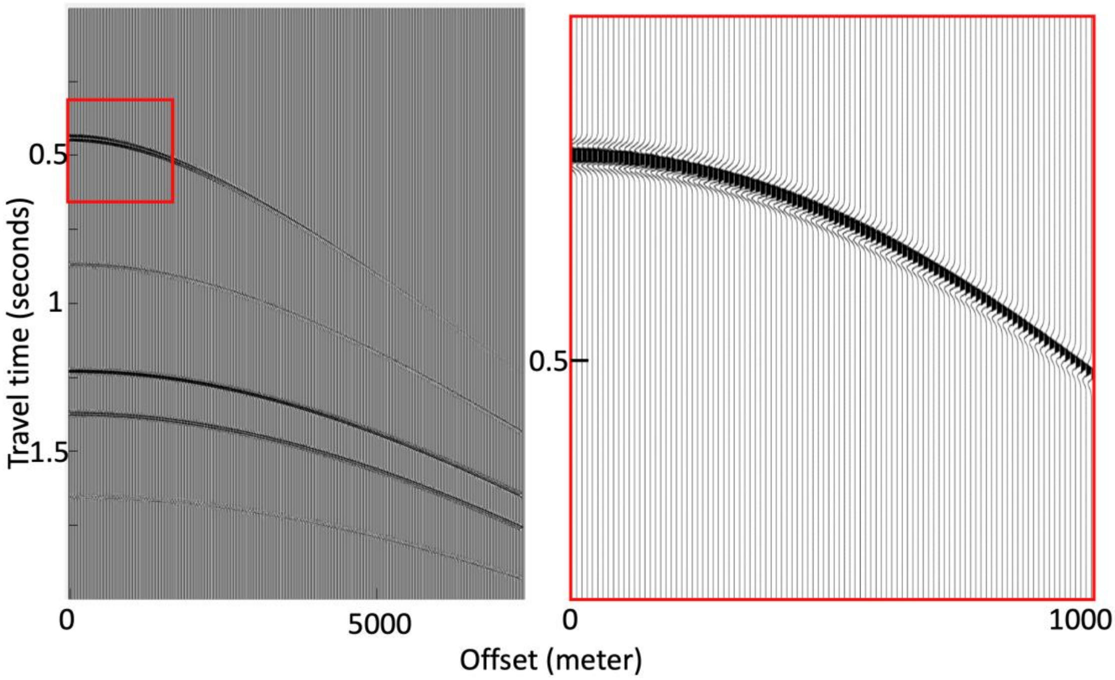

Figure 5-9 *Synthetic seismograms in ATRAK that produced from simple velocity model. Zoom in synthetic seismic (right side of the figure) indicate the variation of amplitude with offset for first reflection (red box).*

5.4.2 Amplitude versus offset (AVO) curve.

From the synthetic seismic, the AVO responses were produced for each layer. The AVO response were produced for every 1000 psi change in pressure up to 5000 psi through both loading and unloading cycles. **Figure 5-10** shows the results of AVO response during pressure at 1000psi(loading) to 5000psi (loading) and unload back to 1000psi (unloading). Response for horizon 1 were removed due to insignificant change. The most significant change were indicated by AVO response at horizon 3 and 4. Comparison AVO response at the same pressure state during loading and unloading as shows in **Figure** *5-11*. This is allow quantitative analysis of AVO response during stress change and this will be discuss further in the discussion section (5.5.2 Amplitude change during loading and unloading).

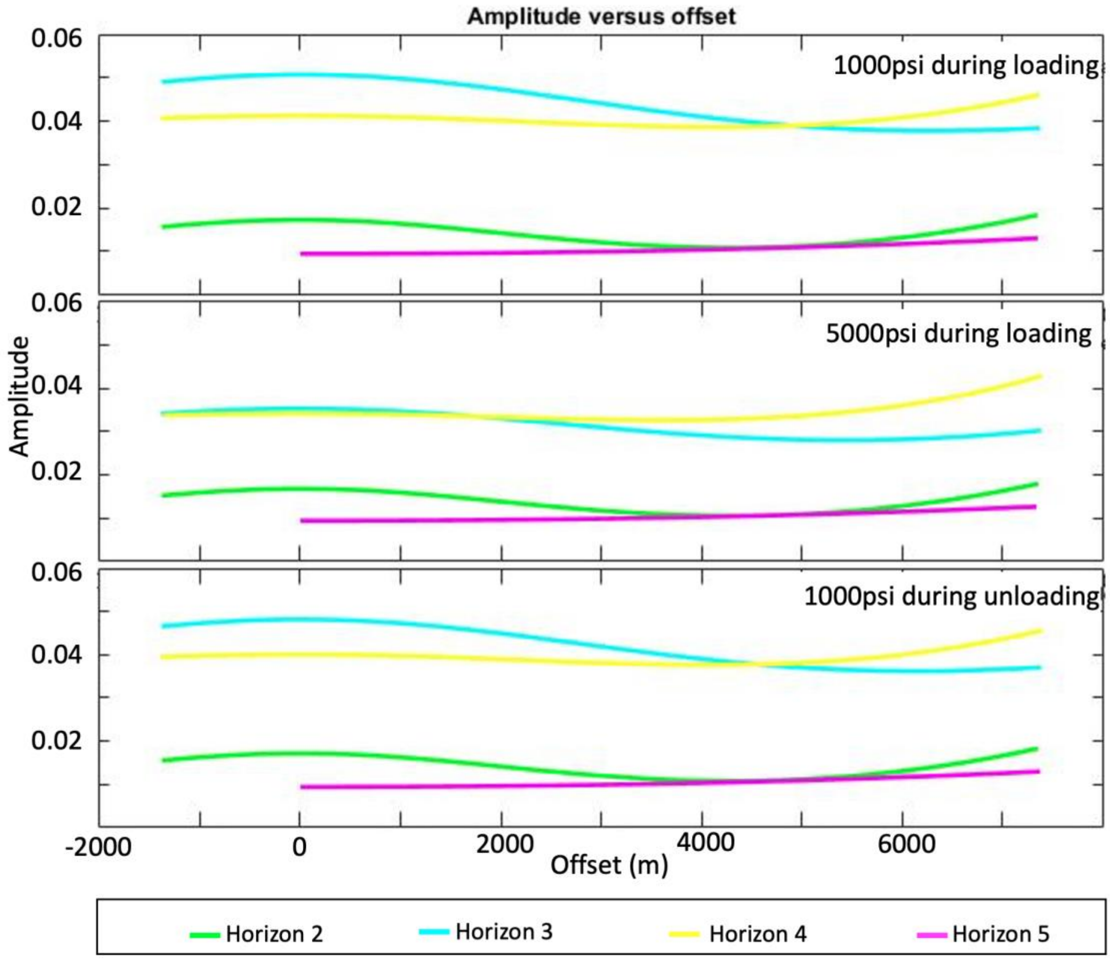

Figure 5-10 *AVO curve shows the seismic reflection coefficients for P-wave with pressure change from loading at 1000psi until 5000psi and then unloading at 1000psi. In this plot, Horizon 1 were removed due to insignificant variation during stress change.*

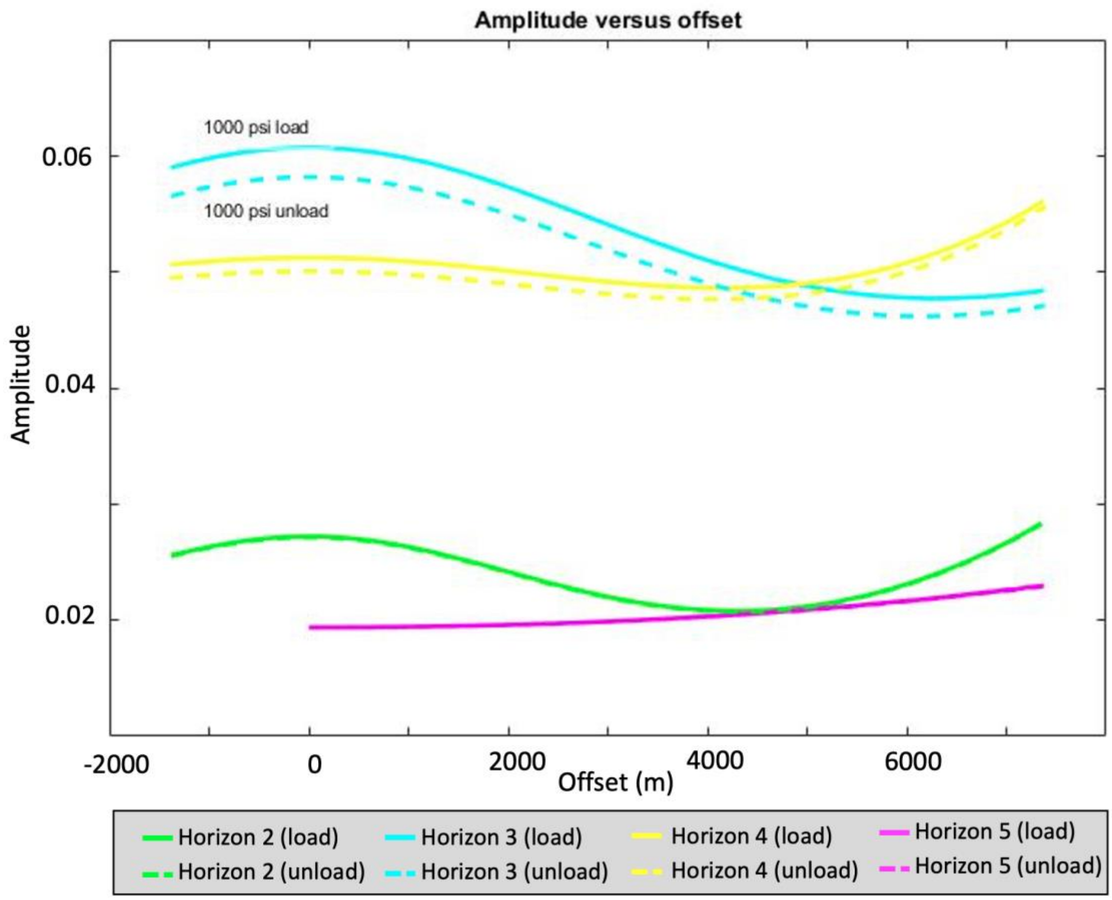

Figure 5-11 *Comparison of AVO response at 1000psi during loading and unloading.*

5.4.3 AVO cross-plot

Amplitude variation in each of the horizons are shown on the cross-plot diagram (**Figure 5-12**). Cross-plot of Horizon 1 data (red) shows an intercept value of 0.118 and gradient -0.162, which are considered as outliers from the other horizons that have range of intercept 0-0.04 and range of gradient within 0 to -0.02. This consideration also reflects that there is small velocity and density contrast at Horizon 1 (**Figure** 5-4). This situation is different for Horizon 2 until Horizon 5, which shows the clear variation of the velocity and density for upper and lower layer of the respected Horizons. The differences of physical properties in Layer 1 have cause the AVO cross-plot for these horizon shows different pattern compare to the other four horizons.

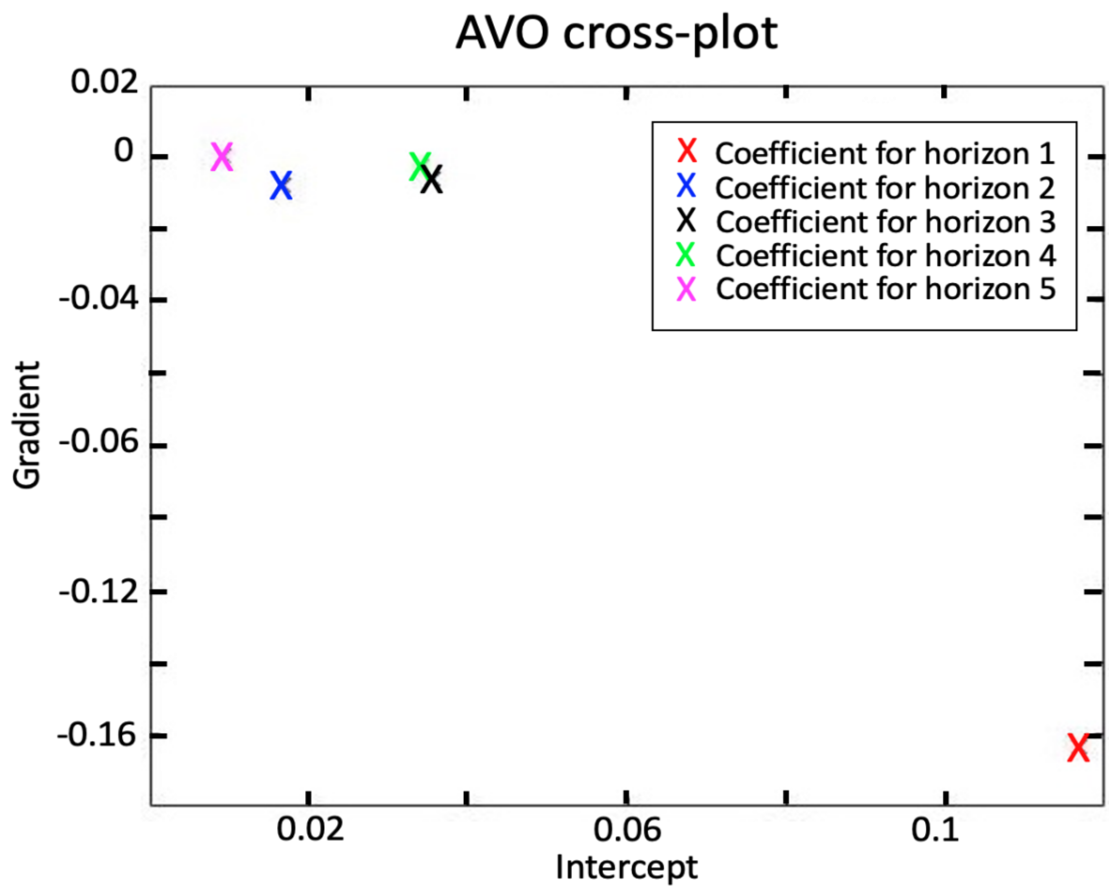

Figure 5-12 *Typical AVO cross-plot for every layer in the model. Red, blue black, green and magenta indicated the first, second, third, fourth and fifth horizon respectively.*

5.4.4 Fluid substitution

The calculated *Vp* and *Vs* during loading and unloading with variation of fluid properties shown in **Table** 5-2**.** This results then plotted as pressure versus velocity curve during fluid substitution shown in **Figure 5-13a.** The results indicate that the stress dependant velocity is also influenced by the existence of fluid in the pore space of the rock as shown by comparison of dry sample and saturated sample (mixture of hydrocarbon and water), which both indicate the velocity variation during stress path change. The results indicate that the P-wave velocity increases as hydrocarbons were replaced by water (from 80% of hydrocarbon to 0% of hydrocarbon) and give significant difference of pressure versus velocity curve and **Figure 5-13*b*** shows the percentage of this variation for each of stage during the fluid substitution. Dry samples give higher velocity variation during stress path change with ranging of 4.2%, while the saturated sample shows the maximum variation ranging from 1.4 to 2.3% depending on the hydrocarbon-water ratio. The cross-plot of bulk modulus during dry and saturated during stress path change from loading to unloading (**Figure 5-14**) as it is known that bulk modulus were change during fluid substitution. The results indicates that the compressibility of the rock samples becomes higher when water replaces hydrocarbon since water has a higher bulk modulus than hydrocarbon with 2.2 GPa versus 1.3 GPa, respectively.

Table 5-2 V_p and V_s during loading and unloading with fluid substitution for reservoir layer (Layer 4).

Stress path	**Pressure (psi)**	***Vp* (m/s)**	***Vs* (m/s)**
Pore filled with 80% oil & 20% water			
Load	1000	2924.49	1673.92
Load	2000	3103.72	1744.33
Load	3000	3207.56	1786.85
Load	4000	3237.88	1818.31
Load	5000	3257.48	1825.39
Unload	4000	3249.28	1822.46
Unload	3000	3228.61	1800.14
Unload	2000	3140.67	1764.77
Unload	1000	2976.23	1710.90
Pore filled with 50% oil & 50% water			
Load	1000	3004.92	1675.36
Load	2000	3172.97	1745.80
Load	3000	3270.84	1788.34
Load	4000	3300.57	1819.82
Load	5000	3319.22	1826.89
Unload	4000	3311.25	1823.97
Unload	3000	3290.83	1801.64
Unload	2000	3207.82	1766.25
Unload	1000	3053.86	1712.36

Pore filled with 20% oil & 80% water			
Load	1000	3104.47	1676.79
Load	2000	3259.36	1747.26
Load	3000	3350.12	1789.83
Load	4000	3379.12	1821.32
Load	5000	3396.63	1828.39
Unload	4000	3388.95	1825.48
Unload	3000	3368.84	1803.14
Unload	2000	3291.72	1767.73
Unload	1000	3150.13	1713.82
Pore filled with 0% oil & 100% water			
Load	1000	3185.28	1677.74
Load	2000	3330.04	1748.24
Load	3000	3415.26	1790.82
Load	4000	3443.65	1822.32
Load	5000	3460.26	1829.39
Unload	4000	3452.82	1826.48
Unload	3000	3432.98	1804.14
Unload	2000	3360.47	1768.72
Unload	1000	3228.44	1714.80

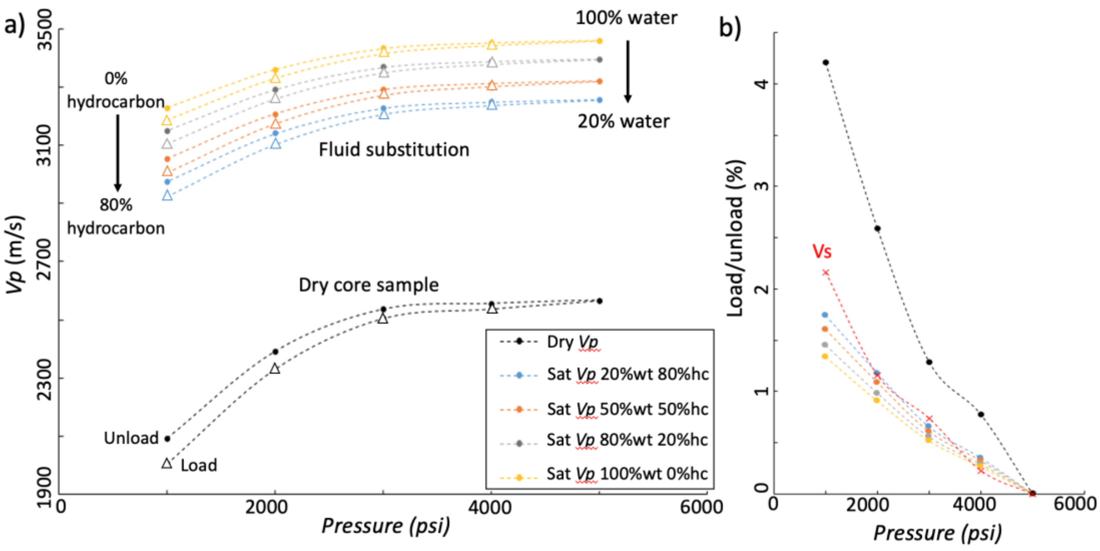

Figure 5-13 *a) Vp variation as a results fluid saturation changes from 80% hydrocarbon (hc) and 20% water (wt) to 0% hydrocarbon and 100% water (via*

Gassmann's substitution theory) during loading and unloading. b) Difference (%) of Vp during loading and unloading for sample with different fluid saturation.

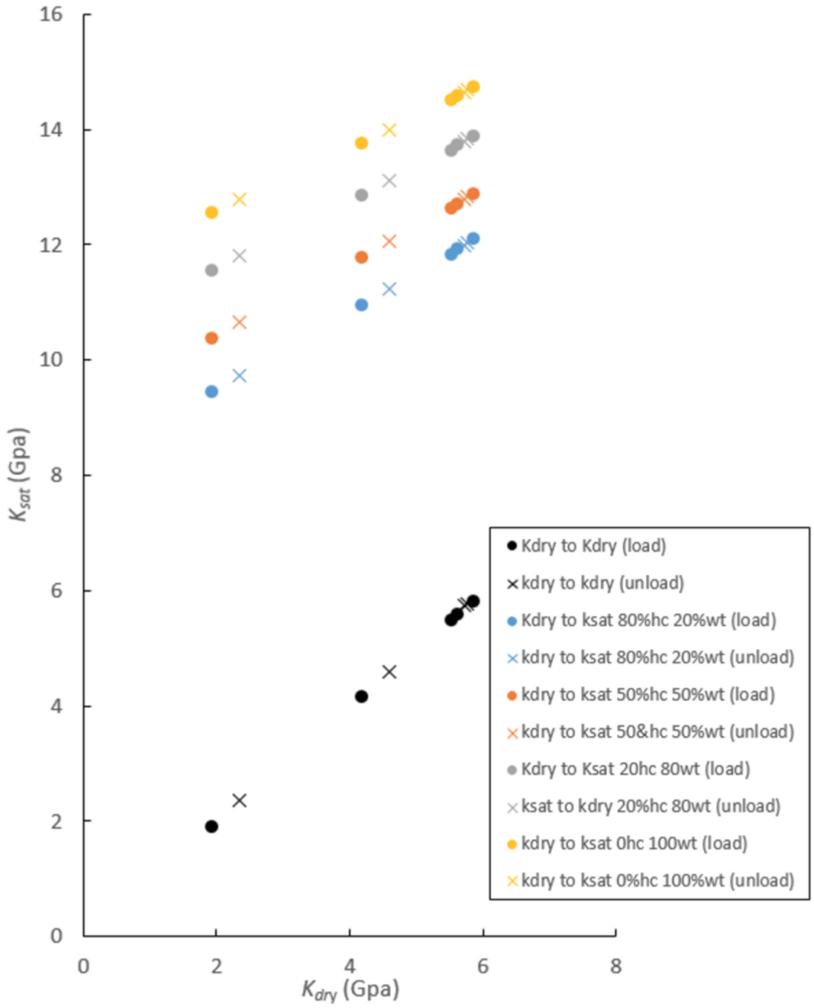

Figure 5-14 *Bulk modulus, k variation during stress path changes and fluid substitution. The different colour of the plot indicates different percentage of hydrocarbon (hc) and water (wt) as the fluid properties.*

5.5 DISCUSSION

The simple six-layer velocity model is used to examine the influence of stress path change in which the reservoir is produced for 10 years before being inflated as a result of water injection. The reduction of pressure in the reservoir layer (estimated drop in 3000psi within 10 years) represented as depletion (loading) effects in the model where is clearly give difference of stress dependant wave velocity curve during re-inflation (unloading) due to water flooding. In this section, comparison of seismic time-shifts and

AVO responses are explored in connection with the stress change in the reservoir. Even though the reasons for the difference in prevalence of slowdown and speedup of seismic wave that cause time-shift in seismic is not entirely clear (Macbeth, 2019). Thus, the sensitivity of seismic response towards velocity changes due to geomechanical and/or fluid change during loading and unloading should be compare in order to justify any potential pattern that may lead seismic prediction misfit.

5.5.1 Time shift during loading and unloading.

The synthetic seismic traces were then gathered for every 1000psi changes of stress during loading and unloading (**Figure 5-15**) **.** To analyse the data in detail, the seismic synthetic from offset $\approx 0^o$ from each of pressure level were acquired then the wave amplitudes were compared between loading and unloading at the same pressure state. Detail analysis of seismic travel-times through loading and unloading cycles shows detectable time-shifts in seismic propagation (**Figure 5-15**). The magnitude of these shifts appears to be increased during lower effective stress (1000 psi).

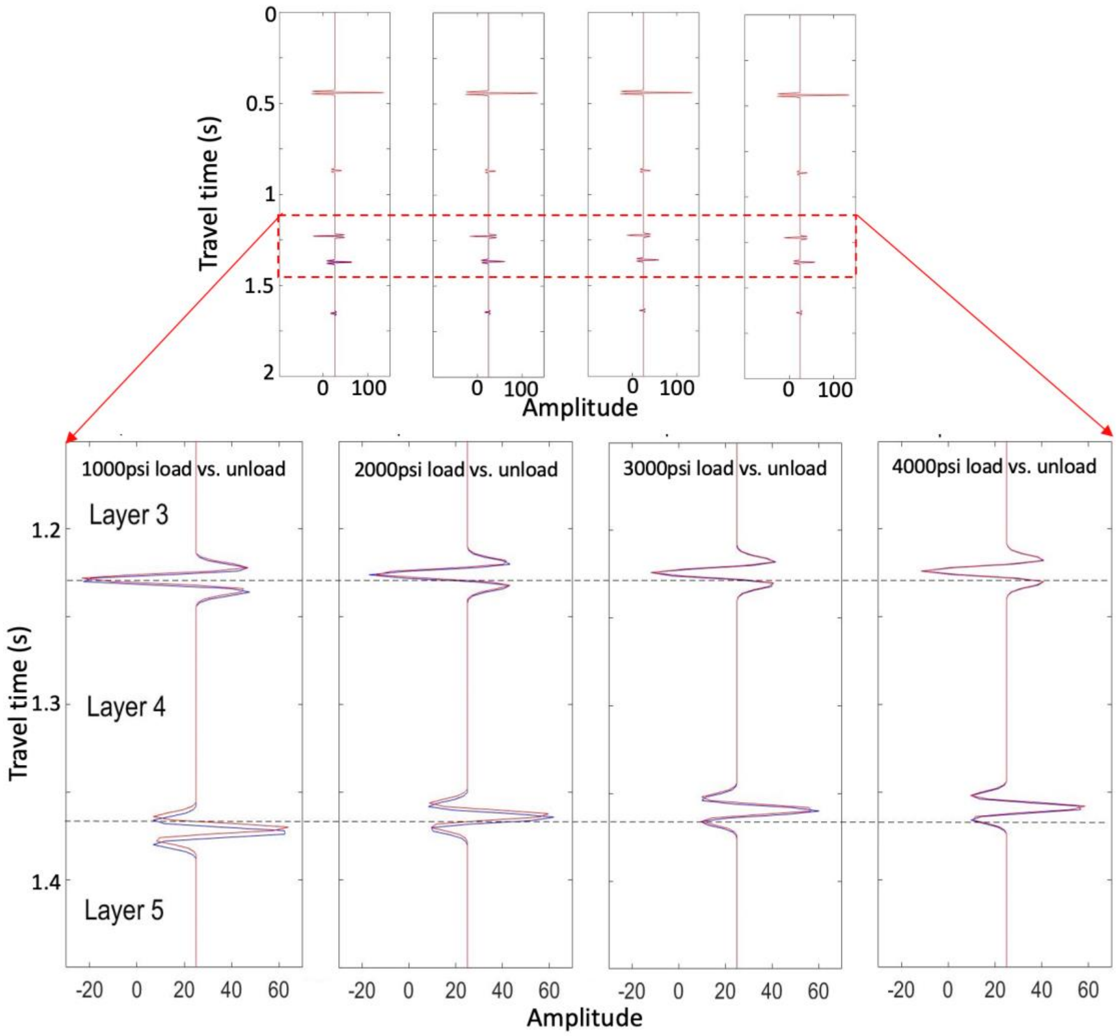

Figure 5-15 *Top) Synthetic signals at zero offset extracted from the seismic synthetic data for every 1000psi changes of pressure for both condition of stress path, load and unload. Bottom) Seismic traces during loading (red) and unloading (blue) cycles.*

Table 5-3 *Time shift during stress path change.*

Stress path	Pressure (psi)			
	1000	2000	3000	4000
Horizon 3				
Travel time during loading (s)	1.228	1.226	1.224	1.224
Travel time during unloading (s)	1.230	1.226	1.224	1.224
Time-shift (s)	0.002	0.00	0.00	0.00
Horizon 4				
Travel time during loading (s)	1.370	1.362	1.360	1.358

Travel time during unloading (s)	1.374	1.364	1.360	1.358
Time-shift (s)	0.004	0.002	0.00	0.00

The variation of time-shifts concurs with the fully-coupled hydro-mechanical simulations of Hawkins *et al.* (2008), who suggest that time-shifts could expressed at the top of the field are less than 2 ms. In this simulation, time-shift of 0.002s (2ms) expressed at the top (Horizon 3) of the reservoir layer and 0.004s (4ms) at the bottom reservoir (horizon 4) (**Table** *5-3*). This time shift were happened during stress change in the reservoir were loading at 1000psi and unloading 1000psi. This also suggest that the variation of the time-shifts getting smaller or undetected for higher pressure. For example, the time-shift did not detected as the pressure at 3000psi or higher. The time-shift behaviour may differ with different effective stress patterns, which also gives larger variation of time-shift at the bottom layer of the reservoir (Horizon 4) compared to the top layer of the reservoir (Horizon 3). The time-shift variations also potentially accommodate the stretching or compacting mechanism in the under- and over-burden during loading (pressure decrease in reservoir layer) and during unloading (pressure increase in reservoir). Small time-shits are observed for the overburden, they are insignificant and almost undetectable for the under-burden.

Table 5-4 *Time shifts during stress change in active reservoir (After MacBeth et al., 2019)*

Reservoir lithology	Field name	Reservoir thickness (m)	Overburden thickness (m)	Time-shift Δt	Reservoir pressure down ΔP (MPa)
Overburden slowdown					
HPHT	Mars	60	1220	15.0	30.0
PC sand	Genesis	60	4000	11.0	20.0
Con sand	Europa	38	1120	8.0	27.5
HPHT	Holstein	85	3700	7.0	20.0
Con sand	Snorre	60	2350	5.0	15.0
Carbonate	Sarawak	55	1650	4.0	4.5
Con sand	SGB	105	2500	2.4	20.0
HPHT	Kristin	110	5000	2.0	30.0
Con sand	Curlew D	250	3050	1.5	33.0
HPHT	Elgin	170	5300	0.8	20.0
Reservoir slowdown					
PC sand	Enfield	52	2100	6.0	11.7
PC sand	Baobab	152	2365	5.0	14.7
Con sand	Norne	225	2500	3.0	20.0
Con sand	Schiehallion	30	1950	1.0	17.0
Chalk	Valhall	40	2400	1.0	2.0
PC sand	**Peace River**	25	545	0.5	5.0
Reservoir speedup					
Chalk	Valhall	40	2400	3	7.0
PC sand	Troll East	175	1330	2	1.5
HPHT	Shearwater	213	4572	2	53.0
Con sand	SGB	150	2100	1.8	12.4
Carbonate	Sarawak	55	1650	1.5	4.5
Con sand	Schiehallion	30	1950	1	15.0
HPHT	Elgin	170	5300	0.4	50.0
Chalk	Ekofisk	175	3000	0.3	4.13
Con sand	Curlew D	250	3050	0.2	34.0

*Poorly consolidated sand (PC sand), consolidated sand (Con sand), high pressure high temperature (HPHT).

The synthetic seismic simulation in this chapter is noise free and simple in geometry. Compare to real field, the reservoir structure are more complex and typically the seismic response in seismogram consist of noise during data acquisition. Even so, based on data from active reservoir around the world (Table 5-4), time shift also detectable and occur in the real field. Typically, the time shift in the overburden is much smaller than that in the reservoir (MacBeth *et al.*, 2019) which similarly shown by synthetic seismic response in this chapter. Some of the overburden shows dramatic time shift with 15ms (slowdown) during the pressure down with 30 Mpa (4351 psi). In some case such as higher pressure situation (more than 3000 psi), small pressure changes produce undetectable time shift, as a results give very small implication in the P-wave velocity. This situation suggest that, the time-shifts could be a valuable thing to look at for the low-pressure settings. But for high-pressure setting or reservoir, the time shift is almost undetectable.

5.5.2 Amplitude changes during loading and unloading

Figure 5-16 and **Figure 5-17** show the change of P-wave reflection magnitude in the AVO curves for horizon 3 (top reservoir layer) and horizon 4 (bottom reservoir layer). The results show the impact of stress path variations induced change in seismic velocity, which is detectable on the P-wave reflection coefficients differences during stress path change and these differences decrease with further offset (e.g., Kudarova *et al.,* 2016). For Horizon 3, there are noticable differences in reflection amplitude changes where every pressure change gives variable range of difference pressure. The amplitude differences were analysed from three different range of offset which is near offset (0-2500m), medium offset (2500m-5000m) and far offset (5000m-7500m) as shown on **Table 5-5**. Near offsets show the biggest difference of seismic amplitude during loading and unloading for Horizon 3 (e.g., at pressure of 1000 psi the difference at 5-4.99%). The differences getting smaller with the increment of the offset as seen in medium offset (e.g., at 1000 psi the amplitude difference at 4.99-4.69%) and far offset indicating the smallest difference (e.g., at 1000 psi the amplitude difference at 4.69-3.64).

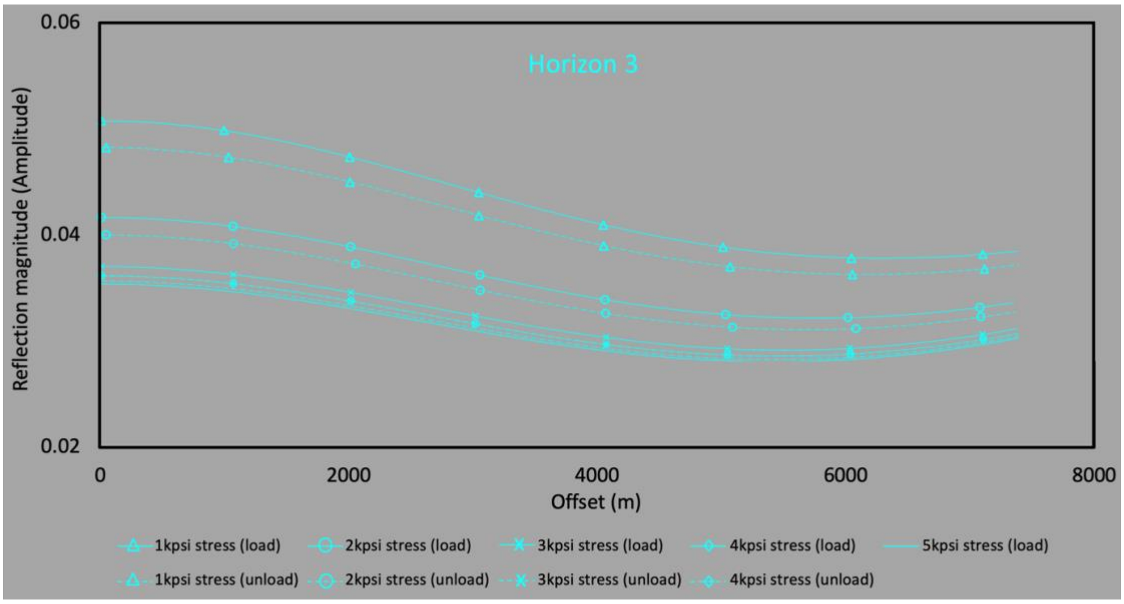

Figure 5-16 *AVO curve for Horizon 3 (top layer of Layer 4) for P-wave during loading (solid line) and unloading (dashed line).*

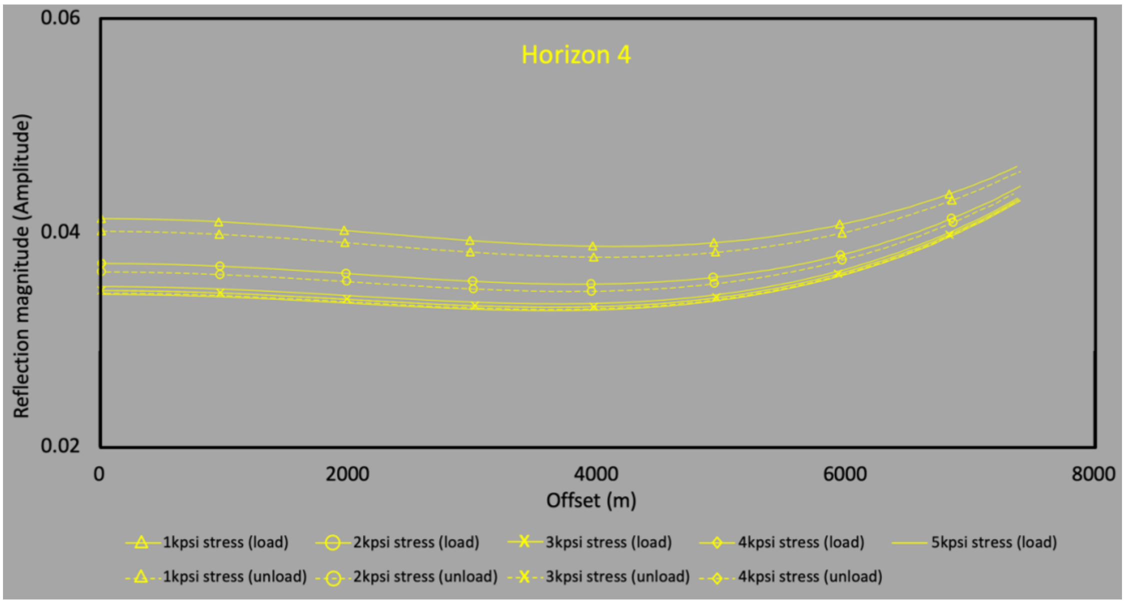

Figure 5-17 *AVO curve for Horizon 4 (bottom layer of Layer 4) for P-wave during loading (solid line) and unloading (dashed line).*

Table 5-5 Amplitude difference during loading and unloading for Horizon 3. Near offset = 0 to 2500m, Medium offset= 2500-5000m, Far offset= 5000-7500m.

Horizon	Pressure (psi)	Offset (m)	Amplitude difference during load vs unload (%)	Full stack amplitude difference (%)
3	1000	Near offset	5.00-4.99 %	
		Medium offset	4.99-4.69%	4.77 %
		Far offset	4.69-3.64%	
	2000	Near offset	4.02-3.97 %	
		Medium offset	3.97-3.59%	3.80 %
		Far offset	3.59-2.61%	
	3000	Near offset	2.33-2.30 %	
		Medium offset	2.30-2.07%	2.20 %
		Far offset	2.07-1.51%	
	4000	Near offset	1.44-1.41 %	
		Medium offset	1.41-1.26%	1.35 %
		Far offset	1.26-0.91%	

The same situation indicated by Horizon 4 in which the bottom part of the reservoir layer with near offset gives higher amplitude difference, which get smaller as offset increases (**Table 5-6**). The partial stacks of near, medium and far offsets were initially generated to analyse the variation of seismic signal with the offset. The partial stacks obtained together with stacking velocities based on interval velocity (Near offset = 0 to 2500m, Medium offset= 2500-5000m, Far offset= 5000-7500m).

Table 5-6 *Amplitude difference during loading and unloading for Horizon 4.*

Horizon	Pressure (psi)	Offset (m)	Amplitude difference during load vs unload (%)	Average amplitude difference (%)
Hor. 4	1000	Near offset	2.83-2.76 %	
		Medium offset	2.76-2.23%	2.51 %
		Far offset	2.23-0.96%	
	2000	Near offset	2.07-2.10 %	
		Medium offset	2.10-1.42%	1.77 %
		Far offset	1.42-0.06%	
	3000	Near offset	1.13-1.08 %	
		Medium offset	1.08-0.81%	0.98 %
		Far offset	0.81-0.29%	
	4000	Near offset	0.68-0.67 %	

	Medium offset	0.67-0.49%	0.59 %
	Far offset	0.49-0.18%	

Although there is no clear mechanism that predicts both the polarity and magnitude of the seismic amplitude, the variation of amplitude could go up to 4.77% within near offset at lower pressure setting (1000psi). This variation could be due to change in geomechanical properties and damage of the rock due to stress change (e.g., Bidgoli & Jing, 2014). The damage in rocks clearly have significant impact during the stress path which also discussed in previous chapters.

5.5.3 AVO cross-plot for stress path change.

The AVO cross-plot during loading and unloading shows the influence of variation of stress change. As the data focusing on variation at Horizon 2 to 5 (**Figure 5-18**), Horizon 3 (between layer 3 and 4) and Horizon 4 (between layer 4 and 5) gave the biggest variation among the other horizon during the stress path change. Horizon 3 more gives more drastic variation compare to Horizon 4 indicated by the gradient of the cross-plot changes. The changes in intercept can be attributed to a change in acoustic impedance, whereas changes in the gradient imply that shear wave velocity is changing too. The velocity contrast between these two layers slightly changes during loading and unloading that cause the seismic response differently as indicated by variation in gradient and intercept in the cross-plot.

The stress path changes influence both the gradient and intercept (**Figure 5-18**), which also suggests that there is change in the Poisson's ratio. Damage to the rock during stress path change as discussed in previous chapter may be relatable with the change in Poisson's ratio experienced by the reservoir rock. Depletion and pressure drop in the reservoir may correspond to a movement in the AVO cross-plot towards dimming at zero-offset but brightening at far-offset. There are time-shift during a load/unload cycle (**Figure 5-15**), but the AVO response gives more significant and sensitive in detecting stress change or path change that happened in the reservoir.

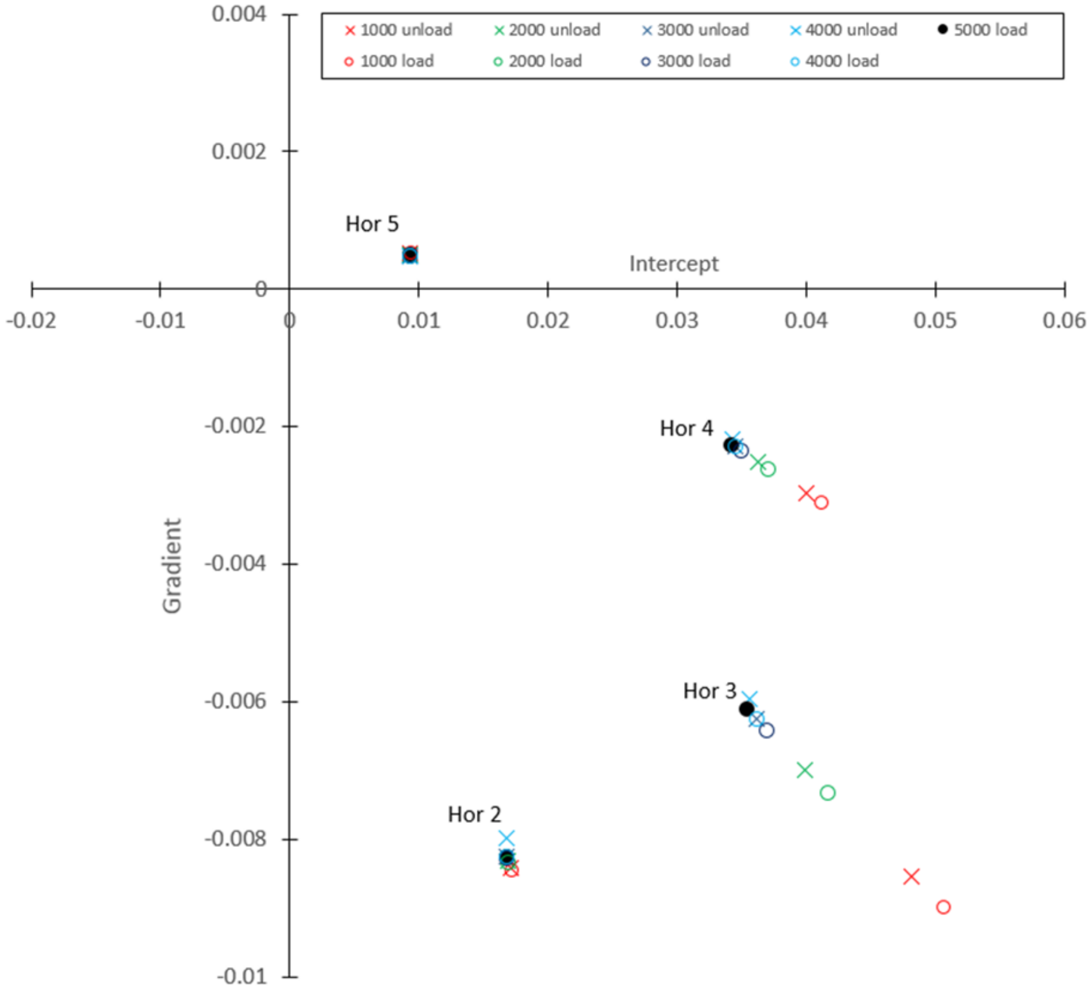

Figure 5-18 *AVO cross-plot for Horizon 2 to 5 (Horizon 1 excluded) during stress path change that applied onto layer 4.*

5.5.4 Impact of changes in fluid saturation & stress path on AVO cross plot

The effect of pressure and fluid saturation changes were combined into one cross-plot (**Figure 5-19)** to summarise their net effect on the AVO cross plot. Technically, a change in pressure is typically associated with a shift in both the intercept (*R*) and gradient (G) directions, suggesting that both acoustic impedance and Poisson's ratio are impacted. Based on the results, the most obvious shift indicated in layer 4 (reservoir) due to stress path change were applied in this layer. The stress path changes between loading and unloading not just affect the reservoir layer but also affect the overburden (layer 3). There is observer able AVO cross plot shift in horizon 3, but not as obvious in reservoir layer. Besides that, the AVO cross plot shift also detected in horizon 5 (under burden layer) but at very small shift.

A change in fluid is associated primarily with a change in the intercept (R) direction, suggesting is its primarily associated with an acoustic impedance change. However, any introduction of fluid moves the AVO response towards zero-gradient which shown by layer 3 and 4. This condition also similarly shown by the typical AVO cross plot response during fluid substitution in the real reservoir (e.g., Wayne, 2015; Umoren & George, 2018). The results also shows that all the AVO cross plot in layers 3 & 4 clearly shifted towards zero as hydrocarbon replaced with water in the model, but the AVO shift is too small and undetected in layer 5.

The effect is more pronounced for layer 4 because of the pressure change and fluid substitution were simulated in this layer as the expected happened in reservoir layer during hydrocarbon extraction and followed by water flooding procedure. Critically for layer 4, the highest-pressure scenarios produce a polarity reversal in the gradient: low pressures will produce a dimming AVO response, whereas higher pressures are associated with brightening.

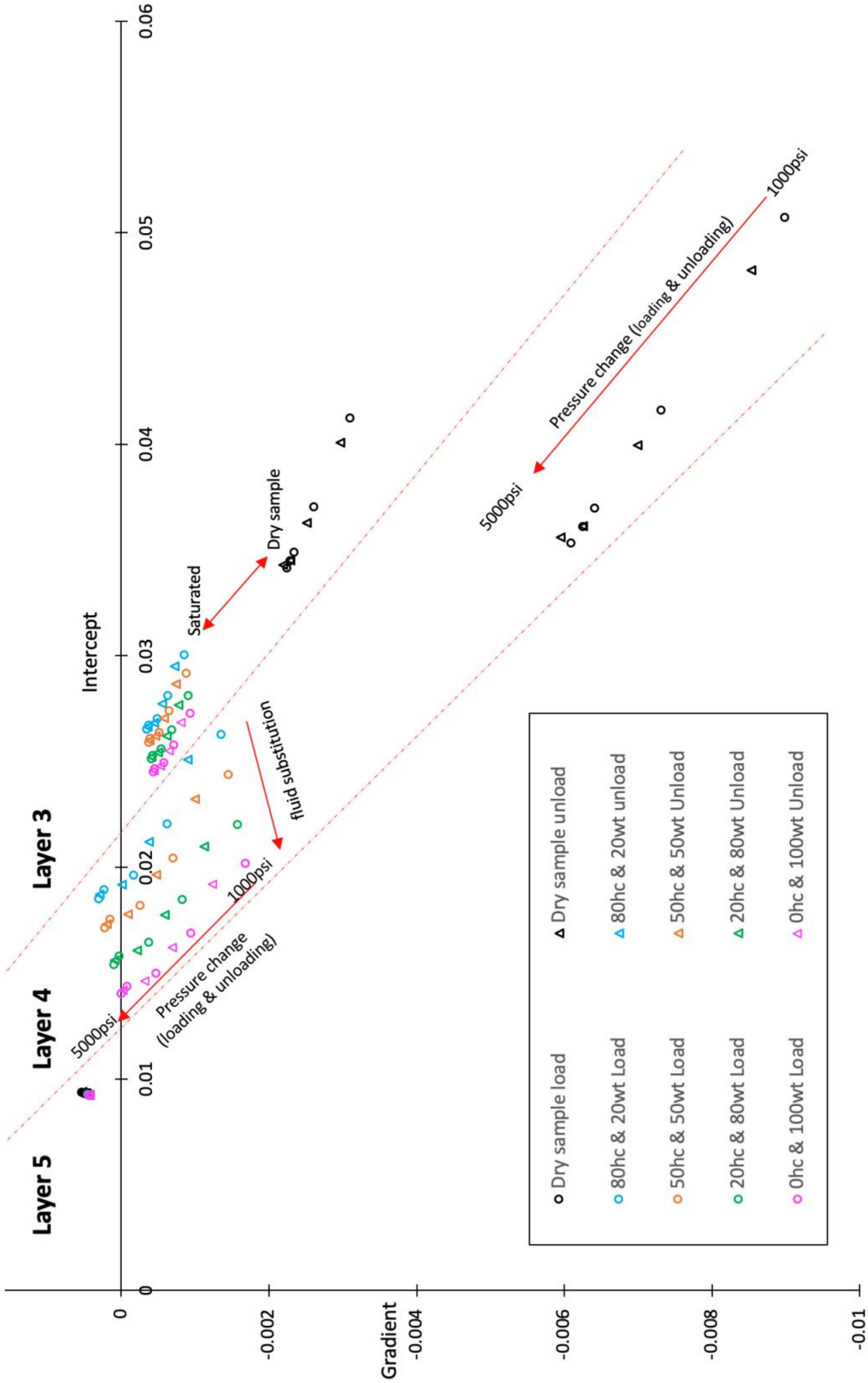

Figure 5-19 *Variation of AVO attribute for Layer 3, 4 & 5 (Layer 1 & 2 has no significant changes) during pressure change and fluid change (hydrocarbon, hc & water, wt).*

Based on the simulation synthetic seismic data, the results could reflect the general ability and sensitivity of time-shifts analysis (**Table** *5-3*) in dynamic reservoir prediction. Even though time-shifts could reveal spatial distribution of geomechanical effects or saturation changes, time-shifts are a cumulative measurement, which do not directly relate to localized sub-surface properties such as velocity change or physical strain (Alaei, 2012). Normal incidence amplitudes such as normal incidence reflection alone could not reveal much of stress path change nor fluid substitution, the analysis of AVO trends proves more useful. The AVO indicates the ability to detect the variation during stress path changes as well as fluid substitution, where AVO cross-plot provide simple plot to distinguish the variation. The AVO cross plot also indicates that a fluid substitution only appears to affect the AVO response in the Intercept (R) direction, whereas both Gradient (G) and Intercept (R) are impacted by pressure.

Generally, there are obvious shift such in Layer 4 (base reservoir) which potentially detectable in the real field. But there also very small shift which happened in the Layer 5 (under burden) which could be totally unnoticeable in the real field due to noise. The synthetic seismic and AVO response in this model is noise free, while seismic data that acquire in the field will contain noise. The appearance of noise in the field could potentially makes the AVO shift during fluid substitution unnoticeable or undetected. Thus, noise free data from this synthetic seismic could arise concern whether the shift of the Intercept-Gradient cross plot is detectable in noisy condition such in the real field. Previous research indicates that, with appearance of 15% random noise, the change in saturation and pressure still recognised clearly at fairly high accuracy with the main features (e.g. Smith et al., 2010; Trani *et al.,* 2011). For the real field situation, Intercept-Gradient cross plot produced by Han *et al.,* 2019, indicated the ability of AVO and Intercept-Gradient cross plot to detect distinguish the present of oil within the base of reservoir.

Pressure change and fluid substitution has impact and shift the AVO response as shown in **Figure 5-19**. Based the shifted pattern in the Intercept-Gradient cross-plot for horizon 4 (Figure *5-20*), pressure change has shifted AVO response on gradient and intercept of the cross-plot. While fluid substitution only gives significant impact on AVO intercept with small variation in gradient. This shows that, the pressure change (1000psi to 5000psi) in the reservoir gives bigger influence towards seismic properties compare to fluid substitution.

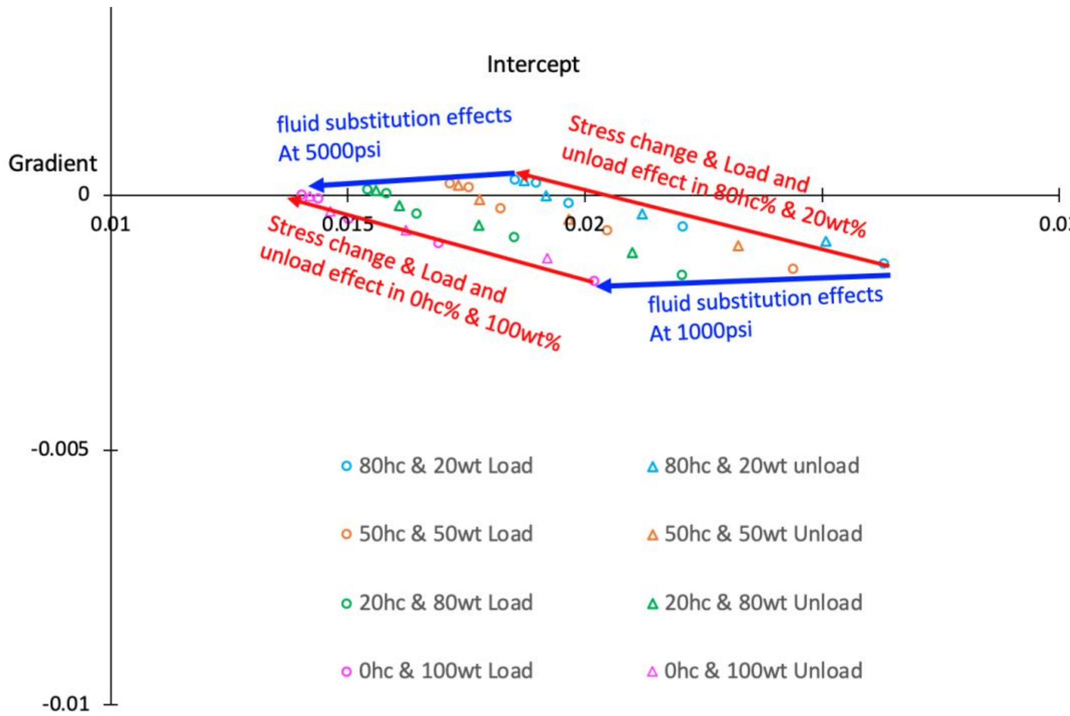

Figure 5-20 *Stress change and fluid substitution impact on AVO response for Horizon 4*

The time-shift and AVO analysis could provide better quantitative evaluation in reservoir characterization which produce better predicted data. Even though the core sample that collected in the reservoir unable to represent and mimic the real dynamics of reservoir in the subsurface, at least it gives significant information on how big the misfit could be appear in predicted and measured data when involving stress path change. From technical perspective, neglecting the effects of stress path change and fluid substitution could lead to produce misfit in predicted and measured data in the field.

5.6 SUMMARY

This chapter has explored the impact of stress path change (loading followed by unloading) on the time-shift and amplitude changes in seismic reflection by using ray tracing approached. Generally, the stress path changes in the model give influence in seismic response, and the simulation based on field model indicates the stress change could affect the over- and under-burden of the reservoir. There are detectable shifted travel time during low pressure (up to 4ms) and deviations in reflection amplitude (up to 4.77%) during stress path change (loading and unloading) were implemented in reservoir layer (Layer 4).

The chapter also explores the impact of fluid saturation variation during stress path change. The modelling results indicate significant change in rock compressibility/bulk modulus. The simulation in this study is using explicitly couple fluid flow - geomechanical and are able to provide enough information on how the geomechanical and fluid change undergone during stress path change. This allow and implementation of the ray-tracing to monitor the seismic response during the stress path change and analyse the effects on the over- and under-burden.

The results from the simulation suggest that both pressure changes and fluid substitution has influence towards seismic response. Based on AVO cross plot analysis, pressure changes indicates more dominant impact towards seismic properties compare to the influence of fluid substitution in the reservoir. Therefore, as suggest by the results, the stress path change should be taken into account during seismic interpretation or reservoir modelling. Considering stress dependant velocity curve are the same during loading and unloading possibility leads to some misinterpretation.

6 CONCLUSION & RECOMMENDATION FOR FUTURE WORK

This research presented in this thesis has focused on the usage of seismic data to characterise rock properties. It covers a range of scales from laboratory core measurement to field scale seismic interpretation and modelling. It is common practice to measure the petrophysical properties of core samples to improve interpretation of subsurface data. Ultrasonic velocity measurements are widely used to help interpretation of seismic data. However, significant uncertainties remain regarding the underlying controls on ultrasonic velocities. For example, velocity is correlated with porosity but the specific causes that control the large amount of scatter around porosity-velocity relationships are poorly understood. , In this thesis, a significant amount of effort was dedicated to improving understanding of the controls on ultrasonic velocities (Chapter 3). A key issue that complicates interpretations of ultrasonic velocity data is the extent to which the samples have been damaged as they have been during and following coring. In particular, pressure and stress in the subsurface is totally different to the surface, which will inevitably change the microstructure and properties of the samples. Chapter 4 addresses this issue and the results indicate that cracks formed during retrieval are random and unpredictable, which makes it difficult to use the laboratory results to predict subsurface behaviour Chapter 5 attempts to model this situation by incorporating measurements conducted on core samples under different stress paths into a coupled fluid-flow geomechanical model. The output from the model is then used to model seismic response which is then compared with the seismic response from a real reservoir.

6.1 Controls on ultrasonic velocities

Chapter 3 examines controls on ultrasonic velocity-porosity relationships is sandstones. A wide range of standard rock physics models have been developed to estimate velocity-porosity relationship. The Raymer-Hunt-Garner, RHG, equation produces the best fit to the velocity-porosity data measured in the laboratory from wide range of sandstone and provides a far more accurate prediction than other rock physics model (Krieff and Voight-Reuss-Hill (VRH), Han and Wyllie). The Krief and VRH rock physics models tend to slightly overestimate the velocity, but the fit is slightly improved for samples with a porosity >10%. The Han equation, which correlates velocity with clay content and porosity, gives a larger misfit as the porosity increases. The Wyllie relationship severely underestimates the velocities and gives the worst prediction for velocity-porosity relationship compared to other rock physics model. Thus, simple approach taken by Wyllie's model is not suitable for a wide variation type of rocks.

The analysis in chapter 3 suggests that, accounting for the clay content, detailed mineralogy or grain-size does not appear to allow a more accurate prediction of ultrasonic velocity than just using porosity. The regression model of predicted vs. measured porosity shows correlation coefficient of 0.671 with removing anhydrite, siderite, magnesite, barite, microcline and pyrite from the equation almost did not give any significant changes to the coefficient value. There is also no significant improvements when velocity-porosity or velocity impedance-porosity relationship were correlated to mineralogy, grain size or pore radius.

6.2 Velocity stress dependent: inverted crack behaviour

A commonly used microstructural (MST) rock physics model has been used to invert the stress dependence of ultrasonic velocities into the crack properties such as aspect ratio and crack density. The inverted values of crack density and aspect ratio are significantly different if inversions were made on based on ultrasonic velocity measurements made during loading or unloading. Strong correlations were not identified between either aspect ratio or crack density and either the composition of the sandstones, their basic petrophysical properties or their microstructure. It seems likely that the velocity dependence on confining pressure is not only controlled by natural features but is also a result of damage to the samples that occurred during or following coring.

It is possible that the stress dependence of the properties of the samples is controlled by a range of extrinsic and intrinsic, which is why strong correlations are not identified between either aspect ratio or crack density and the microstructural, mineralogical or petrophysical properties of the samples. The analysis using data mining also failed to identify similar relationships between aspect ratio values and ultrasonic velocities. A sensitivity study was therefore conducted by using the MST model to assess the impact of aspect ratio and crack density on velocity – stress relationships.

The stress dependence of the ultrasonic velocities increases as the crack density increases. The aspect ratio value appears to be related to the curvature of the velocity – stress data. For example, the velocity of samples with a low aspect ratio values (i.e., long thin cracks) tends to increase rapidly as confining pressure is increased and then velocity tends to be less stress sensitive at higher confining pressures; this results in a distinct non-linearity to the stress vs. velocity relationship. On the other hand, the velocity of samples with high aspect ratio values (i.e., more sphere-like cracks) tends to have a more linear relationship with stress.

The aspect ratio during loading (aoL) divided by the aspect ratio during unloading (aoUL) seems to correlate with the aspect ratio during unloading. This is consistent with aspect ratios being partially controlled by the length of grain contacts. In general, aoL/aoUL tends to decrease with increasing porosity. The samples with low porosity show large differences in the aoL/aoUL. Examination of the micrographs indicates that the lower values tend to have clay between grain contacts whereas the higher values tend to have more quartz-quartz contacts. It is possible that the differences are controlled by grain adhesion. Higher clay content between the crack makes the grain contact more compliant as the result of low porosity value and high aspect ratio values. High aspect ratio value with high porosity caused by small Hertzian contact.

It is important to question whether these laboratory measurements are representative of the subsurface. The fracture networks that were observed after injecting Fields metal into the rock at low confining pressures rapidly closed as confining pressure was increased. It seems very unlikely that such fracture networks existed in the subsurface and were most likely formed as the samples were brought to the surface. If this is the case, the velocity measurements conducted at low stress are certainly not representative of subsurface values and there remain questions as to whether the high-pressure values are also representative of subsurface values.

Overall, it appears that the crack density and aspect ratio terms are essentially parameters to fit measurements of ultrasonic velocity vs. confining pressure. It is also likely that the fracture networks that exist in the laboratory were probably not present in the subsurface. It seems incorrect to generate rock physics models based on these data and then attempt to extrapolate them to subsurface conditions. Great care should be taken when using the MST model used in the current study, or similar rock physics models, which have been calibrated with laboratory measurements of the stress dependence of ultrasonic velocities, to predict the stress dependence of seismic velocities in the subsurface.

6.3 Pressure and fluid change in reservoir

Petroleum production leads to changes in pore pressure and often temperature, which results in changes in stress leading to deformation both in and around the reservoir. The compactional deformation within the reservoir may lead to reductions in both porosity and permeability, which may significantly impact fluid-flow in the reservoir (e.g., Heffer *et al.*, 1994; Fredrich *et al.,*1996, 1998; Longuemare *et al.*, 2002; Settari *et al.*, 2002; Angus *et al.*, 2011; Yang *et al.*, 2018;). For more than a decade, there have been numerous studies on reservoir-geomechanical modelling to assess the relative importance of fluid saturation and stress changes due to production-related geomechnaical effects (Molenaar *et al*., 2004; He, 2015; Verdon *et al*., 2008).

A depleted reservoir usually experiences loading (i.e. increase in effective stress) as a result of primary or secondary production. Water flooding or carbon dioxide injection are often implemented to increase oil recovery as an oil field matures and production rates decline, which re-inflates and unloads (reduces effective stress) the reservoir. This stress and fluid change could introduce variation in seismic response before and after the petroleum extraction. As a result, the seismic response comparison was produced with implementation of seismic time-lapse method, which is also a well-known technique for estimating reservoir production-induced physical changes (Lumley, 2001; Nguyen *et al*., 2015).

In chapter 5, a model of reservoir that experience stress path change and fluid substitution are created and seismic response are simulated in that model. The results from the simulation indicate time shift and magnitude change in the seismic response. The seismic response shows different time-shift at different given effective stress patterns, which also gives larger variation of time-shift at the bottom layer of the reservoir (Horizon 4) compared to the top layer of the reservoir (Horizon 3). The time-shift variations also potentially accommodate the stretching or compacting mechanism in the under- and over-burden during loading (pressure decrease in reservoir layer) and during unloading (pressure increase in reservoir). Small time-shits are also observed for the overburden.

Although there is no clear mechanism that predicts both the polarity and magnitude of the time-shift, the results also indicate that, there are variation of time-shift during stress changes. This variation could be due to change in geomechanical properties and damage of the rock due to stress change. Generally, the stress path change in the model give influence in seismic response, and the simulation based on the field model indicates the stress change could affect the over- and under-burden of the reservoir.

The modelling results also indicate significant change in rock compressibility/bulk modulus during fluid substitution. The AVO indicates the ability to detect the variation during stress path changes as well as fluid substitution, where AVO cross-plot provide simple plot to distinguish the variation. The AVO cross plot also indicates that a fluid substitution only appears to affect the AVO response in the Intercept (R) direction, whereas both Gradient (G) and Intercept (R) are impacted by pressure. The assessment from AVO cross-plot reveal that pressure change gives more dominant impact on seismic response compare to fluid substitution.

6.4 Suggestion and recommendations for further work.

The manner in which the research reported in this thesis has progressed makes writing suggestions for further work relatively easy. In particular, the initial aim of the thesis was to investigate the impact of anisotropy on the 4D seismic response in the Elgin Field, North Sea. Unfortunately, changes on staff both at the University of Leeds and our industrial partner meant that after 18 months of study I still hadn't been provided with the basic data that I needed to conduct the study (i.e. core samples, wire-line log data, 4D seismic and the geological model of the field). So a key recommendation would be to undertake the work that was originally planned, which was to build a coupled fluid flow – production simulation model of the field and populate it would anisotropic elastic and mechanical properties measured in the laboratory. It was intended to take the output from the model to estimate 4D seismic response and compare the results with both the results from a non-isotropic model and from the actual 4D response in the field. This would provide insight into the importance of considering seismic anisotropy in the interpretation of 4D seismic.

Based on the work conducted during this study there are several further suggestions. Firstly, a large number or measurements of ultrasonic velocity were made on tight gas sandstones initially while loading the samples to between 5000 and 7000 psi and later in the study measurements were also made during unloading. In retrospect, the confining pressures to which the samples were loaded was in some cases not even as high as that experience at while at in situ prior to gas production let alone as high as they would have experienced during drawdown. The maximum stress (5000psi) that I could measure the samples to was restricted as it was very important that the samples were not damaged as they are to be used for many other types of experiment. However, ideally, the measurements would have been made up to the stresses that would have been experienced at abandonment pressure and during the measurements a series of loading and unloading cycles until would have been conducted until no change in ultrasonic velocities occurred.

It would have also been interesting to attempt to model the key controls on ultrasonic properties. One way that this could have been done would have been to conduct finite difference or finite element modelling of wave propagation through models built from micro-CT scans of the samples analysed. Here the elastic constants of individual minerals could be included. A workflow would need to be developed to include grain boundaries in the model and this is rather non-obvious.

A final recommendation would be to model 4D seismic based on more realistic geometries than was possible using the ray-tracing software ATRAK. One possibility would be to conduct full wave form modelling using finite difference, finite element or the spectral element method. This thesis has discussed the problems encountered in the interpretation of ultrasonic velocity measurements made on core samples through to seismic velocity measurements made at the reservoir scale. However, this research is very much ‘thin end of the wedge’ and has only begun to possible problems and uncertainties in the analysis of seismic data. The following points were considered as the key topics which need to be improved to make the rock physics and time-lapse seismic technique is a more precise and robust geomechanical monitoring tools.

Even after more than 30 years of development, rock physics models are still unable to explain the large amount of scatter in velocity-porosity relationships. This is due to complexity and heterogeneity of the rock properties such as mineralogy, crack analysed that measured in the laboratory. During wave velocity measurement, the wave that travel in the rocks are totally depend on the contacts among the grains in the rock. With implementation of high stress, these mineral grains will collide each other, results change in wave velocity that pass into the rock sample. Most of rock physics model tend to generalise this effects to predict wide range of rocks type. But the response of grain to grain contacts could be unique for each of different minerals. This lead to give different effects on seismic response and cause scatter in the rock physics model. Imaging or simulating the grain to grain contact from various mineral types with implementation of stress could improve the understanding on how the grains response. Micro CT scanner and Electron Backscatter Diffraction (EBSD) technology could help to image the grain-grains response. But it is still challenging to implement stress on the sample and image the sample at same time. This observation is beneficiary and crucial to improve the understanding on intrinsic rock behaviour as well as to produce precise rock physics model.

Analysing big data to produce detail correlation or dependant factors on velocity porosity is quite tough. Thus, application of machine learning are introduced to produce unbiased classification and correlation. Even though the implementation of machine learning in Chapter 3 was still unable to reveal the major controls on velocity-porosity relationship, but the application of machine learning in dealing with wide range types of rock has indicates a huge potential. The machine learning also proven in reducing uncertainties and improve prediction in many field of studies (e.g. Schmidt *et al.,* 2019; Song, 2020). Analysing wider range set of velocity-porosity data with machine learning or deep learning potentially reduce the uncertainty. Moreover, linear and multi linear regression were carried out to investigate any physical parameter of rock sample that give significant influence towards velocity. This analysis could be carried out by using different approach. Recently, Wang *et al.* (2018) produced better permeability prediction by adopts the fuzzy logic algorithm. This approach allows the calculation process to be modelled with the error components which not applicable in linear regression analysis. Application of fuzzy logic algorithm could improve the understating on relationship among the rock physical properties.

Chapter 4 has suggested that there are potential damaged in the rock sample. It is still unclear how big the damage could be happened within the core sample once it took to the surface. This is due to stress difference between stress in the subsurface (in situ) and stress on the surface. Imaging the crack in the core sample that bring to the surface is doable as shown in chapter 4. But it is still challenging to image the crack within the rock in the subsurface, makes the comparison of the crack appearances in subsurface vs. surface is still unclear. If micro crack imaging or micro crack tomography method could be implemented in the reservoir, it could be beneficial to justify the crack behaviour in the real reservoir condition. This crack imaging could be compared with crack image that carried out with the core sample while it on the surface.

Chapter 4 also discussed the differences between crack appearance based on rock physics model (MST) and with crack image from the real rock sample that conducted by Eardly (2017). Obviously, the crack geometry that is assumed in most rock physics models is an oversimplification compared to natural fractures. Improvement and production of more realistic rock physics model based on real crack properties in the rock sample such as shape and behaviour should be a breakthrough to this problem. Moreover, to produce such rock physics model could require challenging task, thus analysing of crack properties in detail and robust model on grain to grain contact behaviour during stress change could improve the rock physics model. Rock properties correlation is another element that crucial to improve rock physics model.

In Chapter 5, simulated seismic response in reservoir model has indicate that there are time-shift and amplitude change during stress path change. Note that the reservoir model that used in the simulation is too simple, but this simplification is require to analyse and detect the impact of small stress changes on seismic response. Real reservoirs usually have far more complex structures. Besides that, seismic wave simulation using ray tracing approach has its own limitation and for some cases, not able to perfectly represent the real wave propagation. Ray based seismic simulation (ATRAK) not easily handle diffraction and a smoothed velocity model a required in order to makes this ray theory works. The smoothing procedure produces a velocity input model with gradually and smooth velocity transition from one layer to another.

This situation usually does not represent the realistic subsurface geometry or geological structure in the subsurface.

The other problem with synthetic seismic in the simulation is that it produces noise free response which is unrealistic in the real world. While to produce more realistic seismic response, the adaptation of noise level in the seismic simulation could be beneficial. This could help to verify either the effect of stress change in reservoir still detectable in the field or not. This could require additional of noise level in the seismic simulation around 10-20% (suggested by Johnson *et al*., 2020). Besides that, adding complex and more realistic structure, such as additional of anisotropic layer in the reservoir model could beneficial in this studies. This application will require additional bedding or fracture orientation in the model. The appearance of anisotropy layer lead to variation in seismic velocity and this effect has been proven by other previous researcher. But this implementation could be challenging since the behaviour of crack during stress change in the subsurface remained unclear as mentioned earlier. Despite of this challenge, producing more realistic subsurface model and wave propagation is a another step forward in improving seismic methods as a better reservoir monitoring tools.

7 REFERENCES

Abd El-Aal, A.K., Salah, M.K. & Khalifa, M.A. 2020. Acoustic and strength characterization of Upper Cretaceous dolostones from the Bahariya Oasis, Western Desert, Egypt: The impact of porosity and diagenesis. *Journal of Petroleum Science and Engineering 187* (2020). 106798. https://doi.org/10.1016/j.petrol.2019.106798.

Abe, S.j., Olowokere, M.T. & Enikanselu, P.A., 2018. Development of model for predicting elastic parameters in 'bright' field, Niger Delta using rock physics analysis. *NRIAG Journal of Astronomy and Geophysics*, Vol. 7 (2), Pp. 264-278, ISSN 2090-9977, https://doi.org/10.1016/j.nrjag.2018.05.006.

Agarwal, B. & Hermansen, H. & Sylte, J.E. & Thomas, L.K. 2000. Reservoir Characterization of Ekofisk Field: A Giant, Fractured Chalk Reservoir in the Norwegian North Sea ? History Match. *SPE Reservoir Evaluation & Engineering*, Vol. 3 (6). Pp. 534-543.

Ahmadi, O., Hedin, P., Malehmir, A., & Juhlin, C. 2013. 3D seismic interpretation and forward modelling – an approach to providing reliable results from 2D seismic data. In: *Johnson, E. (Ed.), Proceeding of the 12th Biennial Meeting: Mineral Deposit Research for a High-Tech World*. Pp. 50-53.

Alaei, B. 2012. Seismic Modeling of Complex Geological Structures in Ed. Masaki Kanao, 2012. *Seismic Waves - Research and Analysis*. IntechOpen.

Alber, M. 2014. Experimentally based relation between dynamic and static elastic moduli of various sandstones and a quartzite. In *Alejano, Perucho, Olalla & Jiménez (Eds). 2014. Rock Engineering and Rock Mechanics: Structures in and on Rock Masses*. Taylor & Francis Group, London

Al-Mudhafar, W.J. & Al-Isawi, A. 2015. Multivariate Multiple Linear Regression for Jointly Modeling of Petrophysical Properties. *77th EAGE Conference & Exhibition 2015 - Student Programme IFEMA Madrid, Spain, 1-4 June 2015*

Al-Saddique, M.A.,HamadaMusaed, G.M., Al-Awad, N.J. 2000. State of the Art: Review of Coring and Core Analysis Technology. *Journal of King Saud University - Engineering Sciences*. Volume 12 (1), Pages 117-137.

Alvarez, E., MacBeth, C. & Brain, J. 2017. Quantifying remaining oil saturation using seismic time-lapse amplitude changes at fluid contact. *Petroleum Geoscience, Vol. 23 (2),Pp. 238-250.*

Aminzadeh, F. & Dasgupta, S.N. 2013. Reservoir characterization. In *Ed. Aminzadeh, F. & Dasgupta. 2013. Geophysics for petroleum engineers*. Elsevier, Vol. 60, Pp. 1-282.

Anderson, N., & Cardimona. S. 2002. Forward seismic modelling: The key to understanding reflection seismic and ground penetrating radar (GPR) technique. *Geophysics 2002. The 2nd Annual Conference on the Application of Geophysical and NDT methodologies to Transportation Facilities and Infratructure, Loas Angeles, USA. 15-19 April 2002.*

Anderson, N.L., Hedke, D.E. & Knapp, R.W. 1995. Forward seismic modelling-Application and utility. *Bulletin Kansas Geological Survey.* Vol. 327. Pp. 28-33.

Andreassen, K., Nilssen, E.G. and Ødegaard, C.M. 2007. Analysis of shallow gas and fluid migration within the Plio-Pleistocene sedimentary succession of the SW Barents Sea continental margin using 3D seismic data.

Angus, D.A., Dutko, M., Kristiansen, T.G., Fisher, Q.J., Kendall, J-M., Baird, A.F., Verdon, J.P., Barkved, O.I., Yu, J., &. Zhao, S. 2015. Integrated hydro-mechanical and seismic modelling of the Valhall reservoir: A case study of predicting subsidence, AVOA and microseismicity. *Geomechanics for Energy & the Env.* Vol.2 (2015), Pp. 32-44.

Angus, D.A., Dutko, M., Fisher, Q.J., Kendall, J-M., Baird, A.F., Kristiansen, T.G. Barkved O.I., Yu, J. and Zhao, S. 2013. Integrated hydro-mechanical and seismic modelling of the Valhall reservoir: Predicting subsidence, AVOA and microseismicity. *International Workshop on Geomechanics and Energy – The Ground as Energy Source and Storage Lausanne, Switzerland, 26-28 November 2013.*

Angus, D.A., Fisher, Q.J., Segura, J.M. Verdon, J.P., Kendal, J.-M., Dutko, M. & Crook, A.J.L. 2016. Reservoir stress path and induced seismic anisotropy: results from linking coupled fluid-flow/geomechanical simulation with seismic modelling. *Petroleum Science*, Vol. 13, Pp. 669–684. https://doi.org/10.1007/s12182-016-0126-1

Angus, D.A., Fisher, Q.J. & Verdon, J.P. 2012. Exploring trends in micro crack properties of sedimentary rocks: An Audit of dry and water saturated sandstone core velocity-stress measurements. *Int. J. of Geoscience*, Vol. 3 (4A 2012), Pp. 822-833.

Angus, D.A., Kendall, J-M., Fisher, Q.J., Segura, J.M., Skachkov, S., Crook, A.J.L. & Dutko, M. 2010. Modelling microseismicity of a producing reservoir from coupled fluid–flow and geomechanical simulation. *Geophysical Prospecting*, Vol. 58(5), Pp. 901-914.

Angus, D.A., Verdon, J.P., Fisher, Q.J. & Kendall, J-M. 2009. Exploring trends in micro crack properties of sedimentary rocks: An Audit of dry-core velocity-stress measurements. *Geophysics*, Vol. 74 (5). Pp. E193-E203.

Angus, DA. Verdon, J.P., Fisher, Q.J., Kendall, J.M., Segura, J.M., Kristiansen, T.G., Crook, A.J.L., Skachkov, S., Yu, J. & Dutko, M. 2011. Integrated fluid-flow, geomechanic and seismic modelling for reservoir characterisation. *CSEG Recorder*.

Anifowose, F. & Abdulraheem, A. 2011. Artificial Intelligence Application in Reservoir Characterization and Modeling: Whitening the Black Box. *Conference: 2011 Young Professional Technical Symposium.*

Asef, M. & Najibi, A.R. 2013. The effect of confining pressure on elastic wave velocities and dynamic to static Young's modulus ratio. *Geophysics*, Vol. 78, Pp. 135-D142. 10.1190/geo2012-0279.1.

Avseth, P. 2010. Explorational rock physics- The link between geological processes and geophysical obsevables. In: *Bjorlykke (ed.) Petroleum Geoscience: From sedimentary Environmnet to rock physics*. Pp. 403-426.

Avseth, P., Mukerji, T. & Mavko, G. 2005. Quantitative Seismic Interpretation: Applying Rock Physics Tools to Reduce Interpretation Risk. Cambridge University Press.

Avseth, P., Mukerji, T., Mavko, G. & Gonzalez, E. 2007. Integrating Statistical Rock Physics and Sedimentology for quantitative seismic interpretation.

Avseth, P., Skjei, N. & Mavko, G. 2016. Rock-physics modeling of stress sensitivity and 4D time shifts in patchy cemented sandstones — Application to the Visund Field, North Sea. *The Leading Edge*, Vol. 35, Pp. 868-878. 10.1190/tle35100868.1.

Avseth, P., Skjei, N. & Skålnes, Å. 2013. Rock physics modelling of 4D time-shifts and time-shift derivatives using well log data - a North Sea demonstration. *Geophysical Prospecting.* Vol. 61, Pp. 380-390. 10.1111/j.1365-2478.2012.01134.x.

Asaka,A., Mu Luo,M., Yamatani, T., Kato, A., Yoshimatsu, K., and Knapp, L. 2018. 4D seismic feasibility study: The importance of anisotropy and hysteresis. The Leading Edge, 37, 634-712.

Baker, R.O., Yarranton, H.W. & Jensen, J.L. 2015. *Practical Reservoir Engineering and Characterization,* Gulf Professional Publishing.

Bandyopadhyay, K. 2009. *Seismic anisotropy: Geological causes and its implications to reservoir geophysics*. Stanford, CA: Stan-ford University

Barkved, O.I. & Kristiansen, T. 2005. Seismic time lapse effects and stress changes: example from compacting reservoir. *The leading edge*, Vol. 24 (12).

Barkved, O.I., Kristiansen, T.G., Fjær, E. 2005. The 4D seismic response of a compacting reservoir-Examples from the Valhall Field, Norway. Presented at the 75th Annual Meeting of SEG, Houston, 6-11 November.

Barruol, G. & Kern, H. 1996. Seismic anisotropy and shear-wave splitting in lower-crustal and upper-mantle rocks from the Ivrea Zone—Experimental and calculated data. *Physics of the Earth and Planetary Interiors.* 95. 175-194.

Batzle, M., Han, D-H. & Hofmann, R. 2006. Fluid mobility and frequency-dependent seismic velocity – Direct measurement. *Geophysics*, Vol. 71. 10.1190/1.2159053.

Berryman, J.G. 2007. Seismic waves in rocks with fluids and fractures. *Geophys. J. Int,* Vol. 171, Pp. 954–974.

Bhuiyan, M.H., Holt, R.M., Larsen, I. & Stenebraten, J.F., 2013b. Static and dynamic behaviour of compacted sand and clay: comparison between measurements in Triaxial and Oedometric test systems, *Geophys. Prospect*., 61, 329–340.

Bidgoli, M.N. & Jing, L. 2014. Anisotropy of strength and deformability of fractured rocks, Journal of Rock Mechanics and Geotechnical Engineering, Vol 6 (2), Pp 156-164.

Birch, F. 1960. The velocity of compressional wave in rocks to 10 kilobars. Part 1. *J. of Geophys. Research*. Vol. 65. Pp. 1083-1102.

Botrill, A., Herwenger, J. & Popov, P. 2016. Snøvit geomechanical model for simulation of CO2 into an aquifer. Unpublished

Brahma, J & Sircar, A. 2014. Estimation of the Effect of Anisotropy on Young's Moduli & Poissons ratios of sedimentary rocks using core samples. *International Journal of Geosciences,* 2014, (5), Pp. 184-195.

Bratton, T.R. 2012. Quantifying Anisotropy for Geomechanics. GEO-2010, 10th Middle East Geosciences Conference and Exhibition, Manama, Bahrain, March 4-7, 2012.

Brown, R.J.S. & Korringa, J. 1975. On the dependence of the elastic properties of a porous rock on the compressibility of the pore fluid. *Geophysics*, Vol. 40 (4), Pp. 608–616. doi: https://doi.org/10.1190/1.1440551

Burlini, L., Arbaret, L., Zeilinger, G., & Burg, J-P. 2005. High temperature and pressure seismic properties of a lower crustal prograde shear zone from the Kohistan arc, Pakistan in *High-strain zones:Sstructure and physical properties, Vol. 245, edited by Bruhn, D. & Burlini, L.*, Pp.187-202, Geol. Soc. London Spec. Pub, Bath, UK.

Busch, J. M., Fortney, W. G., and Berry, L. N. 1987. Determination of Lithology from Well Logs by Statistical Analysis: SPE Formation Evaluation, Vol. 2, No. 4, p. 412-418.

Castagna, J.P., Swan, H.W. & Foster, D.J. 1998. Framework for AVO gradient and intercept interpretation. *Geophysics*, Vol. 63 (3).

Carrasquilla, A., Silvab, J. D., and Flexa, R. 2008. Associating Fuzzy Logic, Neural Networks and Multivariable Statistic Methodologies in the Automatic Identification of Oil Reservoir Lithologies through Well Logs: Revista de Geologia, Vol. 21, No. 1, p. 27-34.

Çemen, I., Fuchs, J., Coffey, B., Gertson, R. & Hager, C. 2013. Correlating Porosity with Acoustic Impedance in Sandstone Gas Reservoirs: Examples from the Atokan Sandstones of the Arkoma Basin, Southeastern Oklahoma. *AAPG Annual Convention and Exhibition, Pittsburgh, Pennsylvania, May 19-22, 2013*.

Červený V. and Hron F., 1980. The ray series method and dynamic ray-tracing system for three-dimensional inhomogeneous media. *Bull. Seismol. Soc. Amer*., 70, 47-77.

Chang, H. C., Kopaska-Merkel, D. C., and Chen, H.-C. 2002. Identification of Lithofacies using Kohonen Self-organizing Maps: Computers & Geosciences, Vol. 28, No. 2, p. 223-229.

Chatterjee, R., Mukhopadhyay, M., 2002. Petrophysical and geomechanical properties of rocks from the oilfields of the Krishna-Godavari and Cauvery Basins, India. Bull. Eng. Geol. Environ. 61, 169–178. https://doi.org/10.1007/s100640100137.

Chawre, B. 2018. Correlations between ultrasonic pulse wave velocities and rock properties of quartz-mica schist. *J. of Rock Mechanics and Geotechnical Engineering*, Vol. 10 (3), Pp. 594-602.

Choi, M-K., Bobet, A., Pyrak-Nolte, L.J. 2014. The effect of surface roughness and mixed mode loading on the stiffness ratio k_x/k_z for fractures. *Geophysics*. Vol. 79 (5). Pp. D319-D331.

Chung, D.H. & Buessem, W.R. 2004. The Voigt-Reuss-Hill Approximation and Elastic Moduli of Polycrystalline MgO, CaF_2, β-ZnS, ZnSe, and CdTe. *Journal of Applied Physics,* Vol. 38, Pp. 2535.

Cox, D.R., Newton, A.M.W., Huuse, M. 2020. Chapter 22 - An introduction to seismic reflection data: acquisition, processing and interpretation, *Editor(s): Nicola Scarselli, Jürgen Adam, Domenico Chiarella, David G. Roberts, Albert W. Bally, Regional Geology and Tectonics (Second Edition)*. Elsevier.

Darmawan, E. 2018. C4.5 Algorithm Application for Prediction of Self Candidate New Students in Higher Education. *Jurnal Online Informatika (JOIN)*, Vol 3 (1), Pp. 22-28.

David, E.C., Brantut, N., Schubnel, A. & Zimmerman, R.W., 2012. Sliding crack model for nonlinearity and hysteresis in the uniaxial stress-strain curve of rock, Int. J. Rock Mech. Min. Sci., 52, 9–17.

Dean, O. & Chen, Y. 2011. Recent progress on reservoir history matching: A review. *Computational Geosciences*, Vol. 15, Pp. 185-221. 10.1007/s10596-010-9194-2.

DeBruijn, G., Skeates, C., Greenaway, R., Harisson, D., Parris, M., James, S., Mueller, F., Ray, S., Riding, M., Temple, L. & Wutherich, K. 2008. High pressure high temperature technologies. *Oilfield Review*, Vol. 20 (3), Pp. 46-60.

de Gennaro, Sergio & Onaisi, Atef & Grandi, Andrea & ben brahim, Lotfi & Neillo, V.. (2008). 4D reservoir geomechanics: A case study from the HP/HT reservoirs of the Elgin and Franklin fields. First Break. 26. 10.3997/1365-2397.2008019.

Delfiner, P., Peyret, O., and Serra, O. 1987. Automatic Determination of Lithology from Well Logs: SPE Formation Evaluation, Vol. 2, No. 3, p. 303-310.

Ding, Q-L. & Song, S-B. 2016. Experimental Investigation of the Relationship between the P-Wave Velocity and the Mechanical Properties of Damaged Sandstone. *Advances in Materials Science and Engineering,* Vol. 2016.

Ding, P., Di, B., Wang, D., Wei, J. & Zeng, L. 2018. P and S wave velocity and anisotropy in saturated rocks with aligned cracks. Wave Motion 81 (2018) 1–14

Doornhof, D., Kristiansen, T.G., Nagel, N.B., Pattilo, P.D. & Sayers, C. 2006. Compaction and subsidence. *Oilfield Review*.

Dresen, G., & Gueguen, Y. 2004: Damage and Rock Physical Properties. - In: Gueguen, Y., Bouteca, M. (Eds.), *Mechanics of fluid saturated rocks*, (International Geophysics Series), Elsevier, 169-217.

Dubey, S. & Das, D. 2019. Petroleum System Based Integrated Exploration and Prospect Generation." *Paper presented at the SPE Oil and Gas India Conference and Exhibition, Mumbai, India, April 2019.* doi: https://doi.org/10.2118/194671-MS

Dutta, T., Mukerji, T., Mavko, G. & Avseth, P. 2006. Reservoir quality prediction by integrating sequence stratigraphy and rock physics. SEG Technical Program Expanded Abstracts. New Orleans 2006 Annual Meeting.

Dvorkin, J. & Nur, A. 1998. Time-average equation revisited. *J. Geophysics, 63 (2),* Pp. 460-464.

Dvorkin, J. & Nur, A. 2000. *Critical porosity model*. Department of Geophysics, Stanford University, Stanford

Dvorkin, J., Nur, A. & Rasolovoahangy, E. 2001. Rock physics reservoir characterization. *Stanford University course*.

Eardley., N. 2017. *Improved Reservoir Characterisation and Appraisal of Tight Gas Sandstones*. PhD thesis. University of Leeds.

Fagin, S.W. 1991. *Seismic Modeling of Geologic Structures*: Applications to Exploration Problems. Geophysical Development series, 2. Society of Exploration Geophysicists.

Fawad, M., Hansen, J.A. & Mondol, N.H. 2020. Seismic-fluid detection-a review. *Earth-Science Reviews*, Vol. 210, 103347, ISSN 0012-8252.

Feng, H. & Bancroft, J.C. 2006. AVO principle, processing and inversion. CREWES Research report.

Fink, F. 2015. Enhanced oil recovery, in *Ed. Johannes Fink, 2015. Petroleum Engineer's Guide to Oil Field Chemicals and Fluids (Second Edition)*, Gulf Professional Publishing, Pages 477-565, Foster, D.J., Keys, R.G. & Lane, F.D. 2010. Interpretation of AVO anomalies. *Geophysics*. Vol. 75 (5), Pp. 75A3-75A13.

Fisher, Q. 2019. Petrophysics of tight gas sandstones (PETGAS). University of Leeds. (unpublished).

Fowler, A. C. & Yang, X.S. 2003. Dissolution/precipitation mechanisms for diagenesis in sedimentary basins. *J. Of Geophysical Research*, Vol. 108.

Fredrich, J.T., Arguello, J.G., Thorne, B.J., Wawersik, W.R., Deitrick, G.L., DeRouffignac, E.P., Myer, L.R. & Bruno, M.S. 1996. Three dimensional geomechanical simulation of reservoir compaction and implications for well failures in the Belridge Diatomite. *Paper SPE 36698 presented at the 1996 SPE ATCE, Denver,USA, 6-9 October 1996.* Pp.195-210.

Fredrich, J.T., Deitrick, G.L., Arguello, J.G. & DeRouffignac, E.P. 1998. Reservoir compaction, surface subsidence, and casing damage: A geomechanics approach to mitigation and reservoir management. *The SPE/ISRM Eurock 98 held in Trondheim, Norway, 8-10 July 1998*. *SPE/ISRM 47284*. Pp. 403-412.

Garia, S., Pal, A.K. & Ravi, K. 2019. A comprehensive analysis on the relationships between elastic wave velocities and petrophysical properties of sedimentary rocks based on laboratory measurements. *J Petrol Explor Prod Technol*, Vol. 9, Pp. 1869–1881

Gassmann, F., 1951, Elasticity of porous media. *Vierteljahrsschr der Naturforschenden Gesselschaft*, v. 96, p. 1–23.

Guest, W.S. and Kendall, J-M., 1993. Modelling waveforms in anisotropic inhomogeneous media using ray and Maslov asymptotic theory: applications to exploration seismology. *CJEG*, 29, 78-92.

Gaither, A. 1953. A study of porosity and grain relationships in experimental sand. *J. sedimentary petrology*, Vol. 23(3). Pp. 180-195.

Gardner, G.H.F., Wyllie, M.R.J. and Droschak, D.M. 1965. Hysteresis in velocity-pressure characteristics of rocks. Geophysics, 30, 111-116.

Garia, S., Pal, A.K., Ravi, K & Nair, A.M. 2019. A comprehensive analysis on the relationships between elastic wave velocities and petrophysical properties of sedimentary rocks based on laboratory measurements. *J. of Petroleum Exploration and Production Technology* (2019) 9:1869–1881.

Gou, Y., Hou, Z., Li, M., Feng, W. & Liu, H. 2016. Coupled thermo hydro mechanical simulation of co2 enhance gas recovery with an extended equation of state module for TOUGH2MP-FLAC3D. *J. of Rock Mechanics & Geotechnical Eng*.

Graham, B., Reilly, W.K.., Beinecke, F., Boesch, D.F., Garcia, T.D., Murray, C.A. & Ulmer, F. 2011. *Deep Water the gulf oil disaster and the future of offshore drilling: Report to the president*. National Commission on the BP Deepwater Horizon oil spill and offshore drilling.

Grana, D. 2014. Probabilistic approach to rock physics modelling. *Geophysics*, Vol. 79 (20). Pp. D123-D143.

Greenfield, R.J., Graham, E.K., 1996. Application of the simple relation for describing wave velocity as a function of pressure in rocks containing microcracks. *J. Geophys. Res*. 101, 5643–5652.

Grekov, M.A., Morozov, N.F. 2009. Some modern methods in mechanics of cracks. In: Adamyan V.M. *et al.* (eds) *Modern Analysis and Applications. Operator Theory: Advances and Applications*, Vol 191. Birkhäuser Basel. https://doi.org/10.1007/978-3-7643-9921-4_8

Grossman, E. 2012. North Sea Gas leak: Experts Assess climate impact of ongoing accident. *Inside climate news: Natural Gas & fracking.* Vol 6.

Guilbot, J., and B. Smith, 2002, 4-D constrained depth conversion for reservoir compaction estimation: Application to Ekofisk Field. *The Leading Edge*, 21, 302-308.

Gurevich, B. 2004. A simple derivation of the effective stress coefficient for seismic velocities in porous rocks. *Geophysics*. Vol 69 (2). Pp. 393-397.

Gutierrez, M.A., Dvorkin, J. & Nur, A. 2002. Stratigraphy-guided rock physics. *The Leading Edge*, Vol. 21(1).

Habib, M., Charles, S.P., Guangqing, Y., Danlami, M.S., Congjiao, X., Jakada, H., Abba, H.A. & Omeiza, I.A. 2016. An inversion of reservoir properties based on a concurrent modeling approach: the case of a West African reservoir. *J Petrol Explor Prod Tech* (2016) 6:617–628.

Hall, M., Frank, E., Holmes, G., Pfahringer, B., Reutemann, P., & Witten, I. H. 2009. The WEKA Data Mining Software: An Update, *SIGKDD Explorations*, Vol. 11(1).

Hall, S., Kendall, J.M., Maddock, L. and Fisher, Q.J. 2008. Crack density tensor inversion for analysis of changes in rock frame architecture. *Geophys. J. Int.*, Vol. 173, 577–592.

Han, C. 2019. Spectral Decomposition AVO attributes for identifying potential hydrocarbon related frequency anomalies. *First Break*, Vol. 37.

Han, D.-H. 1986, Effects of porosity and clay content on acoustic properties of sandstones and unconsolidated sediments: Ph.D. thesis, Stanford University.

Han, D.-H & Batzle, M.L. 2004. Gassmann's equation and fluid-saturation effects on seismic velocities. *Geophysics*, Vol. 69, No. 2 (Mar-April 2004), Pp. 398–405,

Hardy, R.G & Tucker, M. 1988. XRD powder diffraction of Sediments. Tucker, M (*ed*) *Technique in Sedimentology.* Blackwell Scientific publication.

Harris, P., Du, Z., MacGregor, L., Olsen, W., Shu, R. & Cooper, R. 2009. Joint interpretation of seismic and CSEM data using well log constraints: an example from the Luva Field. *First break,* volume 27, Pp. 73-81.

Harrison, D.G., Efford, N. D., Fisher, Q. J. and Ruddle, R. A. 2018. PETMiner A Visual Analysis Tool for Petrophysical Properties of Core Sample Data. *IEEE Transactions on Visualization and Computer Graphics,* vol. 24, no. 5, pp. 1728-1741.

Hartley, F. 2001. Facilities sharing, interconnection important in HP/HT developments. Offshore, Vol. 61 (6), Pp. 96-104.

Hassanzadegan, A., Guido, B., Harald, M., Luca, U. & Günter, Z. 2014. The Effects of Temperature and Pressure on the Porosity Evolution of Flechtinger Sandstone. Rock Mechanics and Rock Engineering. 47. 10.1007/s00603-013-0401-z.

Hatchell, P.J. & Bourne, S.J. 2005. Measuring reservoir compaction using time-lapse time shifts. *SEG Technical Program Expanded Abstracts 2005*, 2500-2503

Hatchell, P.J. & Bourne, S.J. 2006. Detecting stress field changes around compacting reservoirs using time lapse seismic. *CWP meeting.*

Hatchell, P., van den Beukel, A., Molenaar, M., Maron, K., Kenter, C., Stammeijer, J., van der Velde, J. and Sayers, C., 2003, Whole earth 4D: reservoir monitoring geomechanics, 73rd. *Ann. Internat. Mtg, Soc. Expl. Geophys*, 1330-1333.

Hawkins, K. Harris, P. & Conroy, G. 2006. Estimating production induced stress changes from 4D finite offset time shifts. *SEG Technical Program Expanded Abstracts* 25(1).

Hawkins, K. 2007. Estimation of 4D anisotropy above the Elgin reservoir from 4D seismic time shift and compaction consideration. 70th Annual meeting, Rome, Italy, E006

Hawkins, K., Howe, S., Hollingworth, S., Conroy, G., Ben-Brahim, L., Tindle, C., Taylor, N., Joffroy, G. & Onaisi, A. 2007. Geomechanical stresses from 4D timeshifts measured around the depleting Franklin and Elgin reservoirs.

He, Y.X. 2015. Seismic waveform simulation using hydro-mechanical reservoir model to asses time-lapse seismic attribute.

He, Y., Angus, D.A., Clark, R.A. & Hildyard, M.W. 2016. Analysis of time-lapse travel-time and amplitude changes to assess reservoir compartmentalisation. *Geophysical Prospecting*, Vol. 64, Pp. 54- 67.

He, Y.-X., Angus, D.A., Blanchard, T.D., Wang, G.-L., Yuan, S.-Y. & Garcia, A. 2016. Time-lapse seismic waveform modelling and attribute analysis using hydromechanical models for a deep reservoir undergoing depletion. *Geophysical Journal International*, Volume 205 (1), Pp. 389–407.

He, Y.X., Angus, D., Yuan, S.Y. & Xu, Y.G. 2015. Feasibility of time-lapse AVO and AVOA analysis to monitor. *Journal of Applied Geophysics*, 122, Pp. 134–148

Heffer, K.J. Koutsabeloulis, N.C., and Wong, S.K. 1994. Coupled geomechanical, thermal and fluid flow modelling as an aid to improving water flood sweep efficiency. *Presented at Eurock SPE/ISRM Rock mechanics in petroleum engineering, Delft The Neteherland 29-31 August. SPE 2808-MS*. Pp. 447-454.

Hermansen, H., Landa, G.H., Sylte, J.E. & Thomas, L.K. 2000. Experiences after 10 years of waterflooding the Ekofisk Field, Norway. *Journal of Petroleum Science and Engineering*. Vol. 26. Pp. 11–18. 10.1016/S0920-4105(00)00016-4.

Herwenger, J.V., Bottrill, A. & Popov, P. 2016. One 4D Geomechanical Model and its Many applications. *78th EAGE Conference & Exhibition 2016 Vienna, Austria, 30 May – 2 June 2016.*

Herwanger, J. & Horne, S.A. 2009. Linking reservoir geomechanics and time-lapse seismics: Predicting anisotropic velocity changes and seismic attributes. *Geophysics*, Vol. 74(4).

Herwanger, J. & Koutsabeloulis, N. 2011. Seismic geomechanics: How to Build and Calibrate Geomechanical Models using 3D and 4D Seismic Data (EET 5). EAGE.

Herwanger, J., Mohamed, F.R., Newman, R. & Vejbæk, O. 2013. Time-lapse seismic data-calibrated geomechanical model reveals hydraulic fracture re-orientation. SEG Houston 2013 Annual Meeting. Pp. 4949-4953.

Herwanger, J., Palmer, E. and Schiott, C.R. 2007. Anisotropic velocity changes in seismic time-lapse data. 77th SEG Annual meeting, san Antonio, USA. Expanded Abstract, 2883-2887.

Hillier, S., 1999. Use of an Air Brush to Spray Dry Samples for X-Ray Powder Diffraction. *Clay Minerals*, **34**, 127-135.

Hillier, S. 2000. Accurate quantitative analysis of clay and other minerals in sandstones by XRD: comparison of a Rietveld and a reference intensity ratio (RIR) method and the importance of sample preparation. Clay Minerals, 35, 291–302.

Hillis, R.R. 1995. Regional Tertiary Exhumation in and around the United Kingdom. *Geological Society Special Publications*, Vol. 88, Pp. 167-190,

Hitlerman, F.J. 1970. Three-dimensional seismic modelling. *Geophysics*. Vol. 35 (6). Pp. 1020-1037.

Holmes, G., Donkin, A., Witten, I. H. 1994. Weka: A machine learning workbench. *Proceedings of the Second Australia and New Zealand Conference on Intelligent Information Systems, Brisbane, Australia*. Retrieved 2007-06-25.

Holt, R.M., Furre, A.-K. & Horsrud, P. 1997. Stress dependent wave velocities in sedimentary rock cores: Why and why not?, *International Journal of Rock Mechanics and Mining Sciences,* Volume 34, Issues 3–4, Pages 128.e1-128.e12, ISSN 1365-1609,

Holt, R.M., Gheibi, S. & Lavrov, A. 2016. Where does the stress path lead? Irreversibility and hysteresis in reservoir geomechanics. *50th US rock mechanics/ geomechanics symposium*, Houston.

Hoffman, N.W & Tobin, H.J. 2004. An empirical relationship between velocity and porosity for undertrust sedimnets in the Nankai Trough accretionary prism.

Hosseini, E., Gholami, R.& Hajivand, F. 2019. Geostatistical modelling and spatial distribution analysis of porosity and permeability in the Shurijeh-B reservoir of Khangiran gas feld in Iran. *J Pet Explor Prod Technol*, Vol. 9, Pp. 1051–1073.

Hssina, B., Merbouha, A., Ezzikouri, H. & Erritali, M. 2014. A comparative study of decision tree ID3 and C4.5. *International Journal of Advanced Computer Science and Applications (IJACSA). Special Issue on Advances in Vehicular Ad Hoc Networking and Applications,* Pp. 13-19.

Huang, L., Stewart, R.R., Sil, S. & Dyaur, N. 2015. Fluid substitution effects on seismic anisotropy. *Journal of geophysical research: Solid earth*. AGU Publication.

Huang, T., Zhou, X., Yang, H., Liao, G. & Zeng, F. 2017. CO2 flooding strategy to enhance heavy oil recovery. *Petroleum*, Vol. 3 (1), Pp. 68-78.

Hussein, M., El-Ata, A.A. & El-Behiry, M. 2020. AVO analysis aids in differentiation between false and true amplitude responses: a case study of El Mansoura field, onshore Nile Delta, Egypt. *J Petrol Explor Prod Technol*, Vol. 10, Pp. 969–989.

Ibrahimli, O. 2019. *Time-shift analysis in the overburden andvreservoir zones from 4D studies across the Norne field.* Norwegian University of Science and Technology. Master’s Thesis.

Jeng, F.S., Weng, M.C., Lin, M.L., Huang, T.H., 2004. Influence of petrographic parameters on geotechnical properties of tertiary sandstones from Taiwan. *Eng. Geol. 73,* 71–91.

Johnson, C. W., Ben-Zion, Y., Meng, H., & Vernon, F. 2020. Identifying different classes of seismic noise signals using unsupervised learning. *Geophysical Research Letters*, Vol. 47. https://doi.org/10.1029/2020GL088353

Kaminskaite, I. 2019. Impact of faults on fluid flow in carbonates. Phd Thesis. University of Leeds.

Katahara, K.W. 1999. Effect of mineral VP/VS on rock VP/VS. *SEG Technical Program Expanded Abstracts 1999*. Pp. 1029-1032.

Katz, S. A., Vernik, L., and Chilingar, G. V. 1999. Prediction of Porosity and Lithology in Siliciclastic Sedimentary Rock using Cascade Neural Assemblies. *Journal of Petroleum Science and Engineering*, Vol. 22, No. 1, p. 141-150.

Kern, H. & Ritcher, A. 1981. Temperature deravatives of compressional and shear wave velocities in crustal and mantle rocks at 6 kbar confining pressure, *J. geophysics*, 49, Pp. 47-56.

King, M.S., 1966. Wave velocities in rocks as a function of changes in overburden pressure and pore fluid saturants, *Geophysics*, Vol.31, Pp.50–73.

Kohout, T., Karlqvist, R., Lasilla, I., Eskelinen, J., Hortling, A., Pesonen, L.J. & Haeggstrom, E. 2013. Ultrasonic Determination of Porosity in Homogeneous Ceramic Samples, *Geophysica* (2013), Vol. 49(1–2), Pp. 25–32.

Korneev, V.A. & Glubokovskikh, S. 2013. Seismic velocity changes caused by an overburden stress. Geophysics 78(5), Pp. 131-C137.

Krebes, E.S. 2004. Seismic Forward Modeling. *CSEG Recorder*, Vol. 30, Pp. 28–39.

Krief, M., Garar, J., Stellingwerff, J. & Ventre, J. 1990. A petrophysical interpretation using the velocities of P and S waves (full- waveform sonic). *The Log Analyst* 31:355–369

Kudarova, A., Hatchell, P., Brain, J. and MacBeth, C. 2016. Offset dependence of production-related 4D time shift: real data examples and modelling. 86th SEG Annual Meeting, Dallas, USA. Expanded Abstracts.

Lacasse M.D., White L., Denli H. & Qiu L. 2018. Full-Wavefield Inversion: An Extreme-Scale PDE-Constrained Optimization Problem. In: Antil H., Kouri D.P., Lacasse MD., Ridzal D. (eds) Frontiers in PDE-Constrained Optimization. *The IMA Volumes in Mathematics and its Applications*, Vol. 163. Springer, New York, NY. https://doi.org/10.1007/978-1-4939-8636-1_6

Lang, X. and Grana, D. 2019. Rock physics modelling and inversion for saturation-pressure changes in time-lapse seismic studies. *Geophysical Prospecting*, Vol. 67: 1912-1928. https://doi.org/10.1111/1365-2478.12797

Lary, D.J., Alavi, A.H., Gandomi, A.H. & Walker, A.L. 2016. Machine learning in geosciences and remote sensing. *Geoscience Frontiers*. Vol. 7, (1), Pages 3-10.

Lim, J.-S., Kang, J. M., and Kim, J. 1999. Interwell Log Correlation Using Artificial Intelligence Approach and Multivariate Statistical Analysis, SPE Asia Pacific Oil and Gas Conference and Exhibition: Jakarta, Indonesia, Society of Petroleum Engineers.

Llana-Funez, S. & Brown, D. 2012. Contribution of crystallographic preferred orientation to seismic anisotropy across a surface analog of the continental Moho at Cabo Ortegal, Spain. *Bulletin*, Vol. 124 (9-10), Pp. 1495-1513. Geological Society of America.

Lorenzen, R. 2018. Multivariate linear regression of sonic logs on petrophysical logs for detailed reservoir characterization in producing fields. *Interpretation*, Vol. 6 (3): T531–T541. doi: https://doi.org/10.1190/INT-2018-0030.1

Longuemare, P., Mainguy, M., Lemonnier, P., Onaisi, A., Gerarad, Ch., & Koutsabeloulis, N. 2002. Geomechanics in Reservoir Simulation: Overview of Coupling Methods and Field Case Study. *Oil and Gas Sci. & Tech*. Vol. 57 (5), Pp. 471-483.

Lumley, D. 2001. Time-lapse seismic reservoir monitoring. *Geophysics*, Vol. 66 (1).

Lynch, T., Fisher, Q.J., Angus, D. & Lorinczi, P. 2013. Investigating stress path hysteresis in co2 injection using coupled geomechanichal fluid flow. Energy Procedia, Vol. 2013 (37). Pp. 3833-3841.

Maaliw, R. R. III. & Ballera, M. A. 2017. Classification of learning styles in virtual learning environment using J48 decision tree. 14th International Conference on Cognition and Exploratory Learning in Digital Age (CELDA 2017)

MacBeth, C., Mangriotis, M-D., Amini, H. 2019. Review paper: Post-stack 4D time-shift: Interpretation and evaluation. *Geophysical prospecting*, 67, Pp 3-31.

Mainprice, D., Barruol, G. & Ben Ismaïl, W. 2000. The Seismic anisotropy of the Earth's mantle: From single crystal to polycrystal. *Shun-Ichiro Karato; Alessandro Forte; Robert Liebermann; Guy Masters; Lars Stixrude. Earth's Deep Interior: Mineral Physics and Tomography From the Atomic Scale to the Global Scale*, 117, American Geophysical Union, pp.237 - 264,

Makse, H, Gland, N., Johnson, D.L., & Schwartz, L.M. 1999. Why effective medium theory fails in granular materials. *Physical Review Letters*, Vol. 83(24). Pp. 5070-5073.

Mandal, D., Suwarlan, W., Mansur, R., Ali, K. & Masoudi, R. 2011. 4D Seismic Improves Reservoir Management- A case Study on Angsi Field. International Petroleum Technology Conference.

Marshall, M. & Strahan, D. 2012. Report reveals earlier problems at North Sea gas site. *Newscientist*, Vol. 2859.

Mavko, G. & Mukerji, T. 2013. Estimating Brown-Korringa constants for fluid substitution in multimineralic rocks. *Geophysics*, Vol 78 (3). Pp. L27-L35.

Mavko, G., Mukerji, T., and Dvorkin, J. 2009. *The Rock Physics Handbook: Tools for Seismic analysis of porous media. 2nd Edition*, Cambridge University Press.

Mavko, G., Mukerji, T., and Dvorkin, J., 1998, *Rock physics handbook: Tools for seismic analysis in porous media*. Cambridge University Press.

Miah, M., Martin, L.B., Foxall, W., Rutqvist, J., Rinaldi, A.P. & Mullen, C. 2015. Development of a Hydro-geomechanical Model to Simulate Coupled Fluid Flow and Reservoir Geomechanics. *TOUGH symposium 2015, Berkeley, California, September 28-30, 2015.*

Minkoff, S.E. Mike Stone, C. & Bryant, S. 2003, Coupled fluid flow and geomechanical deformation modelling. *J. of Petroleum Sci & Eng*. Vol. 38, Pp. 37-56.

Minkoff, S. E., Stone, C.M., Bryant, S. & Peszynska, M. 2004. Coupled geomechanics and flow simulation for time-lapse seismic modelling. *Geophysics*, Vol. 61, Pp.200–211.

Misaghi, A., Negahban, S., Landro, M. & Javaherian, A. 2010. A comparison of rock physics models for fluid substitution in carbonate rocks. *Exploration Geophysics*, Vol. 41 (2)

Mojeddifar, S., Kamali, G.R. & Ranjbar, H. 2015. Porosity prediction from seismic inversion of a similarity attribute based on a pseudo-forward equation (PFE): a case study from the North Sea Basin, Netherlands. *Petroleum Science*. Vol. 12. 10.1007/s12182-015-0043-8.

Molenaar, M.M., Hatchell, P.J. & Van den Beukel, A.C. 2004. Applying Geo-mechanics and 4D: 4D in-situ stress as a complementary tool for optimizing field management. *Presented at 6th North America Rocks Mechanics Symposium (NARMS), in Houston, Texas, June 5-9 2004.*

Mondal, S., Yadav, A. & Chatterjee, R. 2020. Rock-physics forward modelling to predict seismic behaviour: A case study for exploration target in Mahanadi basin, East Coast of India. Geophysical Prospecting, Vol. 68 (7).

Mosquera, J.C., Ghisays, A. & Montes, L. 2013. AVO analysis with partial stacking to detect gas anomalies in the GÜEPAJÉ-3D project. *Geofisica Internacional*. Vol.52 (3), Pp. 249-260.

Mukhopadhyay, P. K. and Subhashis, M. 2011. An Accurate Ray-Based Offset-To-Angle Transform from Normal Moveout Uncorrected Multicomponent Data in a Transversely Isotropic Medium with Vertical Symmetry Axis. *Geophysics, Vol.* 76 (3).

Nagel, N. 2001. Compaction and subsidence issues within the petroleum industry: From Wilmington to Ekofisk and beyond. *Physics and Chemistry of The Earth Part A-solid Earth and Geodesy*, Vol. 26, Pp. 3-14.

Nayfeh, A.H. 1995. Chapter 4 Generalized Snell's law and interfaces. *North-Holland Series in Applied Mathematics and Mechanics,* North-Holland, Vol. 39, Pages 61-70, ISSN 0167-5931, ISBN 9780444890184, https://doi.org/10.1016/S0167-5931(06)80045-8.

Nguyen, P., Nam, M.J. & Park, C. 2015. A review on time-lapse seismic data processing and interpretation. *Geosciences Journal*. 19.

Nichola, J.E. 2017. *Improved reservoir characterisation and appraisal of tight gas sandstones*. Ph.D. Thesis. University of Leeds (School of Earth and Environment).

Nihei, K.T., Hilbert, L.B., Jr., Cook, N.G.W., Nakagawa, S. & Myer, L.R., 2000. Frictional effects on the volumetric strain of sandstone, Int. J. Rock Mech. Min. Sci., 37, 121–132.

Noble, M., Gesret, A. & Belayouni, N. 2014. Accurate 3-D finite difference computation of traveltimes in strongly heterogeneous media. *Geophysical J. Int.*, Vol.199 (3), Pp. 1572–1585, https://doi.org/10.1093/gji/ggu358

Nur, A. 1971. Effects of stress on velocity anisotropy in rocks with cracks. *J. Geophys. Res., 76 (8)*, Pp. 2022– 2034

Nur, A., Mavko, G., Dvorkin, J., & Galmudi, D., 1998. Critical porosity: a key to relating physical properties to porosity in rocks. Leading Edge, 17:357–362.

Nur, A. & Simmons, G. 1969. Stress-induced velocity anisotropy in rock An experimental study. *Journal of Geophysicsal Research*, Vol. 74 (27), Pp. 6667-6674.

Nur, A. & Simmons, G., 1969. The effect of viscosity of a fluid phase on velocity in low-porosity rocks. Earth Planet. Sci. Lett., 7, 99–108.

Olsen, C., H.F. Christensen, and I.L. Fabricius. 2008. Static and dynamic Young's moduli of chalk from the North Sea. *Geophysics*, Vol. 73, 41-50

Osorio, J., Chen, H-Y., Teufel, L. & Schaffer, S. 1998. A Two-Domain, 3D, Fully Coupled Fluid-Flow/Geomechanical Simulation Model for Reservoirs with Stress-Sensitive Mechanical and Fluid-Flow Properties. *Society of Petroleum Exploration*. 10.2118/47397-MS.

Pervukhina, M., Gurevich, B., Dewhurst, D. N. & Siggins, A. F. 2010. Applicability of velocity—stress relationships based on the dual porosity concept to isotropic porous rocks. *Geophysical Journal International*, Vol. 181 (3) DO 10.1111/j.1365-246X.2010.04535.x

Phadke, S. & Ramanjulu, M. 2012. 3D Acoustic and Elastic Wave Modeling on a High-Performance Computing System. Search and Discovery Article.

Pointer, T., Liu, E. & Hudson, J.A. 2000. Seismic wave propagation in cracked porous media. *Geophys. J. Int.*, Vol. 142, Pp.199-231

Price, D., Angus, D.A., Garcia, A. & Fisher, Q.J. 2017. Probabilistic analysis and comparison of stress-dependent rock physics models. *Geophysical Journal International*, Vol. 210(1), Pp. 196-209.

Price, D., Angus, D.A., Garcia, A. & Fisher, Q.J. 2017. Probabilistic analysis and comparison of stress-dependent rock physics models. *Geophysical Journal International*, Vol. 210(1), Pp. 196-209.

Prioul, Romain. 2004. Calibration of Velocity-stress Relationships Under Hydrostatic Stress For Their Use Under Non-hydrostatic Stress Conditions. *Paper presented at the 2004 SEG Annual Meeting, Denver, Colorado, October 2004.*

Prioul, R., Bakulin, A. & Bakulin, V. 2004. Nonlinear rock physics model for estimation of 3D subsurface stress in anisotropic formation: Theory and laboratory verification. *Geophysics*, Vol. 69 (2). Pp. 415-425.

Pyrak Nolte, L.J. & Nolte, D.D. 2012. Approaching a universal scaling relationship between fracture stiffness and fluid flow. *Nature Communication*.

Qiunguo, L., Zhang, X., Mohsin, L., Jiroudi, F. & Alrawahi, A. 2013. 3D geomechnical modelling, wellbore stability analysis improve field's performance. *World Oil*, October 2013, Pp. 53-61.

Quinlan, J. R. 1993. C4.5: Programs for Machine Learning. *Morgan Kaufmann Publishers*.

Raeesi, M., Moradzadeh, A., Doulati Ardejani, F., and Rahimi, M. 2012. Classification and Identification of Hydrocarbon Reservoir Lithofacies and Their Heterogeneity using Seismic Attributes, Logs Data and Artificial Neural Networks: Journal of Petroleum Science and Engineering, Vol. 82, p. 151-165.

Raymer, L.L., Hunt, E.R., and Gardner, J.S., 1.980. An improved sonic transit time-to-porosity transform. Trans. Soc. Prof. Well Log Analysts, *21st Annual Logging Symposium, Paper P.*

Rezaei, Shiba & Babasafari, Amir Abbas & Bashir, Yasir & Sambo, Chico & Ghosh, Deva & Salim, Ahmed. 2020. Time-lapse (4D) Seismic for Reservoir Fluid Saturation Monitoring: Application in Malaysian Basin. *Petroleum and Coal*, Vol. 62, Pp. 712-719.

Reuss, A., 1929. Berechnung der Fliessgrenzen von Mischkristallen auf Grund der Plastizitätsbedingung für Einkristalle. Z. Ang. Math. Mech., 9, 49–58.

Richardson, M. & Briggs, K. 1993. On the Use of Acoustic Impedance Values to Determine Sediment Properties. *Proceedings of the Institute of Acoustics*. Vol. 15 (12).

Roach, J. 2017. *How to extract model data from MPGeomechanics*. Unpublished.

Rob, S. & Mike, B. 2014. *Seismic Amplitude, An Interpreter's Handbook*. Cambridge University Press.

Rosid, M.S., Wahyuni, S.D., & Haidar, M.W. 2016. Carbonate Reservoir Characterization with Pore Type Inversion Using Differential Effective Medium (DEM) Model at "X" Field, East Java. *International Symposium on Current Progress in Mathematics and Sciences 2016 (ISCPMS 2016). AIP Conf. Proc. 1862.*

Ross, C.P. 2000. Effective AVO crossplot modelling: A tutorial. *Geophysics*. Vol.65 (3), Pp. 700-711.

Røste, T. 2007. Monitoring overburden and reservoir changes from prestack time lapse seismic data applications to chalk fields.

Roste, T., Landro, M. and Hatchell, P. 2007. Monitoring overburden layer changes and fault movement from time-lapse seismic data on Valhall Field. Geophysical Journal International, 170, 1100-1118.

Ruiz, H., Seregin, A., Skogly, O.P., Libak, A. & Lien, M. 2020. Accurate Measurement of Seabed Subsidence at the Ormen Lange Field. *Conference Proceedings, EAGE 2020 Annual Conference & Exhibition Online*, *Dec 2020*, Vol. 2020, Pp.1 – 5.

Russell, B.H. 2004. The application of multivariate statistics and neural networks to the prediction of reservoir parameters using seismic attributes. PhD thesis. University of Calgary.

Rwechungura, R., Dadashpour, M. & Kleppe, J. 2011. Advanced History Matching Techniques Reviewed. *The SPE Middle East Oil and Gas Show and Conference, Manama, Bahrain, September 2011*.Paper Number: SPE-142497-MS.

Rybach, L. & Bunterbarth, G. 1982. Relationships between the petrophysical properties density, seismic velocity, heat generation, and mineralogical constitution. *Earth and Planetary Science Letters,* Vol. 57 (2), Pp. 367-376

Saether, M., Lunde, P. & Ersland, G. 2016. Sound velocity measurement methods for porous sandstone. Measurements, finite element modelling, and diffraction correction. *Proceedings of the 39th Scandinavian Symposium on Physical Acoustics, Geilo, Norway, Jan. 31 – Feb. 3, 2016*

Sakamaki, T. 2018. Structure and properties of silicate in: Kono, Y. & Sanloup, C. 2018. Magma under Pressure. *Elsevier*.

Salah, M., Alqudah, M., Abd El Aal, A. & Barnes, C. 2018. Effects of porosity and composition on seismic wave velocities and elastic moduli of lower cretaceous rocks, central Lebanon. *Acta Geophysica*, Vol. 66. 10.1007/s11600-018-0187-1.

Salzberg, S.L. 1994. Book Review: C4.5: Programs for Machine Learning by J. Ross Quinlan. Morgan Kaufmann Publishers, Inc., 1993. *Machine learning*, Vol. 16. Pp. 235-240.

Sambridge, M. 1999. Geophysical inversion with a neighborhood algorithm: I, searching a parameter space. *Geophys. J. Int.*, 138, 479-494.

Sammut, C. & Webb, G.I (eds.), 2011. *Encyclopedia of Machine Learning*, Springer.

Santarelli, F.J., O. Havmøller, and M. Naumann, *Geomechanical Aspects of 15 Years Water Injection on a Field Complex: An Analysis of the Past to Plan the Future*. SPE International, 2008. SPE 112944.

Santarelli, F.J., et al., *Reservoir Stress Path: The Depletion and the Rebound* SPE International, 1998. SPE 47350.

Sayers, C.M. 2002. Stress-dependent elastic anisotropy of sandstones. Geophysical Prospecting, 50, 85-95.

Sayers, C.M. & Chopra, 2009. Introduction to this special section: Seismic modelling. *The leading edge*.

Sayers, C.M. & Kachanov, M. 1995. Microcrack induced elastic wave anisotropy of brittle rocks. *Journal of Geophysical Research*, 100, 4149-4156.

Schmidt, J., Marques, M.R.G., Botti, S. & Marques, M.A.L. 2019. Recent advances and applications of machine learning in solid-state materials science. *npj Comput Mater 5*, Vol. 83. https://doi.org/10.1038/s41524-019-0221-0

Schon, J.H. 2004. *Physical properties of rocks: Fundamental and principles of petrophysics*. Elsevier.

Sebtosheikh, M.A., Motafakkerfard, R., Riahi, M.A. & Moradi, S. 2015. *Iranian Journal of Oil & Gas Science and Technology.* Vol. 4 (2015), No. 2, pp. 01-14

Segura J.M., Fisher, Q.J., Crook, A.J.L., Dutko, M., Yu, J.G., Skachkov, S., Angus, D.A., Verdon, J.P. & Kendal, J.-M. 2011. Reservoir stress path characterization and its implications for fluid flow production simulations. *Petroleum Geoscience.*

Settari, A., Sullivan, R.B, Walters, D.A. & Wawrzynek, P.A. 2002. 3D analysis and prediction of microseismicity in fracturing by coupled geomechnical modelling. *Soc. of Petroleum.* SPE 75714. Pp. 1-8.

Sharma, M.M. & Tutuncu, A.N. 1994. Grain contact adhesion hysteresis: A mechanism for attenuation of seismic waves. *Geophysical Research Letter*, Vol. 21 (21), Pp. 2323-2326.

Shapiro, S. A., & Kaselow, A. 2005. Porosity and elastic anisotropy of rocks under tectonic stress and pore-pressure changes. *Geophysics*, Vol.70 (5), Pp. N27–N38.

Shen, H., Li, X., Li, Q. & Wang, H. 2020. A method to model the effect of pre-existing cracks on P-wave velocity in rocks. J. *of Rock Mechanics and Geotechnical Engineering*, Vol 12 (3), Pp 493-506.

Sheriff, R. E., & Geldart, L. P. 1995. *Exploration seismology*. Cambridge university press.

Shi, G. & Yang, D. 2001. The regression analysis study on velocity and porosity, and clay content of rocks, *Acta Scicentiarum Naturalum Universitis Pekinesis*, Vol. 37, 379–384.

Shuey, R. T. 1985. A simplification of the Zoeppritz equations. Geophysics, Vol. 50(4), Pp. 609-614.

Simm, R., White, R. & Uden, R. 2000. Anatomy of AVO crossplots. The Leading Edge. Vol. 19. Pp. 150-155.

Staples, R., Ita, J., Burrell, R. & Nash, R. 2007. Monitoring pressure depletion and improving geomechanical models of the Shearwater Field using 4D seismic. *The leading edge*, Vol 26 (5).

Smith, M., Gerhardt, A. & Thomas, P. 2010. Quantitative 4D interpretation – Relating the seismic to production changes at Enfield, North West Shelf, Australia. *ASEG Extended Abstracts*, 2010:1, 1-4, DOI: 10.1081/22020586.2010.12041872

Smith, T.D., Sondergeld, C.H. and Rai, C.S. 2003. Gassmann fluid substitutions: A tutorial. Geophysics, Vol. 68 (2), Pp. 430-440.

Smith, T.M., Sayers, C.M & Sondergeld, C. 2009. Rock properties in low-porosity/low-permeability *sandstones. The Leading Edge (January 2009).* Pp.48-59.

Souza, R., Lumley, D., Shragge, J., Davolio, A. & Schiozer, D.J. 2018. Analysis of time-lapse seismic and production data for reservoir model classification and assessment. *J. Geophys. Eng*. Vol. 15, Pp. 1561–1587.

Soete, J., Kleipool, L.M., Claes, H., Hamaekers, H., Kele, S., Ozkul, M., Foubert, A., Reijmer, J.J.G. & Swennen, R., 2015. Acoustic properties in travertines and their relation to porosity and pore types. *Mar. Pet. Geol. Vol 59*, Pp. 320–335. https://doi.org/ 10.1016/ j.marpetgeo.2014.09.004.

Soleimani, F., Hosseini, E. & Hajivand, F. Estimation of reservoir porosity using analysis of seismic attributes in an Iranian oil field. *J Petrol Explor Prod Tech*, Vol. 10, Pp. 1289–1316. https://doi.org/10.1007/s13202-020-00833-4

Somasundaram, S., Mund, B. & Soni, R. 2017. Seismic attribute analysis for fracture detection and porosity prediction: a case study from tight volcanic reservoirs, Barmer Basin, India. *Lead Edge*, Vol. 36(11):947b1–947b7. https ://doi.org/10.1190/tle36 11094 7b1.1

Song, T., Ding, W., Liu, H., Wu, J., Zhou, H. & Chu, J. 2020. Uncertainty Quantification in Machine Learning Modeling for Multi-Step Time Series Forecasting: Example of Recurrent Neural Networks in Discharge Simulations. *Water*, Vol. 12, 912; doi:10.3390/w12030912

Staples, R., Ita, J., Burrell, R. & Nash, R. 2007. Monitoring pressure depletion and improving geomechanical model of the Shearwater field using 4D seismic. *The Leading Edge*, Vol 26 (5).

Subrahmanyam, D. & Rao, P.H. 2008. Seismic attributes. A review. *7th Int. Conference & Exposition on Petroleum Geophysics, Hyderabad 2008.*

Swarbrick, R.E. 2012. Review of pore-pressure prediction challenges in high-temperature areas. *The Leading Edge*, Vol. 31(11), Pp.1288-1294.

Szczerbicki, E. 2001. Management of Complexity and Information Flow, Editor(s): A. Gunasekaran, *Agile Manufacturing: The 21st Century Competitive Strategy*, Elsevier Science Ltd, 2001, Pp. 247-263,

Tang, H., 2009. Successful Carbonate Well Log Facies Prediction using an Artificial Neural Network Method: Wafra Maastrichtian Reservoir, Partitioned Neutral Zone (PNZ), Saudi Arabia and Kuwait. *SPE Annual Technical Conference and Exhibition: New Orleans, Louisiana, Society of Petroleum Engineers.*

Tang, H. and White, C. D. 2008. Multivariate Statistical Log log-facies Classification on a Shallow Marine Reservoir. *Journal of Petroleum Science and Engineering*, Vol. 61 (2), Pp. 88-93.

Tavassoli, Z. Carter, J. & King, P. 2004. Errors in History Matching. *SPE Journal*, Vol. 9, 10.2118/86883-PA.

Tiab, D. & Donaldson, E.C. 2016. Chapter 3 - Porosity and Permeability, *Editor(s): Djebbar Tiab, Erle C. Donaldson, Petrophysics (Fourth Edition),* Gulf Professional Publishing.

Tod, S. R. 2002. The effects of stress and fluid pressure on the anisotropy of interconnected cracks. *Geophysics J. Int.,* Vol. 149, 149–156.

Trani, M., Arts, R., Leeuwenburgh, O. & Brouwer, J. 2011. Estimation of changes in saturation and pressure from 4D seismic AVO and time-shift analysis. *Geophysics,* Vol. 76 (2). P. C1–C17, 10.1190/1.3549756.

Tutuncu, A.N., Podio, A.L. & Sharma,M.M., 1998. Nonlinear viscoelastic behavior of sedimentary rocks: II. Hysteresis effects and influence of type of fluid on elastic moduli, *Geophysics,* Vol. 63, Pp. 195–203.

Thai, N.B., Tran, X.V., Do, K.Q., Hoang, Q.T. & Nguyen, T.M. 2017. Applying the evaluation results of porosity-permeability distribution characteristics based on hydraulic flow units (HFU)to improve the reliability in building a 3D geological model, GD field, Cuu Long Basin. *J. Petrol Explor Prod Technol*, Vol. 7, Pp. 687–697.

Umoren, E.B. & George, N.J. 2018. Time lapse (4D) and AVO analysis: A case study of Gullfaksfield, NorthernNorth Sea. *NRIAG Journal of Astronomy and Geophysics*, Vol. 7 (62)–7777

Usman, M. 2018. *Predictive analysis on large data for actionable knowledge: emerging research and opportunity*. IGI Global.

Van der Linden, A., Korndorffer, F., Dudley, J., Yassir, N. & Christian L. 2006. The effect of stress path on the sonic response of Pierre Shale. Paper presented at the *Golden Rocks 2006, The 41st U.S. Symposium on Rock Mechanics (USRMS), Golden, Colorado, June 2006.*

Vejbæk, O.V., Mohamed, F.R. & Herwanger, J.V. 2014. 4D seismic, 4D geomechanics and hydraulic stimulation in the low permeability South Arne chalk field. *First Break*, Vol. 32 (6).

Verdon, J.P. 2012. Microseismic monitoring and geomechanical modelling of CO2 storage in subsurface reservoirs. *Springer Theses Recognizing Outstanding Ph.D. Research.* Springer.

Verdon, J., Angus, D.A., Kendall, J.M. and Hall, S. 2008. The effects of microstructure and nonlinear stress on anisotropic seismic velocities. *Geophysics*, Vol. 73(4), D41–D51.

Vernik, L. and Nur, A. 1992. Petrophysical classification of siliciclastics for lithology and porosity prediction from seismic velocities. *AAPG Bull. 76 (9): 1295-1309.*

Vilhelm, J. Ivankina, T., Lokajíček, T. & Rudajev, V. 2016. Comparison of laboratory and field measurements of P and S wave velocities of a peridotite rock. *Int. J. of Rock Mechanics and Mining Sci*, Vol. 88, Pp. 235-241, ISSN 1365-1609, https://doi.org/10.1016/j.ijrmms.2016.07.027.

Voigt, W., 1907. Bestimmung der Elastizitätskonstanten von Eisenglanz. *Ann. Phys.*, Vol. 24, Pp. 129–140.

Wang, L. & Alexander, C.A. 2016. Machine learning in big data. *International Journal of Mathematical, Engineering and Management Sciences*, Vol. 1 (2), Pp. 52–61.

Wang, X., Yang, S., Wang, Y., Zhao, Y. & Ma, B. 2018. Improved permeability prediction based on the feature engineering of petrophysics and fuzzy logic analysis in low porosity–permeability reservoir. *Journal of Petroleum Exploration and Production Technology*, Vol. 9, Pp. 869–887. https://doi.org/10.1007/s13202-018-0556-y

Wang, Z. 2001. Fundamental of seismic rock physics. *Geophysics*, Vol. 66(2), Pp.398-412.

Watt, J. P., Davies, G. F. & Richard J.O. 1976. The elastic properties of composite materials, Reviews of Geophysics, *Rev. Geophys*, 14 (4), Pp 8755-1209.

Wayne, M. 2015. AVO attributes plugin for the open source seismic interpretation platform, Opend Tect (http://www.opendtect.org/). P. 10.E.B.

Wikel, K. 2011. Geomechanics Bridging the Gap from Geophysics to Engineering in Unconventional Reservoirs. *CSEG Recorder*.

Wollner, U., and Mavko, G. 2017. Brown and Korringa constants for heterogeneous thinly layered poroelastic media, J. *Geophys. Res. Solid Earth*, Vol. 122, Pp. 895– 905 doi:10.1002/2016JB013672.

Wyllie, M. R. J., Gregory, A.R., and Gardner, G. H. F., 1958. An experimental investigation of factors affecting elastic wave velocities in porous media. Geophys., 23, 459–493.

Wyllie, M. R. J., Gregory, A.R., and Gardner, L.W., 1956. *Elastic wave velocities in heterogeneous and porous media. Geophys., 21, 41–70.*

Yang, X., Pan, Y., Fan, W., Huang, Y., Zhang, Y., Wang, L., Wang, L., Teng, Q., Qiu, K., Zhao, M. & Shan, F. 2018. Case Study: 4D Coupled

Reservoir/Geomechanics Simulation of a High-Pressure/High-Temperature Naturally Fractured Reservoir. *Society of Petroleum Engineers Journal*., Vol. 23 (5). 2018. Pp.1518-1538.

Yilmaz, O., 2001, *Seismic data analysis*. Society of Exploration.

Yu, C., Ji, S., Li, Q., 2016. Effects of porosity on seismic velocities, elastic moduli and Poisson's ratios of solid materials and rocks. J. Rock Mech. Geotech. Eng. 8, 35–49. https://doi.org/10.1016/j.jrmge.2015.07.004.

Zatsepin, S.V. & Cramplin, S. 1997. Modelling the compliance of crustal rock- I. Response of shear-wave splitting to differential stress. *Geophys. J. Int*. Vol. 129. Pp. 477-494.

Zhang, Y., Bhark, E., Phale, H. & Dehghani, K. 2014. Case Studies: The Ensemble-based Approach to History Matching and Model Parameter Estimation. *Proceedings - SPE Annual Technical Conference and Exhibition*, Vol.3, Pp. 2022-2038. 10.2118/170726-MS.

Zhong et al. 2014. A novel EBSD based finite element wave propagation model for investigating seismic anisotropy.

Zhu, Q. & Shao, J. 2017. Micromechanics of rock damage: Advances in the quasi-brittle field. *Journal of Rock Mechanics and Geotechnical Engineering*, Vol. 9 (2017), Pp. 29-40.

Zimmer, M., Prasad, M., Mavko, G. & Nur, A. 2007. Seismic velocities of unconsolidated sands: Part 2 Influence of sorting and compaction-induced porosity variation. *Geophysics*, Vol. 72 (1).

Zoback, M. 2007. *Reservoir Geomechanics*. Cambridge University Press.

8 APPENDIX

Software utilized

- **ATRAK**

The program ATRAK is a package to solve seismic wave propagation in anisotropic media based on ray theory. ATRAK tracks seismic rays in form of compressional, shear and converted waves which travel through 2.5D generally anisotropic, inhomogeneous and multi-layered media (Guest & Kendall, 1993). The program is written in FORTRAN, and is developed and maintained by Outer Limits Seismic Software. Using the ray tracing results, the program is capable of generating 2D 3-components synthetic seismic sections. Carrying out the ray-tracing program, three steps need to be followed:

(i) building an ATRAK model

(ii) running ATRAK program,

(iii) generating synthetic seismograms.

Furthermore, with the complementary tools, the following displays can be generated:

- transmission and reflection coefficients between two media;
- group velocity and slowness surfaces from model elastic constants;
- reflection amplitudes, ray-paths and travel-times.

The software is fast to implement and can generate clear synthetics from defined horizons without multiples. Both 'ray shooting' (by setting incidence and azimuthal phase angle) and 'normal incidence' (zero offset for horizontal interface) modes can be implemented. For models having more complex structure with sharp elasticity variations, more advanced full-waveform algorithms, such as finite-difference and finite-element full-waveform simulation, should be employed.

- **MATLAB**

  MATLAB is a commercial programming and numeric computer platform. This software package has wide applications in numerical computing such as signal processing, 2D/3D visualization, etc. In this thesis, there are a lot diagram and results were generated by using this software. The program command are written in Matlab scripts and some of the simulation such in ATRAK programme written in UNIX shell script.

- **PETMiner**

  PETMiner developed by PETRIVA LTD is a sophisticated data visualization and data mining tool. This software is capable to carry out the integration and analysis of microstructural and petrophysical data. The software package is implemented in Python, uses Matplotlib for visualization, and SQLAlchemy for database access. Python's introspection capabilities have allowed a novel use of SQLAlchemy's object-relational mapping to provide a user defined backend database schema, which can by amended by the user during usage of the application. Most of correlation analysis for the laboratory data were analyses using this software. This software also allow simple linear regression or multiple linear regression were carried out with friendly graphical user interface.

Output during ultrasonic measurement

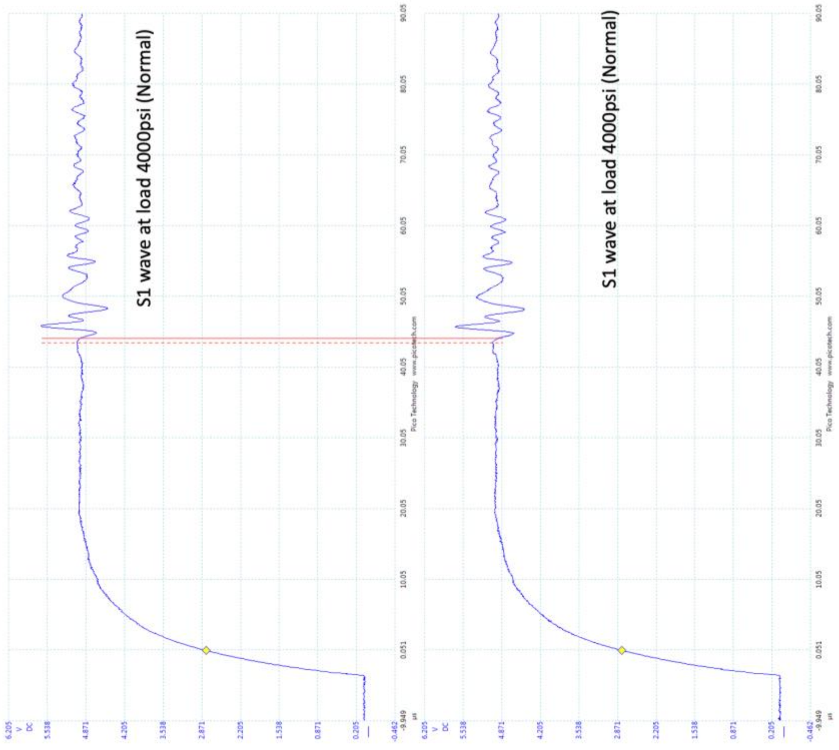

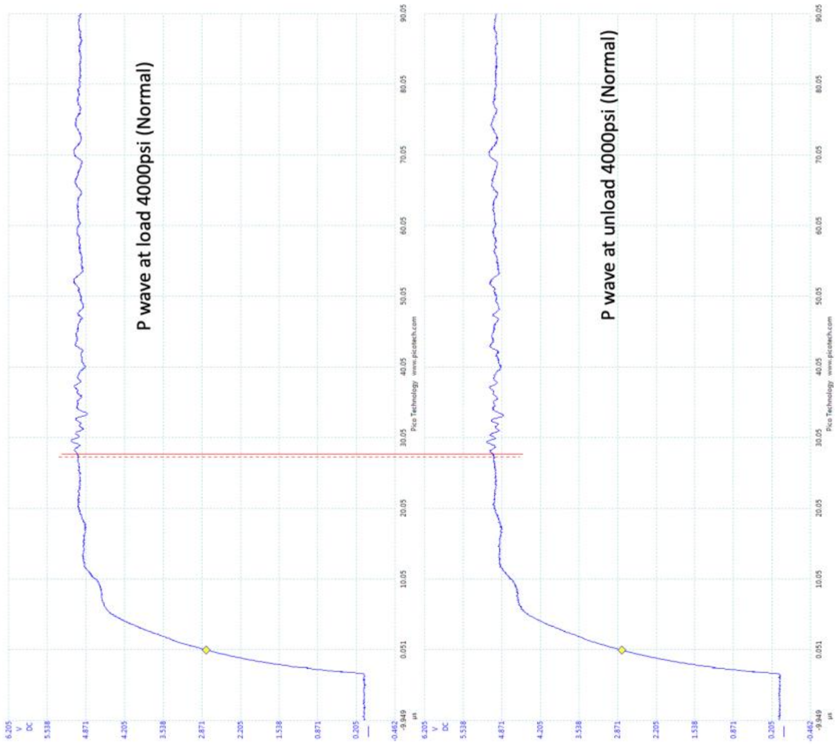

Classification analysis by WEKA

Classifier output

```
=== Run information ===

Scheme:       weka.classifiers.trees.J48 -C 0.25 -M 2
Relation:     Crack_density-weka.filters.unsupervised.attribute.Remove-R1-2,7,21,23-29,32-33,36-41
Instances:    74
Attributes:   23
              grain_size
              grain_sorting
              Microstructural rock type
              Porosity
              Quartz
              Albite
              Microcline
              Calcite
              Dolomite
              Mica
              Illite-smectite
              Kaolinite
              Chlorite
              Pyrite
              Siderite
              Barite
              Anhydrite
              Clay
              a0_load
              e0_load
              a0_unload
              e0_unload
              e0_load/unload_class_type
Test mode:    10-fold cross-validation

=== Classifier model (full training set) ===

J48 pruned tree
------------------

e0_unload <= 0.135049: AL (56.0/9.0)
e0_unload > 0.135049
|   a0_unload <= 0.000163: e0H (8.0)
|   a0_unload > 0.000163: AL (10.0/2.0)

Number of Leaves  :     3

Size of the tree :      5
```

```
Time taken to build model: 0 seconds

=== Stratified cross-validation ===
=== Summary ===

Correctly Classified Instances          54               72.973  %
Incorrectly Classified Instances        20               27.027  %
Kappa statistic                          0.2915
Mean absolute error                      0.1438
Root mean squared error                  0.3268
Relative absolute error                 66.2593 %
Root relative squared error            101.2917 %
Total Number of Instances               74

=== Detailed Accuracy By Class ===

                 TP Rate  FP Rate  Precision  Recall   F-Measure  MCC      ROC Area  PRC Area  Class
                 ?        0.000    ?          ?        ?          ?        ?         ?         H
                 0.500    0.031    0.714      0.500    0.588      0.548    0.809     0.494     e0H
                 0.222    0.092    0.250      0.222    0.235      0.137    0.839     0.349     a0H
                 0.855    0.632    0.797      0.855    0.825      0.242    0.728     0.859     AL
Weighted Avg.    0.730    0.485    0.719      0.730    0.721      0.271    0.753     0.748

=== Confusion Matrix ===

  a  b  c  d   <-- classified as
  0  0  0  0 |  a = H
  0  5  0  5 |  b = e0H
  0  0  2  7 |  c = a0H
  0  2  6 47 |  d = AL
```